

The Mozambique Ridge
—
**Evolution of a Large Igneous Province and its implication
for palaeocean circulation**

**Kumulative Dissertation
zur Erlangung des akademischen Grades
Dr. rer. nat.
am Fachbereich Geowissenschaften
der Universität Bremen**

Maximilian David Fischer

Mai 2017

Erklärung

Hiermit versichere ich,

Maximilian David Fischer
Friedenstraße 11
34121 Kassel

dass ich

- (1) die Arbeit ohne unerlaubte fremde Hilfe angefertigt habe,
- (2) keine anderen als die von mir angegebenen Quellen und Hilfsmittel benutzt habe und
- (3) die den benutzten Werken wörtlich oder inhaltlich entnommenen Stellen als solche kenntlich gemacht habe.

Bremerhaven, den

Maximilian David Fischer

Die vorliegende Dissertation wurde am 11.08.2017 an der Universität Bremen verteidigt. Der Prüfungsausschuss bestand aus Prof. Dr. Wilfried Jokat (erster Gutachter), Prof. Dr. Katrin Huhn-Frehers (zweite Gutachterin), Prof. Dr. Cornelia Spiegel, Prof. Dr. Dierk Hebbeln, Dr. Stefan Wenau und Steffen Brandt.

Zusammenfassung

Neue geophysikalische Daten aus dem südwestlichen Indischen Ozean liefern den ersten hochauflösenden Mehrkanal-Reflexionsseismik Datensatz der den kompletten südlichen Mosambikrücken (MozR) überspannt. Während der Forschungsexpedition mit FS Sonne wurden insgesamt ~4200 km reflexionsseismische Profillinien aufgenommen, die als Grundlage für eine Beurteilung des MozR hinsichtlich seiner Grundgebirgsstruktur und Entstehung dienen sollen. Ein weiteres Ziel der Interpretation der Daten umfasst die mögliche Auswirkung des Rückens auf die Paläozirkulation im sich öffnendem Südozean während der Kreide, dem Tertiär und dem Quartär. Die Basis dieser Dissertation bildet ein neu entwickeltes seismostratigrafisches Model, welches die gewonnenen reflexionsseismischen Daten mit Ergebnissen der Tiefseebohrung auf dem nördlichen MozR (DSDP Leg 25 Site 249) und einem vorhandenen seismostratigrafischen Model korreliert.

Die Entstehung der vier geomorphologischen Einheiten des MozR fällt in den Zeitraum des Gondwana Aufbruchs. Der genaue Ursprung des Rückens und die Entwicklung seit seiner Entstehung sind jedoch heftig umstritten. Die vorhandenen Theorien reichen von der Annahme eines kontinentalen Ursprungs der Struktur bis hin zur Ansprache des Rückens als kontinentales Fragment eingebettet in ozeanische Kruste. Weitwinkelseismik legt eine Interpretation des südlichen MozR als magmatische Großprovinz (engl.: Large Igneous Province, LIP) nahe und wird von Ergebnissen der magnetischen Vermessung der Struktur gestützt.

Die neuen reflexionsseismischen Untersuchungen lassen mächtige und großflächige Lavaflußsequenzen und eine Vielzahl von Extrusionszentren erkennen. Diese Beobachtungen sprechen für eine Charakterisierung des MozR als LIP. Diese Annahme wird durch die errechnete Fläche und das magmatische Volumen des Rückens bekräftigt, welche die postulierten Mindestwerte für LIPs bei Weitem übersteigen.

Die beobachteten Geometrien der seismischen Reflexionen suggerieren eine sequenzielle Entstehung der einzelnen Segmente des MozR durch gewaltige, jedoch nach geologischem Maßstab, kurze magmatische Eruptivphasen. Die Annahme einer sequenziellen Entstehung des MozR wird durch weitere bereits veröffentlichte geophysikalische Daten aus dem Gebiet des MozR gestützt. Anhand des errechneten magmatischen Volumens, sowie unter Berücksichtigung von publizierten gemittelten magmatischen Ausflussraten und einer aktuellen plattentektonischen Rekonstruktion, wird die Entstehung des südlichen MozR auf den Zeitraum zwischen 131 und 125 Ma datiert.

Die Entstehung der MozR LIP fällt somit in die finale Phase der Trennung von Afrika, Antarktis und Südamerika, und ergänzt die Fülle an kretazischen LIPs in Atlantik, Indik und dem Pazifischem Ozean. Die reflexionsseismischen Daten liefern zudem Hinweise auf eine magmatisch-tektonische Reaktivierung des MozR entlang seiner Flanken während des späten Neogens. Dies könnte im Zusammenhang mit einer meerwärtigen Ausbreitung des westlichen Ausläufers des Ostafrikanischen Grabenbruchs stehen.

Die sedimentären Ablagerungen im Gebiet des südlichen MozR dienen als Archiv für den Wassermassenaustausch zwischen Indik und Südatlantik durch die Afrika-Südozean (A-SO) Passage, da durch strömungskontrollierte Sedimentation charakteristische Sedimentstrukturen (Konturite) entstehen. Durch die Interpretation der Konturite können Aussagen über die Stärke, den Verlauf und Richtungsänderungen der Paläozirkulation abgeleitet werden.

Die reflexionsseismischen Daten deuten auf eine Ablagerung terrigener Sedimente ohne Strömungseinfluss im Anschluss an die initiale Bildungsphase des MozR hin. Ergebnisse der Tiefseebohrung (DSDP Leg 25 Site 249) zeigen einen erhöhten Anteil organischen Kohlenstoffs in den Sedimenten und lassen auf eine Ablagerung unter euxinischen Bedingungen schließen. Dies wird als Indiz für eine Abschottung der A-SO Passage durch topografische Barrieren (z.B., Falkland Plateau)

gegenüber der allmählich aufkommenden Paläozirkulation im Südozean interpretiert.

Das Vorkommen von vulkanischen Lagen im Bohrkern zusammen mit einem starken Anstieg der Reflexionsamplituden deutet auf eine magmatische Reaktivierung des Rückens zum Ende der Unterkreide hin. Der nachfolgende Interval, der sich bis in die späte Oberkreide zieht, ist durch einen langanhaltenden Hiatus geprägt. Dieser ist als Folge der Anhebung des MozR durch dessen magmatische Reaktivierung und dem Beginn einer starken oberflächennahen Zirkulation im Gebiet der A–SO Passage entstanden.

Oberkreidezeitliche Konturite am südlichen MozR sind das Ergebnis flacher, strömungskontrollierter Sedimentation aufgrund der Abnahme der Strömungsintensität. Einer der Auslöser für die verringerte Strömungsintensität war die Trennung des Rio Grande Rise vom Walvis-Rücken, die möglicherweise zu einer Ablenkung des Oberflächen- und Zwischenwassers westlich der A–SO Passage geführt hat. Die Konturite belegen somit den Beginn des oberflächennahen Wassermassenaustauschs zwischen Indik und Südatlantik durch die Passage im späten Campanium (~75 Ma).

Ein etwa 50 Millionen Jahre umfassender Hiatus am MozR wird als Konsequenz eines kräftigen südäquatorialem Stroms im Indischen Ozean (pre-Indian Ocean SEC) gedeutet. Umfassende klimatische (z.B., Vergletscherung der Westantarktis) und tektonische Veränderungen (z.B., sukzessive Schließung des Indonesischen Seeweges) während des Neogens sorgten für eine Verlagerung des Zustroms des Antarktischen Bodenwassers (AABW) und eine Ablenkung des Nordatlantischen Tiefenwassers (NADW) im Gebiet der A–SO Passage. Diese Modifikationen werden durch erneute Ablagerung von Konturiten in Tiefenbereichen des AABW und NADW belegt. Die dünne Sedimentbedeckung und das vermehrte Auftreten von Erosionsstrukturen in Tiefen des heutigen Antarktischen Zwischenwassers (AAIW) deuten auf eine anhaltende kräftige Zirkulation in diesen Tiefen hin.

Eine Pliozäne Diskordanz im Gebiet der A–SO Passage wird als Übergang zur modernen thermohalinen Zirkulation (THC) interpretiert. Der Übergang geht einher mit einer Verlagerung des AABW Zuflusses in die A–SO Passage durch die Agulhas Passage im Westen und ist dokumentiert durch Konturite entlang der südlichen tiefen Flanken des MozR. Gleichzeitig zeichnet sich anhand der beobachteten Sedimentstrukturen eine Veränderung der NADW Zirkulation entlang des MozR ab, welche auf eine Aufteilung des NADW in der A–SO Passage in einen nördlichen und einen südlichen Strom schließen lassen.

Diese Beobachtungen signalisieren den Beginn der tiefen THC zwischen dem Atlantik und Indik durch die A–SO Passage ohne eine starke Beeinflussung der Zirkulation durch den MozR im Quartär. Die Zunahme von Konturiten im Tiefenbereich des AAIW deutet auf eine Verringerung der Strömungsgeschwindigkeit hin. Die Quartären Veränderungen der Paläozirkulation sind die Folge weitreichender paläo-ozeanografischer Ereignisse wie etwa die finale Schließung der Meerenge von Panama und des Indonesischen Seeweges, sowie dem Beginn der Vergletscherung in der nördlichen Hemisphäre. Die Ergebnisse zeigen, dass die Interpretation der Sedimentablagerungen am südlichen MozR eine detaillierte Rekonstruktion der Ozeanzirkulation seit der Unterkreide liefern und zu einem besseren Verständnis der Auswirkungen tektonischer und klimatischer Veränderungen beitragen.

Summary

New geophysical data acquired in the southwest Indian Ocean represent the first high-resolution multi-channel seismic (MCS) reflection survey covering the complete southern Mozambique Ridge (MozR). During RV Sonne expedition SO232 ~4200 km of MCS reflection data were gathered. This data is used to evaluate the basement structure and the origin of the southern MozR. Another objective of the interpretation of the data is to investigate the possible impact of the structure on palaeocean circulation in the evolving Southern Ocean during the Cretaceous, Tertiary and Quaternary. The foundation for this dissertation is based on a new seismostratigraphic model that correlates the acquired MCS reflection data with the results of DSDP Leg 25 Site 249 and a previously published seismic stratigraphy.

The four geomorphological segments of the MozR were formed during the Gondwana breakup, but the precise origin and evolution of the ridge since its development are highly debated. Some authors propose a continental provenance of the structure, while others suggest continental fragments embedded in oceanic crust. Recent wide-angle seismic data favours a Large Igneous Province (LIP) origin of the southern MozR, a view supported by geomagnetic anomaly data.

Investigation of the new MCS reflection data shows the occurrence of thick and laterally extensive lava flow sequences and a great number of extrusion centres. These observations suggest a LIP origin of the southern MozR. Evaluations of its areal extent and magmatic volume provide further support for this assumption, as they exceed the required minimum values for LIPs by far.

The observed geometries of the seismic reflections suggest a sequential emplacement of the individual segments of the MozR by massive but geologically short magmatic pulses. Additional geophysical data recorded in the area of the MozR are also in favour of a sequential formation of the ridge. Based on the calculated magmatic volume, published time-averaged volumetric volcanic output rates and a recent plate tectonic reconstruction, a rapid sequential emplacement of the southern MozR between 131 and 125 Ma is proposed.

The formation of the MozR LIP therefore coincides with the final separation of Africa, Antarctica and South-America, and complements the already vast list of Cretaceous LIPs in the Atlantic, Indian and Southern Oceans. The MCS reflection data provide evidence for a late Neogene tectono-magmatic reactivation of the MozR along its flanks. This may indicate a seaward propagation of the Western branch of the East African Rift System.

The sedimentary record in the area of the southern MozR acts as an archive for the water mass exchange between the Indian and South Atlantic Oceans through the African–Southern Ocean (A–SO) gateway. Characteristic sedimentary structures (contourites) are deposited by current controlled sedimentation and allow for an interpretation of the intensity, pathway and direction of the palaeocean circulation.

The MCS reflection data suggest deposition of terrigenous sediments without an influence by circulation subsequent to the initial ridge formation. Results of DSDP Site 249 show an increased amount of TOC in the Lower Cretaceous sediments that infer deposition under euxinic conditions. This is interpreted as evidence for the isolation of the A–SO gateway by topographic barriers (e.g., Falkland Plateau) against the emerging palaeocean circulation in the Southern Ocean.

The occurrence of volcanogenic sediment layers at DSDP Site 249 together with an observed distinct increase in reflection amplitudes suggest a magmatic reactivation of the MozR in mid-Cretaceous times. The following interval, which continues into the late Upper Cretaceous, is characterized by a long-lasting hiatus. The hiatus is a result of the uplift of the MozR due to its magmatic reactivation, and the onset of a vigorous shallow circulation in the A–SO gateway.

Observed Upper Cretaceous contourites at the southern MozR are evidence of a shallow current

controlled sedimentation due to decreased current intensities. One of the reasons for the decrease in current intensities may be the separation of the Rio Grande Rise from the Walvis Ridge that probably caused a deflection of the surface and intermediate waters west of the A–SO gateway. The observed contourites indicate the inception of a shallow water mass exchange between the Indian and South Atlantic Oceans through the gateway in late Campanian times (~75 Ma).

The occurrence of a ~50 Myr long hiatus at the MozR is attributed to the vigorous pre-Indian Ocean South Equatorial Current. Extensive climatic (e.g., West Antarctic Glaciation) and tectonic (e.g., gradual closing of the Indonesian seaway) modifications during the Neogene caused a shift of the inflow of Antarctic Bottom Water (AABW) and a deflection of North Atlantic Deep Water (NADW) in the A–SO gateway. These changes are documented by renewed contourite deposition in depths similar to AABW and NADW. The thin sedimentary cover and the occurrence of a number of erosional structures in depths of modern Antarctic Intermediate Water (AAIW) indicate a sustained vigorous circulation in these depths.

The occurrence of a Pliocene unconformity within the A–SO gateway is interpreted as the transition towards the modern Thermohaline circulation (THC). The transition is accompanied by a shift of the AABW inflow into the gateway through the Agulhas Passage to the west and is documented by the observation of drift structures contouring the southern deep flanks of the MozR. The observed sedimentary structures in NADW depth point to a modification of NADW flow along the MozR, and indicate a separation into a northern and a southern NADW branch.

This suggests the onset of deep THC between the Atlantic and Indian Oceans through the A–SO gateway without major interference by the MozR. The increase in the number of contourites in AAIW depths implies a slowing down of current velocities. The Quaternary modifications of the palaeocean circulation are the consequence of extensive palaeoceanographic events, such as the final closure of the Central American Seaway and the Indonesian Seaway, and the onset of Northern Hemisphere Glaciation. The results show that the interpretation of the sedimentary deposits at the southern MozR provide a detailed reconstruction of the palaeocean circulation since the Early Cretaceous, and contribute to a better understanding of the impacts related to tectonic and climatic modifications.

Contents

Zusammenfassung	I
Summary	III
List of Figures	XI
List of Tables	XIII
Nomenclature	XV
1. Introduction and motivation	1
1.1. Large Igneous Provinces and their environmental impact.....	1
1.2. Ocean circulation	2
1.3. The African–Southern Ocean gateway	4
1.4. Research questions	5
2. Datasets and methods	7
2.1. Datasets.....	7
2.1.1. Seismic reflection data	8
2.1.2. Borehole data	9
2.2. Methods	10
2.2.1. Seismic data processing.....	10
2.2.2. Seismic stratigraphy	11
2.2.3. Identification of magmatic structures within seismic reflection data	11
2.2.4. Identification of palaeocean circulation pathways	12
3. Contribution to scientific journals	15
3.1. The Mozambique Ridge: a document of massive multistage magmatism.....	15
3.2. Late Cretaceous onset of current controlled sedimentation in the African–Southern Ocean gateway	16
3.3. Neogene modifications of circulation in the African–Southern Ocean gateway.....	16
4. The Mozambique Ridge: a document of massive multi-stage magmatism	19
4.1. Introduction	20
4.2. Geological and tectonic background.....	21
4.3. Data and methods	22
4.3.1. Seismic reflection data	22
4.3.2. DSDP data.....	23
4.4. Results	24
4.4.1. Seismic stratigraphy	24
4.4.1.1. Basement	24
4.4.1.2. Seismic units S1 and S2	24
4.4.2. Regional basement structure.....	29
4.4.2.1. Central Mozambique Ridge.....	29
4.4.2.2. Southwestern Mozambique Ridge	29
4.4.2.3. Southeastern Mozambique Ridge	30
4.4.3. Magmatic structures	30

4.4.4. Faults.....	32
4.5. Discussion	32
4.5.1. Intrabasement reflections and extrusion centres.....	32
4.5.2. Post-sedimentary magmatism at the Mozambique Ridge.....	33
4.5.3. Magmatic volume of the southern Mozambique Ridge and implications for its emplacement history.....	35
4.5.3.1. Volume of magmatism at the southern Mozambique Ridge.....	35
4.5.3.2. Timing and duration of emplacement of the Mozambique Ridge	38
4.6. Conclusion.....	41
4.7. Acknowledgements.....	41
5. Late Cretaceous onset of current controlled sedimentation in the African–Southern Ocean gateway	43
5.1. Introduction.....	44
5.2. Background and settings.....	45
5.2.1. Tectonic and palaeoceanographic setting	45
5.2.2. Contourite drifts	47
5.2.3. Seismic stratigraphy	47
5.3. Methods.....	49
5.4. Results	50
5.4.1. Distribution of seismic units	50
5.4.1.1. Basement.....	50
5.4.1.2. Early Cretaceous unit S1.....	51
5.4.1.3. Late Cretaceous unit S2a.....	52
5.4.2. Current controlled sedimentation in the study area.....	53
5.4.2.1. Late Cretaceous (late Campanian to late Maastrichtian) sediment drifts.....	54
5.4.2.2. Erosional structures.....	54
5.5. Discussion	56
5.5.1. Early Cretaceous (until ~100 Ma; unit S1).....	56
5.5.2. Late Cretaceous hiatus (~100–75 Ma).....	58
5.5.3. Late Cretaceous (~75–68 Ma).....	60
5.6. Conclusion.....	62
5.7. Acknowledgements.....	63
6. Neogene modifications of circulation in the African–Southern Ocean gateway	65
6.1. Introduction.....	66
6.2. Background and settings.....	67
6.2.1. Geologic and palaeoceanographic setting	67
6.2.2. Seismic stratigraphy	68
6.3. Methods.....	70
6.4. Results.....	71
6.4.1. Distribution of seismic unit S2b (≤ 15 Ma).....	71
6.4.1.1. Subunit S2b-I (~15–5 Ma).....	72
6.4.1.2. Subunit S2b-II (≤ 2.6 Ma).....	74
6.4.2. Contourites and erosional structures.....	75
6.4.2.1. Mid–Miocene to early Pliocene structures (~15–5 Ma; unit S2b-I).....	76
6.4.2.2. Pleistocene to Holocene structures (≤ 2.6 Ma; unit S2b-II).....	77
6.5. Discussion	78
6.5.1. Mid-Miocene to early Pliocene palaeoceanographic implications (unit S2b-I) ...	79

6.5.2. Implementation of the modern circulation scheme in the A–SO gateway (unit S2b-II)	80
6.6. Conclusion	82
6.7. Acknowledgements.....	83
7. Seismostratigraphic model of the southern Mozambique Ridge.....	85
8. Conclusion	87
9. Outlook	90
10. Bibliography.....	95
11. Danksagung.....	115
Appendix	A-1

List of Figures

Figure 1.1.	Global distribution of Large Igneous Provinces	1
Figure 1.2.	The global Thermohaline Circulation and modern circulation in the study area	3
Figure 2.1.	Logo of the expedition SO232 to the Mozambique Ridge	7
Figure 2.2.	Overview of acquired data during cruise SO232	7
Figure 2.3.	Simplified sketch of seismic data acquisition.....	8
Figure 2.4.	Equipment used for seismic data acquisition.....	9
Figure 2.5.	Results of DSDP Leg 25 Site 249.....	9
Figure 2.6.	Schematic sketches of magmatic features in the study area.....	11
Figure 2.7.	Characteristics of mounded drift types	12
Figure 2.8.	Principal drift development in the Southern Hemisphere.....	13
Figure 4.1.	Map of the study area with location of shown profiles	20
Figure 4.2.	Seismostratigraphy of the study area	23
Figure 4.3.	Seismic profile across the central Mozambique Ridge from NW to SE	26
Figure 4.4.	Seismic profile across the central Mozambique Ridge from NE to SW	26
Figure 4.5.	Maps of basement depth, sedimentary thickness and magmatic features	27
Figure 4.6.	Seismic profile across the SW Mozambique Ridge from WNW to ESE	29
Figure 4.7.	Extrusion centre and onlapping intrabasement reflections	30
Figure 4.8.	Seismic profile across the SE Mozambique Ridge from N to S.....	31
Figure 4.9.	Free-air gravity anomaly map of the southern Mozambique Ridge	34
Figure 4.10.	Simplified <i>P</i> -wave velocity model of the SW Mozambique Ridge.....	36
Figure 4.11.	Comparison of areal extent and crustal volume of Large Igneous Provinces.....	37
Figure 4.12.	Duration of emplacement phases of the southern Mozambique Ridge	39
Figure 4.13.	Schematic sketch of the emplacement model for the Mozambique Ridge.....	40
Figure 5.1.	Circulation pathways south of Africa and map of the study area	45
Figure 5.2.	Cretaceous seismostratigraphy of the study area	48
Figure 5.3.	Depth maps of the Cretaceous seismic units in the study area.....	50
Figure 5.4.	Seismic profile between the SW and central Mozambique Ridge	51
Figure 5.5.	Isopach maps of the Cretaceous seismic units in the study area.....	52
Figure 5.6.	Late Cretaceous sedimentary features and current pathways	53
Figure 5.7.	NE to SW trending seismic profile at the SW flank of the Mozambique Ridge	55
Figure 5.8.	Cretaceous palaeoceanographic evolution of the study area.....	57
Figure 6.1.	Map of the study area with inset showing circulation pathways off South Africa	66
Figure 6.2.	Cenozoic seismostratigraphy of the study area.....	69
Figure 6.3.	Depth map of the Cretaceous unit and isopach map of the Cenozoic unit.....	71
Figure 6.4.	Seismic profile between the SW and central Mozambique Ridge	72
Figure 6.5.	WNW to ESE trending seismic profile W of the SW Mozambique Ridge	73
Figure 6.6.	Isopach and depth maps of the Neogene seismic unit in the study area	73
Figure 6.7.	Seismic profile across the SE Mozambique Ridge from N to S.....	74
Figure 6.8.	Isopach and depth maps of the Quaternary seismic unit in the study area.....	75
Figure 6.9.	Neogene sedimentary features and inferred circulation scheme	77
Figure 6.10.	Quaternary sedimentary features and inferred circulation scheme	78
Figure 7.1.	Merged version of the seismostratigraphy of the study area	85

Figure 8.1.	Graphic summary of the Cretaceous to Quaternary events	88
Figure 9.1.	Map of the study area showing the proposed seismic profiles and drill sites	90
Figure 9.2.	Interpreted seismic section with proposed Drill Site B.....	91
Figure A.1.	Map of the study area with locations of the 22 seismic profiles.....	A-1
Figure A.2.	Time-migrated profile AWI-20140201	A-3
Figure A.3.	Time-migrated profile AWI-20140202	A-4
Figure A.4.	Time-migrated profile AWI-20140203	A-5
Figure A.5.	Time-migrated profile AWI-20140204	A-6
Figure A.6.	Time-migrated profile AWI-20140205	A-7
Figure A.7.	Time-migrated profile AWI-20140206	A-8
Figure A.8.	Time-migrated profile AWI-20140207	A-9
Figure A.9.	Time-migrated profile AWI-20140208	A-10
Figure A.10.	Time-migrated profile AWI-20140209	A-11
Figure A.11.	Time-migrated profile AWI-20140210	A-12
Figure A.12.	Time-migrated profile AWI-20140211	A-13
Figure A.13.	Time-migrated profile AWI-20140212	A-14
Figure A.14.	Time-migrated profile AWI-20140213	A-15
Figure A.15.	Time-migrated profile AWI-20140214	A-16
Figure A.16.	Time-migrated profile AWI-20140215	A-17
Figure A.17.	Time-migrated profile AWI-20140216	A-18
Figure A.18.	Time-migrated profile AWI-20140217	A-19
Figure A.19.	Time-migrated profile AWI-20140218	A-20
Figure A.20.	Time-migrated profile AWI-20140219	A-21
Figure A.21.	Time-migrated profile AWI-20140220	A-22
Figure A.22.	Time-migrated profile AWI-20140221	A-23
Figure A.23.	Time-migrated profile AWI-20140222	A-24

List of Tables

Table 2.1. Seismic processing steps.....	10
Table 4.1. Seismic stratigraphy of the study area	25
Table 4.2. Values used in the volumetric calculations of the Mozambique Ridge.....	35
Table 5.1. Seismic stratigraphy of the Cretaceous units in the study area	49
Table 6.1. Seismic stratigraphy of the Cenozoic units in the study area.....	70
Table 7.1. Merged version of the seismic stratigraphy of the study area	86
Table 9.1. Parameters of proposed drill sites A and B	91
Table A.1. Parameters of seismic reflection profiles	A-2

Nomenclature

A–SO	African–Southern Ocean
AABW	Antarctic Bottom Water
AAIW	Antarctic Intermediate Water
AC	Agulhas Current
ACC	Antarctic Circumpolar Current
AGC	Automatic Gain Control
AP	Agulhas Plateau
APa	Agulhas Passage
AWI	Alfred-Wegener-Institut Helmholtz-Zentrum für Polar- und Meeresforschung
BC	Basement Complex
bsl	below sea level
CDP	Common Depth Point
cMozR	central Mozambique Ridge
DSDP	Deep Sea Drilling Program
e.g.	for example
EAG	Equatorial Atlantic Gateway
EARS	East African Rift System
EC	Extrusion Centre
GEBCO	General Bathymetric Chart of the Oceans
GPS	Global Positioning System
ISOW	Intermediate Southern Ocean Water
LIP	Large Igneous Province
Ma	Million Years ago
mbsf	metres below seafloor
MCS	Multi-channel seismic
MIOJet	Miocene Indian Ocean Equatorial Jet
MozR	Mozambique Ridge
Myr	Million Years
NADW	North Atlantic Deep Water
nMozR	northern Mozambique Ridge
NV	Natal Valley
PSM	Post-sedimentary magmatism OR post-sedimentary magmatic
RV	Research Vessel
RWS	Rio Grande Rise–Walvis Ridge System
SEC	South Equatorial Current
seMozR	southeastern Mozambique Ridge
swMozR	southwestern Mozambique Ridge
TB	Transkei Basin
TWT	Two Way Time
UNAW	Upper North Atlantic Water
UPW	Upper Pacific Water

1. Introduction and motivation

1.1. Large Igneous Provinces and their environmental impact

Massive magmatic events have repeatedly occurred within geologic history both on land and in the ocean. Large Igneous Provinces (LIPs) are the expression of these enormous magmatic outpourings and several mechanisms have been proposed to explain their formation. A widely supported theory connects LIP development to the presence of a mantle plume (Coffin and Eldholm, 1994; White and McKenzie, 1995; Saunders, 2005; Campbell, 2007). During the life cycle of a plume, a massive plume-head is developed in a first step that rises through the mantle in a geologically short time. At the base of the lithosphere the plume head expands due to decompression and erupts massive flood basalts with a large buoyancy flux (Courtilot *et al.*, 2003). Other models explain the massive outpourings of magma as the result of edge-driven convection (King and Anderson, 1998), or lithosphere delamination (Elkins-Tanton, 2005).

LIPs can be divided into four types: continental flood basalts, volcanic rifted margins, oceanic plateaus and ocean basin flood basalts (Figure 1.1). All four types share their common intraplate tectonic setting, thus were emplaced by processes distinct from those observed at modern plate boundaries (Bryan and Ernst, 2008). While most LIPs are of mafic to ultramafic composition (e.g., Shatsky Rise in the Pacific Ocean; Figure 1.1), some are dominated by silicic magmatism (e.g., Whitsunday LIP east of Australia).

Bryan and Ernst (2008) defined LIPs as magmatic provinces with areal extents $>0.1 \times 10^6 \text{ km}^2$, igneous volumes $>0.1 \times 10^6 \text{ km}^3$ and maximum lifespans of ~ 50 Myr. They are characterized by igneous pulse(s) of short duration ($\sim 1\text{--}5$ Myr), during which a large proportion (>75 per cent) of the total igneous volume was emplaced. It has been suggested that the magmatism associated with the emplacement of all LIPs taken together account for ~ 10 per cent of the mass and energy transfer from

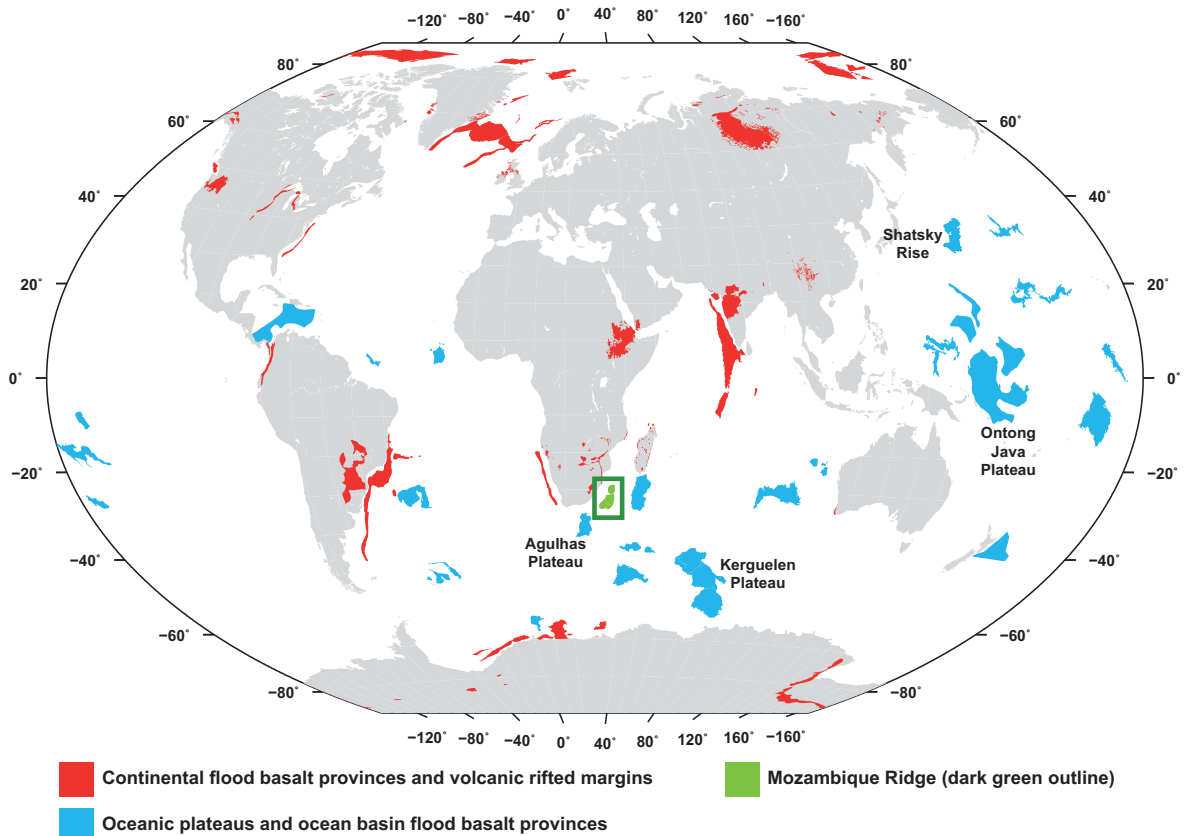


Figure 1.1. Global distribution of Large Igneous Provinces. Continental flood basalts and volcanic rifted margins are shown in red, oceanic plateaus and ocean flood basalt provinces are shown in blue. The Mozambique Ridge is illustrated in green. LIPs addressed in the text are labelled. Modified after Bryan and Ferrari, 2013.

the Earth's deep interior to the surface (Sleep, 1992).

For several decades LIPs have been of great interest because of their dramatic impact on the Earth's atmosphere, oceans and biosphere (Neal *et al.*, 2008). Correlations between large basaltic eruptions and disturbances of the global environment are well-documented. Historic examples include two volcanic eruptions in Iceland (934 and 1783 CE), both of which were followed by historically cold summers in the Northern Hemisphere (Stothers, 1998).

In contrast, the magmatic eruptions associated with LIP formation exceed the duration and strength of both events by several orders of magnitude. They have been linked to climate shifts and mass extinction events by ejecting large amounts of greenhouse gases (e.g., CO₂, SO₂) and heat into the atmosphere (Sobolev *et al.*, 2011; Armstrong Mckay *et al.*, 2014; Kerr, 2014). The emplacement of several Cretaceous oceanic plateaus such as the Ontong Java and Kerguelen Plateaus (Figure 1.1) eventually culminated in oceanic anoxic events and significant deposition of black shales (Kerr, 1998, 2005; Saunders, 2005; Kerr, 2014). According to Bond and Wignall (2014) almost all of Earth's most severe biotic crises, including four of the "Big 5" Phanerozoic extinction events, were associated with LIP formation. The global occurrences of these biotic crises highlight the far-reaching changes caused by LIP emplacement.

Directly or indirectly, these changes in the atmosphere-ocean system may also have caused disturbance of the ocean circulation (Self *et al.*, 2006). This applies in particular to the Cretaceous, which, because the CO₂ content in the atmosphere was three to seven times higher than that of today, was thus perhaps more susceptible to perturbations in atmosphere-ocean dynamics (Neal *et al.*, 2008). LIP-induced global warming may have increased water temperatures in the polar regions, thereby effectively slowing down circulation by decreasing the pole-to-equator temperature gradient (Kerr, 2005; Wignall, 2005). Furthermore, oceanic plateaus represent large-scale seafloor elevations and can thus severely obstruct water circulation within the ocean basins. This is documented by the occurrence of erosional unconformities, contourites and distinct geochemical signatures at a number of LIPs such as the Agulhas and Kerguelen Plateaus (Figure 1.1; Tucholke and Carpenter, 1977; Tucholke and Embley, 1984; Uenzelmann-Neben, 2001, 2002; Murphy and Thomas, 2012, 2013).

1.2. Ocean circulation

Modern-day ocean circulation is relatively well-understood, with the global Thermohaline Circulation (THC; Figure 1.2) considered to be the main conveyor of global heat transfer and one of the driving forces behind the earth's climate (Rahmstorf, 2002; Kuhlbrodt *et al.*, 2007; van Aken, 2007). According to Wunsch (2002) the ocean is best described as a mechanically driven fluid engine, capable of importing, exporting, and transporting vast quantities of heat and freshwater. Its engine is fuelled by differences in temperature and salinity causing density loss or gain and therefore up- or downwelling of water masses in specific regions.

Warm and saline surface water (red paths in Figure 1.2) flows towards high latitudes where the three main deep water formation regions (northern North Atlantic, Ross Sea and Weddell Sea; yellow ovals in Figure 1.2) are located. It becomes denser and downwells due to its lower temperature and higher salt content (Rahmstorf, 2002; Wunsch, 2002; Kuhlbrodt *et al.*, 2007; van Aken, 2007). The denser water then recirculates at depth (blue paths in Figure 1.2), thereby getting warmer and less salty due to mixing. Consequently, the water upwells again, eventually starting a new cycle of heat and salt transport towards the high latitudes.

Otto-Bliesner *et al.* (2002) and Via and Thomas (2006) suggested that deep water formation was already active during the Late Cretaceous or early Palaeogene by mechanisms similar to the present. However, continental configuration prevented a global circulation until plate tectonic movements

allowed for interoceanic exchange of water masses. Important steps towards initiation of the global THC include:

- Middle to Late Cretaceous reorganization of the oceanic circulation that governed the termination of the hot Cretaceous greenhouse as a consequence of the opening of the Equatorial Atlantic Gateway (Friedrich *et al.*, 2012).
- Late Eocene to early Oligocene Antarctic glaciation and initiation of the Arctic Circumpolar Current due to the Drake Passage opening (Katz *et al.*, 2011).
- Late Neogene intensification of North Atlantic Deep Water circulation as a result of the closure of the Central American Seaway, which may have facilitated the onset of Northern Hemisphere Glaciation (Schneider and Schmittner, 2006).

The opening and closing of ocean gateways have therefore substantially altered ocean circulation during most of geologic history, which in turn affected the global climate (Sijp *et al.*, 2014; Donnadiou *et al.*, 2016; Uenzelmann-Neben *et al.*, 2016). These palaeoceanographic events left their footprints in the sedimentary record and can be reconstructed based on the analysis of geochemical proxy signatures (e.g., $\delta^{18}\text{O}$, $\delta^{13}\text{C}$, ϵ_{Nd} ; Frank *et al.*, 2002; Friedrich *et al.*, 2012). Furthermore, sedimentary sequences that have been deposited and shaped by these long-term currents reveal information about flow paths, strengths and directions, and thus yield information about palaeocurrent attributes and changes (Rebesco *et al.*, 2014; for further details please refer to chapter 2.2.4). A detailed reconstruction of palaeocurrent flow paths improves the knowledge of oceanic gateways and palae-

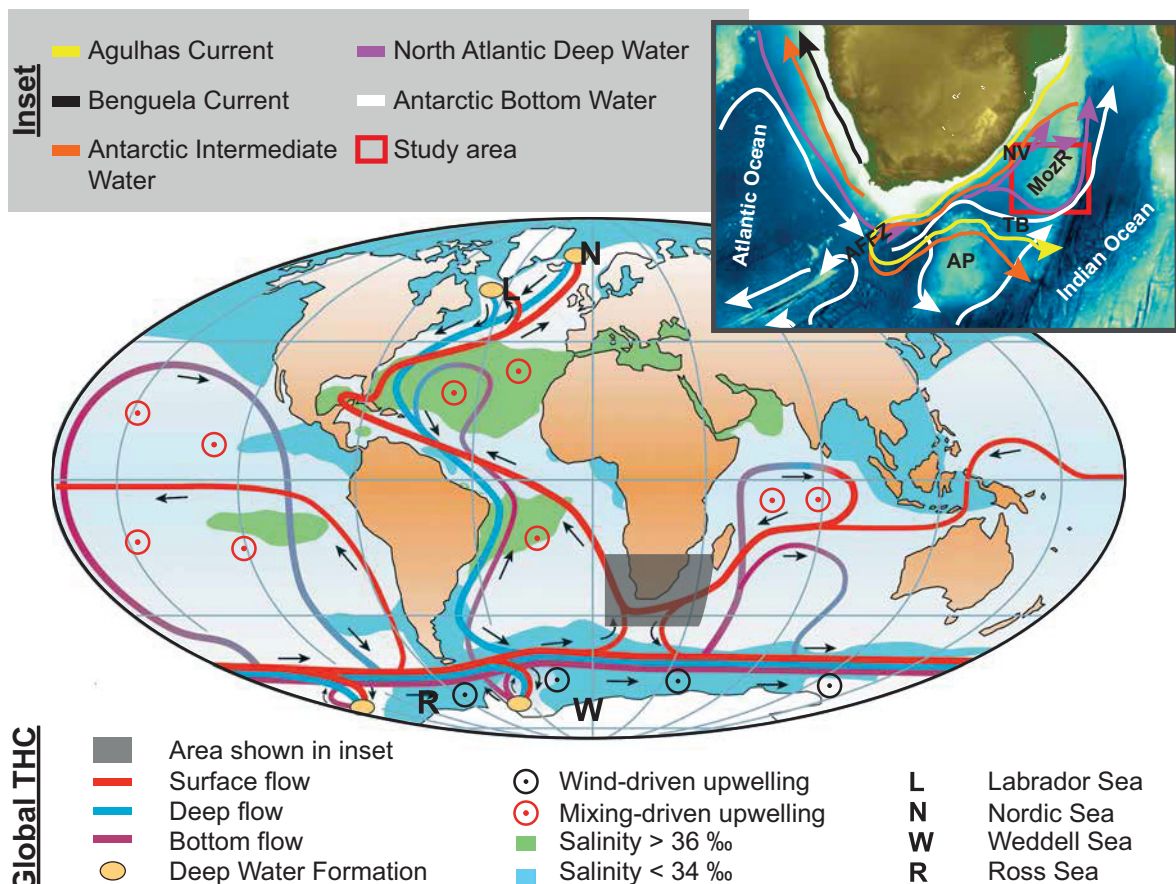


Figure 1.2. Simplified sketch of the global Thermohaline Circulation (THC). Modified after Rahmstorf, 2002 and Kuhlbrodt *et al.*, 2007. Inset shows a bathymetric map (Weatherall *et al.*, 2015) of the African–Southern Ocean gateway along with important structural units and the main flow paths (Lutjeharms, 2006; Uenzelmann-Neben *et al.*, 2007; Gruetzner and Uenzelmann-Neben, 2016) of the water masses circulating within the gateway.

oclimatic conditions and can lead to a better understanding of their development. This, in turn, can improve future forecast models for changes in global climate.

1.3. The African–Southern Ocean gateway

The African–Southern Ocean gateway (A–SO gateway; inset in Figure 1.2) represents an area that has been of great interest for studies about the effects of climatic and tectonic modification on circulation. Here, cold and warm water masses circulating through the Atlantic, the Indian and the Southern oceans meet and mix (Lutjeharms, 1996). The gateway thus plays an important role in maintaining the global THC. Nowadays, the upper ~2000 m of the water column are circulated by the warm and saline Agulhas Current (surface water; yellow arrow in inset of Figure 1.2) and the colder and denser Antarctic Intermediate Water (orange arrow in inset of Figure 1.2; Tomczak and Godfrey, 1994; You *et al.*, 2003; Lutjeharms, 2006). The deeper water masses comprise the North Atlantic Deep Water (depth below ~2000 m; purple arrows in inset of Figure 1.2) and the Antarctic Bottom Water (depth below ~3500 m; grey arrows in inset of Figure 1.2; Tucholke and Embley, 1984; van Aken *et al.*, 2004; Lutjeharms, 2006), both of which are strongly affected by seafloor topography (Lutjeharms, 2006).

The seafloor topography within the gateway is characterized by several structural units, whose structure, composition and development are still not fully understood (inset in Figure 1.2). The area developed as a consequence of Gondwana breakup between 170 and 160 Ma (Lawver *et al.*, 1992; Storey, 1995; Ghidella *et al.*, 2002; Jokat *et al.*, 2003; Jokat *et al.*, 2004; Bernard *et al.*, 2005) with a shallow water basin covering the area of the Mozambique Basin and Riser Larsen Sea. The opening of the South Atlantic started between 137 and 126 Ma (Gladczenko *et al.*, 1997; Hinz *et al.*, 1999), with the earliest traces of oceanic crust in the Natal Valley yielding an age of ~130 Myr (Goodlad *et al.*, 1982; König and Jokat, 2010). The circulation within the evolving Southern, Atlantic and Indian oceans were entirely different and characterized by separated shallow basins and a sluggish, restricted circulation under mainly euxinic conditions (Lawver *et al.*, 1992; Robinson *et al.*, 2010; Donnadiou *et al.*, 2016; Uenzelmann-Neben *et al.*, 2016). According to König and Jokat (2006) separation of the Falkland Plateau from Africa between ~110 and 100 Ma resulted in the inception of a deep water connection between the Indian and South Atlantic oceans.

Observed Late Cretaceous black shales in the Transkei Basin (TB; inset of Figure 1.2) indicate that a restricted and euxinic deep circulation within the A–SO gateway probably continued until 85 to 80 Ma (Schlüter and Uenzelmann-Neben, 2008a). An Eocene to Oligocene onset of current controlled sedimentation within the gateway is documented by several contourite drifts at the Agulhas Plateau and in the Transkei Basin (Uenzelmann-Neben, 2002; Schlüter and Uenzelmann-Neben, 2008b). Even though modifications of the circulation scheme within the gateway after initial onset of current controlled sedimentation were suggested, for example as a consequence of the mid-Miocene glaciation of West Antarctica, deposition of contourites is suggested to have persisted until the present day (Niemi *et al.*, 2000; Schlüter and Uenzelmann-Neben, 2007; Uenzelmann-Neben *et al.*, 2007; Schlüter and Uenzelmann-Neben, 2008b). As described above, the individual steps of the Gondwana breakup and general circulation history are largely understood.

However, structure, composition and development of the structural units within the A–SO gateway and their influence on palaeocean circulation have been under heavy debate. This applies in particular to the MozR. In general, three completely different theories have been proposed to explain its formation. While several authors favoured a continental provenance of the MozR (Tucholke *et al.*, 1981; Raillard, 1990; Mougnot *et al.*, 1991; Hartnady *et al.*, 1992), Ben-Avraham *et al.* (1995) suggested a partitioning of the MozR into a northern oceanic and a southern continental part.

Recently acquired seismic refraction data is interpreted as strong evidence for a LIP origin of the

southern MozR (Gohl *et al.*, 2011), and supported by gravity and magnetic anomaly data indicating a magmatic origin of the MozR (König and Jokat, 2010). In case of a LIP origin, the MozR would have strongly hindered surface and deep water mass exchange between the evolving Indian and South Atlantic oceans across the A–SO gateway. The results of DSDP Leg 25 Site 249 show the occurrence of two long-lasting hiatuses at the MozR (Simpson *et al.*, 1974). These hiatuses partly involve periods during which contourite deposition was proposed in the A–SO gateway. This indicates that the MozR witnessed a unique depositional history within the gateway.

To answer the question of the origin of the MozR and its possible interaction with palaeocean circulation during the evolution of the A–SO gateway, the Alfred-Wegener-Institut Helmholtz-Zentrum für Polar- und Meeresforschung gathered 22 high-resolution multi-channel seismic (MCS) reflection profiles in 2014 (please refer to chapter 2.1 for further details). The analysis and interpretation of these MCS reflection profiles (plus two additional MCS reflection profiles from a previous survey; see chapter 2.1) form the basis of this dissertation.

1.4. Research questions

In principle, this PhD thesis deals with two different topics: (I) the nature and origin of the basement and its implication for the formation of the Mozambique Ridge, and (II) the late Mesozoic to late Cenozoic sediments deposited on top of the basement and their interpretation as a sedimentary archive for the reconstruction of the palaeocean circulation. The following questions and topics are addressed in detail:

- I. Nature and origin of the basement of the Mozambique Ridge
 - What is the structure of the MozR basement?
 - Do we find evidence for a potential LIP origin of the MozR in the MCS data?
 - What dimensions did the magmatism at the southern MozR have?
 - How was the MozR emplaced, does its formation fit into existing Gondwana break-up models?

- II. Deposits at the Mozambique Ridge as an sedimentary archive
 - What can the sediments tell us about the prevailing conditions during their deposition?
 - When did the water mass exchange through the African–Southern Ocean gateway commence?
 - Do we observe evidence for different periods of palaeocean circulation?
 - Can we deduce the causes for modifications in the palaeocean circulation around the MozR?

The research questions regarding the basaltic basement and formation of the MozR are answered in chapter 4. The sedimentary deposits at the MozR and their use for reconstructing the palaeocean circulation in the African–Southern Ocean gateway are addressed in chapters 5 and 6. Chapter 5 focuses on the Cretaceous depositional environment, while chapter 6 covers the Cenozoic era.

2. Datasets and methods

2.1. Datasets

The geophysical data this study is based on were collected between March and May 2014, during RV Sonne expedition SO 232 as part of the project SLIP to study the structure and petrology of the Mozambique Ridge (Uenzelmann-Neben, 2014). The gathered data comprise 59 dredge samples (magenta inverted triangles in Figure 2.2), swath bathymetry and ~4200 km of high-resolution, multi-channel seismic (MCS) reflection data (red lines in Figure 2.2) across the southern Mozambique Ridge (MozR), parts of the northern MozR and the surrounding basins.

This study is primarily based on the analysis and interpretations of the 22 new MCS reflection profiles (AWI-20140201–AWI-20140222; red lines in Figure 2.2), and supported by incorporating older MCS

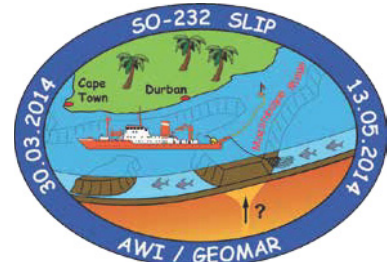


Figure 2.1. Logo of expedition SO232 to the Mozambique Ridge.

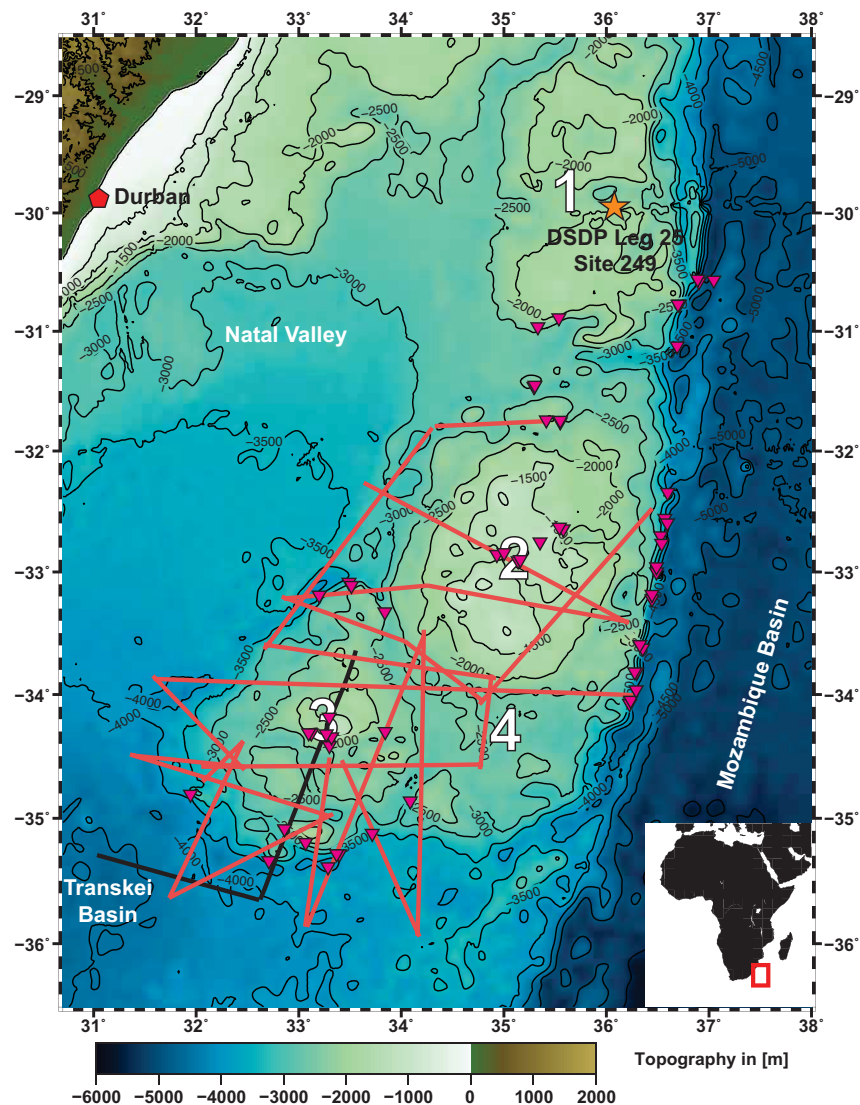


Figure 2.2. Bathymetric map (Weatherall *et al.*, 2015) of the Mozambique Ridge (MozR) off southeast Africa with location of DSDP Leg 25 Site 249 (star) and Durban, South Africa (pentagon). The red lines illustrate the MCS reflection profiles gathered during SO 232, whereas the black lines show the locations of the two MCS reflection profiles of SO 182. The magenta inverted triangles indicate the locations of the 59 samples dredged during SO 232. 1 = northern MozR, 2 = central MozR, 3 = swMozR, 4 = seMozR. The inset map shows the location of the study area (red frame) in context of the African continent.

reflection (AWI-20050017, AWI-20050018; black lines in Figure 2.2) and borehole data (DSDP Leg 25 Site 249; orange star in Figure 2.2).

2.1.1. Seismic reflection data

Seismic reflection profiling is a widely-used geophysical method to image the subsurface. It involves the measuring the two-way travel time (TWT) of seismic waves, emitted from the source of the acoustic signal (here: cluster of airguns) and reflected back to the receiver (here: hydrophone array) at interfaces between contrasting geological layers. The emitted seismic signal is reflected only when there is a contrast in the acoustic impedance caused by differences in seismic velocity (v), and in the density (ρ) of the geological layers. The amplitude of the reflected signal is the product of the strength of the contrast in the acoustic impedance, and is recorded along with the two-way travel time. An example of such seismic wave propagation is shown in Figure 2.3.

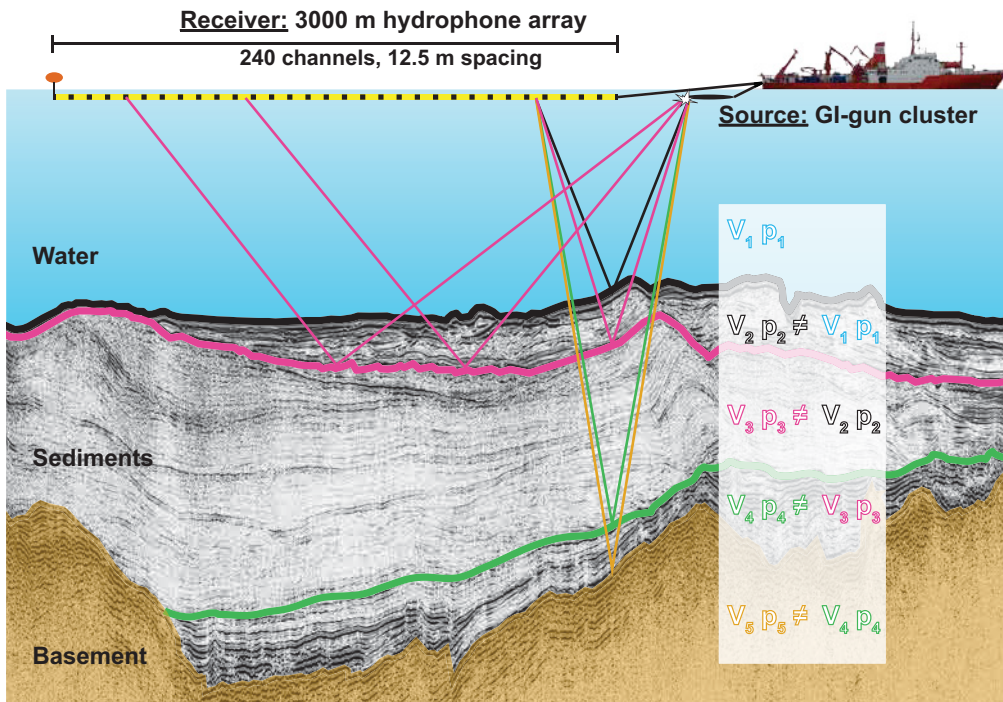


Figure 2.3. Simplified sketch of seismic reflection data acquisition showing a time slice recorded during SO 232. The source generates a seismic signal that travels through the water column, gets reflected at a boundary layer and is recorded at the receiver. Ray pathways are illustrated as an example.

To be able to resolve individual structures in the underground, they have to be separated from each other by one quarter of the wavelength (λ) of the seismic source (Claerbout, 1985b). If the dominant frequency of the source (f) and the P-wave velocity of the signal (v) are known, the vertical resolution (R_v) is calculated by:

$$R_v = \frac{\lambda}{4} = \frac{v}{4f}$$

The spatial resolution (R_s) is defined by the Fresnel zone (Sheriff, 1977), which in a two-dimensional case can be expressed in terms of a product of wavelength (λ) and depth (d) by:

$$R_s = \sqrt{\frac{\lambda d}{2}} = \sqrt{\frac{vd}{2f}}$$

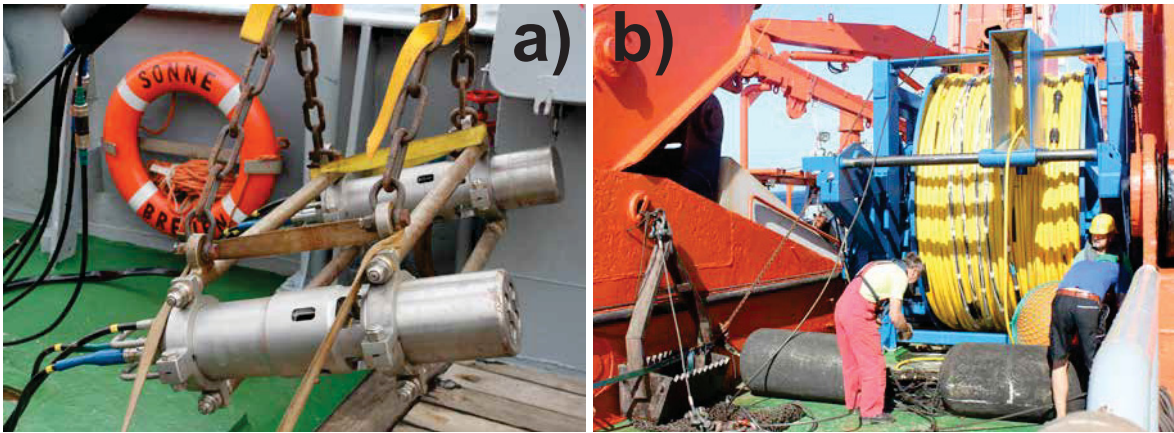


Figure 2.4. Equipment used for the acquisition of seismic reflection data during SO 232 (pictures taken by M.D. Fischer). **(a)** Two of the four GI-guns representing the seismic source. **(b)** The 3000 m long hydrophone array (streamer). The dredge used for the dredge operation during SO 232 is depicted in the left part of the picture.

During the RV Sonne cruise SO 232 the seismic signal was produced by a cluster of four GI-guns (Figure 2.4a). Each GI-Gun is composed of a generator chamber (0.72 l) and an injector chamber (1.68 l). The dominant frequencies of the seismic signal are between 20 and 55 Hz. The guns were towed ~20 m behind the vessel at a depth of 2 m, and were fired every 10 s, which corresponds to a nominal shot spacing of 25 m. The injector chambers were triggered with a 33 ms delay to suppress the bubble effect. The reflected waves from the subsurface were recorded by a 3000 m long 240-channel hydrophone array (Sercel SEAL™) at a sample rate of 1 ms (Figure 2.4b). Navigation data were specified by GPS.

2.1.2. Borehole data

I used the geological borehole data of DSDP Leg 25 Site 249 (orange star in Figure 2.2) for the interpretation of the MCS reflection data of the southern MozR. No direct correlation of the DSDP drill data with the MCS reflection data was possible, since the profiles did not cross Site 249 located on the northern MozR. A direct correlation with results from the drill site would have been difficult anyway because there is a deep depression between the northern and southern MozR (Figure 2.2). Nonetheless, the drilling results provide general information about the nature of unconformities observed in the sedimentary column and, in the absence of a more direct possibility of dating, they were used to constrain the seismic stratigraphy presented in chapter 2.2.2 and described in more detail in chapters 4 to 6.

Site 249 was drilled at a water depth of 2088 m and cored 408 m of sediments and sedimentary rocks of late Cenozoic and Cretaceous age prior to reaching the basaltic basement (Figure 2.5; Simpson *et al.*, 1974).

A thin segment of basaltic basement (3.1 m) was recovered, but due to severe weathering of the rock samples, no radiometric age dating was possible. Based on the age of the overlying sediments, Simpson *et al.* (1974) suggested an early Neocomian age of the tholeiitic basalt. Three major lithological units and two subunits were recognized by means of lithological and

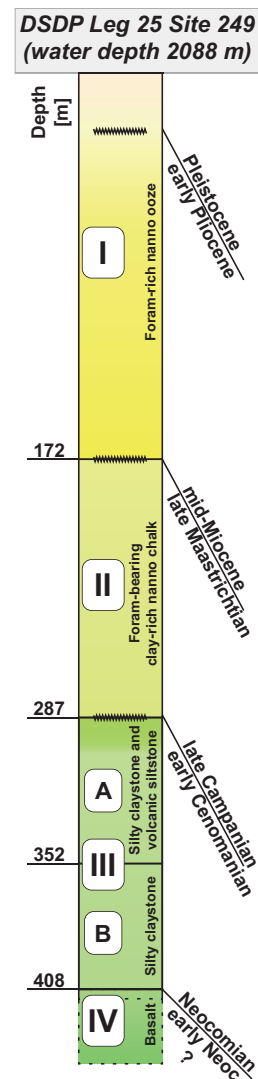


Figure 2.5. Graphical illustration of the results of DSDP Leg 25 Site 249 (Simpson *et al.*, 1974).

biostratigraphic characteristics (Simpson *et al.*, 1974). ~121 m of Neocomian to early Cenomanian deposits overlie the basement and comprise two subunits (IIIB and IIIA) that mainly consist of silty claystone. The subunits can be distinguished from each other based on the occurrence of volcanic siltstones within subunit IIIA.

An early Cenomanian to late Campanian unconformity (287 mbsf) representing ~25 Myr separates lithological unit III from the 115 m thick foram-bearing clay-rich nanno chalk of unit II. Another prominent unconformity is observed at 172 mbsf, where the complete late Maastrichtian to mid-Miocene (~50 Myr) sedimentary record is missing (Simpson *et al.*, 1974). Biostratigraphic age determinations of the foram-rich nanno ooze of lithological unit I suggests the occurrence of a ~2 to 3 Myr hiatus separating the Neogene from the Quaternary sediments in the upper part of the ~172 m thick unit.

2.2. Methods

2.2.1. Seismic data processing

Processing of the MCS reflection data was performed using the Echos© 2011.3 software package by Paradigm®. The main objective of seismic data processing is to enhance its signal-to-noise ratio. The following is a summary of the processing steps that were applied to the data prior to interpretation. For further information, please refer to, for example, Claerbout (1985a) and Yilmaz (2001). The corresponding Echos© software modules of the individual steps are shown in Table 2.1.

Processing of the seismic data started with the geometry definition using the ship's navigation data

Table 2.1. Seismic processing steps with corresponding software modules in Paradigm© Echos© 2011.3

Processing step	Module	Purpose, Remarks
Set up of geometry	GENERATE, LINE, PATTERN, SOURCE	Bin size of 25 m, conducted onboard SO 232 (G. Uenzelmann-Neben)
CDP sorting	SORT	Arrange traces by common depth point, CDP spacing of 25 m (G. Uenzelmann-Neben)
Velocity-depth analysis	VELDEF	Conducted every 50 th CDP, interval decreased in case of complex features or steep flanks
Normal moveout (NMO) correction	NMO	Corrects arrival time on offset traces to zero-off-set time
Correction for spherical divergence	SPHDIV	Compensates energy loss with radial distance
Stacking	MEDSTK	Increases the signal-to-noise ratio of the NMO corrected data. Iterative mean stacking algorithm was used, with four iterations and a gradual decrease of admitted samples to each iteration.
Migration	MIGFX	Omega-x finite-difference migration was used to collapse diffraction hyperbolas, method was chosen because it is accurate for steeply dipping reflectors and lateral velocity variations
Filtering	FILTER	For display purpose, band pass filtering with tapering (Hanning window; 5–30/200–250 Hz) was applied to the migrated data
Muting of	MUTE	A water column mute was applied for better visualization of the data

and Common Depth Point (CDP) sorting with a CDP spacing of 25 m. A precise velocity analysis was performed by picking the seismic velocities every 50th CDP. In areas prone to steep dipping flanks, or in case of small-scale and complex features the interval was decreased. The resulting stacking velocity was used for normal moveout (NMO) correction, which is used to reduce the delays in travel time of the signal due to the spatial differences of the receiver locations.

NMO correction was followed by correction for spherical divergence to account for the loss of seismic wave energy due to spherical expansion. An iterative mean stacking algorithm was applied to enhance the signal-to-noise ratio of the data. Four iterations have been performed with a stepwise exclusion of samples larger or smaller $\pm 25/20/15/10$ times the standard deviation from the mean during the individual iterations.

A post-stack time-migration of the data was carried out using an omega-x finite-difference migration, an algorithm especially useful in case of steep dipping reflectors and all types of velocity variations. For display purpose, I applied a band pass filter with tapering (Hanning window) with the boundaries 5–30 and 200–250 Hz. A water column mute was used for better visualization of the data. Since seismic amplitude information was used for the interpretation, we avoided Automatic Gain Control (AGC) filtering so that amplitudes depicted in the profiles represent values relative to the maximum of the entire section.

2.2.2. Seismic stratigraphy

Based on the correlation of the new MCS reflection data with borehole data (chapter 2.1.2; Simpson *et al.*, 1974) I developed a seismostratigraphic model of the southern Mozambique Ridge that incorporates and extends the seismostratigraphic concept by Uenzelmann-Neben *et al.* (2011). Three seismic units (basement, S1 and S2) and three subunits (S2a, S2b-I and S2b-II) were identified in the study area with the interfaces between the units representing distinct changes in seismic reflection characteristics. To avoid repetition I here refer to chapters 4, 5 and 6 for a detailed explanation of the seismic stratigraphy of the study area. A graphic and tabular summary is shown in chapter 7. The processed MCS reflection data were migrated into the Halliburton Landmark SeisWorks© software to implement the seismic stratigraphic concept by tracking and picking the seismic horizons throughout the study area.

2.2.3. Identification of magmatic structures within seismic reflection data

In order to evaluate a possible Large Igneous Province (LIP) origin of the southern MozR, I interpreted the MCS reflection data in terms of occurrences of magmatic features. Magmatic structures that can be identified with the seismic reflection method require to exceed the seismic resolution limit and have a significant impedance contrast compared to the surrounding underground.

LIPs are typically associated with a large number of extrusion centres, laterally and vertically extensive lava flow sequences, and features indicative of magmatic reactivation (Uenzelmann-Neben *et al.*, 1999; Sager *et al.*, 2013b; Pietsch and Uenzelmann-Neben, 2015). Extrusion centres (ECs; Figure 2.6a) are characterized by a convex upward shape that typically forms local basement highs. Lateral extents of more than 20 km have been reported for ECs at the Manihiki Plateau (Pietsch and Uenzelmann-Neben, 2015). The overlying sediments onlap the ECs, in-

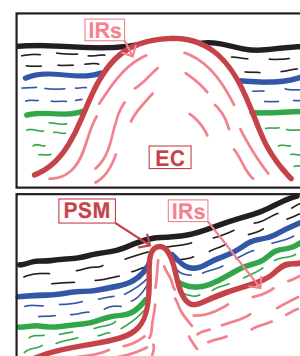


Figure 2.6. Schematic sketches of (a) an extrusion centre (EC) with onlap of sediments, and (b) a post-sedimentary magmatic (PSM) structure with pull up of sediments. Thin red lines illustrate intrabasement reflections (IRs), thick red line is top of magmatic basement. Overlying green, blue and black lines indicate individual sedimentary units.

ferring a pre-sedimentary origin of the magmatic structures.

ECs are usually associated with laterally continuous and thick lava flow sequences that emerge, dip away and extend downhill from the local basement highs in opposing directions (Uenzelmann-Neben *et al.*, 1999). Such lava flow sequences are imaged in MCS reflection data as intrabasement reflections (IRs; Figure 2.6). They are suggested and partly proven to either represent subaerial lava flows (Frey *et al.*, 2000), alternations of different types of lava flows (Inoue *et al.*, 2008), or alterations of lava flow packages with thick sediment layers that accumulated during times of magmatic repose (Sager *et al.*, 2013b).

While most of the features associated with late stage magmatism or reactivation of magmatic activity display characteristics similar to ECs (convex upward shape, emerging IRs), they are usually of smaller dimensions and show a pull up of adjacent sedimentary layers (Lancelot and Embley, 1977; Jackson, 2012; Pietsch and Uenzelmann-Neben, 2016). This implies a post-sedimentary magmatic (PSM) origin of these structures (Figure 2.6b). For a detailed review of the observed structures and the evaluation of a possible LIP origin of the MozR, please refer to chapter 4.

2.2.4. Identification of palaeocean circulation pathways

The history of ocean circulation and climate can be derived from contourite drifts using seismic images of the subsurface. MCS reflection data enables visualization of drift geometries, internal reflections configuration and seismic facies, thereby providing information on bottom current pathways and on modifications in bottom current strength and direction during deposition (Faugères *et al.*, 1999; Rebesco and Stow, 2001; Stow *et al.*, 2002).

A bottom current is defined as any semipermanent water current that affects the seafloor by resuspending, transporting or controlling the deposition of sediments (Rebesco *et al.*, 2008; Stow and Faugères, 2008). Drifts can be used to reconstruct circulation pathways of bottom water during deposition of the individual structures and are classified as either sheeted or mounded drifts. Mounded drifts are further divided into a number of drift types (giant elongated drifts, channel related drifts,

Mounded drifts: migration and aggradation any type of reflections, except horizontal	Giant elongated drifts	Plastered drift - alongslope migration (downstream of the current flow) - down and upslope migration	
	Giant elongated drifts	Separated drift - alongslope migration (downstream of the current flow) - upslope migration	
	Confined drifts	- predominant down-current migration - limited lateral migration	

Figure 2.7. Characteristics and schematic sketches of three of the five different mounded drift types (not illustrated are detached drifts and channel-related drifts). Brown structures = substrata (e.g., basement), green structures = contourite drift bodies. Black circle and dashed contours indicate location of current core (highest velocities). Modified after Faugères and Mulder, 2011.

confined drifts), but there is some overlap of the different types (Faugères and Mulder, 2011; Rebesco *et al.*, 2014). Examples of different drift types and their characteristics are shown in Figure 2.7.

Under the prerequisite of unrestricted circulation, Coriolis force deflects currents to the left in flow direction in the Southern Hemisphere, thereby eroding the right flank of the drift, whereas slower flow and deposition occurs on the left flank of the drift (Figure 2.8a).

Where the flow is constrained along a topographic high (e.g. a ridge), the Coriolis effect again deflects the flow to the left (Southern Hemisphere), effectively constraining the flow against the ridge. As a result, the flow intensifies, erosion occurs and a moat develops (Figure 2.8b). Lower velocities to the right of the flow favour deposition and drift construction, with the drift tending to migrate towards the ridge and to decrease its relief downstream (Faugères *et al.*, 1999; Rebesco and Stow, 2001; Stow *et al.*, 2002). Drifts often form a part of a Contourite Depositional System, which is an association of several drifts and erosional structures (e.g., moats) where occurrence of the erosional structures usually correspond to the location of the palaeo current core (Hernández-Molina *et al.*, 2008; Hernández-Molina *et al.*, 2010; Faugères and Mulder, 2011; Rebesco *et al.*, 2014).

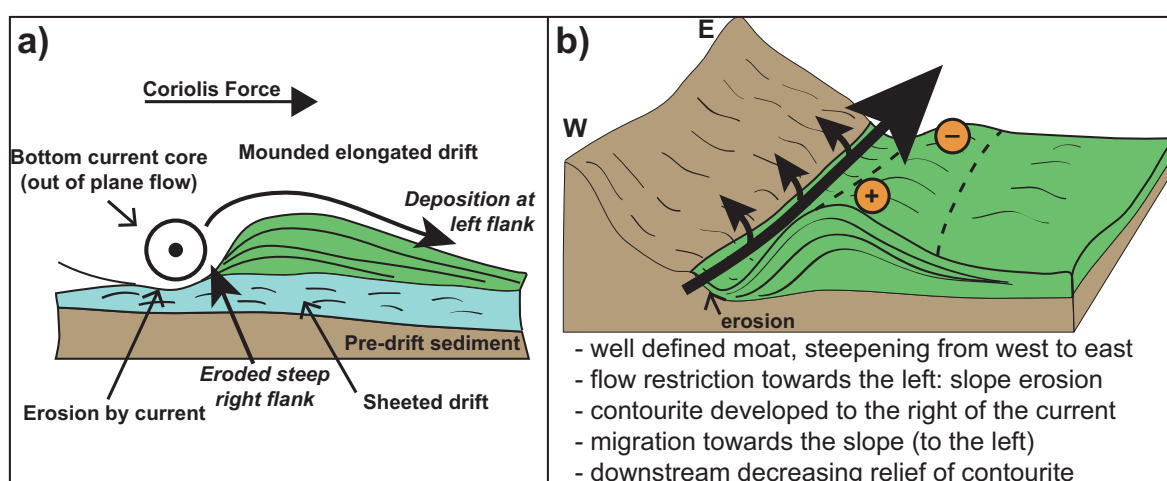


Figure 2.8. Principal drift characteristics in the Southern Hemisphere. **(a)** Mounded drift deposited (green) on top of a sheeted drift (blue). In case of an unrestricted bottom current flow (out of plane) the Coriolis force deflects the current to the left in the Southern Hemisphere, thereby eroding the right flank of the drift. Accumulation of sediments takes place at the left flank of the drift where current velocities are lower. Modified after Stow *et al.*, 2002. **(b)** Where the flow is directed along an obstacle (e.g., ridge), the Coriolis force again deflects the flow to the left (Southern Hemisphere). The current intensifies, erosion occurs and a moat develops. A drift develops on the right side of the flow, where the current velocity is lower. Modified after Faugères *et al.*, 1999.

3. Contribution to scientific journals

In this chapter, I present a brief summary of the scientific publications that were prepared during the PhD project. Each summary includes an overview of the contributions of the individual authors. The publications can be found in the subsequent chapters (4, 5 and 6) of this thesis. The dataset used, and the applied processing steps and methods have been explained in chapter 2. If not, they are explained in the individual manuscripts.

3.1. The Mozambique Ridge: a document of massive multistage magmatism

Fischer, M.D.¹, Uenzelmann-Neben, G.¹, Jacques, G.^{2,3}, Werner, R.²

¹Alfred-Wegener-Institut Helmholtz-Zentrum für Polar- und Meeresforschung

²GEOMAR Helmholtz-Zentrum für Ozeanforschung

³Bundesanstalt für Geowissenschaften und Rohstoffe

Geophysical Journal International (2017) 208, 449–467. doi: 10.1093/gji/ggw403.

This publication (see chapter 4) comprises a seismostratigraphic analysis of the southern Mozambique Ridge and addresses the question of its nature and origin by focussing on its basement structure. We present a seismic stratigraphic model of the entire southern Mozambique Ridge by correlating new high-resolution MCS reflection data gathered during SO 232 in 2014 and two MCS profiles recorded during SO 182 in 2005 with geological information from DSDP Leg 25 Site 249 (Simpson et al., 1974) and a pre-existing seismic stratigraphy of the southwestern ridge segment (Uenzelmann-Neben et al., 2011). Based on our observations we promote a Large Igneous Province origin of the ridge and present a new model of its initial formation. Furthermore we propose a link between a Neogene magmatic and tectonic reactivation of the ridge with a southward propagation of the East African Rift System.

I conducted the velocity analysis, NMO correction, time migration and filtering of the 22 MCS profiles recorded during RV Sonne expedition SO 232 (AWI-20140201–AWI-20140222) and defined the revised seismic stratigraphic model of the Mozambique Ridge. I traced and picked the top basement reflector and the top reflector of the sedimentary unit (= seafloor) throughout the 24 MCS profiles covering the study area (SO 232: AWI-20140201–AWI-20140222; SO 182: AWI-20050017, AWI-20050018). Based on the interpretation I calculated the depths of the two seismic horizons and the thickness of the sedimentary succession. In addition I picked the extrusion centers and post-sedimentary structures throughout the study area. Furthermore I performed the volumetric calculations used for the new emplacement model by combining the observed areal extents of the Mozambique Ridge with (1) the seismic refraction model of the swMozR by Gohl et al. (2011), and (2) calculating the thickness of the cMozR and seMozR in consideration of Airy-type isostatic equilibrium between the ridge and the surrounding basins (Recq and Goslin, 1981). I prepared all figures and wrote the manuscript.

G. Uenzelmann-Neben was the chief scientist on board RV Sonne cruise SO 232 and supervised my work. G. Uenzelmann-Neben conducted the pre-processing (geometry and CDP sorting) of the 24 MCS profiles (SO 232: AWI-20140201–AWI-20140222; SO 182: AWI-20050017, AWI-20050018) and processed MCS profile AWI-20050018. P. Schlüter processed MCS profile AWI-20050017. G. Jacques assisted with the petrological interpretation of the data. R. Werner was the coordinator of the petrological work conducted during SO 232 and assisted with the petrological interpretation of the data. All authors revised the manuscript and contributed to the discussion.

3.2. Late Cretaceous onset of current controlled sedimentation in the African–Southern Ocean gateway

Fischer, M.D., Uenzelmann-Neben, G.

Alfred-Wegener-Institut Helmholtz-Zentrum für Polar- und Meeresforschung

Under review at Marine Geology since March 2017. Submitted in February 2017.

In this publication (see chapter 5), we used my seismic stratigraphic model (Fischer et al., 2017) to reconstruct the Cretaceous palaeocirculation at the southern Mozambique Ridge. We propose that the Late Cretaceous hiatus (Simpson et al., 1974; Uenzelmann-Neben et al., 2011; Fischer et al., 2017) following the sluggish Early Cretaceous palaeocirculation is a consequence of both, uplift of the ridge due to renewed magmatic activity and the progressive opening of barriers hindering inflow into the study area. We find evidence for a Late Cretaceous onset of current controlled sedimentation at the Mozambique Ridge, which is significantly earlier as previously suggested (mid-Miocene; Uenzelmann-Neben et al., 2011). We tie this onset of drift deposition at the ridge to palaeogeographic modifications influencing the current pathways in the Southern Atlantic Ocean.

I processed (velocity analysis, NMO correction, time migration, filtering) the 22 MCS profiles recorded during SO 232 (AWI-20140201–AWI-20140222). I used my seismic stratigraphic model (Fischer et al., 2017) to trace and pick the top basement reflector, the top reflector of the Early Cretaceous seismic unit and the top reflector of the Late Cretaceous seismic unit throughout the 24 MCS profiles covering the study area (SO 232: AWI-20140201–AWI-20140222; SO 182: AWI-20050017, AWI-20050018). I calculated the depths of the seismic horizons and the thicknesses of the two Cretaceous sedimentary units. I interpreted the Cretaceous sedimentary units in terms of sedimentary and erosional structures, and used the locations and characteristics of these structures and depocentres for development of a Cretaceous circulation model in the African–Southern Ocean gateway. I prepared all the figures and wrote the manuscript.

G. Uenzelmann-Neben conducted the pre-processing (geometry and CDP sorting) of the 24 MCS profiles (SO 182 and SO 232) and processed the MCS profile AWI-20050018. In addition G. Uenzelmann-Neben supervised my work, provided helpful comments during the preparation of the manuscript and revised the manuscript. P. Schlüter processed the MCS profile AWI-20050017 (SO 182).

3.3. Neogene modifications of circulation in the African–Southern Ocean gateway

Fischer, M.D., Uenzelmann-Neben, G.

Alfred-Wegener-Institut Helmholtz-Zentrum für Polar- und Meeresforschung

Under review at Deep-Sea Research Part I since April 2017. Submitted in April 2017.

In this publication (see chapter 6), we focus on the reconstruction of the mid-Miocene to Holocene palaeocean circulation in the African–Southern Ocean gateway. We present a refined seismic stratigraphic model for the Late Cenozoic unit (Fischer et al., 2017) that correlates distinct differences in the seismic characteristics between the upper and lower part of the unit to a regional Pliocene unconformity (Simpson et al., 1974; Niemi et al., 2000). Our observations show that the late Pliocene onset of Northern Hemisphere Glaciation (Bartoli et al., 2005) along with the final closure of the Indonesian

gateway (Gourlan et al., 2008) were the likely causes of inception of the modern circulation scheme in the African–Southern Ocean gateway that has persisted until today.

I conducted the velocity analysis, NMO correction, time migration and filtering of the 22 MCS profiles covering the southern Mozambique Ridge (AWI-20140201–AWI-20140222). I refined the seismic stratigraphy of the late Cenozoic seismic unit (Fischer et al., 2017). I used my refined seismic stratigraphy to trace and pick the top reflector of the pre-Cenozoic unit and both Cenozoic units throughout the 24 MCS profiles (SO 232: AWI-20140201–AWI-20140222; SO 182: AWI-20050017, AWI-20050018) and calculated the depths of the three horizons and the thicknesses of the Cenozoic units. I analysed the 24 MCS profiles in terms of late Cenozoic sedimentary and erosional structures and developed a model of the late Cenozoic circulation in the African–Southern Ocean gateway. I prepared all the figures and wrote the manuscript.

G. Uenzelmann-Neben conducted the pre-processing (geometry and CDP sorting) of the 24 MCS profiles recorded during SO 182 and SO 232 and processed the MCS profile AWI-20050018 (SO 182). Furthermore G. Uenzelmann-Neben supervised my work, provided helpful comments during the preparation of the manuscript and revised the manuscript. P. Schlüter processed the MCS profiles AWI-20050017 (SO 182).

4. The Mozambique Ridge: a document of massive multi-stage magmatism

Maximilian D. Fischer¹, Gabriele Uenzelmann-Neben¹, Guillaume Jacques^{2,3}, Reinhard Werner²

¹Alfred-Wegener-Institut Helmholtz-Zentrum für Polar- und Meeresforschung, ²GEOMAR Helmholtz-Zentrum für Ozeanforschung, ³Bundesanstalt für Geowissenschaften und Rohstoffe

published in **Geophysical Journal International** (2017) 208, 449–467, doi: 10.1093/gji/ggw403

Abstract

The Mozambique Ridge, a prominent basement high in the southwestern Indian Ocean, consists of four major geomorphological segments associated with numerous phases of volcanic activity in the Lower Cretaceous. The nature and origin of the Mozambique Ridge have been intensely debated with one hypothesis suggesting a Large Igneous Province origin. High-resolution seismic reflection data reveal a large number of extrusion centres with a random distribution throughout the southern Mozambique Ridge and the nearby Transkei Rise. Intrabasement reflections emerge from the extrusion centres and are interpreted to represent massive lava flow sequences. Such lava flow sequences are characteristic of eruptions leading to the formation of continental and oceanic flood basalt provinces, hence supporting a Large Igneous Province origin of the Mozambique Ridge. We observe evidence for widespread post-sedimentary magmatic activity that we correlate with a southward propagation of the East African Rift System. Based on our volumetric analysis of the southern Mozambique Ridge we infer a rapid sequential emplacement between ~131 and ~125 Ma, which is similar to the short formation periods of other Large Igneous Provinces like the Agulhas Plateau.

4.1. Introduction

For several decades Large Igneous Provinces (LIPs) have been of great interest because of their immense sizes and potential far-reaching impact on biosphere and atmosphere leading to climate shifts and mass extinctions (Wignall, 2001), their role in plate motion by thickening of oceanic crust (Miura *et al.*, 2004), and their association with continental breakup and supercontinent cycles (Bryan and Ernst, 2008; Bryan and Ferrari, 2013). The term LIP was initially proposed by Coffin and Eldholm (1991) and is used for large ($>0.1 \times 10^6 \text{ km}^2$) marine and terrestrial areas overprinted by massive volcanic activity (Bryan and Ernst, 2008; Coffin and Eldholm, 1994; Kerr, 2014). Episodes of excessive magmatism have repeatedly formed LIPs on Earth by eruptions from a system of fissures or vents (Uenzelmann-Neben, 2013). Three proposed models to explain these massive outpourings of magma are the impact of a rising plume head at the base of the lithosphere, edge-driven convection, or lithospheric delamination (Coffin and Eldholm, 1994; White and McKenzie, 1995; Campbell, 2007; Saunders, 2005). In Cretaceous times, an increase in development of LIPs occurred globally, e.g. Manihiki Plateau in the Pacific Ocean and Rio Grande Rise in the Atlantic Ocean (Coffin and

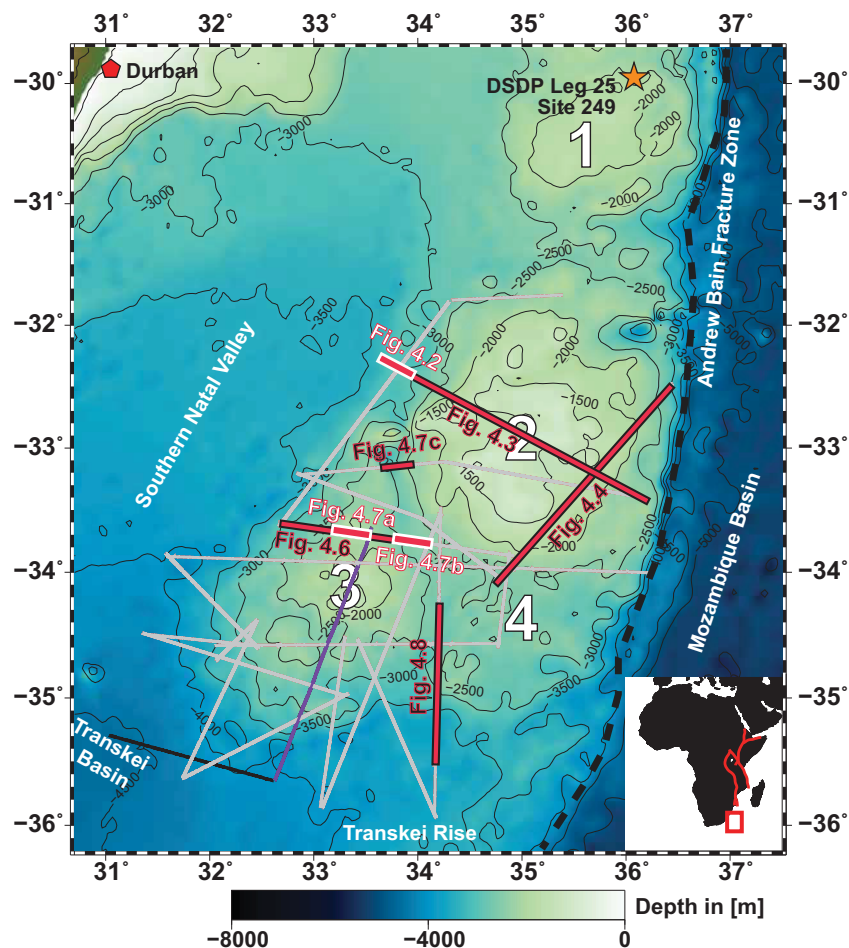


Figure 4.1. Bathymetric map (GEBCO_08; 500 m contour lines in black) of the study area in the southwestern Indian Ocean with location of DSDP Leg 25 Site 249 (star) and Durban, South Africa (pentagon). MCS profiles of SO 232 are shown in grey, those of SO 182 in black and purple. Seismic refraction profile interpreted by Gohl *et al.* (2011) is coincident with NNE–SSW striking MCS profile AWI-20050018 of SO 182 depicted in purple (Gohl *et al.*, 2011; Uenzelmann-Neben *et al.*, 2011). White outlines depict the segments of the Mozambique Ridge: 1 = northern Mozambique Ridge, 2 = central Mozambique Ridge, 3 = southwestern Mozambique Ridge, 4 = southeastern Mozambique Ridge. Red bars (black outline) indicate the locations and lateral extent of presented seismic data. White outlines are used if the respective figures represent an extract of shown seismic data. The inset shows the location of the study area off South Africa (red rectangle) and the major rift features of the East African Rift System (after Tikku *et al.*, 2002; Chorowicz, 2005; Macgregor, 2015).

Eldholm, 1994). In the Indian Ocean emplacement of several structures such as the Kerguelen Plateau (Frey *et al.*, 2000) and the Agulhas Plateau (Parsiegla *et al.*, 2008) are associated with massive volcanic events and classified as LIPs.

The Mozambique Ridge (MozR) is located in the southwestern Indian Ocean (Figure 4.1), an area where Gondwana breakup between Africa, South America and Antarctica occurred during the Cretaceous. The areal extent ($\sim 2 \times 10^5 \text{ km}^2$) of the elongated aseismic ridge is nearly twice the size of Iceland. The MozR is limited to the east by an abrupt, more than 2000 m deep step-down into the Mozambique Basin (dashed line in Figure 4.1), which owes its existence to the NNE-SSW striking Andrew Bain fracture zone (Ben-Avraham *et al.*, 1995; Sclater *et al.*, 2005). To the north, the MozR is bound by the Northern Natal Valley, to the west by the Southern Natal Valley and to the south by the Transkei Basin and Transkei Rise (Figure 4.1). Geomorphologically it is divided into four segments, termed here as northern MozR (nMozR), central MozR (cMozR), southwestern MozR (swMozR), and southeastern MozR (seMozR). Together the latter three form the southern MozR (Figure 4.1). The first samples from the basement of the MozR were collected at DSDP Leg 25 Site 249 on the nMozR, where 3.1 m of tholeiitic basalt was recovered (Simpson *et al.*, 1974).

Authors have proposed several hypotheses about the nature and origin of the MozR, ranging from a continental provenance (Tucholke *et al.*, 1981; Raillard, 1990; Mougénot *et al.*, 1991; Hartnady *et al.*, 1992), to an oceanic origin (Hales and Nation, 1973; König and Jokat, 2010), to being partitioned into continental and oceanic parts (Ben-Avraham *et al.*, 1995). Seismic refraction and reflection data collected across the swMozR are interpreted as strong evidence for an oceanic LIP origin of the southern MozR (parallel to the purple line in Figure 4.1; Gohl *et al.*, 2011). A LIP origin of the whole MozR could have had an immense influence on climate during the Early Cretaceous with the emission of gases and heat into atmosphere and ocean and in addition implications on the development of the South African gateway with the formation of obstacles for surface and deep circulation.

The main objective of this paper is to resolve the structure and evolution of the MozR by focusing on the questions of formation and magmatism using seismic reflection data. This will provide parameters required for future studies about the reconstruction of the paleo-ocean current circulation and its implications for climate.

4.2. Geological and tectonic background

The origin of the MozR is still unclear. In general, three totally different theories have been proposed to explain its development history. Tucholke *et al.* (1981) suggested a continental provenance of the MozR based on a comparison of 1d seismic refraction data from Hales and Nation (1973) and Chetty and Green (1977) with seismic refraction data from the Agulhas Plateau that was interpreted to be a continental fragment of South Africa. Dredge samples presented by Raillard (1990), Mougénot *et al.* (1991), and Hartnady *et al.* (1992) supported a continental origin of the MozR. Ben-Avraham *et al.* (1995) favoured a partitioning of the MozR into a northern oceanic and a southern continental part. They suggested a microcontinental fragment embedded into oceanic crust at the southern MozR based on low-resolution seismic refraction data of Hales and Nation (1973) and Raillard (1990), gravity data (Doucouré and Bergh, 1992; Lyakhovskiy *et al.*, 1994), and rock samples (Raillard, 1990; Mougénot *et al.*, 1991; Hartnady *et al.*, 1992; Ben-Avraham *et al.*, 1995).

Based on the interpretation of gravity anomaly data and a recent magnetic survey, König and Jokat (2010) contradicted this model by excluding the presence of large continental blocks throughout the MozR. According to their observations, high amplitude magnetic anomalies at the major structural boundaries suggest that the different segments of the ridge were formed at different times. They

described the MozR as the result of long lasting volcanic activity between 140 Ma (magnetic anomaly ~M15n) and 122 Ma (magnetic anomaly C34n, onset of Cretaceous Normal Superchron) and proposed an oceanic origin for the whole ridge. The findings of Erlank and Reid (1974), Simpson *et al.* (1974), and Thompson *et al.* (1982), who dated the basaltic basement at Site 249 (location see Figure 4.1) as Early Cretaceous, support the postulated timeframe of emplacement.

A more than 22 km thick crust was identified for the MozR during a 1-D seismic refraction study (Hales and Nation, 1973; Chetty and Green, 1977). Chetty and Green (1977) concluded that the over-thickened crust lacks characteristic velocities of the continental basement and therefore a basement of continental crust was not strongly supported. The interpretation of 2-D seismic refraction data showed that the MozR is characterized by over-thickened (16–22 km), seismically homogeneous, lower crustal units making up between half to two-thirds of the crustal column with *P*-wave velocities of more than 7.0 km s⁻¹ (Gohl *et al.*, 2011). According to them these velocities suggest that large volumes of mantle-derived material accreted in the lower crust and indicate a formation of MozR and Agulhas Plateau at the same magmatic province (Gohl and Uenzelmann-Neben, 2001; Parsiegla *et al.*, 2008). As a consequence of their studies Gohl *et al.* (2011) proposed a LIP origin of the MozR and speculated on the existence of a Southeast African LIP consisting of the MozR, the Agulhas Plateau and other fragments. Preliminary petrological-geochemical results of the basaltic rock samples dredged during SO 232 favour a deep-plume source and support a LIP origin of the MozR (Uenzelmann-Neben, 2014; Jacques *et al.*, 2015).

4.3. Data and methods

4.3.1. Seismic reflection data

This study is based on 24 high-resolution MCS reflection profiles with a total length of about 4600 km acquired by the Alfred Wegener Institute, Helmholtz Centre for Polar and Marine Research on board RV Sonne during expeditions SO 182 in 2005 (black and purple lines in Figure 4.1) and SO 232 in 2014 (grey lines in Figure 4.1). The seismic profiles cover the cMozR, the swMozR, and the seMozR of the MozR, as well as the transition zone to the adjacent basins (Figure 4.1). A cluster of four GI-guns were triggered at a nominal interval of 25 m (shot interval of 10 s), generating seismic signals of up to 500 Hz with dominant frequencies between 20 and 55 Hz. Each GI-gun produces a primary pulse (Generator) with a volume of 0.72 litres, which is followed by a delayed (33 ms) secondary signal (Injector volume 1.68 l) to suppress the bubble effect. The data were received by a 240-channel hydrophone array with a total active length of 3000 m. Navigation data were specified by GPS.

Pre-stack processing of the multichannel seismic data included geometry definition using the ship's navigation data, and common depth point (CDP) sorting with a CDP spacing of 25 m. A detailed velocity analysis (every 50 CDP) was carried out and used for normal moveout correction. Where needed, the interval for the velocity analysis was decreased (e.g., for complex, small scale features). Stacking was carried out using a mean iterative algorithm together with spherical divergence correction and was followed by an Omega-X finite-difference migration (Yilmaz, 2001). This migration method is very useful for the imaging of strongly inclined reflectors as caused by, for example, volcanic structures or tectonic processes. Since seismic amplitude information was used for the interpretation we avoided AGC (Automatic Gain Control) filtering so that amplitudes depicted in the profiles represent values relative to the maximum of the entire section. For better visualization of the seismic data, band pass filtering with tapering (Hanning window; boundaries 5–30 Hz and 200–250 Hz) and a water column mute were applied.

4.3.2. DSDP data

Site 249 was drilled during DSDP Leg 25 and recovered a thin segment of basaltic basement (3.1 m) from a depth of 408 meters below seafloor (mbsf). Due to severe weathering of the rock samples no radiometric age dating was possible, but major and trace element analysis showed compositional similarities with mid-ocean ridge tholeiites (Erlank and Reid, 1974). Based on the age of the overlying sediments, Simpson *et al.* (1974) inferred an Early Neocomian age of the tholeiitic basalt. Three lithological units were identified by means of lithological and biostratigraphic characteristics

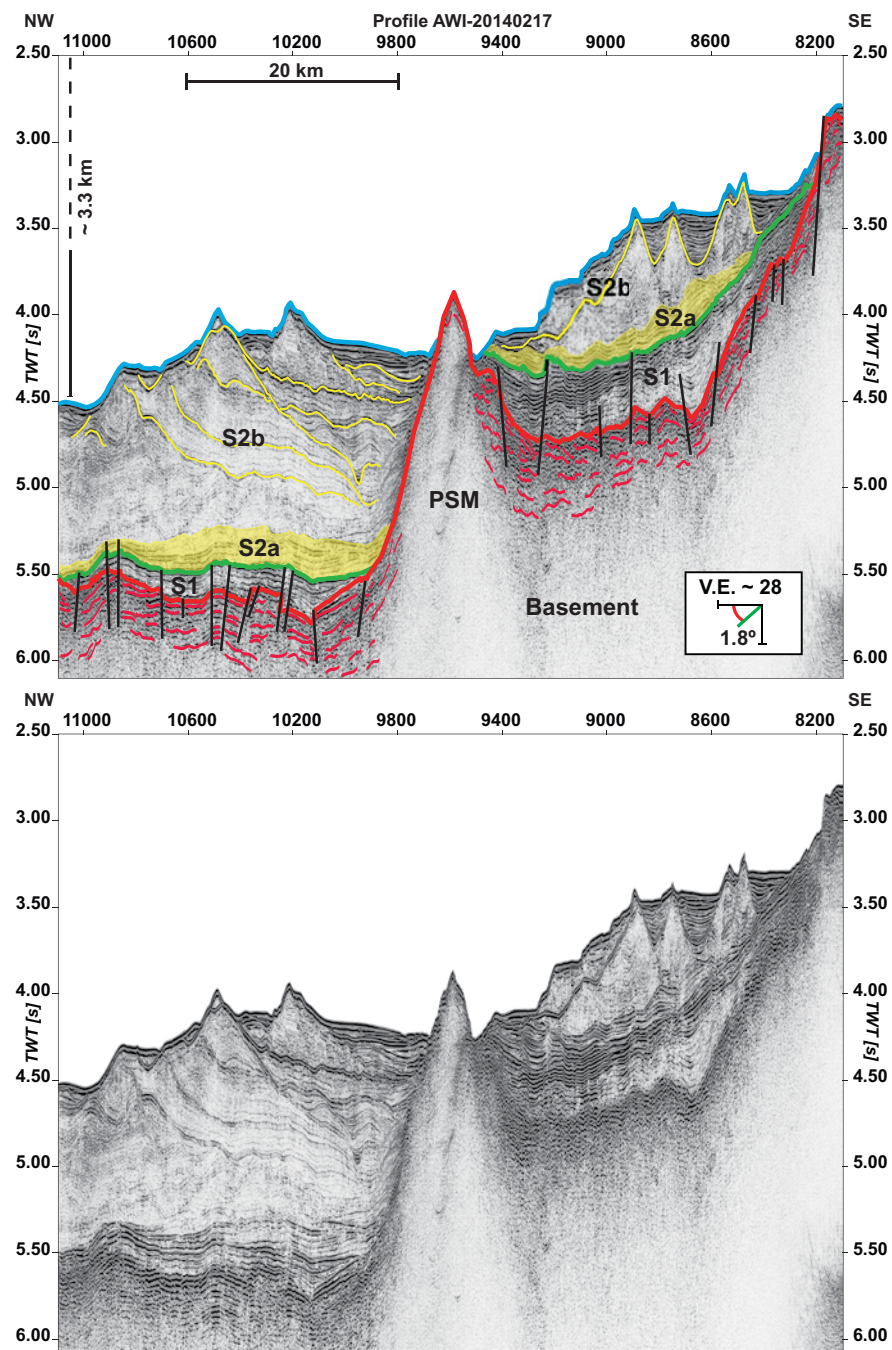


Figure 4.2. Seismic stratigraphy of the study area together with the uninterpreted section. Location of profile is shown in Figure 4.1. For a detailed description of the units refer to chapter 4.4.1 and Table 4.1. Thick blue line = seafloor, thin yellow lines = discontinuities within subunit S2b, the yellow shaded area = subunit S2a, thick green line = top of unit S1, thick red line = top of basement, thin red lines = intrabasement reflections, black lines = faults. PSM = post-sedimentary magmatic structure. For slope angles and vertical exaggeration refer to the legend.

(Simpson *et al.*, 1974). Those units are separated by two prominent hiatuses: a Campanian to Cenomanian unconformity (287 mbsf) representing ~25 Myr and a Middle Miocene to Maastrichtian unconformity (172 mbsf) representing ~50 Myr. Sedimentation rates of 5 m Myr⁻¹ and 20 m Myr⁻¹ were determined for the Neocomian to Early Cenomanian and the Late Campanian to Maastrichtian, respectively, and a sedimentation rate of about 19 m Myr⁻¹ was calculated for the Miocene (Simpson *et al.*, 1974).

No direct correlation of the DSDP data to our seismic reflection data was possible since our profiles did not cross Site 249 located on the nMozR (Figure 4.1). Nonetheless, the drilling results provide general information on the nature of unconformities observed in the sedimentary column and, in the absence of a more direct possibility of dating, thus were used to constrain our seismic stratigraphy.

4.4. Results

4.4.1. Seismic stratigraphy

Three seismic units (basement, S1 and S2) were identified within the study area with the interfaces between the units representing distinct changes in seismic reflection characteristics (seismic stratigraphy; Vail *et al.*, 1977; Cross and Lessenger, 1988). Based on their reflection characteristics (e.g., frequency, amplitude and continuity) the seismic units were correlated with the lithological results of DSDP Leg 25 Site 249 (Simpson *et al.*, 1974) and the seismic units defined by Uenzelmann-Neben *et al.* (2011) to obtain a timeframe for their deposition. For the location of the MCS profile used by Uenzelmann-Neben *et al.* (2011) please refer to Figure 4.1 (purple line crossing the swMozR). We present an overview of the seismic units and the correlations in Figure 4.2 and Table 4.1.

4.4.1.1. Basement

The lowermost unit shows high amplitude, low frequency reflections (e.g., Figure 4.2 CDPs 10200–10600). Intrabasement reflections can be deep reaching (e.g., up to 500 ms TWT in Figure 4.2 CDPs 9000–9400). The intrabasement reflections are strongest and appear most continuous near the top of the unit and become increasingly weaker and less continuous with depth due to scattering and attenuation of the seismic signal. Individual reflections can typically be traced for 5–15 km. The intrabasement reflections dip away from local highs and form subparallel sequences that in places overlap (e.g., Figure 4.3 CDPs 4000–4200 and Figure 4.4 CDPs 1800–2200). The unit's top (red horizon in all shown MCS profiles) is defined by a strong impedance contrast with a sudden velocity increase to its overlying unit, appears rugged and hummocky, and shows a wide range in observed depths (Figure 4.5a).

Our observations match those described for the magmatic basement of the MozR by Simpson *et al.* (1974) and Uenzelmann-Neben *et al.* (2011), we thus interpret this unit as magmatic basement. Several faults disrupt the top basement reflection (e.g., Figure 4.2 CDPs 10200–10600) and basement peaks piercing the sedimentary column appear locally (e.g., Figure 4.2 CDPs 9300–9900).

4.4.1.2. Seismic units S1 and S2

Two seismic units (S1 and S2) overlie basement. Reflection characteristics of the well stratified older unit S1 show low to medium frequency reflections with weaker amplitudes in its lower part and medium to strong amplitude reflections in its upper part. The mostly conformable reflections of the unit are more continuous in the upper part (Figure 4.2 CDPs 8400–9400). The top of unit S1 (green horizon in

Table 4.1. Seismic stratigraphy of the study area.

Seismic units of the Mozambique Ridge	Thickness [ms TWT]	Estimated age [Ma] ^{a,c}	Material ^a	Seismic characteristics	Correlation with published seismic stratigraphies ^{a, b}	Remarks
Unit S2 (S2a & S2b)	0-1600	S2b: 15-0 ^a S2a: 75-68 ^a	S2b: nanno ooze S2a: clay-rich nanno chalk	S2b: sporadically subhorizontal strong amplitude reflections of lower frequency in the uppermost part; mostly continuous internal reflections with weak to moderate amplitudes and low to medium frequency; occasionally strong amplitude reflections; discontinuities; S2a: discontinuous medium to high amplitude reflection band of lower frequency	Units I & II ^a ; Unit S2 ^b	Hiatus on top of S2a; S2a can only partly be distinguished from S2b
Unit S1	0-500	<128.66-100 ^{a,c}	silty claystone and volcanics, clay content increases towards the base	medium to strong amplitude reflections (upper part); weaker amplitude reflections (lower part); low to medium frequency reflections; less continuous reflections in lower part	Subunit IIIA ^a ; Unit S1 ^b	Hiatus on top of S1; age of oldest deposits decrease to the S due to younger basement
Basement		130.86-124.90 ^c depending on respective segment of MozR	basalt	strong impedance contrast at top; high amplitude, low frequency reflections; subparallel sequences of internal reflections; piecewise continuous and up to 800 ms TWT deep	Basement ^{a,b}	

^aSimpson *et al.* (1974); ^bUenzelmann-Neben *et al.* (2011); ^cThis study.

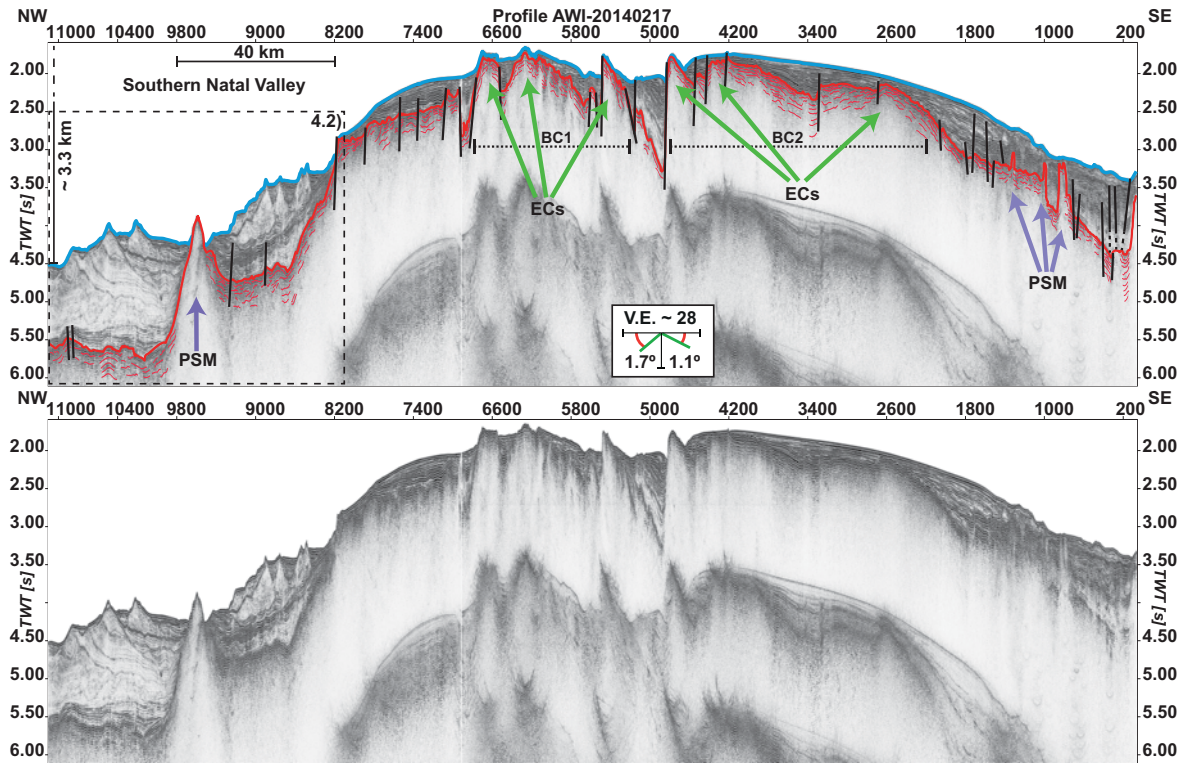


Figure 4.3. MCS profile AWI-20140217 crossing the central Mozambique Ridge in a NW–SE direction. Location of profile is shown in Figure 4.1. Dashed frame indicates location of Figure 4.2. Thick blue line= seafloor, thick red line= top of basement, thin red lines= intrabasement reflections, black lines = faults, green arrows = extrusion centres (ECs), purple arrows = post-sedimentary magmatism (PSM). BC1 = Basement complex 1, BC2 = Basement complex 2. For slope angles and vertical exaggeration refer to the legend.

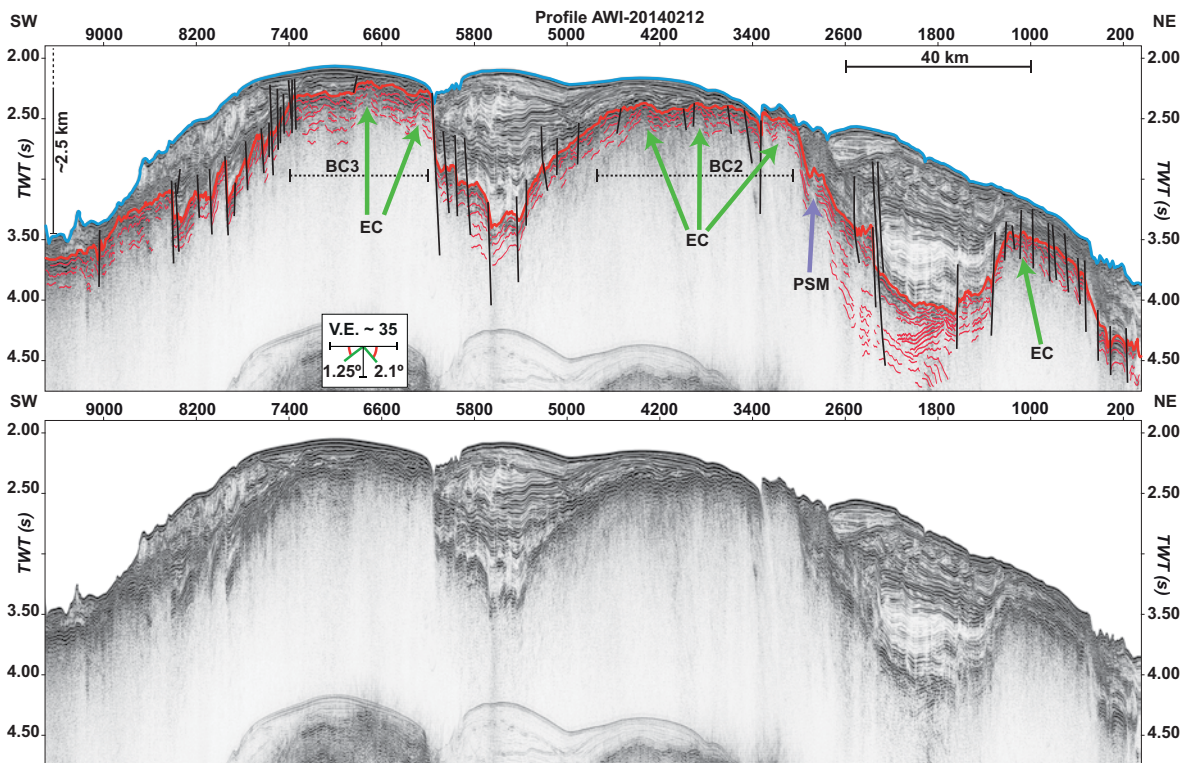


Figure 4.4. MCS profile AWI-20140212 crossing the central Mozambique Ridge in a NE–SW direction. Line and arrow colours as in Figure 4.3. BC2 = Basement complex 2, BC3 = Basement complex 3. For slope angles and vertical exaggeration refer to legend. Location of profile is shown in Figure 4.1.

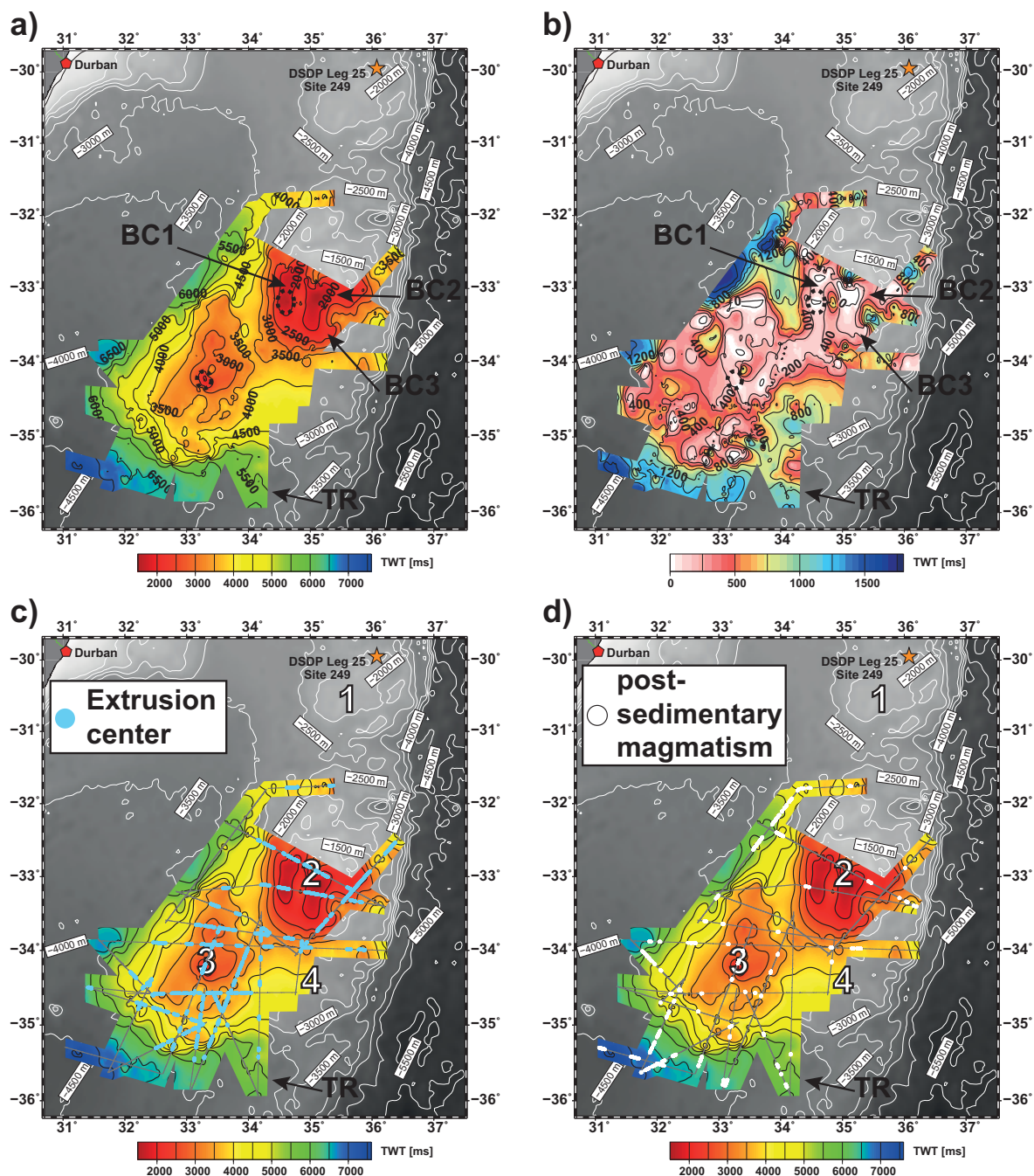


Figure 4.5. (a) Depth map (TWT) of top basement reflection (500 ms TWT contour lines in black) on top of greyscale bathymetric map (GEBCO_08; 500 m contour lines in white). Map shows location of DSDP Leg 25 Site 249 (star) and Durban (pentagon). BC1, BC2 and BC3 indicate the location of the basement complexes of the cMozR, the black dashed ellipses mark prominent basement highs, and TR stands for Transkei Rise. (b) Isopach map (TWT) of the sedimentary deposits in the study area (200 ms TWT contour lines in black). (c) Locations of extrusion centres (cyan dots) within the study area on top of the basement depth map (Figure 4.5a). Location of MCS profiles is shown in thin black lines. White numbers depict the segments of the Mozambique Ridge: 1 = northern Mozambique Ridge, 2 = central Mozambique Ridge, 3 = southwestern Mozambique Ridge, 4 = southeastern Mozambique Ridge. (d) Map of the observed post-sedimentary magmatic features (white dots) plotted on top of the basement depth map (Figure 4.5a).

Figure 4.2) seems to be affected by erosional truncation and is marked by a strong amplitude reflection. The unit has a thickness of up to 500 ms TWT and drapes the local morphology of the strongly faulted basement (Figure 4.2 CDPs 8200–9500). Towards the surrounding basins (Natal Valley, Transkei Basin) and towards basement highs, unit S1 thins and in places is missing completely. The reflection characteristics of our unit S1 are similar to the reflection characteristics of lithological

unit IIIA at Site 249 and to those of unit S1 described by Uenzelmann-Neben *et al.* (2011). Therefore, we correlate our seismic unit S1 with lithological unit IIIA of Site 249. The recovered deposits of unit IIIA at Site 249 consist of silty claystone and volcanic siltstone of Early Cretaceous (Neocomian to Early Cenomanian) age. The unit's top reflection (green horizon in Figure 4.2) is described by Uenzelmann-Neben *et al.* (2011) as well and is correlated with the ~25 Myr hiatus (Early Cenomanian to Late Campanian) identified at Site 249 (Simpson *et al.*, 1974).

With a thickness of up to 1600 ms TWT (e.g., Figure 4.2 CDPs 10200), seismic unit S2 constitutes the largest part of the deposits covering the basement. The top of unit S2 is marked by the light blue horizon in Figure 4.2. The unit typically thins towards basement highs (e.g., Figure 4.2 CDPs 8200–9000) and can be divided into two subunits (S2a & S2b) based on their reflection characteristics. In the lower part of unit S2 a thin (max. 250 ms TWT) discontinuous medium to high amplitude reflection band of lower frequency can be observed (Figure 4.2 CDPs 8600–9400).

The reflections onlap onto unit S1 and we observe a significant difference in reflection amplitude and frequency when comparing it to the more transparent nature of the overlying part of unit S2 (shaded in yellow in Figure 4.2 CDPs 8500–9400 and 9800–11100). We define this reflection band as subunit S2a. Subunit S2a cannot be observed throughout the study area and usually thins towards basement highs. The thickest successions are observed within the surrounding basins of the MozR or within local depressions.

The Late Cretaceous (Late Campanian to Maastrichtian) lithological unit II drilled at Site 249 shows a variable thickness and thins towards the basement highs (Simpson *et al.*, 1974). It is topped by a hiatus (Maastrichtian to Middle Miocene) as the result of erosion (Simpson *et al.*, 1974). The seismic characteristics of lithological unit II resemble the characteristics of subunit S2a. Consequently, we correlate subunit S2a with the Late Campanian to Maastrichtian rocks drilled at Site 249. Uenzelmann-Neben *et al.* (2011) sporadically observed lower frequencies and stronger amplitude reflections in the lower 100 m of their seismic unit S2. Even though they could not correlate these reflections with certainty to the data of Simpson *et al.* (1974), they interpreted this lower part to represent lithostratigraphic unit II.

The majority of seismic unit S2 consists of subunit S2b (thickness up to 1400 ms TWT), which shows a more transparent nature compared to the subjacent units (Figure 4.2 CDPs 9800–11050). Its amplitudes are weak to moderate but occasionally strong and feature a low to medium frequency. We observe two groups of reflections characterized by significant differences in their seismic appearance in the uppermost part of unit S2b: a set of weak to moderate amplitude reflections of medium frequency, and a series of almost horizontal, well-layered strong amplitude reflections of lower frequency (e.g., Figure 4.2 CDPs 8500–8800 and 10100–10600). The undulating, mostly continuous internal reflections of subunit S2b represent discontinuities (yellow lines in Figure 4.2) such as erosional truncation and onlap termination (e.g., Figure 4.2 CDPs 10000–10400).

We correlate the significant change in reflection characteristics between S2a and S2b to a distinct change in clay fraction content between lithological unit II (high clay fraction content of up to 60%) and lithostratigraphic unit I (clay fraction content <20 per cent; Leclaire, 1974; Simpson *et al.*, 1974). Uenzelmann-Neben *et al.* (2011) correlated the major part of their seismic unit S2 with lithostratigraphic unit I. We observe a similar thickness proportion of subunit S2b in relation to subunit S2a as Uenzelmann-Neben *et al.* (2011) described for the lower and upper parts of their seismic unit S2. We hence suggest that subunit S2b consists of the pelagic sediment of mid-Miocene to Holocene age of lithostratigraphic unit I recovered at Site 249.

4.4.2. Regional basement structure

4.4.2.1. Central Mozambique Ridge

The basement at the cMozR has a rounded morphology (2 in Figure 4.1) and gentle slopes that show a slight increase in dip to the NW and NE (Figure 4.3 and Figure 4.4). A ~15 km wide and 1600 ms TWT high basement peak on the NW flank disrupts the overall symmetry of the cMozR (Figure 4.3 CDPs 9300-9900). The segment is built up of at least three basement complexes (BC1, BC2 and BC3, Figure 4.3, Figure 4.4 and Figure 4.5a). The shallowest area of the top basement reflection identified in seismic reflection data is located in the southern part of BC1 with a depth of 1590 ms TWT below sea level (bsl; south of BC1 in Figure 4.3; black dashed ellipse in Figure 4.5a and b). In this part the cMozR rises up to 3650 ms TWT above the basement in the Natal Valley.

We observe only a thin sedimentary cover on top of basement highs (e.g., Figure 4.4 CDPs 3400–4200 and Figure 4.5b). The individual basement complexes are separated by depressions (e.g., Figure 4.4 CDPs 4800-6200). Faults associated with the depressions show offsets of up to 1500 ms TWT (Figure 4.3 CDP 4800). The intrabasement reflections at the cMozR can be identified up to 800 ms TWT deep, and individual reflections are typically traced for 5-15 km. Onlaps of intrabasement reflections onto other intrabasement reflections are observed, for example, between basement complex 2 and a 20 km wide basement high in the northeast of the cMozR (Figure 4.4 CDPs 1800–2200).

4.4.2.2. Southwestern Mozambique Ridge

The basement at the swMozR (3 in Figure 4.1) has gentle slopes and a rounded morphology that is slightly elongated to the N (Figure 4.5a and Figure 4.6). The shallowest area of the top of the basement covered by seismic reflection data has a depth of 1920 ms TWT bsl (black dashed ellipse in Figure 4.5a and b; fig. 2 in Uenzelmann-Neben *et al.*, 2011). We observe a thinning of the sedimentary cover towards basement highs (e.g., black dashed ellipse in Figure 4.5b and Figure 4.6 CDPs

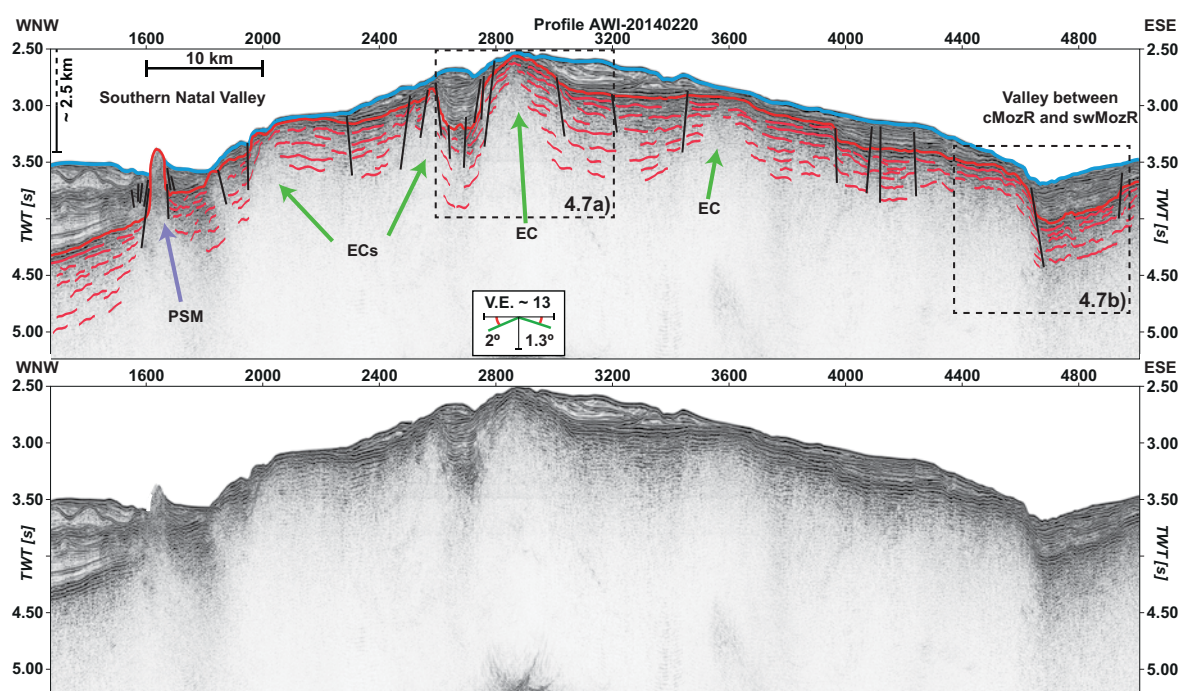


Figure 4.6. MCS profile AWI-20140220 crossing the southwestern Mozambique Ridge in a WNW–ESE direction. Line and arrow colours as in Figure 4.3. For slope angles and vertical exaggeration refer to legend. The dashed frames indicate the locations of Figure 4.7a and b. Location of profiles is shown in Figure 4.1.

2800–2950).

The swMozR is not as elevated as the cMozR, but still rises above the abyssal seafloor basement by up to 3500 ms TWT (Figure 4.5a and Figure 4.6). The swMozR is separated from the cMozR by a NNW–SSE striking valley (Figure 4.5a). The valley seems to have an asymmetrical shape as can be seen in Figure 4.6 (CDPs 4600–5000) and Figure 4.7c. We observe a greater abundance of faults and larger fault throws in the southern part of the swMozR with the result that the basement appears more fragmented than in the north. With a depth of up to 800 ms TWT below the top of basement the maximum depth of the observed intrabasement reflections is comparable to the cMozR (Figure 4.6 CDPs 1300–1550 and CDPs 3000–3400). Within the valley between the cMozR and the swMozR intrabasement reflections emerging from local basement highs of the cMozR show onlap onto those emerging from local highs of the swMozR (Figure 4.7b and c).

4.4.2.3. Southeastern Mozambique Ridge

In contrast to the cMozR and the swMozR, the seMozR (4 in Figure 4.1) seems to have a smoother and more homogeneous basement topography, even though it is difficult to make a general statement based on the low data coverage of the seMozR. Seismic data suggest a rather uniform basement depth in east-west direction and a gentle dip of basement to the south (Figure 4.5a and Figure 4.8). The depth ranges between ~3500 ms TWT in the north and more than 4800 ms TWT in the south (Figure 4.5a and Figure 4.8). Basement hence lies significantly deeper than on the other segments (Figure 4.5a). Intrabasement reflections reach up to 600 ms TWT deep and follow the general southward dipping trend of top basement (Figure 4.8 CDPs 4200–4600).

South of the seMozR we observe a smooth transition onto the Transkei Rise (Figure 4.1 and Figure 4.8). The depth of top of basement is between 5500 and 6000 ms TWT bsl and thus lies about 1000 to 2000 ms TWT deeper than at the seMozR (Figure 4.5a). Intrabasement reflections at the Transkei Rise show a maximum depth of 450 ms TWT below the top of basement.

4.4.3. Magmatic structures

The magmatic basement of the MozR and the Transkei Rise is characterized by prominent convex upward shaped

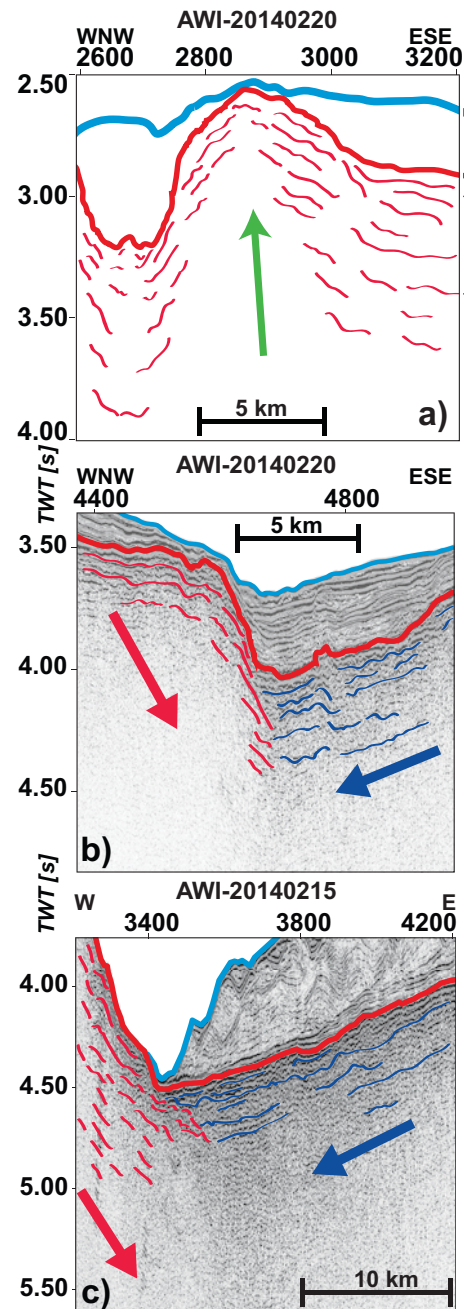


Figure 4.7. (a) Extrusion centre with lava flow sequences emerging and dipping away from it. Line colours as in Figure 4.3b and c. (b) and (c) Figures showing the area of the valley between the southwestern and central Mozambique Ridge. Line colours as in Figure 4.3, except thin red lines = intrabasement reflections emerging from the southwestern Mozambique Ridge, thin blue lines = intrabasement reflections emerging from the central Mozambique Ridge. The arrows (red and blue) show the observed flow direction of the respective intrabasement reflections.

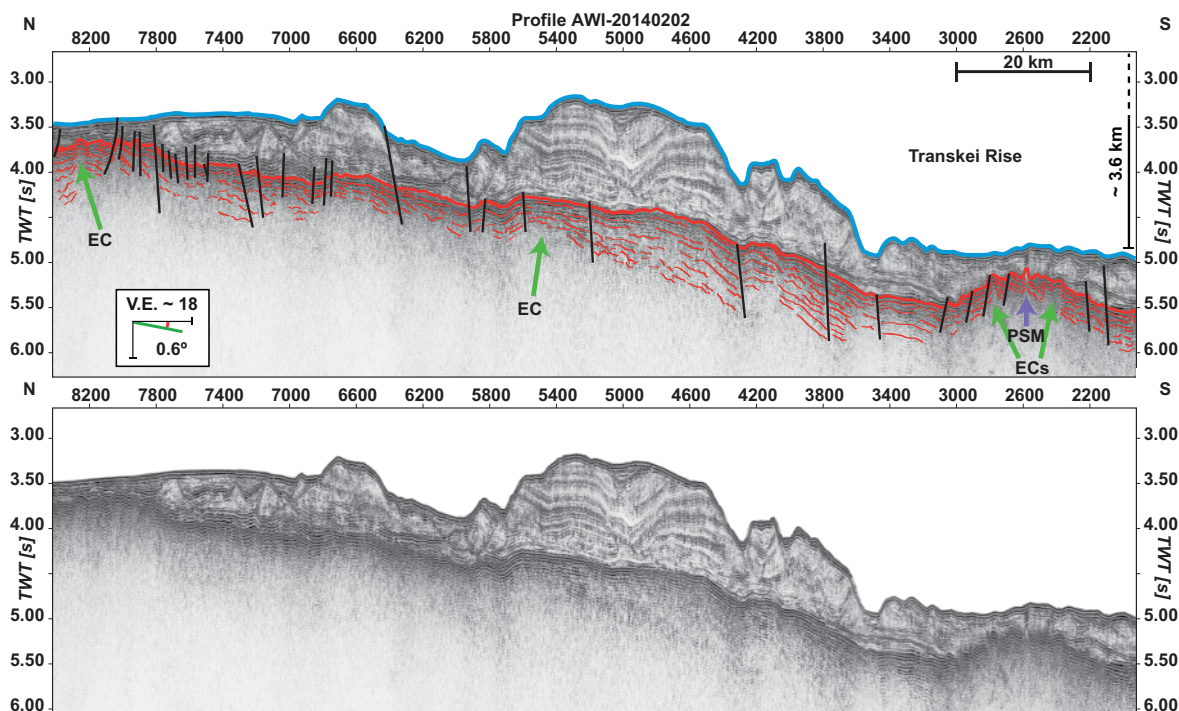


Figure 4.8. N–S striking MCS profile AWI-20140202 across the southeastern Mozambique Ridge. Line and arrow colours as in Figure 4.3. For slope angles and vertical exaggeration refer to legend. Location of profile is shown in Figure 4.1.

structures (e.g., Figure 4.3 CDPs 2400–2800, Figure 4.4 CDPs 4200–4400), which form local highs. The structures are distributed randomly and do not seem to follow any apparent trend (Figure 4.5c). The lateral extent of these structures can be up to 10 km (e.g., Figure 4.3 CDPs 2400–2800, Figure 4.6 CDPs 2700–3100, Figure 4.7a). Parallel (e.g., Figure 4.3 CDPs 3400–4200) and subparallel (e.g., Figure 4.6 CDPs 3200–4000) sequences of intrabasement reflections emerge, dip away and extend downhill from these local basement highs in opposing directions.

Reflections at the summit are nearly horizontal and not as continuous as those on the flanks, and we observe nearly no intrabasement reflections beneath the summits (e.g., Figure 4.3 CDPs 2400–2800). Our observations resemble structures identified at the Manihiki Plateau, Shatsky Rise, and the Agulhas Plateau (Uenzelmann-Neben *et al.*, 1999; Sager *et al.*, 2013b; Pietsch and Uenzelmann-Neben, 2015), which have been interpreted as extrusion centres (ECs). Sedimentary deposits onlap the ECs indicating pre-sedimentary magmatism (e.g., Figure 4.3 CDPs 3400–4200).

We observe a second type of magmatic structures characterized by a pull up of sedimentary layers suggesting a predominantly post-sedimentary development (Figure 4.2 CDPs 9300–9900) here called post-sedimentary magmatic (PSM) structures. All PSM structures cause deformation up to seismic unit S2b, even though not all of them pierce into the mid-Miocene to Holocene deposits. This is due to considerable differences in height from less than 100 m to more than 1200 m (using an averaged seismic velocity of 1500 m s^{-1}). The lateral extent of the conical to cylindrical PSM structures usually ranges from 1 to 4 km (e.g., Figure 4.6 CDPs 1600–1700) thus much smaller than the observed ECs. The structures are mainly concentrated on the flanks of the segments, whereas only a few are observed adjacent to ECs (Figure 4.5d).

4.4.4. Faults

We observe numerous breaks in lateral continuity of seismic units within the study area, some of them with small offsets of <20–80 ms TWT only affecting basement and the intrabasement reflections (e.g., Figure 4.4 CDP 3900, Figure 4.6 CDP 3950, Figure 4.8 CDP 3500). The majority of the vertical offsets affect basement and seismic unit S1 (offsets up to 180 ms TWT; e.g., Figure 4.4 CDP 6000, Figure 4.6 CDP 2500, Figure 4.8 CDP 7200) with some causing deformation up to the seafloor with offsets greater than 1000 ms TWT (e.g., Figure 4.3 CDP 4800, Figure 4.6 CDP 2800, Figure 4.8 CDP 8050).

Vertical offsets or breaks in lateral continuities of seismic units, and kinking or bowing of seismic reflections are typical expressions of faults (Hajnal *et al.*, 1996; Sager *et al.*, 2013a). Depending on the age of the deformed strata the observed faults can be divided into three groups: (I) faults only affecting basement that probably developed during or shortly after emplacement of the basement, (II) faults dissecting basement and sedimentary deposits of seismic unit S1 with a minimum age of ~100 Ma, and (III) faults deforming the whole sedimentary pile including basement and a maximum age of ~15 Ma. The latter can be observed in multibeam data recorded at the swMozR during SO 232 as well and show a predominantly EW to WNW–ESE strike (Uenzelmann-Neben, 2014).

4.5. Discussion

4.5.1. Intrabasement reflections and extrusion centres

The seismic data show a large number of ECs randomly distributed across the three segments of the southern MozR (Figure 4.5c). Defining characteristics of the convex upward shaped ECs are up to 15 km long parallel and subparallel sequences of intrabasement reflections diverging from their summits and the onlap of overlying sedimentary strata onto its surface, suggesting emplacement of the ECs before deposition of sediments took place. The intrabasement reflections vary in their reflection amplitude and continuity, and can be identified as deep as 800 ms TWT below the top of basement (Figure 4.4 and Figure 4.6). Similar observations of massive intrabasement reflections with varying geometries and amplitude characteristics have been reported for other locations around the world (e.g. Shatsky Rise, Agulhas Plateau, Kerguelen Plateau, Manihiki Plateau).

Deep intrabasement reflections are characteristic for oceanic plateau eruptions (Sager *et al.*, 2013b) and have been interpreted and in parts proven via drilling as lava flow sequences (Uenzelmann-Neben *et al.*, 1999; Frey *et al.*, 2000; Inoue *et al.*, 2008; Parsiegla *et al.*, 2008; Sager *et al.*, 2013b; Pietsch and Uenzelmann-Neben, 2015). We hence interpret the observed intrabasement reflections at the MozR to represent lava flow sequences. This interpretation is backed by a rise in interval velocity from less than 2600 m s⁻¹ within seismic units S1 and S2 to values of 3500 to 5000 m s⁻¹ below the top of basement derived from velocity analyses of CDP gathers and the *P*-wave velocity-depth distribution model for the swMozR by Gohl *et al.* (2011).

The lava flow sequences observed in the seismic reflection data form successions of at least 1.4–1.7 km thickness converting the observed thicknesses in ms TWT into m using a velocity of 4.25 km s⁻¹. The lava flow sequences represent only a small proportion of up to 22 km thick crust proposed to be built up by large volumes of mantle-derived magma (Gohl *et al.*, 2011). This type of crust implies that either eruptive phases were long lasting or eruption rates were high. The postulated short time frame of only ~13 Myr during which emplacement of the southern MozR took place (König and Jokat, 2010) supports high eruption rates as the primary cause for the thick lava flow deposits.

According to Coffin and Eldholm (1994), Self *et al.* (2008) and Sager *et al.* (2013b) high eruption rates are typical for LIPs and the reason for their distinctive low slopes and thick lava sequences.

We therefore propose that the observed low slopes and thick successions of lava sequences (e.g., Figure 4.6) were caused by high eruption rates during emplacement of the southern MozR and thus favour a LIP origin of the MozR.

The geometry of the lava flow sequences is highly variable (e.g., dip angles and dip directions; Figure 4.4 CDPs 1800–2200). The large number of ECs from which the intrabasement reflections emerge (e.g., Figure 4.6 CDPs 2600–3200), and the observation of parallel and sub-parallel stratified sequences of intrabasement reflections, which overlap and onlap each other (e.g., Figure 4.4 CDPs 1400–2200), points towards several eruptive phases during emplacement.

LIPs are proposed to be constructed of eruptions from multiple locations (Jerram and Widdowson, 2005; Bryan *et al.*, 2010). The observation of onlaps (Figure 4.7b and c) of lava flow sequences emplaced at the cMozR onto lava flow sequences emerged from the swMozR are interpreted as evidence for an asynchronous emplacement of both segments: while magmatic output ceased at the swMozR, lava flow sequences were still being emplaced at the cMozR. Strong magnetic anomalies associated with the boundaries of the individual segments interpreted as evidence for formation of the segments at different ages (König and Jokat, 2010), which agrees well with our observations. We therefore suggest that the thick pile of lava flow sequences forming the southern MozR were emplaced during several eruptions via the randomly distributed ECs and favour sequential development of the southern MozR with the youngest segment located in the southeast.

4.5.2. Post-sedimentary magmatism at the Mozambique Ridge

Magmatic structures of proposed post-sedimentary magmatic (PSM) origin (deformation of above lying sedimentary sequences with a pull-up at the structure's flanks, e.g., Figure 4.3 CDPs 1300–1400, in places piercing of the seafloor, e.g., Figure 4.6 CDPs 1600–1700) can be identified on the MozR. With their small diameters and steep flanks the PSM structures resemble piercement structures as described for the Kerguelen Plateau and interpreted as subvolcanic intrusives by Ramsay *et al.* (1986). Some of the PSM structures seem to coincide with the faults that deform a large proportion of the up to 15 Myr old seismic unit S2b (e.g., Figure 4.6 CDPs 1600–1700).

The majority of PSM features are concentrated within the transition zone of the segments to the surrounding basins (Figure 4.5d and e.g., Figure 4.3 CDPs 9300–9900) with a distinct increase in abundance of PSM structures in the southwestern and northwestern part of the study area (Figure 4.5d). All observed PSM structures led to deformation of parts of the overlying seismic unit S2b. This points to the onset of PSM activity after deposition of seismic unit S2b had already begun, thus after 15 Ma. This age corresponds to the probable onset of faulting associated with the breaks in lateral continuity, which in places affect seismic unit S2b up to seafloor (e.g., Figure 4.3 CDP 200). Faulting of the mid-Neogene to Quaternary strata might thus be an ongoing process.

According to Chorowicz (2005), neotectonic and Neogene magmatic activity in East Africa are interconnected and a consequence of the East African Rift System. The rift valleys of the East African Rift System (EARS) form two main lines, the Eastern and Western rift branches, which have shown a general southward propagation since initiation of the EARS (inset in Figure 4.1; Ebinger *et al.*, 1989; Kampunzu *et al.*, 1998; Calais *et al.*, 2006). Parts of the onshore Western rift branch terminate in the Mozambique Coastal Plains north of the study area (Stamps *et al.*, 2008; Saria *et al.*, 2014; Wiles *et al.*, 2014). Magmatic activity in the western branch commenced ~11 Ma in the north and ~8.6 Ma in the south, thus following the general southward trend of rift propagation of the EARS (Kampunzu *et al.*, 1998; Macgregor, 2015).

Several authors suggested a seaward propagation of the Eastern branch of the EARS but there is a strong dissent about whether there exists an offshore extension of the Western branch (Mougenot *et al.*, 1986; Hartnady *et al.*, 1992; Kampunzu *et al.*, 1998; Stamps *et al.*, 2008; Saria *et al.*, 2014;

Wiles *et al.*, 2014; Franke *et al.*, 2015; Klimke *et al.*, 2015). Hartnady *et al.* (1992) and Ben-Avraham *et al.* (1995) related neotectonic activity in the vicinity of the MozR to a propagation of the Western branch of the EARS into the Natal Valley. Tikku *et al.* (2002) supported a seaward extension of the Western branch of the EARS into the northeastern Natal Valley on the basis of free-air gravity lows interpreted as neotectonic faults. A seaward propagation was recently revisited by Wiles *et al.* (2014) as a probable cause for up to 31 km long and 18 km wide seafloor mounds observed northwest of the MozR. Other authors proposed that the western boundary of the Lwandle microplate traces along the eastern border of the MozR (Stamps *et al.*, 2008; Saria *et al.*, 2014; Stamps *et al.*, 2014), thus presenting another probable connection of neotectonic activity to a southward propagation of the EARS in the vicinity of the MozR.

We suggest that both PSM structures and neotectonic activity creating the faults deforming seismic unit S2b are caused by seaward propagation of the Western branch of the EARS in Late Miocene times. This is based on the age of the deformed seismic unit S2b (<15 Ma) and its chronological correlation to the onset of rifting in the Western branch of the EARS (Nyblade and Brazier, 2002). If we follow the proposed southward decrease in age of volcanism at the onshore Western branch and its onset in the south ~8.6 Ma (Kampunzu *et al.*, 1998; Macgregor, 2015), it is likely that post-sedimentary magmatism at the MozR commenced after 8.6 Ma. The observed piercing of the sedimentary deposits up to seafloor supports this.

We speculate that the over-thickened oceanic crust of the MozR (Gohl *et al.*, 2011) acted as a 'barrier' for a continuation of southward propagation of the EARS thus leading to a concentration of PSM structures at the flanks and margins of the LIP. Several authors proposed that development of the Eastern and Western branches of the EARS are controlled by stress concentrations from rheological contrasts (Petit and Ebinger, 2000; Chorowicz, 2005; Corti *et al.*, 2007). The rigid crust of the MozR

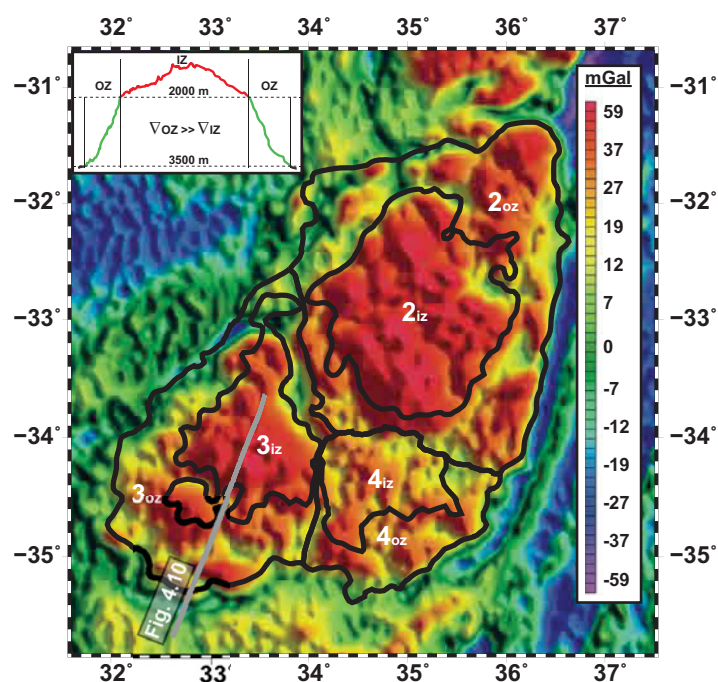


Figure 4.9. Free-air gravity anomaly map (after Sandwell and Smith, 2009) with subdivision of the individual plateaus of the Mozambique Ridge into an inner (iz) and outer zone (oz). The inner zones were constructed within the closed 2000 m depth contour at the central Mozambique Ridge (2iz), the closed 2500 m depth contour at the southwestern Mozambique Ridge (3iz) and the closed 2750 m depth contour at the southeastern Mozambique Ridge (4iz). The outer zones (2oz/3oz/4oz) were constructed between the outlines of the respective inner zones and the 3500 m isoline. The grey line illustrates the location of the P-wave velocity depth model of the swMozR by Gohl *et al.* (2011) shown in Figure 4.10. The inset in the upper left corner shows the basis for differentiation between iz and oz using the example of the central Mozambique Ridge. ∇ = gradient of basement depth.

could represent such a rheological contrast and thus re-directed the tectonic stress towards zones of structural weakness where it created pathways for igneous material. The thinner parts of the MozR as well as the transition into oceanic crust represents an ideal location for those areas of weakness.

4.5.3. Magmatic volume of the southern Mozambique Ridge and implications for its emplacement history

We have seen that the magmatic basement of the MozR is characterized by a large number of extrusions centres (EC). This in combination with thick lava flow sequences within the basement resemble observations from other LIPs (e.g., Pietsch and Uenzelmann-Neben, 2015) and are therefore interpreted as strong evidence for a LIP origin of the MozR. The predominantly basaltic composition of the 59 rock samples dredged during SO 232 and preliminary geochemical results in favour of a plume component in the source of MozR volcanism also support this interpretation (Uenzelmann-Neben, 2014; Jacques *et al.*, 2015). The presence of an up to 22 km thick over-thickened equivalent of oceanic layer 3 (Gohl *et al.*, 2011) and the suggested emplacement of the MozR within a relatively short timespan of ~18 Myr (König and Jokat, 2010) add to our interpretation of the southern MozR as a LIP (Bryan and Ernst, 2008; Kerr, 2014). The duration of magmatic activity as well as the volume of magmatic material emplaced are further important parameters, which will be studied in the following.

4.5.3.1. Volume of magmatism at the southern Mozambique Ridge

The excess crustal volume acts as an important measurement for quantifying the amount of magmatic material involved in a LIP formation. In order to calculate the volume of magmatism of the MozR parameters like the crustal thickness, the areal extent and the thickness of the surrounding oceanic crust are needed.

In order to calculate the total areal extent of the southern MozR and account for the crustal thinning of LIPs at their marginal areas we constructed an inner and an outer zone for each segment (Figure 4.9). The outlines of the outer zones were assigned to the 3500 m bathymetric depth contour bordering the positive free-air gravity

Table 4.2. Values used in the volumetric calculations of the Mozambique Ridge. Areal extents of the individual segments are derived from Figure 4.9. Excess volume stands for total volume excluding oceanic crust of 6 km (Reznikov *et al.* 2005). LCB stands for lower crustal body. Duration of main pulse based on a time-averaged volumetric volcanic output rate (Q_o) of $9 \times 10^{-1} \text{ km}^3 \text{ a}^{-1}$, duration of phase of reduced magmatic activity based on Q_o of $1 \times 10^{-1} \text{ km}^3 \text{ a}^{-1}$ (Coffin *et al.* 2002; White *et al.* 2006).

Segment	Area inner zone [x 10 ⁴ km ²]	Area outer zone [x 10 ⁴ km ²]	Total area [x 10 ⁴ km ²]	Averaged crustal thickness inner zone [km]	Averaged crustal thickness outer zone [km]	Total volume [x 10 ⁶ km ³]	Excess volume [x 10 ⁶ km ³]	Volume of extruded upper crust [x 10 ⁶ km ³]	Volume of intruded crust and LCB [x 10 ⁶ km ³]	Magmatic main pulse (75 per cent of total volume) [Myr]	Reduced magmatic activity (25 per cent of total volume) [Myr]	Total duration of formation [Myr]
cMozR	3.212	4.358	7.570	23.68	21.76	1.709	1.255	0.192	1.063	1.046	3.137	4.182
swMozR	1.750	2.912	4.662	21.45	19.53	0.944	0.665	0.106	0.559	0.554	1.661	2.215
seMozR	1.114	1.171	2.286	20.34	18.42	0.442	0.305	0.050	0.255	0.254	0.763	1.018
Σ	6.076	8.441	14.517	-	-	3.096	2.224	0.348	1.877	-	-	-

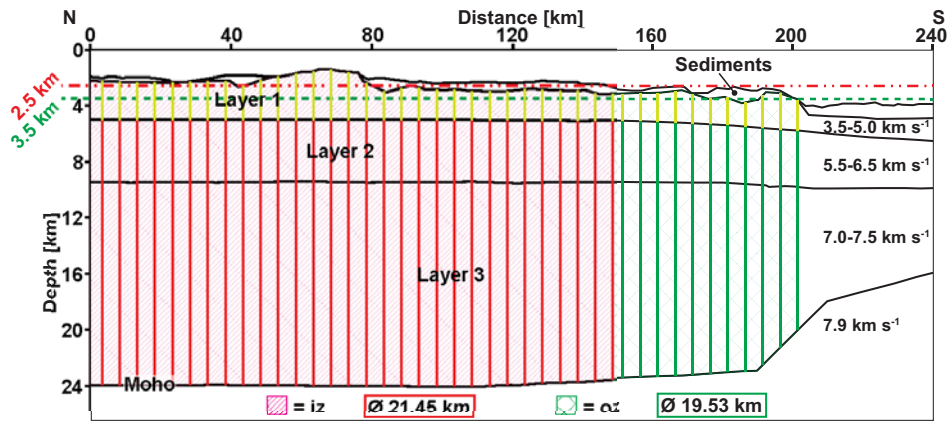


Figure 4.10. Simplified P -wave velocity depth model (after Gohl *et al.*, 2011) that was used to determine the average thickness of the inner zone (iz; dashed in red) and the outer zone (oz; dashed in green) of the southwestern Mozambique Ridge. Horizontal dashed lines represent bathymetric depth contours (*cf.* Figure 4.9) used for construction of the inner zone (2500 m; in red) and the outer zone (3500 m; in green). Thickness was measured every 5 km within the zones. Yellow vertical lines were used to calculate the average thickness of the extruded upper crust (layer 1), red vertical lines (incl. associated yellow vertical lines) for calculating the average thickness of the inner zone, and green vertical lines (incl. associated yellow vertical lines) for calculating the average thickness of the outer zone. Velocities, layers, depth and profile distance based on Gohl *et al.* (2011). Refer to chapter 4.5.3.1 for a detailed description.

anomalies (Sandwell and Smith, 2009) associated with the magmatic basement of the MozR (Figure 4.9). The outlines of the inner zones were constructed based on the observation of distinct variations in gradient (∇) of basement depth at each segment. Whereas the outer zones display a high ∇ , the inner zones demonstrate only a low ∇ (inset in Figure 4.9). To construct closed inner zones in areas where no information about basement depth (and thus ∇) is available, we linked the boundaries to their corresponding bathymetric depth contours. The inner zones of the cMozR, swMozR and seMozR were therefore constructed within the closed 2000, 2500 and 2750 m depth contour (Figure 4.9).

We calculated an areal extent of $6.1 \times 10^4 \text{ km}^2$ for the inner zones and $8.4 \times 10^4 \text{ km}^2$ for the outer zones (Table 4.2). With a total area of $1.45 \times 10^5 \text{ km}^2$ the southern MozR surpasses the suggested threshold value for classifying LIPs of $1 \times 10^5 \text{ km}^2$ (Bryan and Ernst, 2008) by ~ 45 per cent.

For the purpose of volume calculations the thickness of the swMozR was measured every 5 km within the inner and outer zones of the crustal velocity-depth model (Gohl *et al.*, 2011) and averaged for the inner (hatched in red in Figure 4.10) and outer zone (hatched in green in Figure 4.10). This leads to an average thickness of 19.53 km for 3_{oz} and 21.45 km for 3_{iz} , and a total crustal volume for the swMozR of $0.94 \times 10^6 \text{ km}^3$ (Table 4.2).

Only 1-D crustal thickness estimates of low resolution exist for the cMozR and the seMozR. Assuming Airy type isostatic equilibrium between the ridge and the adjacent oceanic basins (Hales and Nation, 1973; Recq and Goslin, 1981; Maia *et al.*, 1990) we used the Airy-Heiskanen model to determine the crustal thickness of the cMozR and the seMozR. A 6 km thick oceanic crust (Reznikov *et al.*, 2005) and an average basement depth of 6.3 km within the adjacent oceanic basin (Schlüter and Uenzelmann-Neben, 2007) were used as reference values together with a water density of 1000 kg m^{-3} and a mantle density of 3300 kg m^{-3} . The density of the crust at the MozR was calculated to be 2944 kg m^{-3} based on the P -wave velocity depth model of the swMozR (Gohl *et al.*, 2011) and the empirical density-velocity relation of Barton (1986).

This led to an average crustal thickness of 23.68 and 21.76 km for the inner and outer zones of the cMozR, and 20.34 and 18.42 km for the inner and outer zones of the seMozR, respectively (Table 4.2). The crustal volume of the cMozR is thus estimated to be $1.71 \times 10^6 \text{ km}^3$, and of the seMozR $0.44 \times 10^6 \text{ km}^3$ (Table 4.2). The sum of the crustal volumes of the three segments is $3.10 \times 10^6 \text{ km}^3$ including extrusive and subvolcanic (upper crustal) intrusive volumes, and middle and lower crustal

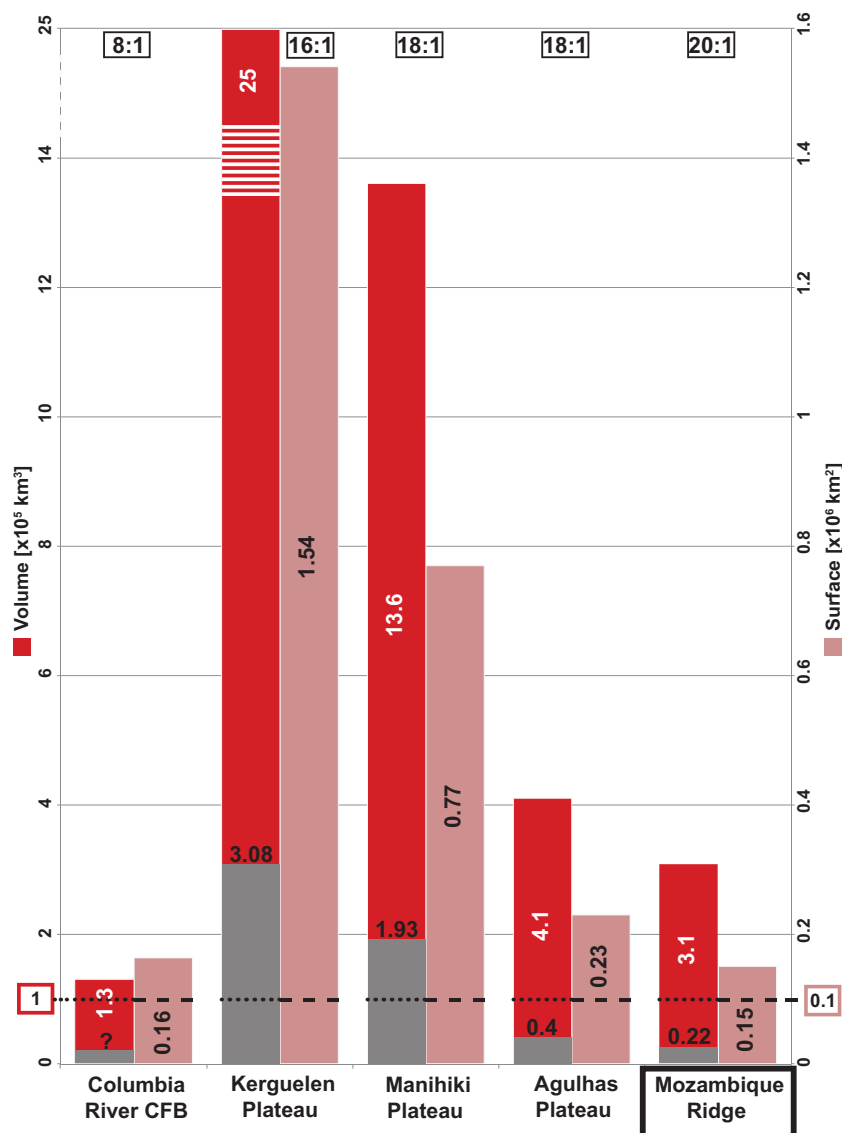


Figure 4.11. Graph illustrating the areal extent (light red bar) and crustal volume (dark red bar: extruded upper crust + intruded crust + lower crustal body; grey: extruded upper crust) of the southern Mozambique Ridge, selected oceanic plateau LIPs and the Columbia River Continental Flood Basalt Province (no data available for volume of extruded upper crust). Dashed lines represent threshold values for size ($0.1 \times 10^6 \text{ km}^2$) and volume of extruded crust ($0.1 \times 10^6 \text{ km}^3$) of a LIP suggested by Bryan and Ernst (2008). Proportions stated in the uppermost part of the graph yield ratios of total crustal volume to areal extent of each LIP. (Agulhas Plateau: Parsiegla *et al.*, 2008; Columbia River CFB: Hooper, 1988; Baksi, 1989; Coffin and Eldholm, 1994; Kerguelen Plateau: Coffin and Eldholm, 1994; Frey *et al.*, 2003; Manihiki Plateau: Coffin and Eldholm, 1994; Inoue *et al.*, 2008).

components (Table 4.2). The results should only be considered as a tentative minimum estimate and do not account for the whole MozR due to the lack of data for the northern MozR.

Eldholm and Coffin (2000) summarized that volumes of LIPs range from $0.7 \times 10^6 \text{ km}^3$ to $44.4 \times 10^6 \text{ km}^3$. Our results for the southern MozR thus fall into the lower range. Examples of areal extent and volumetric distribution of several LIPs including the southern MozR are shown in Figure 4.11, with the southern MozR having a size and volume that equals ~ 70 per cent of the Agulhas Plateau. Comparison of the crustal volume to area ratio shows that the southern MozR has a $\sim 20:1$ ratio, which is slightly higher than the ratios of the oceanic LIPs of Agulhas Plateau, Kerguelen Plateau and Manihiki Plateau (Figure 4.11).

Continental LIPs, for example, the Columbia River Continental Flood Basalt Province, show a significant lower crustal volume to area ratio than the oceanic LIPs and the southern MozR (Figure 4.11).

We interpret this similarity of crustal volume to area ratios of oceanic LIPs with those of the MozR as support for an oceanic LIP origin of the MozR.

Subtracting the volume of a 6 km thick layer of oceanic crust as observed for the adjacent basin (Reznikov *et al.*, 2005) leads to a magmatic excess volume of the southern MozR of $2.22 \times 10^6 \text{ km}^3$. We distinguish between an intruded crust/lower crustal body and an extruded upper crust in our calculations. Following the method used by Parsiegla *et al.* (2008) we estimated the extruded upper crustal component by picking the thickness of layer 1 characterized by velocities between 3.5 and 5 km s^{-1} in the velocity-depth model of the swMozR (Gohl *et al.*, 2011) every 5 km (yellow vertical lines in Figure 4.10).

The average thickness within the inner zone is 2.5 km and within the outer zone 2.1 km. We calculated the ratio of extruded upper crust to total crustal thickness for the inner (11.87 per cent) and outer zone (10.73 per cent) of the swMozR. By applying these ratios to the crustal thicknesses of both other segments we were able to estimate the extruded upper crustal component at the cMozR ($2_{iz} = 2.81 \text{ km}$; $2_{oz} = 2.33 \text{ km}$) and the seMozR ($4_{iz} = 2.42 \text{ km}$; $4_{oz} = 1.98 \text{ km}$).

Based on these estimates the amount of extruded material of the three segments is found to be $3.48 \times 10^5 \text{ km}^3$ (Table 4.2). The calculated volume of extruded material of the MozR exceeds the minimum specifications for a LIP of $1 \times 10^5 \text{ km}^3$ (Bryan and Ernst, 2008) by almost 250 per cent, supporting a LIP origin of the MozR as postulated by Gohl *et al.* (2011). The remaining excess volume of $1.88 \times 10^6 \text{ km}^3$ (Table 4.2) intruded into the oceanic crust and accounts for the strongly increased thickness of the seismically homogeneous, lower crustal units (Gohl *et al.*, 2011).

Based on our results the southern MozR shows an intrusive to extrusive ratio (I:E) of $\sim 5:1$. Following Bryan and Ernst (2008) the volume of the intruded and lower crustal body of a LIP can be up to ten times larger than the associated extruded upper crust. Their statement rests on the findings of Crisp (1984) who examined a loosely constrained I:E ratio of 3:1 to 16:1 for mafic rock volumes worldwide. The results for the I:E ratio of the MozR show a high proportion of extruded upper crust, which bear witness to the highly eruptive nature of the MozR.

4.5.3.2. Timing and duration of emplacement of the Mozambique Ridge

White *et al.* (2006) calculated time-averaged volumetric volcanic output rates (Q_v) based on volcanic eruption data published from 1962 to 2005, and proposed a Q_v of $9 \pm 2 \times 10^{-1} \text{ km}^3 \text{ a}^{-1}$ for flood basalt provinces and oceanic plateaus. But magma output rate is not constant over time. Coffin *et al.* (2002) observed that following the peak in magma production ($Q_v = 9 \times 10^{-1} \text{ km}^3 \text{ a}^{-1}$) at the Southern Kerguelen Plateau magmatic output waned by nearly an order of magnitude to $\sim 0.1 \times 10^{-1} \text{ km}^3 \text{ a}^{-1}$. Karlstrom and Richards (2011) suggested magmatic activity of LIPs on two distinct timescales: an intrusion-dominated regime with only minor eruptions lasting the total active lifetime of a LIP, and a distinctively shorter 'main stage' during which most of its volume is emplaced. The main pulse can be very brief (less than 1 Myr), but accounts for more than 75 per cent of the total volume of magmatic output (Camp *et al.*, 2003; Courtillot and Renne, 2003; Bryan and Ernst, 2008).

Karlstrom and Richards (2011) proposed that terminations of main eruption phases are a probable result of shutoff of dike propagation from the deep crust. It was suggested that the transition from the main eruption phase to the phase of strongly decreased magmatic output happens abruptly (Coffin *et al.*, 2002). Bryan *et al.* (2002) and Jerram and Widdowson (2005) related the interval of reduced magmatic output to a waning and more protracted phase of volcanism where the volume of eruptions rapidly decreases and may become more widely distributed or focused when rifting occurs.

Adopting a presumed magmatic activity on two distinct timescales (e.g., Karlstrom and Richards,

2011) and following Coffin *et al.* (2002) and White *et al.* (2006) we apply a Q_e of $9 \times 10^{-1} \text{ km}^3 \text{ a}^{-1}$ for estimating the duration of the magmatic main pulse (75 per cent of the total volume), and a Q_e of $1 \times 10^{-1} \text{ km}^3 \text{ a}^{-1}$ to calculate the duration of the phase of reduced magmatic activity (remaining 25 per cent of the total volume; Figure 4.12). Using our estimates of the magmatic volume of the southern MozR (Table 4.2) this results in the duration of the main pulse of $\sim 1.1 \text{ Myr}$ for the cMozR, $\sim 0.6 \text{ Myr}$ for the swMozR and $\sim 0.3 \text{ Myr}$ for the seMozR (Figure 4.12 and Table 4.2). The length of the phase of reduced magmatic activity amounts to $\sim 3.1 \text{ Myr}$ for the cMozR, $\sim 1.6 \text{ Myr}$ for the swMozR and $\sim 0.7 \text{ Myr}$ for the seMozR (Figure 4.12 and Table 4.2).

Based on the analysis of magnetic anomalies König and Jokat (2010) proposed a formation of the MozR between 140 and 120 Ma. We have updated their ages of magnetic anomalies using the age calibration of Ogg (2012). König and Jokat (2010) distinguish four phases of formation: Segment 1 was formed between 140 and 135.32 Ma (prior to magnetic anomaly M11n, Figure 4.13a), a simultaneous onset of formation of the cMozR and the swMozR with no clear specification for the commencement (sometime after 135.32 Ma, i.e. magnetic anomaly M11n) but a cessation of formation of the swMozR at 128.66 Ma (magnetic anomaly M3n) while the cMozR continued to grow until 125.93 Ma (magnetic anomaly M0r), and the seMozR formed between 125.93 Ma (magnetic anomaly M0r) and $\sim 120 \text{ Ma}$.

Using our estimated durations for the main magmatic pulses and later emplacement periods in combination with König and Jokat (2010)'s reconstruction results in the tentative scenario for the development of the MozR shown in Figure 4.13. Anomaly M3n forms a tie point in their model because the swMozR at that time had already been formed to its full extent while the cMozR continued to grow (Figure 4.13c). Since König and Jokat (2010) have no clear evidence for the onset of magma emplacement at the cMozR and the swMozR we use anomaly M3n (128.66 Ma) to calculate the onset of formation of the swMozR as 130.86 Ma (128.66 Ma + 0.6 Myr main pulse + 1.6 Myr reduced magmatic phase; Figure 4.13b).

Build-up of the cMozR then continued for another 2 Myr with a cessation of magma production at $\sim 126.66 \text{ Ma}$ (Figure 4.13d). That eruptive activity of the cMozR exceeded that of the swMozR is supported by the onlaps of intrabasement reflections originating from ECs of the cMozR onto intrabasement reflections emerging from the swMozR (Figure 4.7b and 7c). Whether magma flux of the cMozR and the swMozR diminished abruptly or gradually is open to interpretation and cannot be determined based on the seismic data. The seMozR started to develop shortly after M0r with its main eruption phase beginning $\sim 125.90 \text{ Ma}$ probably while passing the Astrid Ridge. The main eruption phase of the seMozR lasted about 0.3 Myr (Figure 4.13e). The final phase of intrusive processes and minor eruptions started at about $\sim 125.6 \text{ Ma}$ and lasted for $\sim 0.7 \text{ Myr}$ (Figure 4.13f).

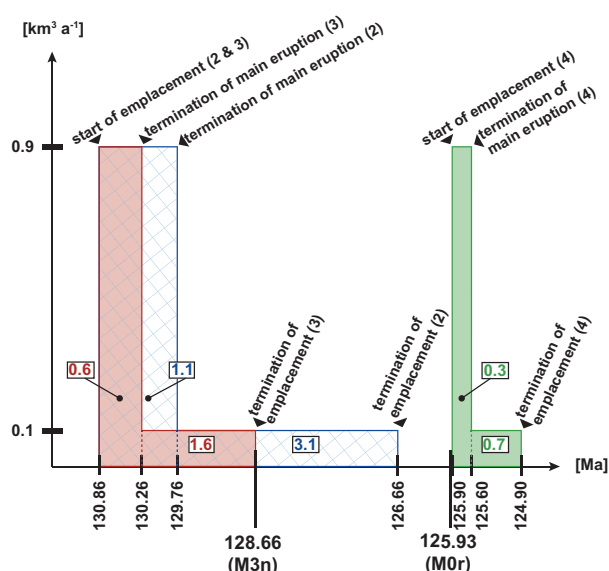


Figure 4.12. Illustration of duration of emplacement phases (numbers within white boxes) of the individual segments. Central Mozambique Ridge: blue bar with hatching, southwestern Mozambique Ridge: red bar, southeastern Mozambique Ridge: green bar. The onset and termination of each phase is marked on the x-axis (refer to chapter 4.5.3.2 for explanation), whereas the y-axis indicates the used time-averaged volumetric volcanic output rates (Q_e ; Coffin *et al.*, 2002, White *et al.*, 2006) the calculations are based on.

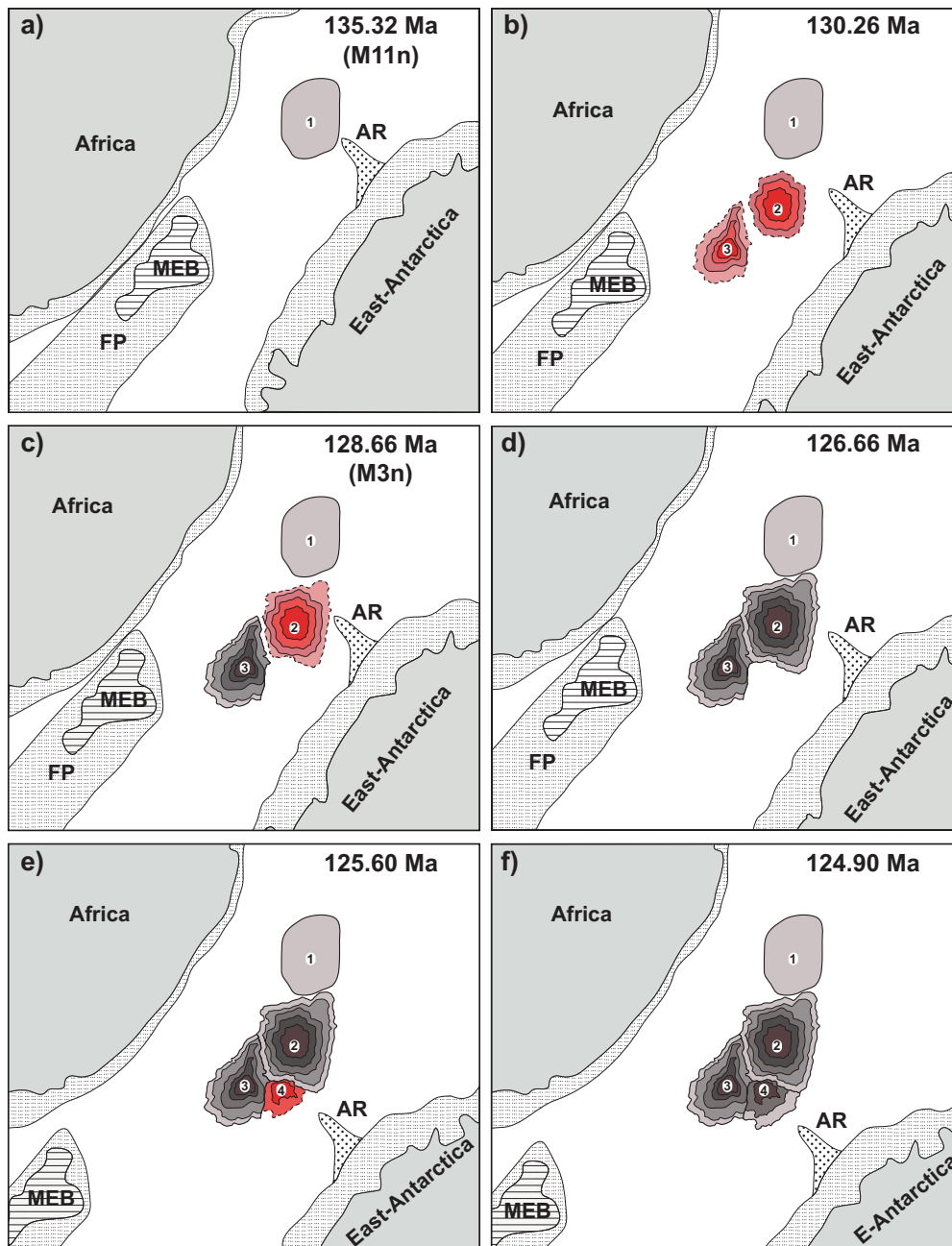


Figure 4.13. Schematic sketch of the proposed emplacement model for the southern Mozambique Ridge. The framework conditions of the model are based on the plate tectonic reconstruction by König and Jokat (2010). Life spans of the individual segments are based on time-averaged volcanic output rates (Figure 4.12; Coffin *et al.*, 2002; White *et al.*, 2006). Age calibration is based on Ogg (2012). 1 = northern Mozambique Ridge (nMozR), 2 = central Mozambique Ridge (cMozR), 3 = southwestern Mozambique Ridge (swMozR), 4 = southeastern Mozambique Ridge (seMozR), AR = Astrid Ridge, FP = Falkland Plateau, MEB = Maurice Ewing Bank. **(a)** nMozR was formed prior to M11n between 140 and 135.32 Ma (König and Jokat, 2010). **(b)** Onset of magmatic activity at cMozR & swMozR started ~130.86 Ma. Main eruption phases terminated ~130.26 Ma at swMozR and continued for another ~0.5 Myr at cMozR. **(c)** Emplacement of swMozR was completed ~128.66 Ma (M3n) after a ~1.6 Myr lasting phase of intrusive processes and minor eruptions. **(d)** phase of reduced magmatic activity at cMozR lasted ~3.1 Myr with formation of cMozR being completed ~126.66 Ma. **(e)** emplacement of seMozR started shortly after M0r (125.93 Ma) about 125.90 Ma and main eruption phase terminated ~125.60 Ma; **(f)** Phase of decreased magmatic output of seMozR lasted for ~0.7 Ma, thus formation of the southern MozR was completed ~124.90 Ma.

4.6. Conclusion

The analysis of the first high-resolution MCS reflection dataset covering the three southern segments of the MozR provided detailed information on its structure and development.

- (1) Seismic stratigraphy identifies two sedimentary units and the basaltic basement showing deep reaching intrabasement reflections known from other study areas and classified as lava flow sequences typical for LIPs.
- (2) Based on a comprehensive analysis of our data we can conclude that MozR can be classified as a LIP. Amongst others this classification is based on the presence of numerous extrusion centres, deep reaching lava flow sequences and size and crustal volume of the MozR.
- (3) The MozR is constructed of four segments, and the three southern segments are a consequence of sequential development by excessive volcanic activity.
- (4) We propose emplacement of the individual segments between 130.9–126.7 Ma (cMozR), 130.9–128.7 Ma (swMozR) and 125.9–124.9 Ma (seMozR).
- (5) Besides extrusion centres corresponding to the initial development of the segments post-sedimentary magmatic features are observed within the study area. We suggest that late stage magmatism corresponds to a seaward propagation of the Western branch East African Rift System in Late Miocene.

4.7. Acknowledgements

We want to express our gratitude to Captain Detlef Korte and his officers and crew of RV *Sonne* for their professional and enthusiastic engagement and service during the scientific program of this leg. The cruise leg SO 232 and the project SLIP were primarily funded by the German Federal Ministry of Education and Research (BMBF) under project number 03G0232A. Additional funding has been provided by the Alfred-Wegener-Institut. We thank M. Coffin, R. Reece and G. Laske (editor) for their detailed and helpful comments that improved our manuscript.

5. Late Cretaceous onset of current controlled sedimentation in the African–Southern Ocean gateway

Maximilian D. Fischer, Gabriele Uenzelmann-Neben

Alfred-Wegener-Institut Helmholtz-Zentrum für Polar- und Meeresforschung, Am Alten Hafen 26, 27568 Bremerhaven, Germany

In review in **Marine Geology** (02/2017)

Abstract

During the breakup of Gondwana the Mozambique Ridge, a Large Igneous Province emplaced between 140 and 125 Ma, was located in the evolving African–Southern Ocean gateway. Therefore, it represents an archive of the evolving exchange of water masses between the South Atlantic and Indian Oceans via the development of surface, intermediate, and bottom circulation. Two Cretaceous seismic units (S1 and S2a) were deposited on top of magmatic basement separated by a hiatus. Unit S1 mostly shows seismic reflections parallel to the top of the basement and no indications of current activity. Within seismic unit S2a we observe the first evidence of current controlled sedimentation with several sediment drifts. Based on our observations we propose deposition under partly euxinic conditions in the area of the Mozambique Ridge until ~100 Ma. The onset of a strong shallow circulation affecting deposition at the Mozambique Ridge is inferred by the Late Cretaceous ~25 Myr hiatus reported by drilling results and documented in the seismic records, whereas black shales deposited in the nearby deep Transkei Basin indicate a restricted deep circulation at least until ~85–80 Ma. We propose that the observed hiatus might be a consequence of a late Early Cretaceous uplift of the Mozambique Ridge and the progressive opening of the Agulhas Passage allowing inflow into the study area. The intense circulation that caused the hiatus seems to have weakened in Campanian times, which is documented by the occurrence of sediment drifts in seismic unit S2a. We suggest that the onset of current controlled sedimentation was caused by palaeogeographic modifications in the Atlantic Ocean along with relocation of circulation pathways.

5.1. Introduction

For several decades Large Igneous Provinces (LIP) like the Mozambique Ridge (MozR) have been of great interest because of their potential far-reaching impact on biosphere and atmosphere leading to climate shifts and mass extinctions (e.g., Coffin and Eldholm, 1994; Wignall, 2001; Saunders, 2005). Despite the probable influence of palaeo-climate by emission of greenhouse gases during emplacement of the MozR, its elevation and location off South Africa in the southwestern Indian Ocean (Figure 5.1a) presents another criterion that might have influenced palaeo-climate: the obstruction of ocean currents circulating in the evolving Southern Ocean (e.g., Durgadoo *et al.*, 2008). A prominent example of such an impact on palaeocean circulation is the Rio Grande Rise/Walvis Ridge System, which acted as a barrier for deep water circulation between the North and South Atlantic Ocean until its Late Cretaceous subsidence (Wagner and Pletsch, 1999; Murphy and Thomas, 2013; Voigt *et al.*, 2013).

The modern oceanographic setting of the southwestern Indian Ocean is characterized by a four-layer structure consisting of surface (Agulhas Current), intermediate (Antarctic Intermediate Water), deep (North Atlantic Deep Water) and bottom water masses (Antarctic Bottom Water) that probably developed during the late Eocene or early Oligocene as a consequence of the Antarctic Circumpolar Current (Figure 5.1a; Tomczak and Godfrey, 1994; Uenzelmann-Neben, 2001; Lutjeharms, 2006; Uenzelmann-Neben and Huhn, 2009; Katz *et al.*, 2011; Uenzelmann-Neben and Clift, 2015). In Early to Late Cretaceous times the oceanic setup was entirely different, mainly due to considerable differences in palaeogeography, palaeotemperature and CO₂ levels (Poulsen *et al.*, 2001; Leckie *et al.*, 2002; MacLeod *et al.*, 2011; Donnadieu *et al.*, 2016).

Various authors focused on the evolution of water masses in the Southern Ocean and inferred a late Early Cretaceous onset of deep water formation and thus of palaeocean circulation in the Indian sector (e.g., Poulsen *et al.*, 2001; Robinson *et al.*, 2010; Murphy and Thomas, 2012, 2013). It is a matter of ongoing debate whether Northern Component Water or Southern Component Water acted as driving mechanism of Late Cretaceous ocean circulation, but circulation evolved from a sluggish and partly regional to an ocean wide and open deep water circulation until the end of the Mesozoic era (e.g., Huber *et al.*, 1995; MacLeod *et al.*, 2011; Robinson and Vance, 2012; Murphy and Thomas, 2013; Donnadieu *et al.*, 2016). Most of these studies are based on the analysis of neodymium (ϵ_{Nd}), oxygen ($\delta^{18}O$) and carbon isotope data ($\delta^{13}C$).

The study of contourite drifts offers another approach to reconstruct palaeoceanography because the observed morphologic, stratigraphic and seismic characteristics allow for the interpretation of the pathway and approximate flow intensity of the water mass that was responsible for their development (Faugères *et al.*, 1999; Hernández-Molina *et al.*, 2006; Müller-Michaelis *et al.*, 2013). The analysis of sediment drifts led to a proposed middle Tertiary onset of current controlled sedimentation in the Transkei Basin SW of the MozR (Schlüter and Uenzelmann-Neben, 2007), whereas onset of current controlled sedimentation at the MozR was suggested for ~15 Ma (Uenzelmann-Neben *et al.*, 2011). In this paper we focus on the Early to Late Cretaceous sediments deposited in the study area to gain insight into the palaeoceanographic conditions during their deposition and the probable influence of the MozR on these conditions. The location of the MozR in the gateway between the evolving South Atlantic and Indian Ocean and its entire emplacement by ~125 Ma lends it a crucial importance to better understand the establishment of the deep water connection between the South Atlantic and the Southwest Indian Oceans (König and Jokat, 2006, 2010; Fischer *et al.*, 2017). We present high-resolution multichannel seismic (MCS) reflection data recorded in the area of the Mozambique Ridge (MozR) during RV Sonne expedition SO 232 in 2014 to identify seismic characteristics typical for changes in current strength and spatial and temporal variations in the location of these currents.

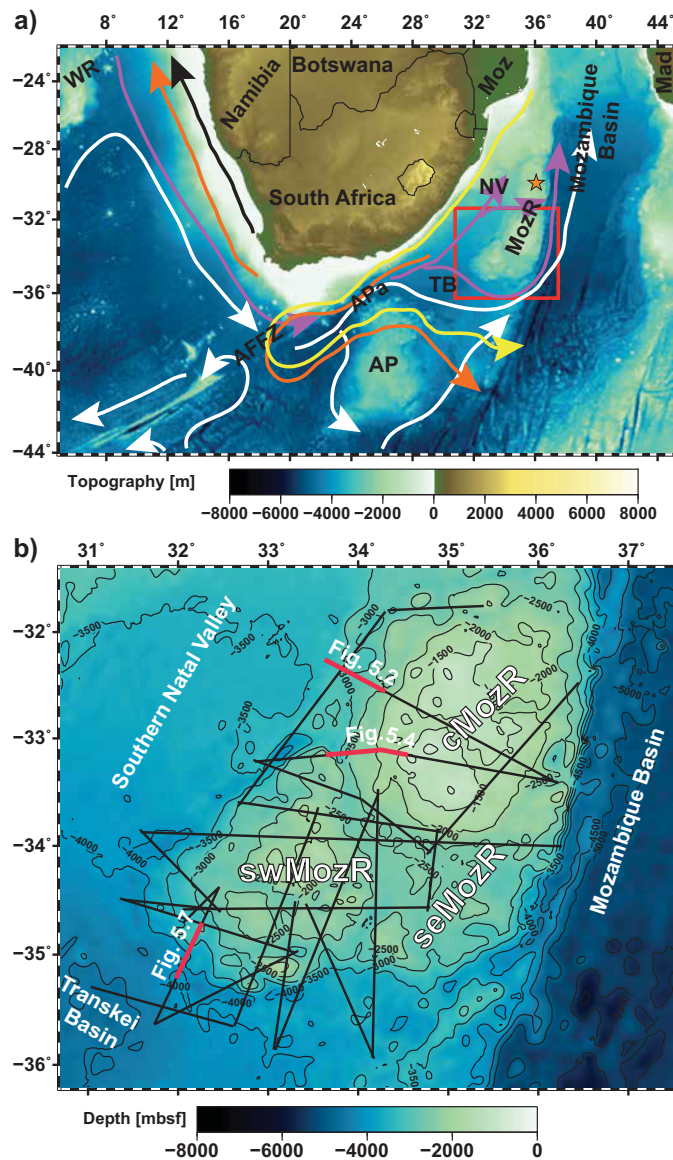


Figure 5.1. (a) Bathymetric map (Weatherall *et al.*, 2015) of S Africa with parts of the South Atlantic and SW Indian Ocean. The arrows show the schematic flow paths of surface currents and deeper water masses (Lutjeharms, 2006; Uenzelmann-Neben *et al.*, 2007; Gruetzner and Uenzelmann-Neben, 2016): Agulhas Current (yellow), Benguela Current (black), Antarctic Intermediate Water (orange), North Atlantic Deep Water (purple) and Antarctic Bottom Water (white). Orange star marks the location of DSDP Leg 25 Site 249 on the northern Mozambique Ridge. Red box indicates study area shown in Figure 5.1b. AFFZ = Agulhas Falkland Fracture Zone; AP = Agulhas Plateau; APA = Agulhas Passage; Mad = Madagascar; Moz = Mozambique; MozR = Mozambique Ridge; NV = Natal Valley; TB = Transkei Basin; WR = Walvis Ridge. (b) Bathymetric map (Weatherall *et al.*, 2015) of the study area in the southwestern Indian Ocean (500 m contour lines in black). MCS profiles of SO 182 and 232 are shown in black. Thick red lines mark intervals of MCS profiles shown in figures. cMozR = central Mozambique Ridge, swMozR = southwestern Mozambique Ridge, seMozR = southeastern Mozambique Ridge.

5.2. Background and settings

5.2.1. Tectonic and palaeoceanographic setting

The palaeogeography of the Cretaceous Southern Ocean can be divided into three regions: Atlantic, Indian and Pacific (Robinson *et al.*, 2010). The basins of the Indian region surrounding the MozR started to form as a consequence of the opening between Africa and Antarctica during the early

stages of Gondwana breakup in Middle Jurassic (Mozambique Basin), and during the early opening between South America and Africa ~136 to 134 Ma (Natal Valley; Goodlad *et al.*, 1982; König and Jokat, 2006, 2010). An exact age of the Transkei Basin southwest of the MozR cannot be determined precisely because its formation commenced subsequent to the Natal Valley during the Cretaceous Normal Superchron (Dingle and Camden-Smith, 1979; Schlüter and Uenzelmann-Neben, 2007). With a suggested emplacement of the LIP between 140 and 125 Ma the development of the MozR therefore accompanied the formation of three Mesozoic basins (König and Jokat, 2010; Fischer *et al.*, 2017).

Until Albian times only small, semi-isolated deep ocean basins existed in the South Atlantic and southern Indian Ocean regions (Dingle and Lavelle, 2000). Similar restricted and partly euxinic conditions can be inferred for the MozR during deposition of the Early Cretaceous sedimentary unit based on organic carbon rich intervals (average amount of 1.5% organic carbon) drilled at DSDP Site 249 (orange star in Figure 5.1a) at the northern MozR (Girdley, 1974; Simpson *et al.*, 1974). Uenzelmann-Neben *et al.* (2016) inferred that a weak transport of intermediate water through the Drake Passage into the South Atlantic and further on through the African-Southern Ocean gateway into the evolving Indian Ocean was already being established in Albian times. Murphy and Thomas (2012) also suggested a mechanism of consistent deep water ventilation in the South Atlantic and Indian sector of the Southern Ocean already for the middle Cretaceous, although deep water circulation might have been only sluggish (Robinson *et al.*, 2010) or regionally restricted (Voigt *et al.*, 2013). Increased CO₂ concentrations and palaeogeographic evolution have been proposed as probable driving mechanisms for altering the mid-Cretaceous ocean circulation in the South Atlantic sector (Poulsen *et al.*, 2001). The formation of intermediate and deep waters in the Indian sector of the Southern Ocean during the late Albian supports a mode of meridional overturning circulation characterized by high latitude downwelling prior and during the peak Cretaceous greenhouse in the early Turonian (Murphy and Thomas, 2012).

The transition from an Albian to Turonian palaeogeography led to significant changes in surface and deep oceanic circulation. According to Lawver *et al.* (1992) and König and Jokat (2006) a deep water connection between Indian and South Atlantic Oceans was established ~100 Ma. Combined with the widening of the South Atlantic Ocean, the former regionally restricted circulation in the South Atlantic gave way to meridional overturning circulation ventilating the basins of the Southern Ocean (Poulsen *et al.*, 2001). Donnadiou *et al.* (2016) suggested only sluggish deep water circulation in the western Indian Ocean during the Turonian, while an increase in salinity in the southern latitudes might have temporarily enhanced convection in the Indian Ocean during the peak of the Cretaceous greenhouse in the early Turonian (Poulsen *et al.*, 2003). The final establishment of an open deep water circulation in the Indian Ocean is inferred ~90 Ma by Lawver *et al.* (1992), even though Schlüter and Uenzelmann-Neben (2008a) reported indications for restricted circulation in the Transkei Basin until the early Campanian.

Multiple authors suggested a trend towards diminished vertical stratification of the water masses during the Late Cretaceous and introduced Northern Component Water or Southern Component Water as driving mechanism of ocean circulation (e.g., Murphy and Thomas, 2013; Voigt *et al.*, 2013). The ongoing opening of the South Atlantic Ocean is proposed to correspond to a marked change in global ocean circulation during the Campanian (e.g., Martin *et al.*, 2012), and great importance is assigned to the subsidence of the Rio Grande Rise/Walvis Ridge System (RWS) enabling water mass exchange between the North and South Atlantic through the Equatorial Atlantic Gateway (Robinson and Vance, 2012; Moiroud *et al.*, 2016). Gradual seafloor spreading and subsidence of parts of barriers like the Kerguelen Plateau promoted Southern Component Water flow into the southwestern Indian Ocean and is suggested to have constantly altered the Late Cretaceous regional circulation pattern (Robinson *et al.*, 2010; Murphy and Thomas, 2013).

5.2.2. Contourite drifts

Contourite drifts are sediments deposited or significantly affected by the action of semipermanent bottom currents, usually resulting from thermohaline and/or wind-driven circulation in the oceans (Stow *et al.*, 2002; Rebesco *et al.*, 2008; Stow and Faugères, 2008; Rebesco *et al.*, 2014). The term semipermanent is used because bottom currents are highly variable in intensity, direction and precise location at any one time (Stow *et al.*, 2002). Those variations in bottom current intensities are responsible for accumulation of mounded and sheeted drifts (moderate intensities) as well as for episodes of non-deposition or erosion (increased intensities), which generate erosional structures or hiatuses (Faugères *et al.*, 1999; Stow *et al.*, 2002; Shanmugam, 2008; Stow *et al.*, 2009). Such events can have either a climatic origin, linked to the variation in the extent of polar ice caps and sea ice, or a tectonic cause, for example the opening and closing of gateways that control bottom water exchange between ocean basins (Faugères *et al.*, 1999; Rebesco *et al.*, 2014).

The architecture of deposits within a drift is complex and marked by an alternation of periods of sedimentation and erosion or non-deposition resulting in discontinuities and variations of seismic reflection characteristics (e.g., Faugères *et al.*, 1999). While homogenous seismically transparent units may point towards stable moderate flow intensities, high amplitude reflector sequences can indicate large temporary changes in current strength or sediment supply (Nielsen *et al.*, 2008). The identification and description of contourite drifts and erosional structures based on seismic reflection data therefore offers the possibility to study changes in palaeocean circulation and correlate them with changes in palaeogeography or climate events.

5.2.3. Seismic stratigraphy

The Alfred Wegener Institute, Helmholtz Centre for Polar and Marine Research acquired 24 high-resolution MCS reflection profiles with a total length of about 4600 km on board RV *Sonne* during expeditions SO 182 in 2005 and SO 232 in 2014 in the area of the MozR (black lines in Figure 5.1b). The seismic profiles cover the three segments of the southern MozR, in particular the central MozR (cMozR), the southwestern MozR (swMozR), and the southeastern MozR (seMozR), as well as the transition zone to the adjacent basins (Figure 5.1b). The data were correlated with results of DSDP Site 249 (orange star in Figure 5.1a; Simpson *et al.*, 1974) and a palaeoceanographic interpretation of a seismic profile recorded during cruise So 182 (Uenzelmann-Neben *et al.*, 2011). We here apply the seismic stratigraphy shown in Table 5.1 and explained in detail in Fischer *et al.* (2017).

The lowermost unit is characterized by piecewise-continuous high amplitude, low frequency reflections reaching up to 800 ms TWT below the unit's top (Figure 5.2). The top of the unit is defined by a strong impedance contrast with a sudden velocity increase to its overlying unit, appears rugged and hummocky, and shows a wide range in observed depths. Fischer *et al.* (2017) correlate the unit with the Lower Cretaceous basaltic basement drilled at Site 249 that erupted either subaerially or in shallow waters (Girdley *et al.*, 1974; Simpson *et al.*, 1974; Jacques *et al.*, 2015).

Two Cretaceous seismic units, the largely Early Cretaceous unit S1 (<128.66–100 Ma), and the Late Cretaceous unit S2a (75–68 Ma) overlie basement (Fischer *et al.*, 2017). The uppermost seismic unit S2b is of Late Cenozoic age (≤ 15 Ma) and will therefore not be discussed here. Please refer to Fischer *et al.* (2017) for a description of that particular seismic unit. Seismic unit S1 fills and drapes the magmatic basement. The unit shows low to medium frequency reflections with weaker amplitudes in its lower part and medium to strong amplitude reflections in its upper part. The reflections are mostly conformable and appear more continuous in the upper part of the unit. The top of unit S1 seems to be affected by erosional truncation and is marked by a strong amplitude reflection and a distinct difference in geometry to the overlying unit. Fischer *et al.* (2017) correlated the unit to the Neocomian

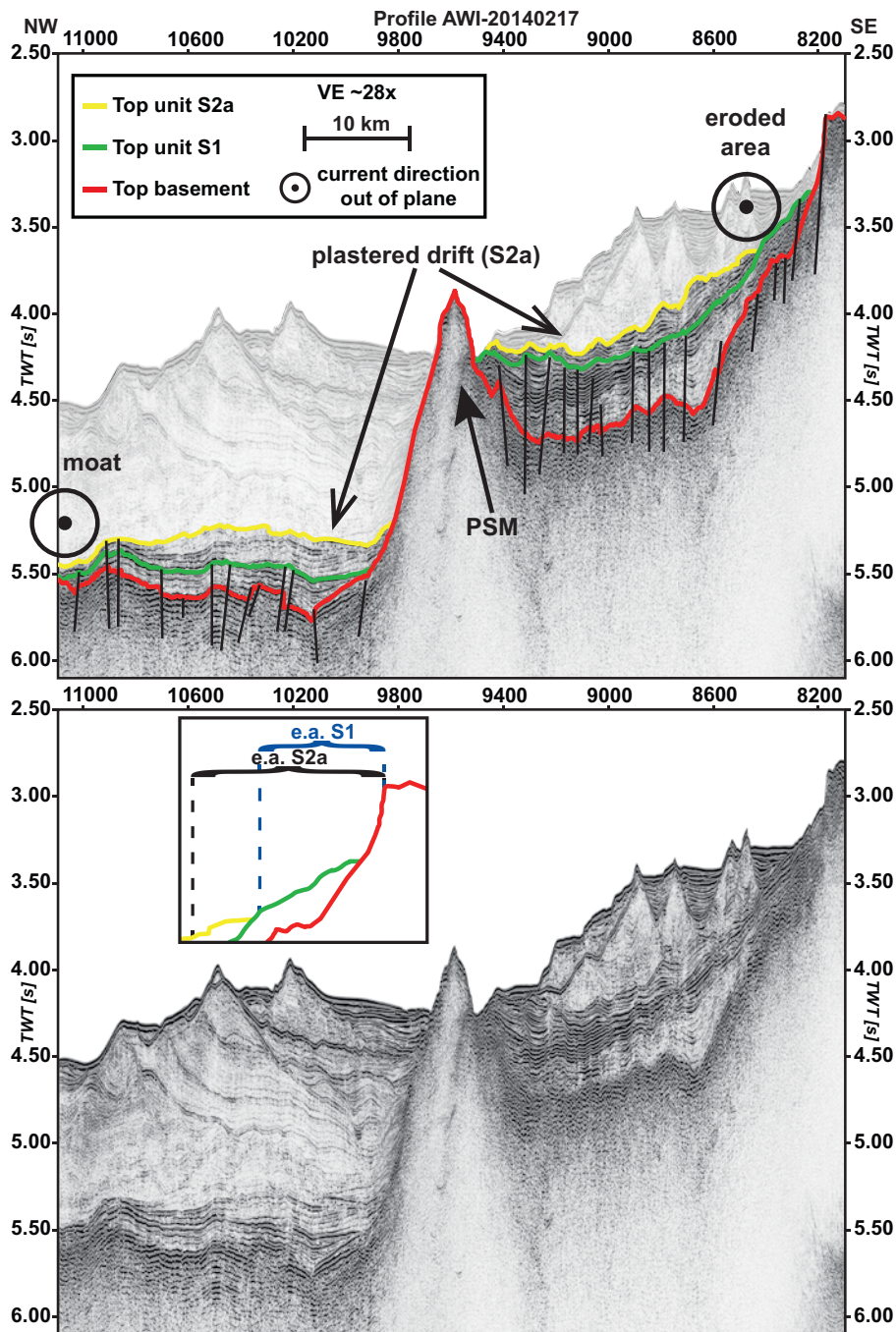


Figure 5.2. Part (interpreted/uninterpreted) of MCS profile AWI-20140217 showing the seismic stratigraphy of the Cretaceous units in the study area. Location of profile is shown in Figure 5.1b. For a description of the units refer to chapter 5.2.3. Thick yellow line = top of late Campanian to late Maastrichtian unit S2a, thick green line = top of Barremian to early Cenomanian unit S1, thick red line = top of basement. Black circle denotes current direction during deposition of the late Campanian to late Maastrichtian unit. Black lines indicate faults. PSM = Post-sedimentary Neogene magmatism. The younger deposits are masked in the interpreted section. For horizontal scale and vertical exaggeration refer to legend. The inset illustrates the increase in width of the eroded areas (e.a.) of seismic unit S2a (in black) compared to that of seismic unit S1 (in blue).

to Albian terrigenous silty claystone and volcanic siltstone of Site 249, which are topped by a ~25 Myr hiatus (Girdley *et al.*, 1974; Simpson *et al.*, 1974).

The overlying seismic unit S2a usually thins towards basement highs and, where deposited, roughly follows the topography of unit S1. The reflections are characterized by discontinuous medium amplitudes of lower frequencies that onlap onto unit S1. In some parts the unit seems to be almost transparent (e.g., Figure 5.2 CDPs 10200-10600). The unit's reflections show a wavy geometry and

differ significantly from the reflections of seismic unit S1. Fischer *et al.* (2017) correlated unit 2a with the Late Cretaceous (Campanian to Maastrichtian) biogenic sediments (clay-rich nanno chalk) described by Simpson *et al.* (1974), which are topped by a ~50 Myr hiatus.

Table 5.1. Seismic stratigraphy of the Cretaceous seismic units in the study area.

Cretaceous seismic units of the southern Mozambique Ridge	Unit S2a	Unit S1	Basement
Thickness (ms TWT); RMS thickness (ms TWT)	0–840; 160	0–611; 131	
Age (Ma) ^a	75–68	<128.66–100	130.86–124.90
Material ^a	Clay-rich nanno chalk (biogenic)	Silty claystone (terrigenous) and volcanoclastics	Basalt
Seismic characteristics ^b	discontinuous reflections with moderate amplitudes and low to medium frequency; occasionally more continuous reflections with stronger amplitudes	Medium to strong amplitude reflections of lower frequency; stronger amplitudes and more continuous in upper part; weaker amplitudes in lower part	Strong impedance contrast at top; high amplitude, low frequency reflections; subparallel sequences of internal reflections, piecewise continuous and up to 800 ms TWT deep
Remarks	Hiatus on top of S2a	Hiatus on top of S1; age of oldest deposits decrease to the South due to younger basement; layers with TOC up to 1.7%	

^aSimpson *et al.* (1974); ^bFischer *et al.* (2017)

5.3. Methods

For the study of the Early to Late Cretaceous depositional conditions at the MozR we applied the seismostratigraphic model of Fischer *et al.* (2017) and mapped the seismic units throughout the study area. Due to the spacing of the seismic reflection data the resulting maps (e.g., Figure 5.3) are afflicted with uncertainties in the uncovered areas. Nonetheless, the general thickness and depth trend of the depicted sedimentary deposits are correct.

We calculated the depth of the three seismic horizons, which were used to compute the thickness of both sedimentary units S1 and S2a. The isolines of the root mean square (rms) thickness were used to define the outlines of sediment depocentres. The orientation and location of those features are interpreted with respect to the prominent basement elevations of the MozR and the morphology of the underlying horizon. Depocentres may indicate whether sedimentation was mainly gravity or bottom current controlled, that is depocentres oriented parallel to the slope are interpreted to document dominance of bathymetric contour-parallel sediment transport, whereas a depocentre perpendicular to the bathymetric contours is interpreted to indicate dominance of down-slope sediment transport (Uenzelmann-Neben and Gohl, 2014).

Our interpretation of the pathways and intensities of the palaeocurrents is based on the identification and classification of sediment drifts and erosional structures under the assumption that bottom currents in the southern hemisphere are deflected to the left by Coriolis force and erode the left flank of the drift, whereas slower flow and deposition occurs on the right flank (Faugères *et al.*, 1999). Variations in bottom current activity at the MozR were correlated with palaeoceanographic events

and tectonic and palaeogeographic changes to develop a reconstruction of Early to Late Cretaceous current circulation in the study area.

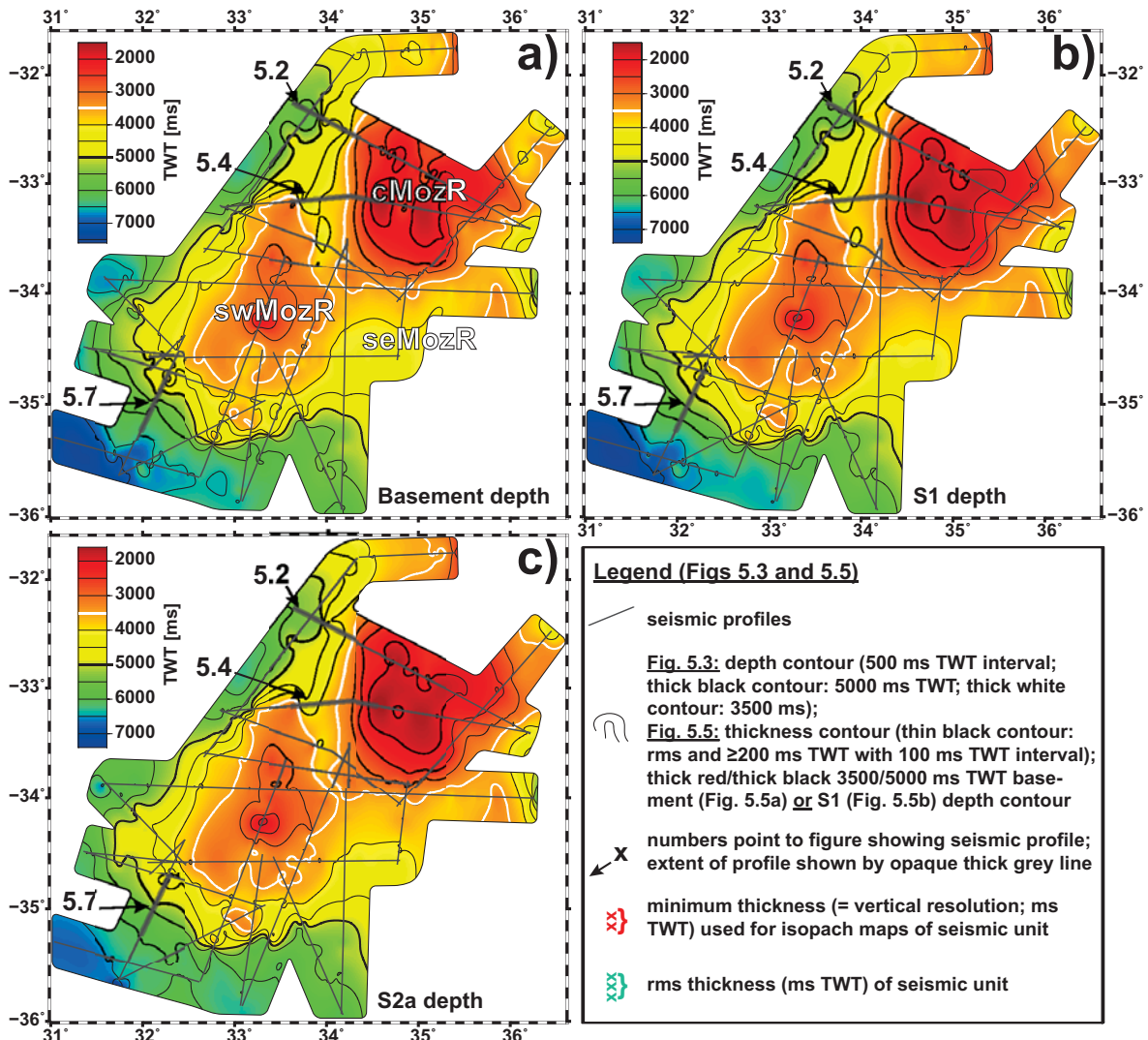


Figure 5.3. Depth maps (ms TWT) of top Early Cretaceous basement (a), top Barremian to early Cenomanian seismic unit S1 (b) and top late Campanian to late Maastrichtian seismic unit S2a (c). cMozR = central Mozambique Ridge, swMozR = southwestern Mozambique Ridge, seMozR = southeastern Mozambique Ridge. Refer to legend for further description.

5.4. Results

5.4.1. Distribution of seismic units

5.4.1.1. Basement

With its highest areas reaching up to 1600 ms TWT below sea level (Figure 5.3a, 34.6°E/33.1°S; Figure 5.4 CDPs 1000-1500) the segments of the southern MozR significantly contrasts with the basement topography of the surrounding basins. To the W and S the basement depth increases sharply to depths more than 5000 ms TWT (Figure 5.2; thick black contour in Figure 5.3a) with the maximum depth of 7550 ms TWT (Figure 5.3a, 31°E/35.3°S) being located in the northeastern branch of the Transkei Basin. Overall, the basement has a rms depth of 4533 ms TWT.

We observe a roughly N-S striking basement trough between the cMozR and the swMozR (Fig-

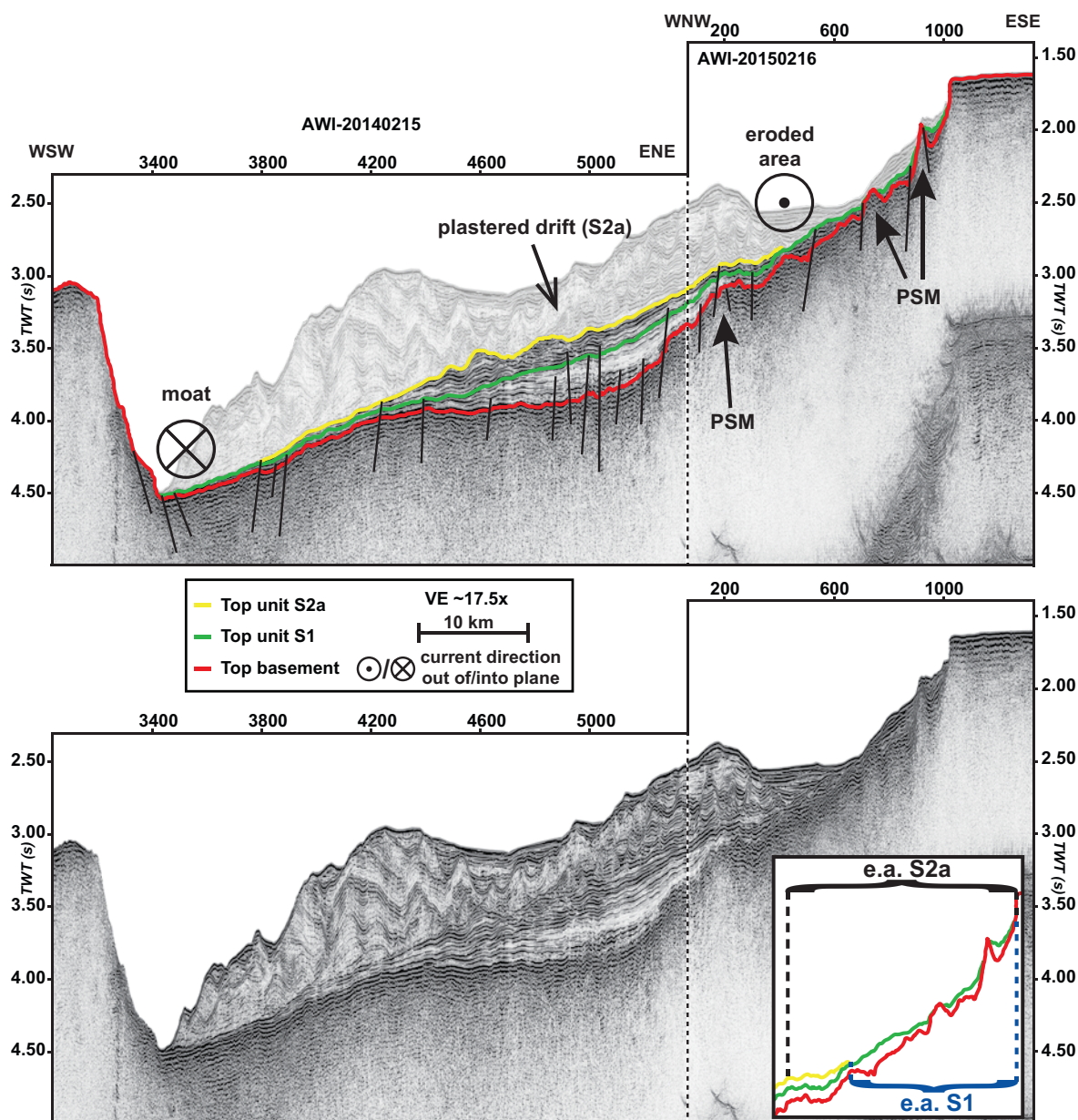


Figure 5.4. Part (interpreted/uninterpreted) of MCS profiles AWI-20140215 and AWI-20140216 showing the seismic stratigraphy of the Cretaceous units in the study area. Location of profile is shown in Figure 5.1b. For a description of the units refer to chapter 5.2.3. For line colours, symbols, horizontal scale and vertical exaggeration refer to legend. PSM = Post-sedimentary magmatism. The younger deposits are masked in the interpreted section. The inset illustrates the increase in width of the eroded areas (e.a.) of seismic unit S2a (in black) compared to that of seismic unit S1 (in blue).

ure 5.3a; Figure 5.4 CDPs 3300-5300) and several local depressions (Figure 5.3a, 33.2°E/34.6°S, 36.1°E/32.8°S, 35°E/32.9°S). Additional basement peaks can be observed along the flanks and on top of the segments of the southern MozR, locally deforming the overlying Cretaceous sedimentary units (Figure 5.2 CDPs 9300-9800). These basement peaks were proposed to be of post-sedimentary magmatic (PSM), probably Neogene origin by Fischer *et al.* (2017).

5.4.1.2. Early Cretaceous unit S1

Early Cretaceous unit S1 lies above the seismic basement and drapes the basement topography (Figure 5.2 CDPs 8200-9400). Due to the rugged basement below, the thickness of unit S1 is highly

variable ranging from 0 to 611 ms TWT and usually decreases towards basement highs (Figure 5.2 and Figure 5.5a). The depocentres are defined by a thickness of more than 131 ms TWT (= rms thickness). We observe a rather random distribution of depocentres with no indications for deposition parallel to the bathymetric contours (thick black and magenta basement depth contours in Figure 5.5a). Several depocentres are located in local basement depressions on top of the MozR segments (e.g., Figure 5.5a, 35°E/32.9°S).

The top of unit S1 shows the same attributes as the underlying top of basement but with a smoother, more gradual increase in depth away from the MozR (Figure 5.3b). Again, we observe a NS trending trough between the cMozR and the swMozR that appears narrower and slightly shallower than at basement depth level due to the sedimentary load of unit S1 (Figure 5.3b; Figure 5.4 CDPs 3300–5300). With a rms depth of 4355 ms TWT unit S1 is roughly 180 ms TWT shallower than the basement. The unit's rms thickness, average seismic velocity and age yield a sedimentation rate of $\sim 6 \text{ m Myr}^{-1}$, which is slightly higher than the published sedimentation rate for the northern MozR of 5 m Myr^{-1} (Simpson *et al.*, 1974).

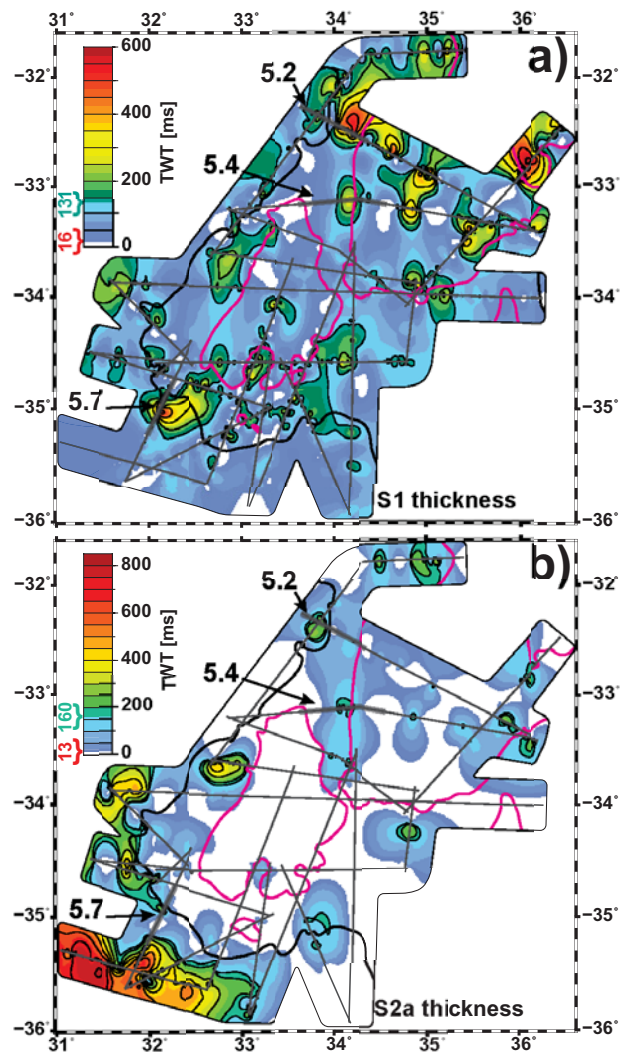


Figure 5.5. Isopach maps (ms TWT) of Barremian to early Cenomanian seismic unit S1 (a) and late Campanian to late Maastrichtian seismic unit S2a (b). Colours and symbols described in legend of Figure 5.3.

5.4.1.3. Late Cretaceous unit S2a

Deposits of the late Campanian to late Maastrichtian seismic unit S2a show a highly variable thickness ranging from 0 to 840 ms TWT (Figure 5.5b). Depocentres are characterized by a thickness greater than 160 ms TWT (= rms thickness) and are primarily located below the 5000 ms TWT unit S1 depth contour (thick black contour in Figure 5.5b). Most of the depocentres are elongated parallel to the bathymetric contours of the underlying seismic unit S1 (Figure 5.2 CDPs 8450–9450, 9800–11100, and Figure 5.4 CDPs 3550/AWI-20140215–400/AWI-20140216; thick red and black contour in Figure 5.5b).

We observe a pronounced depocentre in the SW of the study area (Figure 5.5b) whose vast extent is the main reason for a 22% increase in rms thickness relative to unit S1. We find little to no sedimentary cover above ~ 3500 ms TWT (Figure 5.2 CDPs 8100–8450, and Figure 5.4 CDPs 400–1350; thick red contour in Figure 5.5b). There are two exceptions to this observation, small depocentres located in local depressions (e.g., Figure 5.5b, 34.9°E/33.2°S), and two larger depocentres located on the eastern flank of the cMozR (Figure 5.5b, 35.8°E/33.2°S and 36.1°E/32.8°S).

The depth map shows only slight variations on top of the MozR segments (≤ 3500 ms TWT; thick white line in Figure 5.3c) but changes significantly in the transition to the surrounding basins (Figure

5.3c). Due to most of the unit's deposits being located below the 5000 ms TWT depth contour (thick black contour in Figure 5.3c and Figure 5.5b) the unit's rms depth increases to 4654 ms TWT. Compared to the underlying unit S1, the sedimentation rate strongly increases to $\sim 24 \text{ m Myr}^{-1}$, which is slightly higher than the 20 m Myr^{-1} stated for the northern MozR (Simpson *et al.*, 1974).

5.4.2. Current controlled sedimentation in the study area

Seismic characteristics typical of current controlled sedimentation and sediment drifts have been investigated by several authors in great detail (e.g., Faugères *et al.*, 1999; Stow *et al.*, 2002; Uenzelmann-Neben *et al.*, 2007; Nielsen *et al.*, 2008; Rebesco *et al.*, 2014), and are summarized by Müller-Michaelis *et al.* (2013) to comprise of high- to moderate amplitude reflections caused by changes in current attributes (e.g., velocity), (basal) erosional unconformities due to intense currents with onlap or low-angle downlap of overlying reflections, a general orientation of deposits along the bathymetric contours, and distinct drift geometries (e.g., plastered drifts or mounded drifts).

Based on the identification of those characteristics we found two locations in the study area where previously unknown Late Cretaceous ($\sim 75\text{--}68 \text{ Ma}$) sediment drifts (red lines in Figure 5.6) can be observed: at the flanks of the MozR and within the trough between the swMozR and the cMozR (Figure 5.4 CDPs 3550/AWI-20140215–400/AWI-20140216).

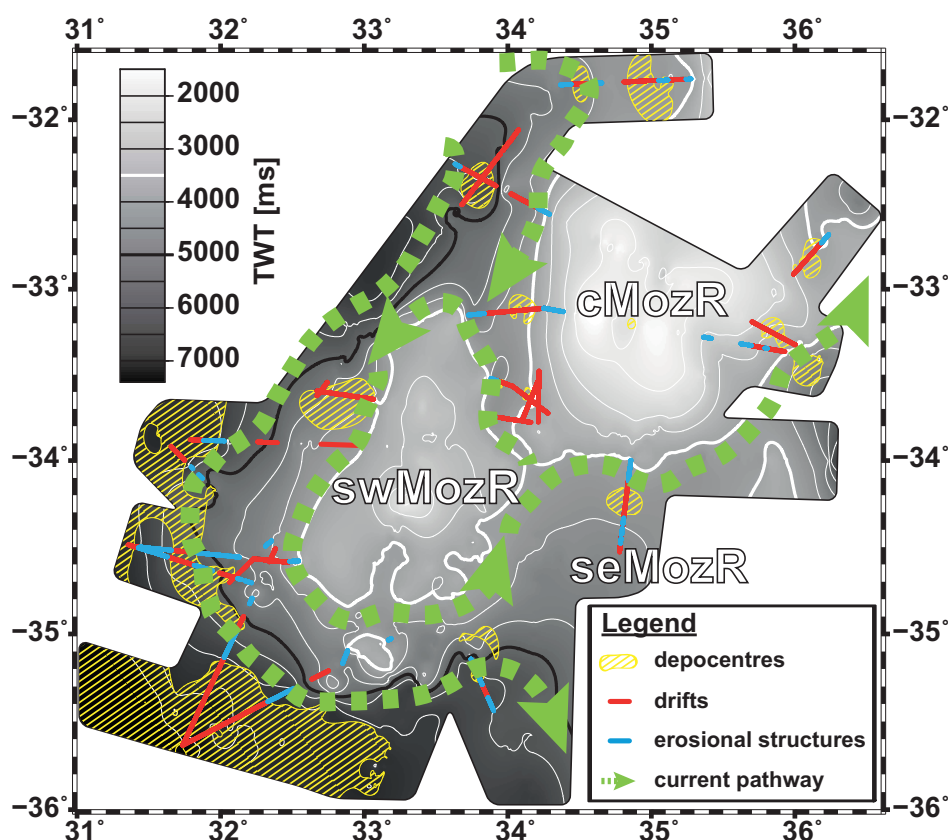


Figure 5.6. Greyscale depth map (ms TWT) of top seismic unit S1 with observed depocentres (thickness > rms value; hatched in yellow), drift bodies (red lines) and erosional structures (blue lines) of the late Campanian to late Maastrichtian seismic unit S2a. Thin white 500 ms TWT S1 depth contour lines (thick white contour line = 3500 ms TWT depth; thick black contour line = 5000 ms TWT depth). The green dashed arrow shows the inferred current pathway during deposition of seismic unit S2a.

5.4.2.1. Late Cretaceous (late Campanian to late Maastrichtian) sediment drifts

Late Cretaceous seismic unit S2a shows several drift bodies plastered onto the flanks of the MozR that either show a very low-relief geometry typical for sheeted drifts (Figure 5.2 CDPs 8450–9450, 9800–10900, and Figure 5.7 CDPs 3800–4350), or are associated with a moat and a slope break (steep to gentle) typical for separated drifts (Figure 5.7 CDPs 2650–3050). At the western flank of the cMozR a plastered drift is located that is dissected by a ~12.5 km wide PSM structure (Figure 5.2 CDPs 9300–9800). The drift shows a maximum thickness of ~225 m and decreases in thickness towards its flanks (Figure 5.2 CDPs 8450–9450, 9800–10900). The lateral extent in NW-SE direction is approximately 60 km. It has a broad low-mounded geometry and is deposited on top of the early Cenomanian to late Campanian unconformity.

The seismic reflections are of moderate amplitude, discontinuous and in some parts the drift appears more or less transparent. We observe several discontinuities and pinch out of the seismic reflections at the base of the overlying Maastrichtian to middle Miocene unconformity. Southwest of the swMozR we observe remnants of a separated sediment drift (Figure 5.7 CDPs 2650–3050). The strongly eroded drift body is confined to the northeast by a moat (Figure 5.7 CDPs 2150–2300) and pierced by two PSM structures (Figure 5.7 CDPs 2300–2400, 2650–2700). The moat is located at a slope break of the swMozR from steep in the NE to gentle in the SW. The separated drift has a maximum thickness of ~300 m and an extent of ~17.5 km in NE-SW direction. The drift seems to extend further to the north roughly following the 5000 ms TWT S1 depth contour (thick black contour in Figure 5.6) and coinciding with the extent of the depocentre (yellow shaded area in Figure 5.6, 31.6°E/33.7°S to 32.1°E/35°S). We observe a consistent depth of ~4800 ms TWT at its top and ~5250 ms TWT at its base in all seismic profiles crossing the drift body. The seismic reflections are of low to medium amplitude and mostly discontinuous.

We observe a second drift body in the southwest of the swMozR that is located at least ~1500 ms TWT deeper than the separated drift described before (Figure 5.7 CDPs 3800–4350). Based on our seismic data we observe a maximum thickness of ~400 m (~300 m in Figure 5.7 CDP 4200) and a maximum extent of ~65 km in NE-SW direction (Figure 5.6, 31.7°E/35.6°S to 32°E/35.1°S). The discontinuous seismic reflections are of low to medium amplitude and show a slight increase in amplitude and continuity to the top. Due to its morphological context it can best be described as a sheeted drift that probably extends into the abyssal plain.

Within the trough between the cMozR and swMozR a ~26 km wide (E-W) drift complex plastered onto the westward dipping flank of the cMozR is observed (Figure 5.4 CDP 4400 of AWI-20140215 to CDP 200 of AWI-20140216). The low-mounded drift body has a maximum thickness of ~275 m that decreases on its margins. We observe medium to strong amplitude with alternating transparent intervals. The sub-parallel, discontinuous reflections pinch out at the basal reflector of the overlying unit. Similar drifts seem to occur at several locations within the trough (Figure 5.6, red lines between 33.1°S to 33.8°S).

5.4.2.2. Erosional structures

A large number of erosional structures (moats, eroded areas; blue lines in Figure 5.6) are observed that are interpreted to mark the flow axis of the palaeocurrent. These features indicate periodic erosion and/or non-deposition. In the western part of the trough between the cMozR and the swMozR a moat contouring the basement of the swMozR (Figure 5.4 CDPs 3300–4400) is observed. The width of the moat changed from ~20 km in the Early Cretaceous seismic unit S1, to ~27.5 km during deposition of seismic unit S2a, to ~5 km during deposition of the Neogene and Quaternary seismic unit S2b.

Several eroded areas occur in the study area that all show alternating widths with time (e.g., Figure

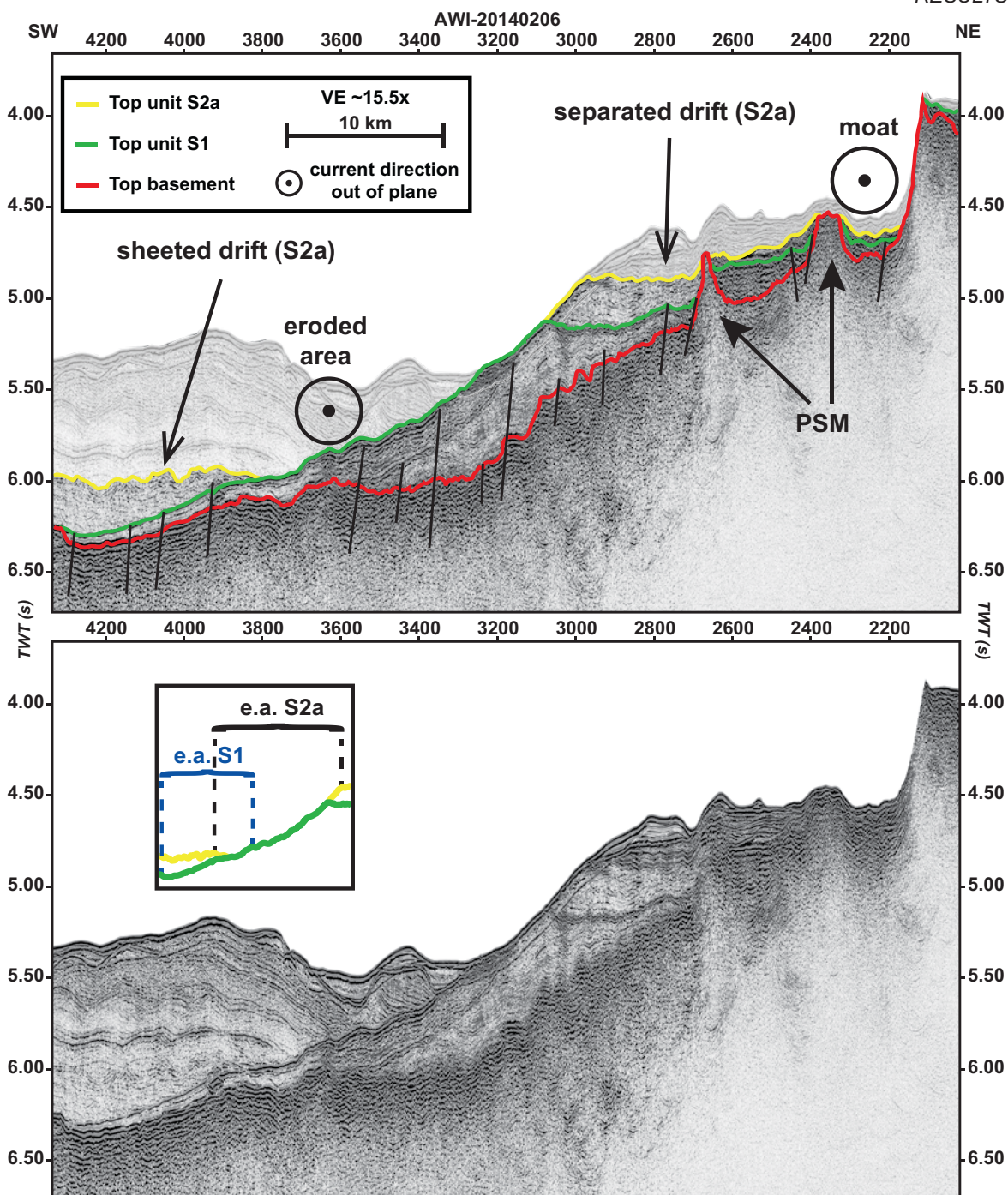


Figure 5.7. Part (interpreted/uninterpreted) of MCS profiles AWI-20140206 showing the seismic stratigraphy of the Cretaceous units in the study area. Location of profile is shown in Figure 5.1b. For a description of the units refer to chapter 5.2.3. For line colours, symbols, horizontal scale and vertical exaggeration refer to legend. PSM = Post-sedimentary magmatism. The younger deposits are masked in the interpreted section. The inset illustrates the increase in width of the eroded areas (e.a.) of seismic unit S2a (in black) compared to that of seismic unit S1 (in blue).

5.2 CDPs 8200–8500 and inset, Figure 5.4 CDPs 200–1000 and inset, Figure 5.7 CDPs 2950–3900 and inset; blue lines in Figure 5.6). Furthermore, we observe a shift from the occurrence of wider eroded areas during Cretaceous to the development of narrower moats during late Cenozoic times. This is documented by the erosional structure at the NW flank of the cMozR that shows a ~5 km wide eroded area (Figure 5.2 CDPs 8200–8400) at the top of seismic unit S1, which increases to ~8.8 km (Figure 5.2 CDPs 8200–8550) during deposition of seismic unit S2a, finally showing a ~3.8 km wide moat in late Cenozoic times (Figure 5.7 CDPs 8300–8450). Similar observations can be made for the erosional structure in the trough between the cMozR and the swMozR (Figure 5.4 CDPs 200–1000).

The eroded area shows an extent of ~15 km (Figure 5.4 CDPs 400–1000; Late Cretaceous seismic unit S1) and ~20 km (Figure 5.4 CDPs 200–1000; Late Cretaceous seismic unit S2a), respectively, and develops into a ~4 km wide moat (Figure 5.4 CDPs 300–700) in the late Cenozoic. The eroded area between the two sheeted and separated drifts in the SW shows a width of ~17.5 km at the top of seismic unit S1 (Figure 5.7 CDPs 3600–4300), widens to ~24 km during deposition of the Late Cretaceous seismic unit S2a (Figure 5.7 CDPs 2950–3900), and separates into a ~10 km (Figure 5.7 CDPs 3000–3400) and a ~5 km wide moat (Figure 5.7 CDPs 3500–3700) in Late Cenozoic times (seismic unit S2b).

5.5. Discussion

In the following we propose a model for the Cretaceous palaeoceanographic circulation in the area of the MozR and its surrounding basins to the west (hereinafter simplified to 'study area'). The model comprises three time intervals: (1) the Early Cretaceous (until ~100 Ma, Barremian to early Cenomanian), (2) the Late Cretaceous hiatus (~100–75 Ma, early Cenomanian to late Campanian), and (3) the Late Cretaceous (~75–68 Ma, late Campanian to late Maastrichtian). It is based on our observations at the MozR and published palaeoceanographic and palaeogeographic data. We used a recent palaeobathymetric reconstruction by Castellino *et al.* (2016) for our model, but need to emphasize that their reconstruction of the African–Southern Ocean (A–SO) gateway is based on certain assumptions and simplifications (e.g., negligible sediment cover over MozR, poor understanding of thermal evolution of LIPs; see publication for further details) and therefore subject to considerable uncertainty. Owing to the sparse data about palaeocirculation in our study area we want to emphasize that the proposed circulation scheme (Figure 5.8) should only be seen as tentative. Nonetheless, we think it provides a good approach to interpret the observed depositional patterns at the MozR in a broader context.

5.5.1. Early Cretaceous (until ~100 Ma; unit S1)

The Early Cretaceous (<128.66–100 Ma) seismic unit S1 at the southern MozR appears as a fill and drape of the magmatic basement with the internal reflector geometry reflecting basement topography (e.g., Figure 5.2 CDPs 10000–10800). The mostly conformable reflections show weaker amplitudes in the lower part of the unit and medium to strong amplitudes with more continuous reflections in the upper part (e.g., Figure 5.2 CDPs 8500–9400). Our observations indicate continuous sedimentation subsequent to the subaerial or submarine emplacement of the MozR. Terrigenous sediments followed by volcanoclastics were observed within the Aptian section at DSDP Site 249 (orange star in Figure 5.1a; Girdley *et al.*, 1974; Sigal, 1974; Simpson *et al.*, 1974; Vallier, 1974). This correlates well with the observed changes in reflection characteristics. Furthermore, we interpret the occurrence of the volcanogenic sediments in the upper part of seismic unit S1 as an indicator of renewed volcanic activity during late Early Cretaceous (~Albian).

The Early Cretaceous deposits drilled at DSDP Site 249 were reported to be rich in organic carbon (average content of 1.5%) resulting from deposition under euxinic conditions (Girdley, 1974; Simpson *et al.*, 1974; Vallier, 1974; Vallier and Kidd, 1977). Vallier and Kidd (1977) interpreted the lithostratigraphy of the Early Cretaceous unit to represent deposition in a relatively deep basin, and Girdley *et al.* (1974) correlated the deposits with the Aptian to Cenomanian marine Domo Formation found in the southern part of Mozambique (Flores, 1973). Flores (1973) proposed that the Domo Formation was deposited as a result of south to north transgression in a graben-like structure where euxinic conditions prevailed and attributed the formation of the structure to Gondwana breakup. Our observation of the partly terrigenous unit S1 on top of the MozR segments (Figure 5.5a) supports a

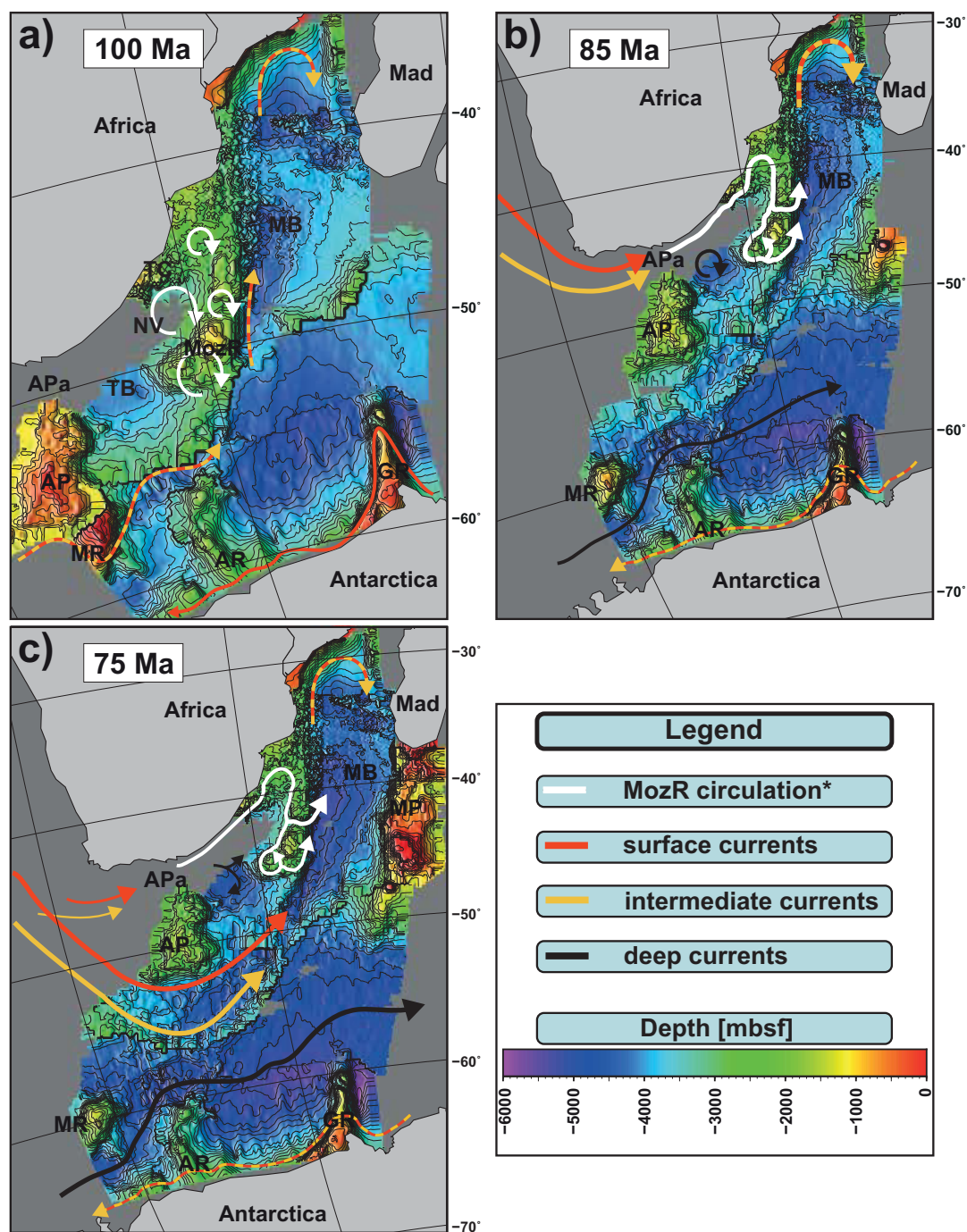


Figure 5.8. Palaeoceanographic evolution of the study area. Modified after the palaeobathymetric reconstruction of the African-Antarctic corridor by Castellino *et al.* (2016) for 100 Ma (a), 85 Ma (b) and 75 Ma (c). Dark grey represent areas not included in their palaeobathymetric reconstruction. White arrows = current pathway in the study area inferred by our data and other studies (Dingle *et al.*, 1978; Dingle and Camden-Smith, 1979; Martin *et al.*, 1982; Meyers and Dickens, 1992). Red/yellow arrows = surface/intermediate current pathways (Donnadieu *et al.*, 2016; Uenzelmann-Neben *et al.*, 2016), black arrows = deep current pathway (Schlüter and Uenzelmann-Neben, 2008b; Donnadieu *et al.*, 2016). Circular arrows = restricted (non-vertical) circulation with partly euxinic conditions. AP = Agulhas Plateau, AR = Astrid Ridge, GR = Gunnerus Ridge, Mad = Madagascar, MB = Mozambique Basin, MozR = Mozambique Ridge, MP = Madagascar Plateau, MR = Maud Rise, NV = Natal Valley, TB = Transkei Basin, TC = Tugela Cone.

submarine deposition of the sediments and indicates that the MozR was subjected to subsidence after emplacement of the basaltic basement. The initiation of a marine depositional environment subsequent to the formation of the MozR was thus probably a consequence of both subsidence of the LIP and the proposed south to north transgression.

Based on the analysis of palaeoenvironmental proxies Dingle and Lavelle (2000) postulated that only small semi-isolated basins existed in the Southern Ocean before Albian times. DSDP and ODP drill results show that deposition of sediments under euxinic conditions was a common phenomenon during most of the Early Cretaceous in the evolving Indian Ocean (Meyers and Dickens, 1992). A recently published study by Uenzelmann-Neben *et al.* (2016) based on seismic reflection data and numerical models suggests that a weak circulation of Upper Pacific Water (UPW), Intermediate Pacific Water and Atlantic Intermediate Water through the A–SO gateway into the Indian Ocean commenced in Albian times (red and yellow arrows in Figure 5.8a). We observe no indications of current influence on the deposition of seismic unit S1. In fact the seismic characteristics throughout unit S1 (e.g., conformable reflections; Figure 5.4 CDPs 4600–5200) point to a rather undisturbed deposition of the sediments. This raises the question why the postulated shallow and intermediate circulation did not affect the Early Cretaceous sedimentation at the MozR. A possible reason might be the Falkland Plateau, the Maurice Ewing Bank and the developing Agulhas–Falkland Fracture Zone obstructing the circulation from entering our study area from the west (Ben-Avraham *et al.*, 1997; König and Jokat, 2010). We hypothesize that together with the MozR and the subaerial Agulhas Plateau, which was emplaced between 105 and 95 Ma (Parsiegla *et al.*, 2008), those structures acted as an entity that hindered inflow into our study area. This resulted in an isolation of our study area, therefore providing the required conditions for a continuous deposition under euxinic conditions (circular white arrows in Figure 5.8a) even after the surface to intermediate circulation between the Southern Atlantic and Indian Oceans commenced.

5.5.2. Late Cretaceous hiatus (~100–75 Ma)

Based on our seismic records the southern MozR seems to be barren of early Cenomanian to late Campanian (~100–75 Ma) deposits. We observe truncation of the Early Cretaceous unit's S1 top and pinch out of its reflections against the overlying Late Cretaceous unit S2a (e.g., Figure 5.2 CDPs 9000–9350, Figure 5.4 CDPs 4500–5000, Figure 5.7 CDPs 7000–7300). The transition from seismic unit S1 (≥ 100 Ma) to the overlying seismic unit S2a (≤ 75 Ma) is marked by a distinct impedance contrast along with an apparent difference in the geometry of the reflections (e.g., Figure 5.2 CDPs 8600–9400 and Figure 5.7 CDPs 2800–3800). The seismic profiles show the occurrence of moats and eroded areas at the top of unit S1 at multiple locations (e.g., Figure 5.2 CDPs 8200–8400, Figure 5.4 CDPs 3300–4000, Figure 5.7 CDPs 3600–4300). Episodes of particularly intense bottom current activity are documented in such erosional features (Faugères *et al.*, 1999; Stow *et al.*, 2002; Stow *et al.*, 2009). We interpret the unconformity associated with the ~25 Myr gap to correspond to the Late Cretaceous hiatus displayed at DSDP Site 249 on the northern MozR (Simpson *et al.*, 1974). According to the palaeobathymetric model by Castelino *et al.* (2016) the shallowest parts of the southern MozR resided in palaeodepths between ~900 (≤ 100 Ma) and ~1500 m (≥ 75 Ma) during the hiatus (Figure 5.8). These palaeodepths would favour an erosive intermediate and deep circulation as the cause for the Late Cretaceous unconformity at the southern MozR. However, the continuous sedimentary record in the nearby Transkei Basin (Schlüter and Uenzelmann-Neben, 2007) questions the occurrence of a Late Cretaceous erosive deep circulation. The absence of a vigorous deep circulation is supported by the observation of Late Cretaceous black shales in the Transkei Basin, which were deposited in palaeodepths of 2200 to 3100 m according to Schlüter and Uenzelmann-Neben (2008a). They attributed their occurrence to the Agulhas Falkland Fracture Zone and the Agulhas Plateau obstructing the pathway for deep circulation through the Agulhas Passage at least until 85 to 80 Ma. The erosive circulation causing the hiatus at the MozR was thus most likely limited to shallower depths.

Girdley *et al.* (1974) proposed a correlation of the hiatus at the MozR with both an uplift of the MozR and a mainland regression discussed by Kent (1974). Evidence for a probable uplift of the MozR is documented by the faulting of the basement and seismic unit S1 (black lines in Figure 5.2, Figure 5.4 and Figure 5.7) for which Fischer *et al.* (2017) proposed an age of ~100 Ma. This timing correlates with the deposition of the volcanogenic sediments in the upper part of seismic unit S1 that show characteristics typical for submarine or subaerial eruptions (Vallier, 1974). A mid-Cretaceous magmatic reactivation of the MozR would have resulted in a decrease of its palaeodepth and thus made it susceptible to a shallow erosive circulation. We therefore hypothesize that an ~Albian to early Cenomanian magmatic reactivation caused an uplift of the MozR, which resulted in the occurrence of the hiatus due to shallow current activity and/or by subaerial erosion. The simultaneous deposition of black shales in the Transkei Basin points towards a strong vertical layering of the water column and thus somewhat euxinic deep circulation possibly due to a tectonic cut-off of this already deep basin (circular black arrow in Figure 5.8b).

At least ~25 Myr of the sedimentary record above the 100±5 Myr old Agulhas Plateau basement is missing (Tuchołke and Carpenter, 1977; Tuchołke and Embley, 1984; Uenzelmann-Neben, 2002). Uenzelmann-Neben (2002) interpreted the ~Albian/Cenomanian to ~Maastrichtian hiatus to be a document of strong erosion. According to Parsieglia *et al.* (2008) parts of the Agulhas Plateau were subaerial at least until ~80 Ma, which offers the possibility that both current activity and subaerial erosion were also affecting sedimentation at this structure during a long period of the Late Cretaceous. Dingle and Camden-Smith (1979) suggested increased current circulation due to deflection by the edges of the Agulhas Plateau as the reason for thinned Late Cretaceous deposits and depressions in the area of the Agulhas Passage (white arrow in Figure 5.8b). The onset of circulation through the Agulhas Passage may be a result of progressive subsidence of the Agulhas Plateau after its emplacement and the Falkland Plateau clearing the tip of Africa (Martin *et al.*, 1982; Dingle *et al.*, 1983; Niemi *et al.*, 2000; Parsieglia *et al.*, 2008).

A Turonian (~91 Ma) unconformity (McDuff) has been observed at the southeast African shelf, the Tugela Cone and in the Central Terrace of the Natal Valley that affected deposition during most of the Cenomanian to Turonian (Ludwig *et al.*, 1968; Flores, 1973; Dingle *et al.*, 1978; Martin *et al.*, 1982; Dingle and Robson, 1985). The authors correlated the unconformity with the hiatus expressed at the MozR. We therefore suggest that the erosive circulation in the study area commenced ~91 Ma during the Turonian. According to Dingle *et al.* (1978) the McDuff unconformity is not expressed north of the Almirante Leite Ridge (~26.5°S in Figure 5.1a) and shows a general southward dip in the Central Terrace to depths slightly below ~4000 ms TWT south of the Central Terrace (~29.8°S in Figure 5.1a). This is in agreement with the south to north transgression that was commencing during late Early Cretaceous (Flores, 1973; Girdley *et al.*, 1974) and may be interpreted as a consequence of progressive Gondwana breakup. Based on the distribution of the McDuff unconformity and the general clockwise circulation in the Southern Hemisphere due to Coriolis force we propose that the circulation in the study area was flowing in a NE direction along the southeast African shelf and the Tugela Cone (white arrow along SE African coast in Figure 5.8b). Circulation then continued further northwards into the Natal Valley where it was deflected southwards at the Almirante Leite Ridge (curved white arrow in Figure 5.8b).

Our seismic records suggest a southward continuation of the circulation along the western flank of the MozR where it contoured all segments of the southern MozR (white arrows around the MozR in Figure 5.8b). The circulation finally left the study area by flowing into the Mozambique Basin in a northward direction along the eastern flank of the MozR thus causing the ridge-wide expression of the hiatus (white arrows at the eastern flank of the MozR in Figure 5.8b). A branch of the circulation may have already left the study area further to the north through the slightly shallower palaeopassage between the northern MozR and the cMozR (white arrow north of cMozR in Figure 5.8b). This passage has previously been suggested as a circulation pathway during Eocene/Oligocene times by

Ben-Avraham *et al.* (1994).

Apart from the regional factors controlling the circulation (e.g., subsidence of the Agulhas Plateau) there were also global palaeoclimate and palaeogeographic events that promoted the initiation of a circulation through the Agulhas Passage. The palaeocean circulation during the early Late Cretaceous was simulated to be very sluggish (Donnadieu *et al.*, 2016; Uenzelmann-Neben *et al.*, 2016). We therefore propose that conditions for an inflow through the Agulhas Passage were not met until the initiation of a long-lasting cooling trend after the Cretaceous thermal maximum in Turonian times (~91 Ma) caused a gradual increase of the temperature gradient between poles and equator (Poulsen *et al.*, 2001; Huber *et al.*, 2002; Poulsen *et al.*, 2003; Friedrich *et al.*, 2012; Murphy and Thomas, 2012).

The termination of the Late Cretaceous greenhouse was probably caused by progressive modification of the continental configuration (e.g., opening and deepening of the Equatorial Atlantic Gateway) and parallel reorganization of ocean circulation since the late Turonian. This correlation is suggested by $\epsilon_{\text{Nd}}/^{13}\text{C}/^{18}\text{O}$ isotope data (Robinson *et al.*, 2010; Murphy and Thomas, 2012, 2013; Linnert *et al.*, 2014; Donnadieu *et al.*, 2016; Moiroud *et al.*, 2016) and a recently published break up model for the Atlantic Ocean (Granot and Dyment, 2015). According to Bice *et al.* (2006) and Linnert *et al.* (2014) a parallel decrease in greenhouse gases may have strengthened the tectonic effects. The timing of the palaeoclimate and palaeogeographic modifications perfectly correlates with the proposed age of the McDuff unconformity (Turonian) by Dingle *et al.* (1978) and the onset of the vigorous circulation causing the hiatus at the MozR.

Uenzelmann-Neben *et al.* (2016) simulated several water masses being active during the Late Cretaceous with UPW mixing with Upper North Atlantic Water (UNAW) and setting into the Indian Ocean via the A–SO gateway (red arrow in Figure 5.8b). Furthermore they proposed a transport of Intermediate Southern Ocean Water (ISOW; yellow arrows in Figure 5.8b) and Upper Southern Ocean Water (red arrow along Antarctic coast in Figure 5.8b) westward along the Antarctic coast and a subsequent recirculation of ISOW through the South Atlantic Ocean. Deepening of the passage south of the Agulhas Plateau (Castelino *et al.*, 2016) gave way to an open deep water circulation between Southern Atlantic and Indian Ocean since ~90 Ma with deep water probably originating in the Weddell Sea region of the Southern Ocean (black arrow pointing towards NE in Figure 5.8b; Lawver *et al.*, 1992; Donnadieu *et al.*, 2016).

We thus suggest that both surface (mixture of UPW and UNAW) and intermediate water (ISOW) were the probable sources for the shallow erosive circulation in the study area. This could explain the observed wide depth range of the hiatus at the MozR. We hypothesize that the bulk of surface and intermediate circulation through the A–SO gateway (red and yellow arrows west of the Agulhas Passage in Figure 5.8b) was at least temporally flowing across our study area and further onwards into the Mozambique Basin. This would specify it as the major contributor to the proposed surface and intermediate circulation in the Mozambique Basin before late Campanian times (yellow and red arrow in Figure 5.8b; Donnadieu *et al.*, 2016; Uenzelmann-Neben *et al.*, 2016). In order to verify this hypothesis one would need to compare Neodymium signatures of Cenomanian to late Campanian deposits in the NW Mozambique Basin with those reported for sites W of the study area (e.g., DSDP Site 361; Murphy and Thomas, 2012).

5.5.3. Late Cretaceous (~75–68 Ma)

Our seismic records show the late Campanian to late Maastrichtian (75–68 Ma) seismic unit S2a to be of highly variable thickness (Figure 5.5b). The depocentres of unit S2a seem to be elongated roughly parallel to the depth contours of seismic unit S1 (e.g., Figure 5.2 CDPs 8450–9450, 9800–11100; thick red and black contours in Figure 5.5b and Figure 5.6). We interpret this to be the result of

current control on sedimentation. This interpretation is supported by the observation of a large number of sediment drifts, moats and eroded areas (Figure 5.2, Figure 5.4 and Figure 5.7; red and blue lines in Figure 5.6) typically resulting from current controlled sedimentation (Faugères *et al.*, 1999; Stow *et al.*, 2002; Stow *et al.*, 2008; Rebesco *et al.*, 2014; Uenzelmann-Neben *et al.*, 2016). Based on the distribution of the depocentres, drifts and erosional structures along the MozR we conclude that the main flow was circulating southward along the ridge before being deflected to the east at the southern flank of the swMozR due to Coriolis force (green dashed arrows in Figure 5.6).

Several drifts at shallower depths and within the trough separating the swMozR and the cMozR favour a counterclockwise circulation around the swMozR, while flow along the cMozR is inferred by deposits on its southern and eastern flanks (green dashed arrows in Figure 5.6). The Campanian to Maastrichtian deposits of unit S2a are characterized by biogenic sediments (Simpson *et al.*, 1974). High organic productivity requires a large supply of nutrients from nutrient-rich intermediate to deep water (Hay, 2011). Since deep current controlled sedimentation in the study area did not commence before late Eocene times (Schlüter and Uenzelmann-Neben, 2008b) we favour intermediate water as the source for the nutrient-rich water at the MozR. After its mid-Cretaceous uplift parts of the MozR were probably still subaerial or submarine. As a consequence we suggest that both surface and intermediate circulation were controlling deposition of seismic unit S2a at the MozR during late Campanian to late Maastrichtian times.

The observed distribution of the sediment drifts and erosional structures at the MozR indicates that the circulation scheme in the study area already active during the Late Cretaceous hiatus was maintained (white arrows in Figure 5.8c), with a slow down to velocities allowing the formation of such features (Brown *et al.*, 1999; McCave and Hall, 2006; Stow *et al.*, 2009). We observe a general increase in the width of the erosional structures cutting into unit S2a when compared to the erosional structures cutting into unit S1 (e.g., Figure 5.2 CDPs 8200–8550 and inset, Figure 5.4 CDPs 3300–4400 and inset, Figure 5.7 inset). This is interpreted as evidence for a subsequent decrease of current velocities and widening of the current's core after termination of the vigorous circulation that caused the Late Cretaceous hiatus.

The sediment drifts show several discontinuities, reflections of alternating amplitudes, and in some parts seem to be almost transparent (e.g., Figure 5.2 CDPs 10000–10800, Figure 5.4 CDPs 4400–5200). Alternating reflection amplitudes and discontinuities incorporated into contourite drifts are usually associated with periods of variations in velocity or location of the circulation system (Faugères *et al.*, 1999; Stow *et al.*, 2002; Nielsen *et al.*, 2008; Stow and Faugères, 2008). This implies repeated modification of the circulation system at the MozR during deposition of seismic unit S2a, which can be correlated to changes in palaeogeography and/or palaeoclimate, e.g., the proposed short-term glaciation event in the early Maastrichtian (Barrera and Savin, 1999; Friedrich *et al.*, 2012).

The Late Cretaceous deposits and sedimentary features are confined to depths below the ~3500 ms TWT S1 depth interval at the swMozR (thick red contour in Figure 5.5b). One explanation might be that parts of the MozR were still exposed above sea level and thus subject to subaerial erosion. However, the cMozR shows an up to ~270 ms TWT thick seismic unit S2a with several drifts and erosional structures well above this depth (thick white contour in Figure 5.6). The lack of an uniform boundary throughout the southern MozR that separates the layer of active deposition and drift formation from the layer of non-deposition or erosion (Figure 5.5b and Figure 5.6) makes non-deposition due to subaerial erosion unlikely. Reports of non-deposition at the Agulhas Plateau even after its subsidence below sea level ~80 Ma (Tucholke and Carpenter, 1977; Tucholke and Embley, 1984; Uenzelmann-Neben, 2002; Parsieglia *et al.*, 2008) also contradict formation of the unconformity due to subaerial erosion.

The formation of Taylor caps above topographic highs accompanied by starvation of sediment supply above the structure's top is a widespread feature (Roberts *et al.*, 1974; Roden, 1991; Chapman

and Haidvogel, 1992). Considering that the segments of the MozR represent topographic highs the shallower parts may have been subject to Taylor cap formation. This could explain the limitation of non-deposition to the prominent basement highs in the study area (MozR and Agulhas Plateau). Due to the shallower depth of the cMozR formation of the Taylor cap and thus starvation of sediment supply also occurred in shallower depths. We interpret this as the cause for the observed differences in the distribution of seismic unit S2a at the cMozR and the swMozR.

The onset of the current controlled sedimentation regime at the MozR between ~75 and 68 Ma is in agreement with a major reorganization of global palaeocean circulation towards common deep and intermediate water masses in the Atlantic and Indian Ocean documented by a simultaneous shift towards less radiogenic Neodymium values (Robinson *et al.*, 2010; Martin *et al.*, 2012; Murphy and Thomas, 2012; Robinson and Vance, 2012; Murphy and Thomas, 2013; Moiroud *et al.*, 2016). These authors attributed the change in Neodymium signatures to the progressive subsidence of Large Igneous Provinces and a reduced inflow of radiogenic water from the Pacific into the South Atlantic caused by a shallower Drake Passage. The initiation of a common circulation in the Atlantic and Indian Ocean basins was accompanied by significant cooling of surface water and bottom water temperatures (Huber *et al.*, 2002; Linnert *et al.*, 2014).

At ~75 Ma multiple ridge jumps separated the former single large-plateau like RWS into an isolated Rio Grande Rise while volcanism continued on the Walvis Ridge (Rohde *et al.*, 2013). The Walvis Ridge still represented a significant barrier to intermediate and deep circulation in the southeastern segment of the South Atlantic during the late Campanian and Maastrichtian (Murphy and Thomas, 2013; Voigt *et al.*, 2013; Moiroud *et al.*, 2016; Uenzelmann-Neben *et al.*, 2016). Flow velocity is a function of flow rate and flow area. Therefore even a slight deflection of the surface (probably UNAW and UPW) and intermediate (probably ISOW) circulation by the RWS to the southwest (thick red and yellow arrows in Figure 5.8c) may have been sufficient to reduce the flow rate of the currents flowing into the study area (thin red and yellow arrows in Figure 5.8c).

As a consequence the bulk of the surface and intermediate water circulated from the South Atlantic into the Indian Ocean through the passage south of the Agulhas Plateau (thick red and yellow arrows in Figure 5.8c). Circulation continued to the NE into the Mozambique Basin where it was joined by the circulation along the eastern flank of the MozR (white arrows in Figure 5.8c). Numerical simulations indicate a southward flow of surface and intermediate water between East Africa and Madagascar (Donnadieu *et al.*, 2016), which is supported by the observation of sediment waves in Late Cretaceous deposits (Castelino *et al.*, 2015).

We therefore suggest a southward turn of surface and intermediate water in the north Mozambique Basin (red and yellow curved arrow in Figure 5.8c). Voigt *et al.* (2013) and Donnadieu *et al.* (2016) proposed a maintenance of the existing eastward circulation of deep water originating in the South Atlantic through the A–SO gateway (black arrow north of Antarctica in Figure 5.8c) during Campanian and Maastrichtian times. Deep circulation into the Transkei Basin through the Agulhas Passage was probably still restricted (Schlüter and Uenzelmann-Neben, 2008a), but the absence of black shales after ~80 Ma indicates oxygenation via vertical exchange between the different water masses in the study area (black arrow in Transkei Basin in Figure 5.8c).

The top of the Late Cretaceous (~75–68 Ma) unit S2a shows evidence of erosional truncation and pinch out of reflections against the overlying seismic unit S2b (e.g., Figure 5.4 CDPs 4400–5000). The Late Cretaceous current controlled sedimentation at the MozR was thus terminated in late Maastrichtian times and followed by another hiatus lasting ~50 Myr until the early Neogene that was attributed to the onset of the erosive pre-Indian Ocean South Equatorial Current by Leclaire (1974).

5.6. Conclusion

With the presented interpretation of new seismic data from the MozR area we aimed at a better understanding of both onset and modification of the current controlled sedimentation in the vicinity of the MozR during the Early and Late Cretaceous. Our results indicate:

- (1) Sedimentation in a restricted basin under euxinic conditions after the MozR was emplaced (~125 Ma). Even though a sluggish circulation in the Southern Ocean may have existed before the Late Cretaceous the circulation did not affect our study area due to several bathymetric structures obstructing the inflow during the Early Cretaceous.
- (2) Occurrence of a Late Cretaceous hiatus (~100–75 Ma) at the MozR as a consequence of a mid-Cretaceous uplift along with an erosive circulation in the study area that commenced in ~Turonian times. This onset of a circulation in the study area was caused by several regional (e.g., opening of the Agulhas Passage) and global modifications (e.g., opening of Atlantic Ocean) of palaeogeography, palaeoclimate and palaeocean circulation.
- (3) Onset of current controlled sedimentation at the MozR in late Campanian times (~75 Ma) as a result of modifications to surface and intermediate water circulation through the Agulhas Passage. Driving factors of the modifications may have been the initiation of deep water mass exchange between the Northern Atlantic, Southern Atlantic and Indian Ocean along with a progressive breaching of the RWS and a diminished inflow of Pacific Water through the Drake Passage.

Current controlled sedimentation in the northern A–SO gateway thus started long before deep circulation affected sediment distribution in late Eocene/early Oligocene times (Ben-Avraham *et al.*, 1994; Schlüter and Uenzelmann-Neben, 2008b). Our data shows that even though bathymetric structures like the MozR and the Agulhas Plateau did not obstruct the circulation completely during the Late Cretaceous they actively altered circulation pathways.

Drill core data and geochemical analyses (especially ϵ_{Nd}) from different sites at the MozR and in the study area would be important for further investigations of the circulation in the A–SO gateway during the Late Cretaceous. This could help to identify the water masses that have caused formation of the depositional features.

5.7. Acknowledgements

We want to express our gratitude to Captain Detlef Korte and his officers and crew of RV *Sonne* for their professional and enthusiastic engagement and service during the scientific program of this leg. The cruise leg SO 232 and the project SLIP were funded by the German Federal Ministry of Education and Research (BMBF) under project number 03G0232A. Additional funding has been provided by the Alfred-Wegener-Institut.

6. Neogene modifications of circulation in the African–Southern Ocean gateway

Maximilian D. Fischer, Gabriele Uenzelmann-Neben
Alfred-Wegener-Institut Helmholtz-Zentrum für Polar- und Meeresforschung, Am Alten Hafen 26,
27568 Bremerhaven, Germany

In review in **Deep-Sea Research Part I** (04/2017)

Abstract

Major palaeoceanographic modifications have characterised the Neogene circulation in the African–Southern Ocean gateway where several water masses originating in the Atlantic, Indian and Southern oceans meet and mix. This palaeo-circulation is reconstructed based on MCS data collected across the southern Mozambique Ridge. The data shows two mid-Miocene to Holocene sedimentary units separated by an early Pliocene to Pleistocene hiatus. The occurrence of contourites and erosional structures in the mid-Miocene to early Pliocene seismic unit are interpreted as evidence for the onset of Neogene current controlled sedimentation as a result of West Antarctic glaciation and the closure of the Indonesian gateway. The Pliocene-Pleistocene transition marks a distinct change in the African–Southern Ocean gateway subsequent to the final closure of the Central American Seaway and the Northern Hemisphere Glaciation with a relocation of bottom water inflow to the Agulhas Passage and the inception of two branches of deep water circulation. Our results show that the two events initiated the onset of free deep circulation from the Atlantic into the Indian Ocean, whereas shallower circulation decreased due to the final closure of the Indonesian gateway. These changes are interpreted as the onset of a modern circulation that has continued up to the present day.

6.1. Introduction

The global thermohaline circulation is strongly affected by the water mass exchange in the African–Southern Ocean (A–SO) gateway. Here, cold and warm water masses originating in the Atlantic, the Indian and the Southern Oceans meet and mix (Figure 6.1; Lutjeharms, 1996). Numerous studies have been carried out around South Africa with the purpose of analyzing the recent circulation scheme (e.g., Arhan *et al.*, 2003; You *et al.*, 2003). Whereas the recent movement of water masses off South Africa is well understood, the palaeocirculation and hence palaeoceanographic and palaeoclimatic conditions remain uncertain. The water masses leave traces of their activity in the sedimentary record, which in turn can be used for reconstruction of palaeocirculation pathways and intensities. These traces may appear as geochemical proxies like ϵ_{Nd} isotope signatures (e.g., Frank *et al.*, 2002), or as sedimentary features (e.g., contourite drifts) in seismic records (e.g., Rebesco *et al.*, 2014).

The Cenozoic history of current controlled sedimentation in the A–SO gateway has been the subject of a number of publications with its onset being proposed in Eocene to Oligocene times following major palaeoceanographic changes (Uenzelmann-Neben *et al.*, 2007; Schlüter and Uenzelmann-Neben, 2008b; Uenzelmann-Neben and Huhn, 2009). However, the occurrence of a late Maastrichtian to mid–Miocene hiatus at the MozR (Simpson *et al.*, 1974; Uenzelmann-Neben *et al.*, 2011; Fischer *et al.*, 2017; Fischer and Uenzelmann-Neben, 2017a) point towards large regional differences in the circulation regime within the gateway. The probable cause of the limitation of the hiatus to the MozR

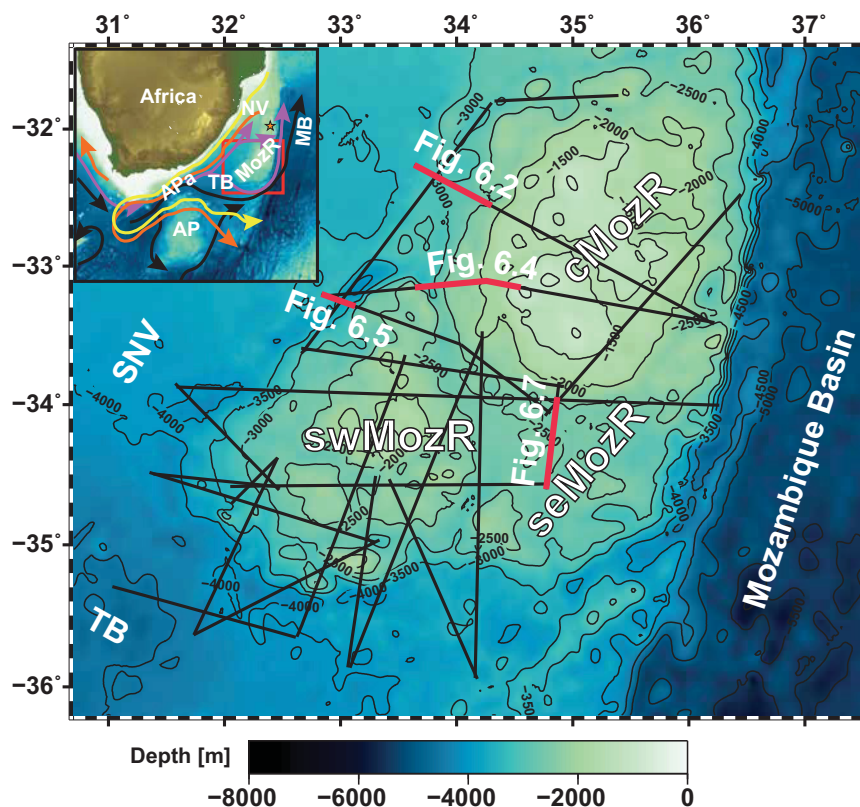


Figure 6.1. Bathymetric map (Weatherall *et al.*, 2015) of the study area in the eastern part of the African–Southern Ocean gateway (500 m contour lines in black). MCS profiles of SO 183 and 232 are shown in black. Thick red lines mark location of the MCS profiles shown in figures. The inset illustrates the main flow paths of surface currents and deeper water masses (Lutjeharms, 2006; Uenzelmann-Neben *et al.*, 2007; Gruetzner and Uenzelmann-Neben, 2016): Agulhas Current (yellow), Antarctic Bottom Water (black), Antarctic Intermediate Water (orange) and North Atlantic Deep Water (purple). Orange star marks the location of DSDP Leg 25 Site 249 on the northern Mozambique Ridge. Red box indicates study area shown in Figure 6.1. AP = Agulhas Plateau; APa = Agulhas Passage; cMozR = central Mozambique Ridge; MB = Mozambique Basin; MozR = Mozambique Ridge; (S)NV = Southern Natal Valley; swMozR = southwestern Mozambique Ridge; seMozR = southeastern Mozambique Ridge; TB = Transkei Basin.

and the somewhat later onset of drift propagation may be that seafloor elevations like the MozR can obstruct and accelerate the flow and therefore influence current pathways (e.g., Roden, 1991; Grützner and Uenzelmann-Neben, 2016).

With the sedimentary record of the MozR being an archive of the major reorganisations of palaeocean circulation in the Atlantic, Indian and Southern Oceans during the Paleogene, Neogene and Quaternary (Leclaire, 1974; Uenzelmann-Neben *et al.*, 2011) the ridge represents an important location within the A–SO gateway. The area is well suited to examine palaeocean circulation because it is topographically isolated from downslope sediment transport from the East African continent. The entire sedimentary record thus formed by a combination of pelagic and current-controlled sedimentation (Leclaire, 1974; Simpson *et al.*, 1974; Uenzelmann-Neben *et al.*, 2011; Fischer and Uenzelmann-Neben, 2017a). Therefore, any reworking or erosion of deposits has resulted from current activity. In this study we focus on the Neogene and Quaternary palaeocirculation at the MozR by investigating new high-resolution multichannel seismic reflection data from the southern part of the topographic high.

6.2. Background and settings

6.2.1. Geologic and palaeoceanographic setting

With a length of up to ~800 km (N to S) and a width of up to ~400 km (E to W) the MozR represents a prominent feature in the African–Southern Ocean gateway (Figure 6.1). The MozR rises up to 3500 m above the ocean floor of its surrounding basins (Mozambique Basin/MB, Natal Valley/NV, and Transkei Basin/TB in Figure 6.1) that developed as a result of Gondwana breakup (Flores, 1973; Coffin and Rabinowitz, 1988; Schlüter and Uenzelmann-Neben, 2007; König and Jokat, 2010). The aseismic ridge consists of a narrower northern and a wider southern part, which comprises three segments: the central MozR (cMozR), the southwestern MozR (swMozR), and the southeastern MozR (seMozR). The distribution of the up to ~1600 ms TWT thick sedimentary sequence at the southern MozR is largely controlled by its underlying basement structure and shows a general thinning towards and on top of the segments (Fischer *et al.*, 2017). Based on the observation of thick lava flow sequences and numerous extrusion centres Fischer *et al.* (2017) proposed a Large Igneous Province origin of the southern MozR and suggested a sequential emplacement of the three segments between ~131 and ~125 Ma.

Since its emplacement the MozR experienced several magmatic and tectonic events (e.g., mid-Cretaceous and Neogene magmatic reactivation) that influenced sediment distribution (Girdley *et al.*, 1974; Fischer *et al.*, 2017; Fischer and Uenzelmann-Neben, 2017a). A first short period of current controlled sedimentation at the southern MozR commenced in the late Campanian (~75 Ma) subsequent to the termination of a phase of vigorous circulation that also affected deposition at other locations in the vicinity (e.g., Agulhas Plateau and Tugela Cone; Dingle *et al.*, 1978; Uenzelmann-Neben, 2002; Fischer and Uenzelmann-Neben, 2017a). Fischer and Uenzelmann-Neben (2017a) linked the inception of the Late Cretaceous (~75–68 Ma) current controlled sedimentation at the MozR to modifications of the South Atlantic palaeocirculation caused by tectonic and palaeogeographic modifications of the Rio Grande Rise–Walvis Ridge System.

Large parts of the Tertiary (~68–15 Ma) were characterized by non-deposition or erosion at the MozR (Simpson *et al.*, 1974; Fischer *et al.*, 2017), which Leclaire (1974) attributed to the strong westward flow of a pre-Indian Ocean South Equatorial Current. According to Uenzelmann-Neben *et al.* (2011) the ~53 Myr hiatus was followed by the mid-Miocene ~15 Ma onset of Neogene current controlled sedimentation at the MozR. The proposed cause for commencing of the current controlled sedimentation was a major reorganisation of deep circulation due to the glaciation of West Antarctica along

with the initiation of the Miocene Indian Ocean Equatorial Jet (MIOJet) that dominated the shallow circulation in the Indian Ocean until ~4 Ma (Zachos *et al.*, 2001; Gurlan *et al.*, 2008; Schlüter and Uenzelmann-Neben, 2008b; Uenzelmann-Neben *et al.*, 2011). A subsequent decrease of the MIO-Jet due to final closure of the Indonesian gateway and the onset of Northern Hemisphere glaciation resulted in modifications of the water masses bathing the MozR (Zachos *et al.*, 2001; Frank *et al.*, 2002; Gurlan *et al.*, 2008; Schlüter and Uenzelmann-Neben, 2008b; Uenzelmann-Neben *et al.*, 2011).

Nowadays, circulation in the African–Southern Ocean gateway is basically driven by four water masses (inset of Figure 6.1) that are either sourced in the Southern Ocean (surface, intermediate and bottom water) or in the North Atlantic (deep water). The Agulhas Current (yellow arrow in inset of Figure 6.1) is the western boundary current of the Indian Ocean and extends to water depths greater than 2000 m (Tomczak and Godfrey, 1994; Lutjeharms, 1996; de Ruijter *et al.*, 1999; Lutjeharms, 2006), while Antarctic Intermediate Water (AAIW; orange arrows in inset of Figure 6.1) circulates through the Indian Ocean in water depths of 700 to 2000 m (Tomczak and Godfrey, 1994; Lutjeharms, 1996; You *et al.*, 2003; Lutjeharms, 2006).

The deeper water masses consist of North Atlantic Deep Water (NADW; purple arrows in inset of Figure 6.1) and Antarctic Bottom Water (AABW; black arrows in inset of Figure 6.1). NADW enters the southwestern Indian Ocean through the Agulhas Passage and resides in water depths between 2000 and 3500 m (Wyrki, 1973; Toole and Warren, 1993; Mantyla and Reid, 1995; You, 1999; van Aken *et al.*, 2004; Lutjeharms, 2006). AABW traverses into the A–SO gateway in depths below 3500 m either by flowing eastwards through the Agulhas Passage, or by flowing into the Transkei Basin east of the Agulhas Plateau (Tucholke and Embley, 1984; Read and Pollard, 1999; van Aken *et al.*, 2004; Lutjeharms, 2006). According to Lutjeharms (2006) bottom topography clearly affects the movement of both NADW and AABW in the Indian Ocean.

6.2.2. Seismic stratigraphy

We here apply the seismo-stratigraphic model by Fischer *et al.* (2017). Their model is based on a correlation of 24 (~4600 km) high-resolution MCS reflection profiles acquired at the southern MozR on board RV *Sonne* (SO 182 and SO 232) by the Alfred Wegener Institute, Helmholtz Centre for Polar and Marine Research (black lines in Figure 6.1) with the drill results of DSDP Leg 25 Site 249 on the northern MozR (orange star in Figure 6.1 inset; Simpson *et al.*, 1974). The seismic profiles cover the three segments of the southern MozR (cMozR, seMozR, swMozR) and the transition zone into the adjacent basins (MB, NV and TB in Figure 6.1). Four seismic units were identified in the MCS profiles, the Early Cretaceous basaltic basement (~131–125 Ma), two Cretaceous sedimentary units with a supposed age of ~128–100 Ma (seismic unit S1) and ~75–68 Ma (seismic unit S2a), and the mid-Miocene to Holocene (≤ 15 Ma) unit S2b (Fischer *et al.*, 2017).

Two long lasting hiatuses were identified at DSDP Site 249 (Simpson *et al.*, 1974) and correlated with major unconformities in the seismic record (Fischer *et al.*, 2017), the first (~100–75 Ma) separating the two Cretaceous units, and the second (~68–15 Ma) the Late Cretaceous unit S2a from the Neogene unit S2b. Owing to the focus of this study on the Cenozoic only those deposits will be discussed here. Please refer to Fischer *et al.* (2017) and Fischer and Uenzelmann-Neben (2017a) for a detailed description of the Cretaceous units at the southern MozR.

Fischer *et al.* (2017) correlated seismic unit S2b with the foram nanno ooze of lithostratigraphic unit I drilled at DSDP Site 249 (Simpson *et al.*, 1974). The unit shows of mainly weak to medium amplitude reflections (Figure 6.2 CDPs 8400–9200). In several areas strong amplitude reflections alternating

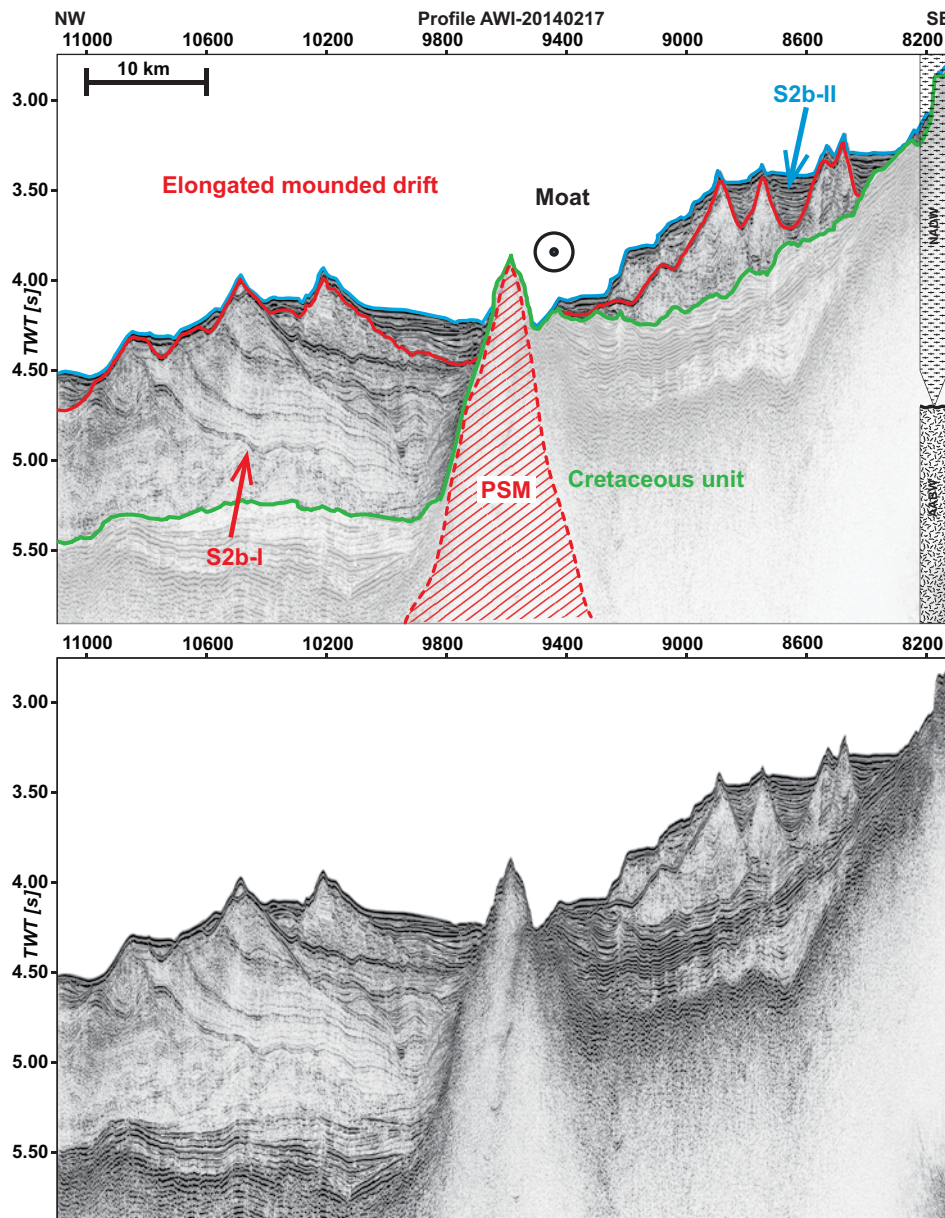


Figure 6.2. Part (interpreted/uninterpreted) of MCS profile AWI-20140217 showing the seismic stratigraphy of the Cenozoic units in the study area. Location of profile is shown in Figure 6.1. For a description of the seismic characteristics of the units refer to chapter 6.2.2. Thick blue line = top of Pleistocene to Holocene unit S2b-II, thick red line = top of mid-Miocene to early Pliocene unit S2b-I, thick green line = top of Cretaceous unit. The Cretaceous is masked in the interpreted section. Red hatched PSM = late Neogene post-sedimentary magmatic structure (Fischer *et al.*, 2017). Colour coded circles denote current during deposition of the respective units (red = S2b-I, blue = S2b-II, black = valid for both intervals). The textured bars indicate the present day depth intervals of the water masses. AABW = Antarctic Bottom Water, AAIW = Antarctic Intermediate Water, NADW = North Atlantic Deep Water. For horizontal scale refer to interpreted section. Vertical exaggeration (VE) of all shown MCS profiles is ~20.

with sets of weaker amplitude reflections were observed (Figure 6.2 CDPs 10200-10600). Fischer *et al.* (2017) identified the strong amplitude reflections as discontinuities such as erosional truncation and onlap termination (Figure 6.2 CDPs 10200–10800, 4600–5000 ms).

We observe a significant difference in the seismic appearance and geometry of the lower and the upper part of seismic unit S2b. In contrast to Fischer *et al.* (2017) who addressed both parts as seismic unit S2b, we here introduce a subdivision into the lower seismic unit S2b-I (red horizon in Figure 6.2 = top of unit S2b-I) and the upper seismic unit S2b-II (blue horizon in Figure 6.2 = top of unit S2b-II/seafloor; Table 6.1). While seismic unit S2b-I is characterized by undulating, mostly weak

to moderate amplitudes, we observe almost horizontal, well-layered strong amplitude reflections in seismic unit S2b-II (Figure 6.2 CDPs 8500–8800). The reflections of the upper part of the unit drape (Figure 6.2 CDPs 9700–10200) and onlap onto reflections of the lower part of the unit (Figure 6.2 CDPs 8400–8900).

Biostratigraphic age determinations by Simpson *et al.* (1974) showed that Pleistocene (~2.6 Ma) sediments unconformably overlie material of early Pliocene (~5 Ma; incomplete Blow's Zone N. 19) at DSDP Site 249. They attributed the unconformity to the occurrence of a hiatus spanning large parts of the Pliocene. We thus suggest that seismic unit S2b-I corresponds to the mid-Miocene to early Pliocene sediments (~15–5 Ma), whereas seismic unit S2b-II correlates with the Pleistocene to Holocene deposits (~2.6–0 Ma).

Table 6.1. Seismic stratigraphy for the Cenozoic units in the study area.

Cenozoic seismic units	Unit S2b-II	Unit S2b-I
Thickness (ms TWT); RMS thickness (ms TWT)	0–596; 138	0–1280; 409
Age (Ma) ^a	0–2.6	15–5
Material ^a	Similar to S2b-I but higher percentage of foraminifera and lower percentage of clay	foram nanno ooze, varying amounts of foraminifera, clay and chalk
Seismic characteristics ^b	subhorizontal moderate to strong amplitude reflections of lower frequency; sporadically continuous weaker amplitude reflections	mostly undulating continuous reflections with weak to moderate amplitudes and low to medium frequency; occasionally strong amplitude reflections; discontinuities
Remarks	unconformably overlying S2b-I	hiatus on top of S2b-I

^aSimpson *et al.* (1974)

^bFischer *et al.* (2017)

6.3. Methods

For the study of the Neogene and Quaternary depositional conditions at the MozR we applied the modified seismostratigraphic model of Fischer *et al.* (2017) described in chapter 6.2.2. We mapped the top reflector of each seismic unit (Cretaceous, S2b-I and S2b-II) throughout the study area and calculated the thicknesses of the late Cenozoic units. The results were used for the computation of the gridded maps (e.g., Figure 6.3). We want to emphasize that the presented maps are afflicted with uncertainties owed to the spacing of the seismic reflection profiles. Nonetheless, the general thickness and depth trends of the depicted sedimentary deposits are correct. The outlines of the depocentres are defined by the root mean square (rms) thickness of the respective unit. The orientation and location of the depocentres are interpreted with respect to the prominent basement elevations of the MozR and the morphology of the underlying horizon.

We here interpret pathways of the palaeocurrents from the location of sedimentary features (e.g., contourite drifts) and erosional features (e.g., moats) under the prerequisite that in the Southern Hemisphere Coriolis force deflects currents to the left thereby eroding the right flank of the drift,

whereas slower flow and deposition occurs to the left (Faugères *et al.*, 1999). Where the flow is constrained along a topographic high (e.g., a ridge), the Coriolis effect again deflects the flow to the left (Southern Hemisphere), effectively constraining the flow against the ridge. As a result, the flow intensifies, erosion occurs and a moat develops. Lower velocities to the right of the flow favour deposition and drift construction, with the drift tending to migrate towards the ridge and to decrease its relief downstream (Faugères *et al.*, 1999; Rebesco and Stow, 2001; Stow *et al.*, 2002). Variations in bottom current activity at the MozR were correlated with palaeoceanographic events and tectonic and palaeogeographic changes to draw conclusions about the driving forces of the Neogene to Quaternary circulation in the study area.

6.4. Results

6.4.1. Distribution of seismic unit S2b (≤ 15 Ma)

The mid–Miocene to Holocene sediments of unit S2b overlie the deposits of the Cretaceous unit (green line in all MCS profiles), which comprises the magmatic basement (~ 131 – 125 Ma), seismic unit S1 (~ 129 – 100 Ma) and seismic unit S2a (~ 75 – 68 Ma). Please refer to Fischer *et al.* (2017) and Fischer and Uenzelmann-Neben (2017a) for a detailed description of the individual Cretaceous units.

We observe a highly variable depth of the Cretaceous unit with its shallowest areas reaching up to ~ 1600 ms TWT (Figure 6.3a $34.6^\circ\text{E}/33.1^\circ\text{S}$, Figure 6.4 CDPs 1000–1300) and its deepest parts in the southwest of the study area reaching almost 7000 ms TWT (Figure 6.3a, $31.7^\circ\text{E}/35.7^\circ\text{S}$). The rms depth contour of the unit (4654 ms TWT; thick magenta contour in Figure 6.3) outlines the segments of the southern MozR, which points towards a strong influence of the magmatic basement on the topography of the unit's top. The areas below the rms depth correlate with the transition zone into the surrounding basins (Figure 6.3a).

The Neogene to Quaternary unit S2b drapes the top of the Cretaceous and shows a highly variable

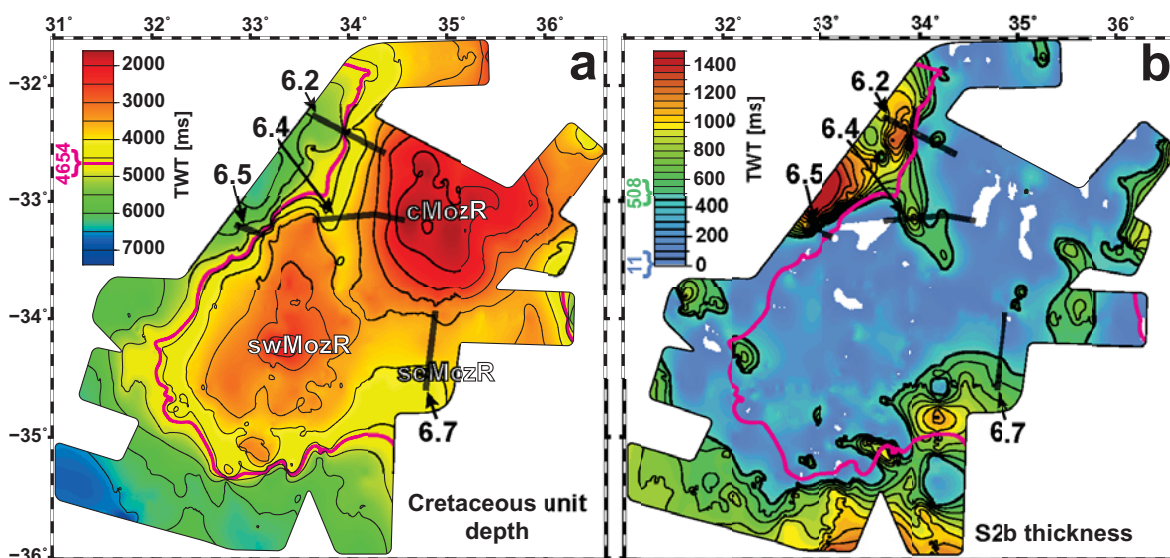


Figure 6.3. (a) Depth map (ms TWT, thin black 500 ms TWT depth contours) of the Cretaceous unit. Thick magenta contour indicates rms depth contour (4654 ms TWT; magenta number alongside colour scale). Opaque thick grey lines along with black arrows and numbers indicate figures showing MCS lines. cMozR = central Mozambique Ridge, swMozR = southwestern Mozambique Ridge, seMozR = southeastern Mozambique Ridge. (b) Isopach map of the Cenozoic seismic unit S2b. Thick black contours represent rms thickness (508 ms TWT; green number alongside colour scale), thin black contour represents thicknesses ≥ 600 ms TWT (interval of 100 ms TWT). Thick magenta contour indicates rms depth contour of underlying Cretaceous. Blue number alongside colour scale indicates minimum vertical resolution.

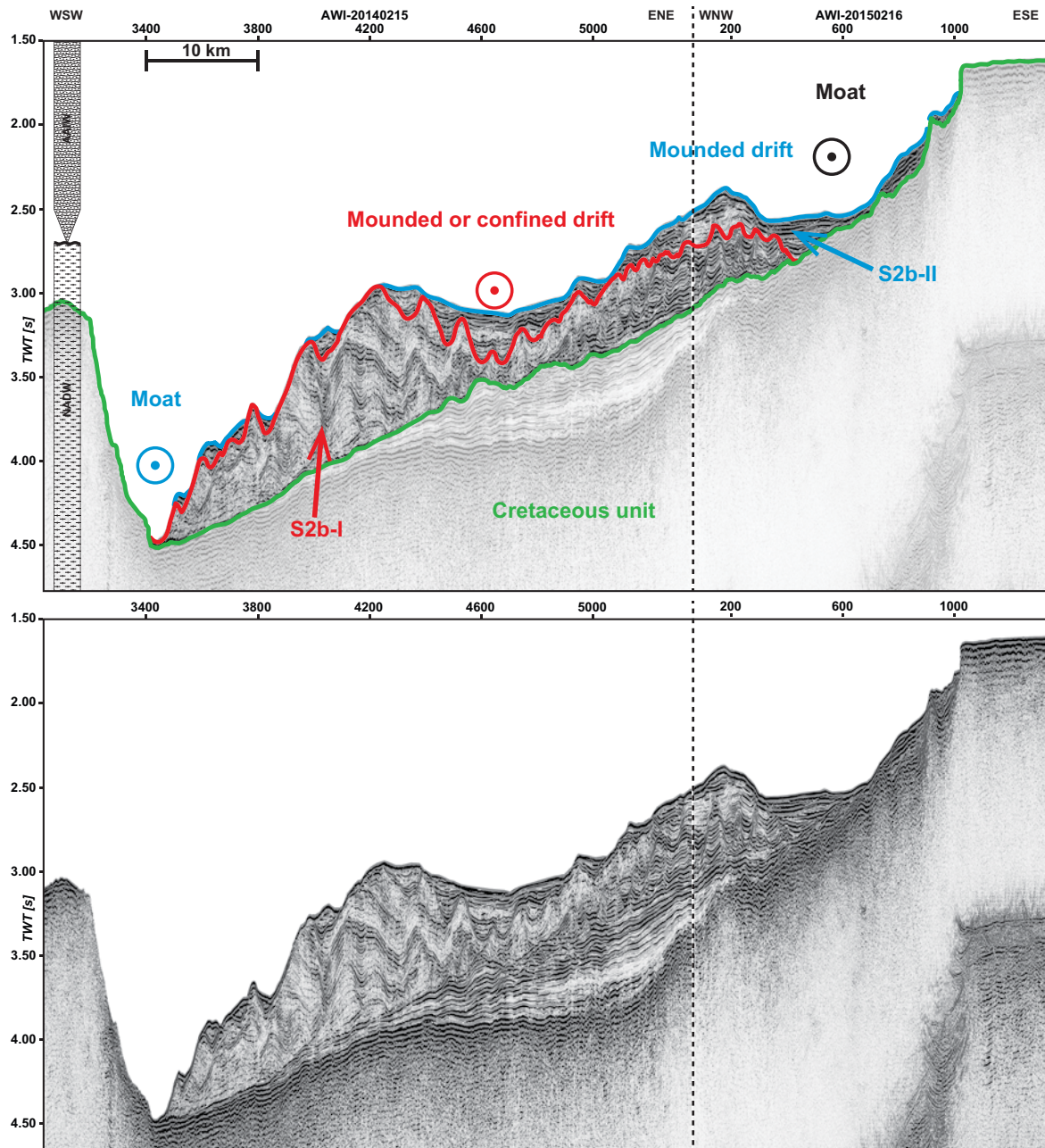


Figure 6.4. Part (interpreted/uninterpreted) of MCS profiles AWI-20140215 (left) and AWI-20150216 (right). Location of the profiles is shown in Figure 6.1. Horizontal scale is shown in the interpreted section. For colours and symbols refer to Figure 6.2.

thickness (max. 1488 ms TWT; Figure 6.3b 32.9°E/33.1°S). Most of the depocentres of seismic unit S2b (≥ 508 ms TWT rms thickness) are located in the transition zone to the surrounding basins (green to red coloured areas in Figure 6.3b; e.g., Figure 6.5 CDPs 4200–4700), whereas the unit's thickness strongly decreases towards the shallower parts of the Cretaceous (Figure 6.2 CDPs 8200–8600, Figure 6.3b).

6.4.1.1. Subunit S2b-I (~15–5 Ma)

With a maximum thickness of ~1280 ms TWT (Figure 6.6a 32.9°E/33.2°S) and a rms thickness of 409 ms TWT subunit S2b-I accounts for ~80% of the total thickness of seismic unit S2b. We observe only a thin sedimentary cover on top of the MozR segments with several areas completely barren of

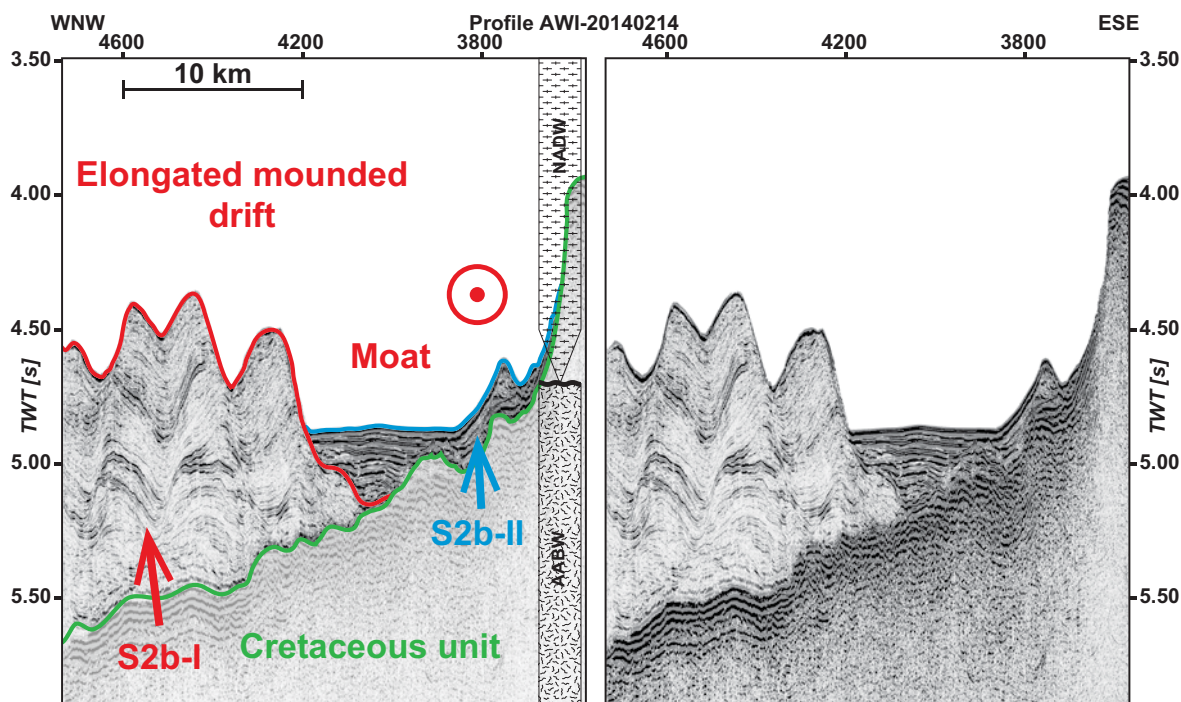


Figure 6.5. Part (interpreted/uninterpreted) of MCS profile AWI-20140214. Location of the profile is shown in Figure 6.1. Horizontal scale is shown in the interpreted section. For colours and symbols refer to Figure 6.2.

mid-Miocene to Pliocene deposits (Figure 6.2 CDPs 8100–8450, Figure 6.4 CDPs 400–1300, Figure 6.5 CDPs 3550–4000, Figure 6.6a). Most of the unit's depocentres (green to red areas in Figure 6.6a) are located below the Cretaceous unit's rms depth contour (thick magenta contour in Figure 6.6a). However, there are a few exceptions to this observation with larger depocentres occurring above the rms depth of the Cretaceous unit east of the cMozR (Figure 6.6a 36.3°E/33.3°S), on top of the seMozR (Figure 6.6a 34.2°E/34.9°S, Figure 6.7 CDPs 1700–3550) and in a depression between the swMozR and the cMozR (Figure 6.4 3450–400, Figure 6.6a 33.9°E/33.1°S). The unit's rms thick-

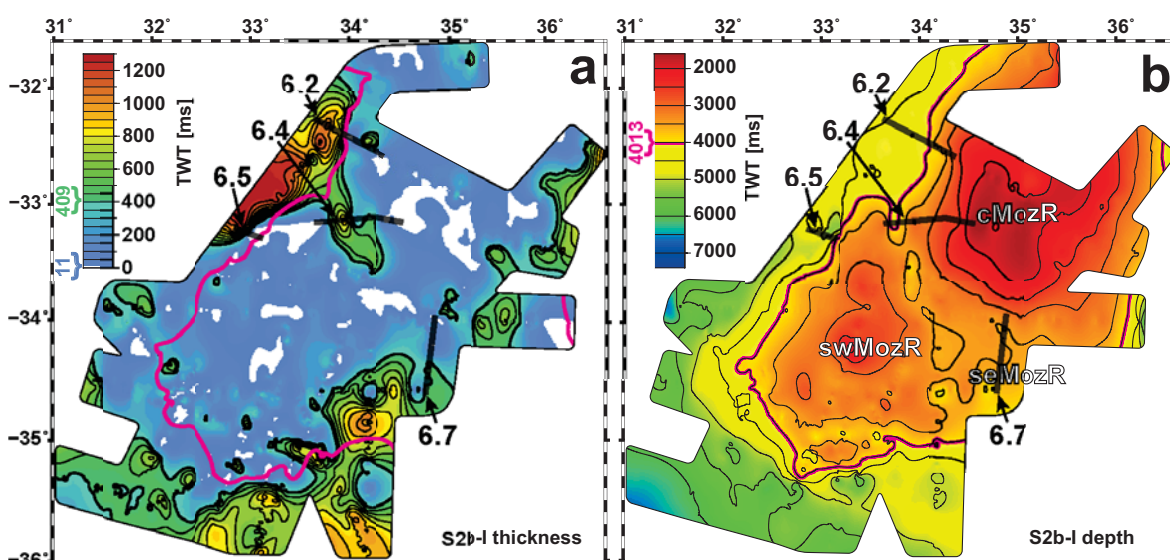


Figure 6.6. (a) Isopach map of the mid-Miocene to Pliocene seismic unit S2b-I. Thick black contours represent rms thickness (409 ms TWT; green number alongside colour scale), thin black contours represent thicknesses ≥ 500 ms TWT (interval of 100 ms TWT). Thick magenta contour indicates rms depth contour of underlying Cretaceous unit. Blue number alongside colour scale indicates minimum vertical resolution. Symbols are described in Figure 6.3. (b) Depth map (ms TWT, thin black 500 ms TWT depth contours, thick magenta rms depth contour) of seismic unit S2b-I. Symbols are described in Figure 6.3.

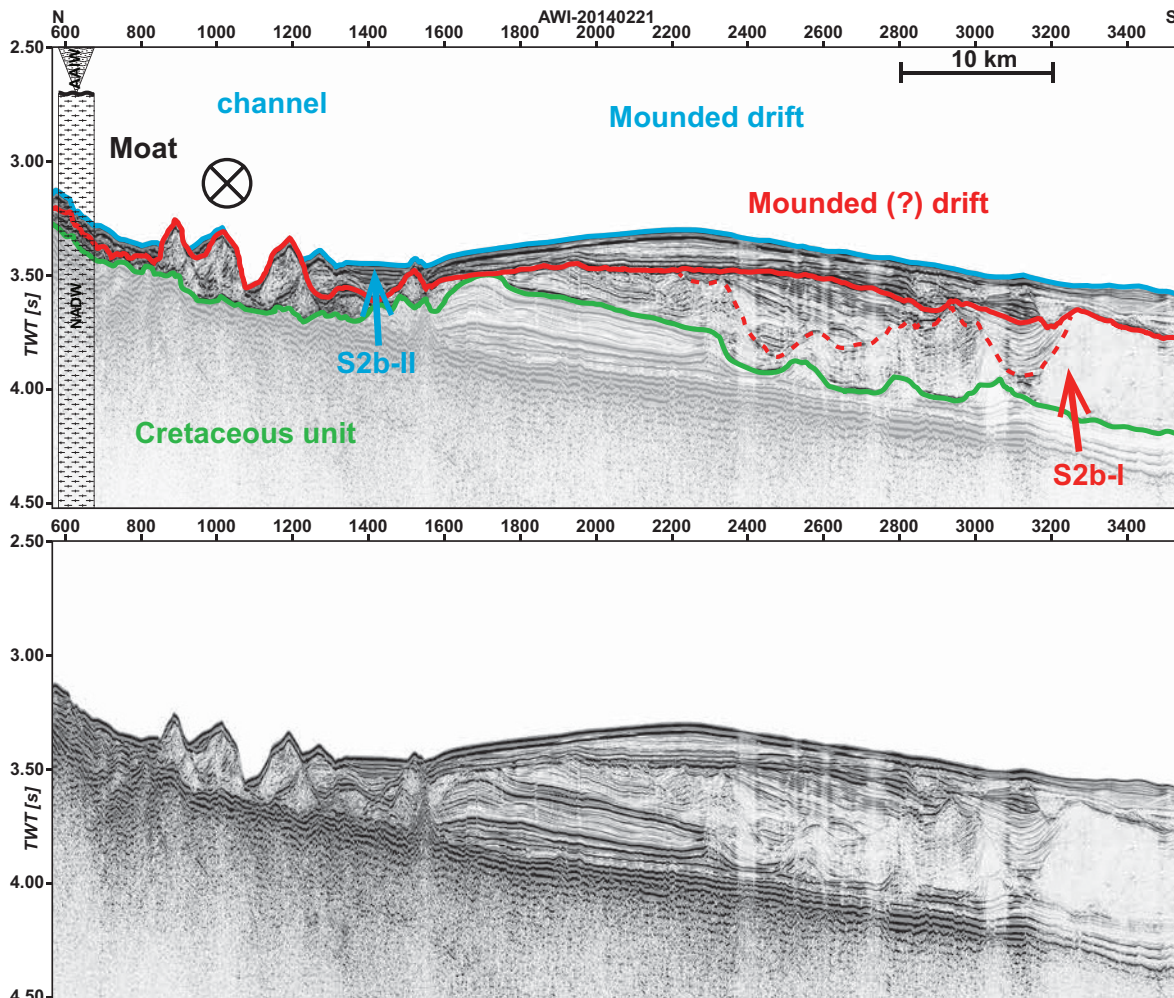


Figure 6.7. Part (interpreted/uninterpreted) of MCS profile AWI-20140221. Location of the profile is shown in Figure 6.1. Horizontal scale is shown in the interpreted section. For colours and symbols refer to Figure 6.2. Dashed red line within seismic unit S2b-I indicates a sudden change in reflection geometries of the Neogene contourite.

ness, average seismic velocity and age results in a sedimentation rate of $\sim 34.8 \text{ m Myr}^{-1}$.

We observe only a slight difference between the depth of subunit S2b-I (Figure 6.6b) and that of the Cretaceous unit on top of the MozR segments (Figure 6.3a). As a consequence of the thick deposits in the transition zone to the surrounding basins the overall appearance of the unit's top is significantly shallower than that of the Cretaceous unit (Figure 6.2 CDPs 9800–11100, Figure 6.5 CDPs 4100–4750, Figure 6.6b). This results in a decrease of the rms depth of seismic unit S2b-I to 4013 ms TWT (thick magenta contour in Figure 6.6b). The maximum depth of 6337 ms TWT is observed in the southwest of the study area (Figure 6.6b $34.2^\circ\text{E}/34.9^\circ\text{S}$).

6.4.1.2. Subunit S2b-II ($\leq 2.6 \text{ Ma}$)

The Pleistocene to Holocene seismic subunit S2b-II comprise predominant subhorizontal reflections of moderate to strong amplitude that drape and onlap the underlying deposits (Figure 6.2 CDPs 8300–9000, 9700–10200). With a maximum thickness of 596 ms TWT (Figure 6.8a $33.3^\circ\text{E}/35.9^\circ\text{S}$) the thickest deposits occur south of the MozR below the rms depth of the Neogene subunit S2b-I (thick magenta contour in Figure 6.8a). Several depocentres (rms thickness $\geq 128 \text{ ms TWT}$; green to red areas in Figure 6.8a) occur on top and at the shallower flanks of the MozR segments (Figure 6.2

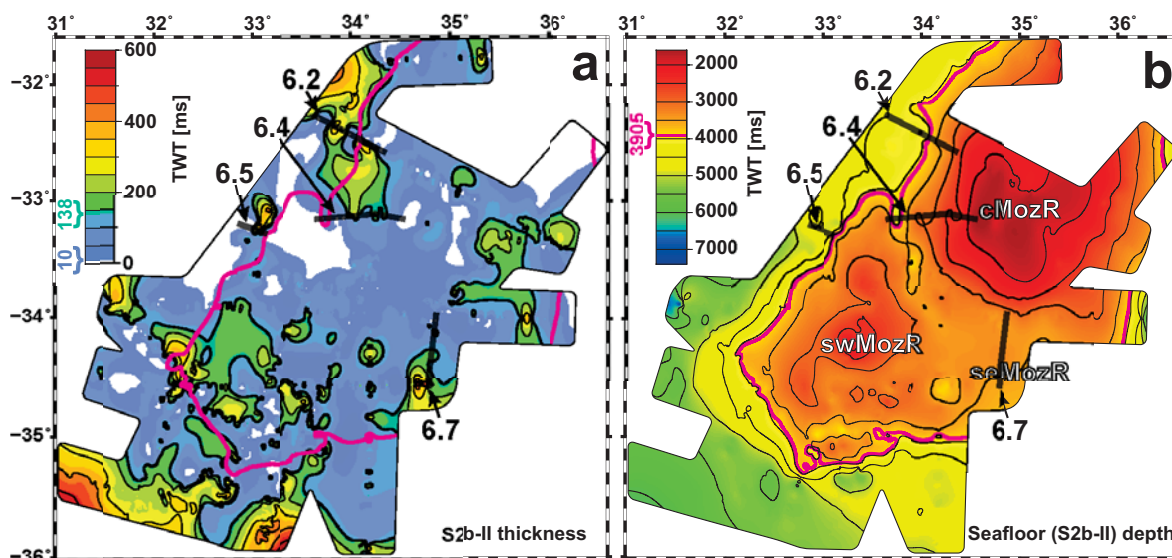


Figure 6.8. (a) Isopach map of the Quaternary seismic unit S2b-II. Thick black contours represent rms thickness (138 ms TWT; green number alongside colour scale), thin black contours represent thicknesses ≥ 200 ms TWT (interval of 100 ms TWT). Thick magenta contour indicates rms depth contour of underlying seismic unit S2b-I. Blue number alongside colour scale indicates minimum vertical resolution. Symbols are described in Figure 6.3. (b) Depth map (ms TWT, thin black 500 ms TWT depth contours, thick magenta rms depth contour) of seismic unit S2b-II (= seafloor). Symbols are described in Figure 6.3.

CDPs 8300–8900, Figure 6.4 CDPs 4400–500, Figure 6.7 CDPs 1900–3450).

At the swMozR we observe a number of small isolated depocentres of random distribution that seem to be confined to depths above the Neogene unit's rms depth (thick magenta contour in Figure 6.8a). However, the larger depocentres seem to be concentrated in depths below the S2b-I rms depth contour (Figure 6.2 CDPs 9700–10050, Figure 6.5 CDPs 3900–4150; thick magenta contour in Figure 6.8a). South of the MozR the depocentres express a slight E-W trend and are separated from the MozR segments by areas of strongly reduced sedimentary cover. Compared to the underlying subunit S2b-I, the sedimentation rate of the unit increases by $\sim 22\%$ to ~ 42.5 m Myr $^{-1}$.

The top of subunit S2b-II's represents the present day seafloor (Figure 6.8b). Considering the different domains (time vs. depth) the gridded S2b-II depth map shows a good correlation with the bathymetric map by Weatherall *et al.* (2015; Figure 6.1). We observe a maximum depth of 6265 ms TWT occurring west of the swMozR (Figure 6.8b 31.5°E/33.9°S), while the shallowest part of the unit is located in the area of the cMozR (1687 ms TWT; Figure 6.8b 35°E/32.2°S). The rms depth of the unit is calculated to be 3905 ms TWT (thick magenta contour in Figure 6.8b).

6.4.2. Contourites and erosional structures

Contourites are sediments deposited or significantly affected by prolonged bottom current activity with long-term mean velocities below 0.5 m s $^{-1}$ (Stow *et al.*, 2002; Stow and Faugères, 2008; Stow *et al.*, 2009; Rebesco *et al.*, 2014). Any semipermanent current that affects the seafloor by resuspending, transporting or controlling the deposition of sediments may be called a bottom current (Rebesco *et al.*, 2008; Stow *et al.*, 2008). The drifts are usually oriented parallel to the bathymetric contours and their geometries are controlled by the bathymetric framework, the current velocity and variability, the amount and type of sediment available, and the length of time over which the bottom current activity has operated (Faugères *et al.*, 1999; Uenzelmann-Neben *et al.*, 2007; Müller-Michaelis *et al.*, 2013).

Bodies of homogeneous weak amplitude reflections are associated with constant current conditions, whereas alternations of weak to moderate amplitude reflections with strong amplitude reflections usually indicate variations in current intensities or pathways (Faugères *et al.*, 1999; Stow *et al.*, 2002). High-velocity currents may also cause erosion or non-deposition of sediments that manifests itself in the occurrence of hiatuses, discontinuities or erosional structures like moats (Faugères *et al.*, 1999; Rebesco and Stow, 2001). The large number of contourites and erosional structures in the study area can be grouped based on their time of development. We will therefore first address structures occurring in subunit S2b-I (~15–5 Ma) followed by those located in subunit S2b-II (≤ 2.6 Ma).

6.4.2.1. Mid–Miocene to early Pliocene structures (~15–5 Ma; unit S2b-I)

Depositional structures resulting from current controlled sedimentation during Mid-Miocene to early Pliocene times occur in all depths throughout the study area (red lines in Figure 6.9a). Moats and scouring of the sedimentary cover are a common feature in the shallower parts of the study area, whereas contourites occur only sporadically. Most of the contourite drifts in the study area are observed at or adjacent to the steep flanks of the southern MozR and are often accompanied by erosional structures like moats (green lines in Figure 6.9a). We observe an up to ~35 km wide (E-W direction) elongated mounded drift contouring the western flank of the southern MozR over a distance of more than 350 km (Figure 6.9a 34.1°E/32.0°S–31.3°E/34.5°S). The drift shows a migration towards the flanks of the ridge (Figure 6.2 CDPs 9700–11000, Figure 6.5 CDPs 4150–4750) and decreases in thickness from more than 1100 m in the north to ~550 m in the south.

The passage between the cMozR and the swMozR is covered by a ~55 km wide elongated mounded and/or confined drift that comprise a large number of consecutive drift structures with dominant upslope migration (Figure 6.4 CDPs 3400/AWI-20140215–400/AWI-20140216). The relief of the contourite decreases towards both, the moat contouring the steep western flank of the cMozR (Figure 6.4 CDPs 400–1000), and the steep eastern flank of the swMozR (Figure 6.4 CDPs 3200–3400). Towards the southern part of the passage we observe well-developed erosional surfaces and an absence of drift structures (green lines around 34.1°E/33.8°S in Figure 6.9a).

In the deeper parts of the study area (below thick light blue contour in Figure 6.9a) we observe a 10 to 15 km wide and up to 700 m deep moat contouring the swMozR and seMozR (e.g., Figure 6.5 CDPs 3700–4200). A more than ~280 m thick (>rms thickness of 409 ms TWT) mounded drift is deposited next to the moat south of the swMozR and seMozR. The east-west trending drift shows a steeper northern and a gentler southern flank. We observe an up to 20 km wide (N-S direction) sediment wave field plastered on top of the gentler southern flank of the mounded drift (white wavy lines on top of red lines in Figure 6.9a). Both the mounded drift and the sediment waves show a northward migration towards the topographic highs of the southern MozR.

Most of the drifts in the study area consist of undulating parallel low to moderate amplitude reflections alternating with reflections of stronger amplitude (e.g., Figure 6.4 CDPs 3800–4600, Figure 6.5 CDPs 4200–4700). Drift bodies often show internal discontinuities and onlap of overlying reflections onto strong amplitude reflections (e.g., Figure 6.2 CDPs 10000–10200, 4500–5000 ms TWT). These discontinuities can be subtle but also more pronounced, as is the case for several contourites at the southern flank of the swMozR and on top of the seMozR. There, we observe widespread erosion of parts of the drifts along with sudden changes of their reflection geometries (e.g., Figure 6.7 CDPs 900–3500). The up to ~380 m thick drift on top of the cMozR shows truncation of its undulating reflections (Figure 6.7 CDPs 1200–3200), a downlap of overlying southward inclined reflections onto the eroded deposits (Figure 6.7 CDPs 2250–3200; separated by dashed red line, and truncation of the uppermost reflections causing its flat relief (Figure 6.7 CDPs 1600–3500).

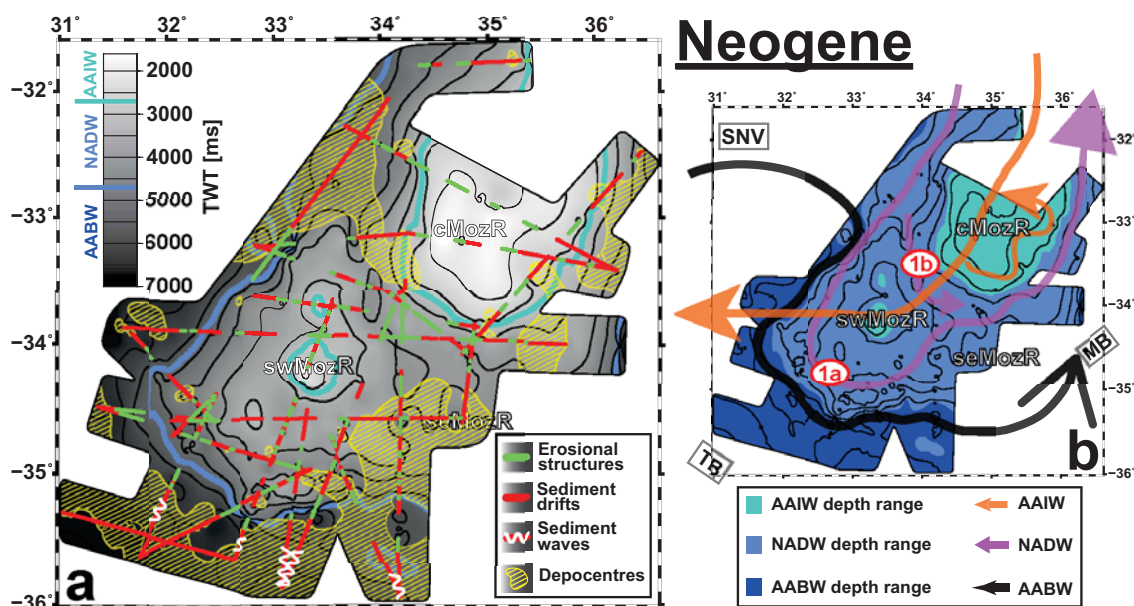


Figure 6.9. (a) Greyscale depth map of the Neogene seismic unit S2b-I (ms TWT, black 500 ms TWT depth contours). The turquoise and light blue depth contours indicate the boundary between Antarctic Intermediate Water (AAIW) and North Atlantic Deep Water (NADW; ~2000 mbsl/2700 ms TWT), and between NADW and Antarctic Bottom Water (AABW; ~3500 mbsl/4700 ms TWT), respectively. Observed depocentres (hatched in yellow), drift bodies (red lines), sediment waves (wavy white lines on top of red lines) and erosional structures (green lines) of seismic unit S2b-I are plotted on top. cMozR = central Mozambique Ridge, seMozR = south-eastern Mozambique Ridge, swMozR = south-western Mozambique Ridge. **(b)** Colour coded depth map of the Neogene seismic unit S2b-I (ms TWT, black 500 ms TWT depth contours). The modern depth intervals of AAIW are shown in turquoise (≤2000 mbsl/≤2700 ms TWT), of NADW in light blue (2000-3500 mbsl/2700-4700 ms TWT) and of AABW in deep blue (≥3500 mbsl/≥4700 ms TWT). The arrows show the inferred current pathways of AAIW (orange), NADW (purple) and AABW (black). The red numbers (1a, 1b) indicate different pathways of NADW. MB = Mozambique Basin, SNV = Southern Natal Valley, TB = Transkei Basin.

6.4.2.2. Pleistocene to Holocene structures (≤2.6 Ma; unit S2b-II)

In the shallower parts of the study area we observe an increase in the number of drift structures when compared to Neogene times along with decreased erosion of the Quaternary deposits by moats. In the passage between the cMozR and the swMozR we observe an up to ~150 m thick and ~12.5 km wide (E-W) mounded drift deposited in a depth of ~2400 ms TWT (Figure 6.4 CDPs 5100/AWI-20140215–300/AWI20140216). The steeper flank of the drift is facing the cMozR, whereas its western flank dips more gently. The drift consists of subparallel strong amplitude reflections that are slightly inclined towards the west. A up to ~10 km wide moat contours the steep western flank of the cMozR in depths above ~2500 ms TWT but causes only a slight decrease in thickness of the deposits (Figure 6.4 CDPs 300–700).

We observe strong spatial variations in the distribution of the deeper Quaternary depositional and erosional structures between the western and southern part of the study area (red and green lines below thick turquoise contour in Figure 6.10a). At the western flanks of the southern MozR drifts and moats occur only adjacent to steep topographic elevations (e.g., east of the PSM structure in Figure 6.2 CDPs 9200–9500). As opposed to that, we observe a large number of drifts and erosional structures in the southern part of the study area and in the deeper parts of the passage between the cMozR and swMozR. Here, the eastern flank of the swMozR is contoured by a moat scouring the Quaternary deposits and eroding parts of seismic unit S2b-I down to the top of the Cretaceous unit (Figure 6.4 CDPs 3400–3500).

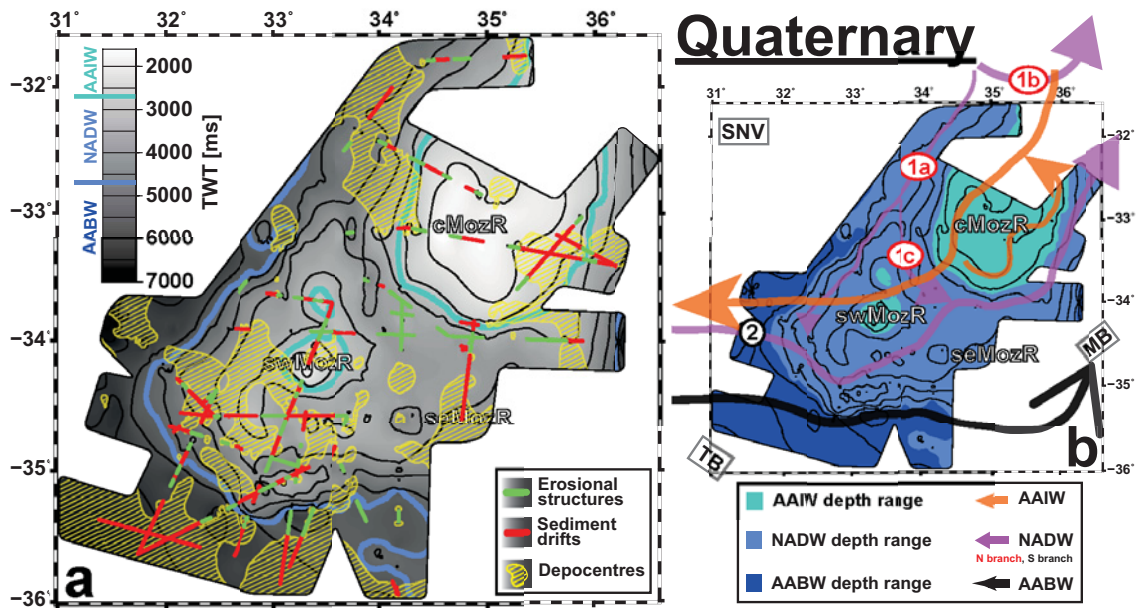


Figure 6.10. (a) Greyscale depth map of seismic unit S2b-II (= seafloor; ms TWT, black 500 ms TWT depth contours) with observed Quaternary depocentres (hatched in yellow), drift bodies (red lines) and erosional structures (green lines) shown on top. Abbreviations and colour code of blue contours as in Figure 6.9a. (b) Colour coded depth map (ms TWT, black 500 ms TWT depth contours) of Quaternary seismic unit S2b-II (= seafloor) with inferred circulation pathways of AAIW, NADW and AABW. Colour code and abbreviations as in Figure 6.9b. The red numbers (1a, 1b, 1c) indicate the pathway of the northern NADW branch, whereas the black '2' indicates the pathway of the southern NADW branch.

We observe several isolated drifts along with moats contouring the southwestern and southern flank of the swMozR in depths between ~3000 to 4500 ms TWT (red and green lines SW and S of swMozR in Figure 6.10a). The drifts comprise mostly subparallel strong amplitude reflections and show several discontinuities. The drifts south of the cMozR and on top of the seMozR show a more homogeneous seismic appearance and geometry. A large mounded drift occurs on top of the seMozR in a water depth of ~3250 ms TWT (Figure 6.7 CDPs 1600–2750). The drift is ~28 km wide and has a maximum thickness of ~130 m (Figure 6.7 CDP 2250). It consists of continuous slightly southward inclined medium to strong amplitude reflections. North of the drift we observe a channel (Figure 6.7 CDPs 1050–1150) next to the moat contouring the southern flank of the cMozR (Figure 6.7 CDPs 550–1000). Within the channel a complete absence of Quaternary deposits occur, whereas the moat only shows partial scouring or non-deposition of deposits.

In depths below ~4500 to 5000 ms TWT we observe an east-west trending moat along the southern MozR (green lines adjacent to thick light blue contour in Figure 6.10a). Within the moat we observe a strongly reduced Quaternary sediment cover and in places erosion into the underlying Neogene deposits. Towards the east we observe a widening of the moat and the occurrence of a sheeted drift covering large parts of the southernmost study area (red lines in southernmost part of Figure 6.10a).

6.5. Discussion

The late Cenozoic period was characterized by major palaeoceanographic, -climatic and tectonic changes. In order to reconstruct the impact of these modifications on the palaeocirculation in the study area we correlated the depth and characteristics of our observed depositional and erosional structures with the present day activity intervals of the water masses bathing the southern MozR (see chapter 6.2.1).

6.5.1. Mid-Miocene to early Pliocene palaeoceanographic implications (unit S2b-I)

The long-lasting Palaeogene to Neogene hiatus at the MozR seems to be a unique feature within the A–SO gateway and was previously attributed to a vigorous pre-Indian Ocean South Equatorial Current bathing the topographic high (Frakes and Kemp, 1972; Leclaire, 1974). The observed mid-Miocene to early Pliocene contourites on top of the unconformity (e.g., Figure 6.5 CDPs 4100–4700) favour a reduction of flow speeds with locally high current velocities indicated by the simultaneous occurrences of moats. The majority of those erosional features are confined to topographic elevations (e.g., Figure 6.4 CDPs 400–700), therefore demonstrating that the MozR severely guided and obstructed the Neogene circulation in the A–SO gateway.

The timing of the onset of current controlled sedimentation at the MozR coincides with major Miocene palaeoceanographic changes in the Southern Ocean. According to Schlüter and Uenzelmann-Neben (2008b) modifications of the Antarctic Circumpolar Current in response to the mid-Miocene cooling and West Antarctic glaciation (Zachos *et al.*, 2001; Shevenell *et al.*, 2008; Cramer *et al.*, 2011) resulted in a north-eastward flow of AABW into the Transkei Basin through a passage east of the Agulhas Plateau. Our observation of a deep moat contouring the western flank of the swMozR in depths below 4700 ms TWT (Figure 6.5 CDPs 3800–4200) suggests that influence of AABW on deposition in the study area was limited to areas south of ~33°S.

Towards the south the deep moat occurs on all of the MCS profiles covering the south-western and southern flanks of the southern MozR below ~4700 ms TWT (~3500 metres below sea-level) and separates it from the depocentres located farther away in the surrounding basins (hatched in yellow in Figure 6.9a). Along with the observed geometries and migration direction of the adjacent contourites this indicates a southward circulation of AABW contouring the western flanks of the swMozR (black arrow in Figure 6.9b). AABW flow then continued eastward along the southern flanks of the swMozR and seMozR before entering the Mozambique Basin southeast of the MozR (black arrow in Figure 6.9b).

It has been suggested that AABW caused a northward deflection of NADW entering the A–SO gateway through the Agulhas Passage (Schlüter and Uenzelmann-Neben, 2008b; Uenzelmann-Neben *et al.*, 2011). We observe a large number of contourites occurring in the activity interval of NADW (red lines between thick turquoise and thick light blue contours in Figure 6.9a, light blue areas in Figure 6.9b) with the ~380 km long elongated mounded drift contouring the western flank of the southern MozR representing the most prominent structure (Figure 6.2 CDPs 9700–11000, Figure 6.5 CDPs 4100–4700). The characteristics of the drift (e.g., eastward migration of drift crest) favour a southward flow of NADW along the steep western flanks of the southern MozR during Neogene times (purple arrow associated with red '1a' in Figure 6.9b). A similar route of NADW flow across the eastern Natal Valley was proposed by Dingle *et al.* (1987) as a result of the Naude Ridge hindering its further northward progress.

The drift geometries (e.g., Figure 6.7 CDPs 900–3500) and distribution of the depocentres (hatched in yellow in Figure 6.9a) in the southern part of the study area suggest that NADW circulation continued east- to north-eastward along the flanks of swMozR and cMozR before leaving the study area towards the northeast (purple arrow with red '1a' in Figure 6.9b). The occurrence of the drift at the western flank of the cMozR facing the swMozR (Figure 6.4 CDPs 3400/AWI-20140215–400/AWI-20140216) point towards parts of NADW circulation happening in a south- to south-eastward direction between both segments through a narrow corridor (purple arrow associated with red '1b' in Figure 6.9b).

Most of the contourite drifts occurring in depths similar to modern AABW and NADW show lower amplitude reflections alternating with stronger amplitude reflections (e.g., Figure 6.4 CDPs 3500–4600)

and sudden changes in reflection geometries (e.g., downlap of southward inclined reflections onto undulating reflections in Figure 6.7 CDPs 2200–3200). We suggest that these observations reflect modifications of current pathways or intensities during mid-Miocene to early Pliocene times. Such modifications can have either a climatic origin, for example due to variations in the extent of polar ice caps and sea ice, or a tectonic origin, for example the closing of gateways that control water mass exchange between ocean basins (Rebesco *et al.*, 2014). It was suggested that late Neogene fluctuations of AABW intensity were driven by alternating glacial and interglacial periods in Antarctica (Ramsay *et al.*, 1994; Pekar and DeConto, 2006). We propose that the observed discontinuities and alternating reflection amplitudes of the drifts located in depths similar to modern AABW may therefore reflect oscillations of Neogene Antarctic glaciation.

Poore *et al.* (2006) resolved late Neogene short-term fluctuations of the percentage of NADW in the Southern Ocean and correlated these with vertical motions of the Denmark Straits. The gradual shoaling of the Central American Seaway (CAS) during the late Neogene largely controlled activity and intensity of NADW in the Southern Ocean (Frank *et al.*, 2002; O’Dea *et al.*, 2016; Uenzelmann-Neben *et al.*, 2016). However, Coates *et al.* (2004) proposed a period of significant deepening of the CAS between 9 and 6 Ma. A stepwise intensification of NADW was postulated during late Miocene between 7.4 and 6.9 Ma (Billups, 2002; Diekmann *et al.*, 2003). We hypothesize that the prominent change in reflection geometries observed in several drifts (e.g., hatched red line in Figure 6.7 CDPs 3500–4600) may represent this stepwise increase during the late Miocene phase of CAS deepening. We therefore suggest that the observed seismic characteristics of the drifts in depths similar to modern NADW (e.g., alternating strong and weak amplitude reflections, discontinuities) were likely a far field effect of tectonic modifications.

We observe only a thin mid-Miocene to early Pliocene sedimentary cover and almost complete absence of depocentres in the depths above ~2700 ms TWT (~2000 metres below sea level; turquoise areas in Figure 6.9b). This is accompanied by the occurrence of several erosional features (green lines enclosed by turquoise contours in Figure 6.9a) that in places truncate the underlying deposits (e.g., Figure 6.4 CDPs 300–1350). We interpret this as evidence for the activity of a strong shallower water mass that caused non-deposition or erosion. Drifts occur only occasionally and are located next to erosional features (red lines enclosed by turquoise contours in Figure 6.9a).

According to Kuhnt *et al.* (2004) and Gourolan *et al.* (2008) the converging Australian and Sunda-land-Eurasian plates led to a major reorganization of Indian Ocean circulation during the mid-Miocene by establishing a strong westward current (MIOJet). It was suggested that the MIOJet strengthened and modified the shallower circulation at the southern MozR during mid-Miocene to early Pliocene times (Uenzelmann-Neben *et al.*, 2011) prior to its decrease due to the final closure of the Indonesian Gateway (Cane and Molnar, 2001; Gourolan *et al.*, 2008).

We therefore suggest that a southwest- to westward intensive AAIW flowed through the study area thereby leading to non-deposition or erosion at the cMozR and the swMozR (southwest directed orange arrow in Figure 6.9b). This pathway is in accordance with a postulated southward flow of AAIW causing erosional patches at the eastern Agulhas Plateau in depths above 2000 m during the Neogene (Uenzelmann-Neben *et al.*, 2007). The occurrences of several smaller drift bodies on the eastern flank of the cMozR indicate parts of AAIW circulated around its flanks (anti-clockwise orange arrow in Figure 6.9b).

6.5.2. Implementation of the modern circulation scheme in the A–SO gateway (unit S2b-II)

The reflections of the Pleistocene to Holocene seismic unit S2b-II unconformably overlie seismic unit S2b-I (e.g., Figure 6.2 CDPs 8300–8800). The well-preserved sedimentary structures of the

underlying unit favour the preceding early Pliocene to Pleistocene hiatus at the southern MozR to be a consequence of non-deposition rather than erosion. Nonetheless, the onset of sedimentation subsequent to the hiatus suggests a renewed decrease in current velocities at the southern MozR. The Quaternary sediments at several other locations off South Africa (e.g., Agulhas Ridge and Transkei Basin) exhibit similar seismic characteristics (subhorizontally stratified strong amplitude reflections, onlap on underlying seismic unit) that were attributed to an increase in the glaciation cycle frequency, responsible for sea level variation and variations in the sediment supply (Dingle and Camden-Smith, 1979; Niemi *et al.*, 2000; Wildeboer Schut *et al.*, 2002; Schlüter and Uenzelmann-Neben, 2007). We thus suggest that the layered strong amplitude reflections document the increase in the Quaternary glaciation cycle frequency.

We observe extensive depocentres in areas south of the MozR corresponding to the depth of AABW (areas hatched in yellow south of thick light blue contour in Figure 6.10a). The depocentres correlate with the occurrence of sheeted drifts that exhibit a continuous northward migration of their crests (red lines south of the MozR in Figure 6.10a). Furthermore, the drifts are separated from the steep flanks of the southern MozR by moats (green lines contouring thick light blue contour in Figure 6.10a). Together these features indicate a steady eastward setting bottom flow at the depth level of AABW along the southern flanks of the MozR. The timing of the termination of the hiatus and the onset of renewed deposition throughout the study area coincides with the final closure of the CAS (O'Dea *et al.*, 2016) and the onset of Northern Hemisphere Glaciation (Bartoli *et al.*, 2005).

These events not only modified NADW circulation (e.g., Frank *et al.*, 2002), but also caused a shift of the main inflow of AABW from south of the Transkei Basin to the Agulhas Passage along with a strong increase in sedimentation rate in the ~6000 ms TWT deep Transkei Basin (Schlüter and Uenzelmann-Neben, 2008b). The calculated ~22% increase in sedimentation rate between unit S2b-I to S2b-II at the southern MozR and the large E-W oriented depocentres and depositional structures south of the MozR confirm the postulated eastward flow of AABW. In accordance with Schlüter and Uenzelmann-Neben (2008b) we thus propose that both the final closure of the CAS and the onset of Northern Hemisphere Glaciation caused AABW to circulate eastward through the A–SO gateway along the southern flanks of the MozR and its continuation into the Mozambique Basin southeast of the seMozR (black arrow in Figure 6.10b).

We observe only weak evidence of current controlled sedimentation in the northwestern part of the study area in depths corresponding to NADW. Here, most of the Quaternary deposits consist of sub-horizontal, well-layered strong amplitude reflections with a smooth top (e.g., Figure 6.2 CDPs 8300–8800, 9700–10100, Figure 6.4 CDPs 4400–5000). We interpret this as an indication for predominant pelagic sedimentation in these areas. However, a large number of drifts and erosional structures (e.g., Figure 6.7 CDPs 575–825, 1050–1150, 1600–2750) indicating strong current control on sedimentation occur in the south of the study area (red and green lines enclosed by thick turquoise and light blue contours in Figure 6.10a).

We propose that the observed difference in strength of current controlled sedimentation between the northwestern and southern study area is the consequence of the existence of two NADW branches since Pleistocene or Pliocene times. In the following we will address the two branches as nNADW (northern NADW branch; purple arrows with red numbers in Figure 6.10b) and sNADW (southern NADW branch; purple arrows with black '2' in Figure 6.10b).

According to van Aken *et al.* (2004) partitioning of NADW is still a feature of today's circulation in the A–SO gateway, with one branch flowing northwards into the Natal Valley and the other one eastward into the Indian Ocean (purple arrows in Figure 6.1). Our seismic data show that nNADW has recirculated southward along the western flank of the MozR similar to its mid-Miocene to Pliocene pathway (purple arrow with red '1a' in Figure 6.10b). Our interpretation of a pelagic sedimentation with only

minor current control implies a weak southward NADW flow with only locally increased current velocities as a consequence of topography interaction (e.g., Figure 6.2 CDPs 9300–9500). The local strong increase of current velocities due to topographic interaction was observed at several locations and verified in modelling approaches (Roden, 1991; Verron and Le Provost, 2006).

We hypothesize that the decreased velocity of nNADW contouring the western flanks of the southern MozR (purple arrow with red '1a' in Figure 6.10b) could be the consequence of a large part of nNADW entering the Mozambique Basin via the gap between the northern and the southern MozR (purple arrow '1b' in Figure 6.10b). In the passage between the swMozR and the cMozR we observe only a thin sedimentary cover and a deep moat contouring the eastern flank of the swMozR (Figure 6.4 CDPs 3300–3500). At the shallower southern exit of the passage the sedimentary cover is strongly scoured by erosion (green lines at 33.9°–34.5°E/33.6°–34°S in Figure 6.10a). This suggests an increased velocity of the initially weak nNADW within the passage (purple arrow with red '1c' in Figure 6.10b). We relate this to southward narrowing and shallowing of the trough constraining the current and therefore increasing its velocity, a mechanism that was also proposed for NADW circulating through the Agulhas Passage (Schlüter and Uenzelmann-Neben, 2007, 2008b).

The observation of erosional structures and contourite drifts in the southern study area suggests a more vigorous eastward flow of sNADW (purple arrow with black '2' in Figure 6.10b). The distribution and geometries of the depositional structures indicate a anti-clockwise circulation of sNADW around parts of the swMozR before turning eastward causing formation of the mounded drift on top of the seMozR (Figure 6.7 CDPs 1600–2750). We hypothesize that the eastward turn of sNADW is a consequence of its interaction with nNADW exiting the passage between the cMozR and swMozR (purple arrow with red '1c' in Figure 6.10b).

The sedimentary features east of the cMozR suggest that sNADW contoured parts of the eastern flank of the cMozR before entering the Mozambique Basin (purple arrow with black '2' along eastern flank of cMozR in Figure 6.10b). Our results indicate that final closure of the CAS along with the onset of Northern Hemisphere Glaciation during Pliocene/Pleistocene were the driving factors behind the onset of a free circulation of deeper water masses (AABW and sNADW) through the A–SO gateway without major obstruction by the southern MozR.

The Quaternary deposits show only a thin cover (<100 ms TWT) in depths similar to modern AAIW (<2000 m). Nonetheless several depocentres do occur on top of the cMozR and swMozR (hatched in yellow in the turquoise areas in Figure 6.10a) and we observe an increase in the number of drift structures compared to unit S2b-I (Figure 6.4 CDPs 5100/AWI-20140215–300/AWI-20140216; red lines in the turquoise areas in Figure 6.10a). We interpret our observations as evidence for a sustained current control on sedimentation.

However, the increased abundance of depositional structures indicate an overall reduction of current velocities compared to mid-Miocene to early Pliocene times. Gurlan *et al.* (2008) proposed a reduction of the strong westward current of the MIOJet during late Pliocene due to the closure of the Indonesian seaway. We therefore suggest the decrease in current velocity of the AAIW to have been a consequence of the closure of the Indonesian seaway. Based on the observed drift geometries and the locations of the erosional structures at the southern MozR we infer that the pathway of AAIW circulation already established in mid-Miocene to early Pliocene was maintained (orange arrows in Figure 6.10b). This is supported by the observation of erosional patches on the eastern Agulhas Plateau caused by a southward setting current in depths above 2000 m (Uenzelmann-Neben *et al.*, 2007).

6.6. Conclusion

The MozR is an important feature within the A–SO gateway witnessing influence of circulation sys-

tems active in the Atlantic, the Indian, and the Southern oceans. A large number of depositional and erosional structures at the southern MozR indicate that throughout most of the late Cenozoic sedimentation has been influenced by persistent bottom currents. Our results indicate:

- (1) The onset of current controlled sedimentation in the mid-Miocene was caused by major palaeo-oceanographic changes (e.g., West Antarctic glaciation) and a subsequent shift of circulation pathways in the A–SO gateway. The occurrence of a large number of contourites and moats in depths >2000 m suggest that both AABW and NADW contoured the southern MozR. The reflection characteristics of the Neogene seismic unit (e.g., alternating weak and strong amplitude reflections) indicate recurring changes of circulation in the A–SO gateway as an effect of climatic (e.g., Antarctic interglacials) or tectonic modifications (e.g., vertical motion of Denmark Strait). The existence of a strong AAIW flow is based on observations of a thin sedimentary cover along with a number of erosional structures in depths <2000 m and may be related to the onset of a strong MIOJet due to narrowing and shallowing of the Indonesian Gateway.
- (2) The Quaternary deposits suggest that the NADW circulation scheme established during the Neogene was maintained, but the chaotic distribution of depocentres and the increased abundance of drifts in the south of the study area indicate the presence of two branches of NADW. The formation of contourite drifts at the southern flanks of the MozR points towards strong current controlled sedimentation during deposition of unit S2b-II and thus increased intensity of NADW. This cannot be observed at the western flank of the southern MozR, where we interpret mainly pelagic sedimentation and lower NADW flow velocities. On-going drift formation in activity depths of AABW suggest relatively stable current velocities since mid-Miocene times, even though our data confirms a shift of the main inflow of AABW into the A–SO gateway after the final closure of the CAS and the onset of Northern Hemisphere Glaciation. Our observations show that AAIW slowed down compared to its vigorous flow during Neogene times, which may be a consequence of the decrease of the MIOJet after the final closure of the Indonesian Gateway. We interpret the inception of the Pleistocene circulation scheme in the A–SO gateway as the initiation of the modern circulation that has persisted until today.

6.7. Acknowledgements

We want to express our gratitude to Captain Detlef Korte and his officers and crew of RV *Sonne* for their professional and enthusiastic engagement and service during the scientific program of this leg. The cruise leg SO 232 and the project SLIP were funded by the German Federal Ministry of Education and Research (BMBF) under project number 03G0232A. Additional funding has been provided by the Alfred-Wegener-Institut Helmholtz-Zentrum für Polar- und Meeresforschung.

7. Seismostratigraphic model of the southern Mozambique Ridge

For the reader's convenience, in the following I provide a graphic (Figure 7.1) and tabular summary (Table 7.1) of the seismostratigraphic model outlined in chapters 4, 5 and 6.

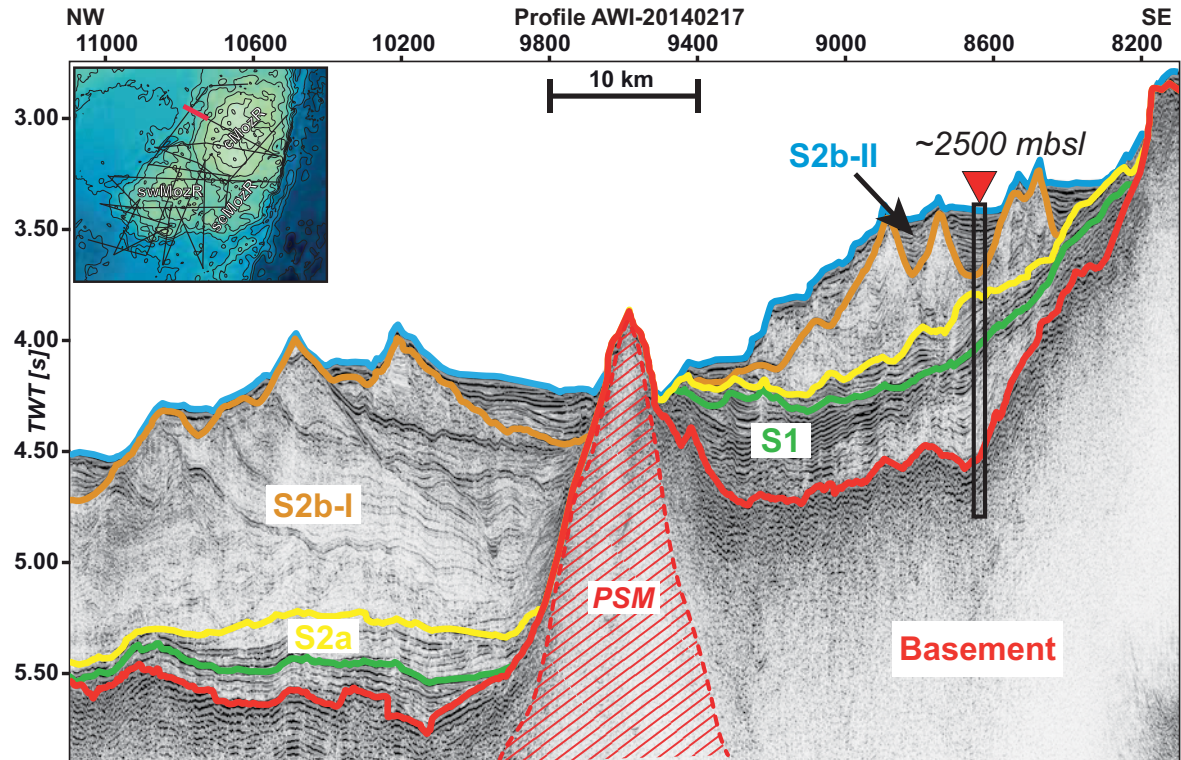


Figure 7.1. Seismostratigraphy of the southern Mozambique Ridge. Thick blue line = seafloor/top of unit S2b-II, thick brown line = top of unit S2b-I, thick yellow line = top of unit S2a, thick green line = top of unit S1, thick red line = top of basement, red dashed line along with red hatched filling = post-sedimentary magmatic structure, see description in chapter 4. The black bar with the red triangle on top indicates the proposed location of Drill Site A, please refer to chapter 9 for further information. For a detailed description of the individual seismic units please refer to Tab.1. The location of the profile is illustrated by the red line in the inset showing the bathymetry of the study area (Weatherall *et al.*, 2015).

Table 7.1. Seismic stratigraphy of the study area

Seismic units of the southern MozR	Thickness; rms thickness [ms TWT] ^{c,d,e}	Estimated age [Ma] ^{a,c}	Material ^a	Seismic characteristics ^{c,d,e}	Correlation with published lithological units and seismic stratigraphies ^{a,b}	Remarks
S2						
S2b		15–0 ^a			Unit I ^a , Unit S2 ^b	
S2b-II	0–596; 138	2.6–0 ^a	S imilar to S2b-I but higher percentage of foraminifera and lower percentage of clay	S ubhorizontal moderate to strong amplitude reflections of lower frequency; sporadically continuous weaker amplitude reflections		Unconformably overlies S2b-I
S2b-I	0–1280; 409	15–5 ^a	F oram nanno ooze, varying amounts of foraminifera, clay and chalk	M ostly undulating continuous reflections with weak to moderate amplitudes and low to medium frequency; occasionally strong amplitude reflections; discontinuities		Hiatus (2–3 Myr) on top of S2b-I
S2a	0–840; 160	75–68 ^a	F oram-bearing clay-rich nanno chalk	D iscontinuous medium to high amplitude reflection band of lower frequency	Unit II ^a , Unit S2 ^b	Hiatus (~50 Myr) on top of S2a
S1	0–611; 131	<128, 66–100 ^{a,c}	S ilty claystone, clay content increases towards the base, volcanics in upper part	M edium to strong amplitude reflections (upper part); weaker amplitude reflections (lower part); low to medium frequency reflections; less continuous reflections in lower part	Subunit IIIA ^a , Unit S1 ^b	Hiatus on top of S1; age of oldest deposits decrease to the S due to younger basement; layers with TOC up to 1.7%
Basement		130.86–124.90 ^c	T holeiitic basalt	S trong impedance contrast at top; high amplitude, low frequency reflections; subparallel sequences of internal reflections, piecewise continuous and up to 800 ms TWT deep	Basement ^{a,b}	Age depending on respective segment of MozR

^aSimpson et al. (1974); ^bUenzelmann-Neben et al. (2011); ^cFischer et al. (2017); ^dFischer and Uenzelmann-Neben (2017a); ^eFischer and Uenzelmann-Neben (2017b)

8. Conclusion

The main objective of this thesis was to resolve the structure and origin of the MozR basement and its influence on ocean circulation since its formation. This chapter summarizes the key findings described and discussed in chapters 4, 5 and 6 with regard to the research questions provided in chapter 1.4.

The new high-resolution MCS reflection data covering the southern MozR enabled a comprehensive analysis of the subsurface for the first time. Its interpretation draws a complex picture of the evolution of the southern MozR. The individual events during the evolution of the MozR and the A–SO gateway that led towards the circulation scheme that persists today are illustrated in Figure 8.1.

The first part of this study (chapter 4) covers a detailed investigation of the MozR basement, which is characterized by the occurrence of thick and laterally extensive lava flow sequences and a large number of ECs typical for LIPs. Further evidence for a LIP origin of the southern MozR is provided by its calculated areal extent and magmatic volume. Both values exceed the threshold values required for qualifying as a LIP by far and suggest its emplacement as a consequence of excessive magmatism during the Early Cretaceous.

Indications for a sequential development of the LIP were identified, which is supported by published magnetic anomaly data (König and Jokat, 2010). Based on the calculated magmatic volume of the southern MozR, its formation can be confined to the time between ~131 and 125 Ma. This timing ties in with a recent plate tectonic reconstruction by König and Jokat (2010) and coincides with the final phase of Gondwana breakup.

This study therefore helps to settle the controversial question concerning the probable origin of the MozR, since my observations suggest that the MozR can be added to the already vast number of Cretaceous LIPs.

The second and third part of the study (chapters 5 and 6) correlate the observed seismic attributes and the characteristics of the Cretaceous and late Cenozoic sedimentary units with postulated palaeoceanographic events. I observed a strong impact of regional and global tectonic and climatic modifications on the depositional conditions in the study area, and strong evidence for the alteration of the water mass exchange between the Atlantic and Indian Oceans by the MozR.

I determined topography to be the controlling factor of the Early Cretaceous depositional environment. Topographic highs, such as the Falkland Plateau and the MozR, effectively blocked the commencing sluggish eastward circulation in the Southern Ocean from entering the A–SO gateway ('Early Cretaceous' box in Figure 8.1). This is documented by a drape of the magmatic basement by sediments deposited under euxinic conditions.

Volcanogenic sediments and a strong increase in reflection amplitudes indicate a mid-Cretaceous magmatic reactivation of the MozR that culminated in its uplift (Chapter 5). A Turonian unconformity observed at several locations within the A–SO gateway was attributed to the existence of a vigorous shallow circulation, and correlated with the ~25 Myr long-lasting hiatus occurring at the MozR ('Mid- to Late Cretaceous' box in Figure 8.1; Dingle *et al.*, 1978). This suggests initiation of a shallow circulation between the Atlantic and Indian Oceans by late Turonian times.

The identification of Late Cretaceous sediment drifts contouring the southern MozR implies a decrease of shallow current velocities. This indicates the onset of shallow current controlled sedimentation in the A–SO gateway long before the first occurrence of deep current controlled sedimentation in late Palaeogene times (Schlüter and Uenzelmann-Neben, 2008b). A Late Cretaceous onset corre-

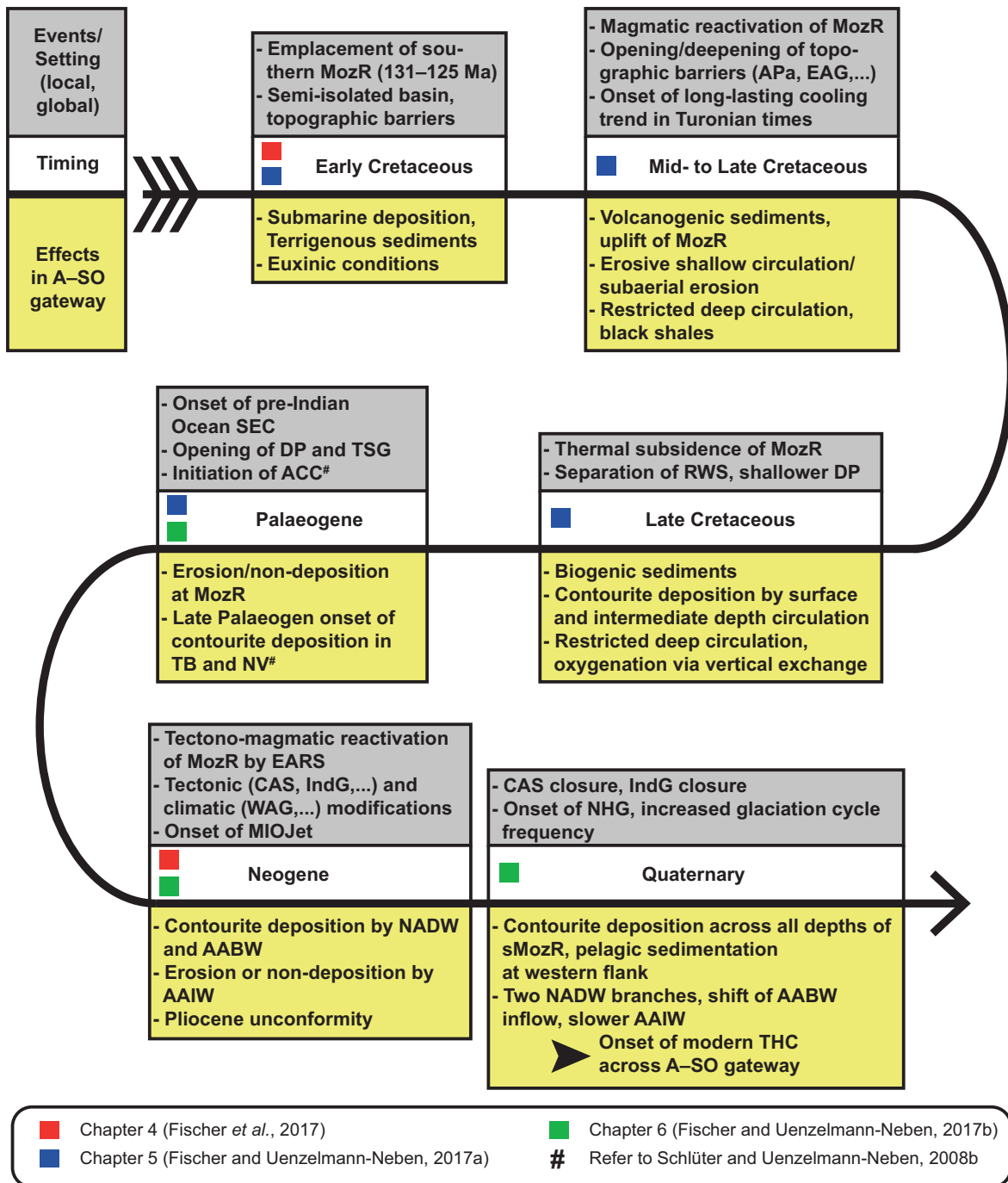


Figure 8.1. Summary of the regional and global events during the period of initial MozR LIP formation and restricted circulation until initiation of modern, unrestricted thermohaline circulation through the African–Southern Ocean (A–SO) gateway. The coloured rectangles/the hashtag refer to the chapters/reference that provide a more detailed discussion of the individual topic. For further information regarding the AABW = Antarctic Bottom Water, AAIW = Antarctic Intermediate Water, ACC = Antarctic Circumpolar Current, APa = Agulhas Passage, CAS = Central American Seaway, DP = Drake Passage, EAG = Equatorial Atlantic Gateway, EARS = East African Rift System, IndG = Indonesian Gateway, MozR = Mozambique Ridge, NADW = North Atlantic Deep Water, NHG = Northern Hemisphere Glaciation, NV = Natal Valley, RWS = Rio Grande–Walvis Ridge System, SEC = South Equatorial Current, TB = Transkei Basin, TSG = Tasmanian Gateway, WAG = West Antarctic Glaciation.

lates well with the major reorganization of global palaeocean circulation driven by extensive tectonic changes in the South Atlantic Ocean ('Late Cretaceous' box in Figure 8.1; Moiroud *et al.*, 2016).

The MozR was affected by a long-lasting Tertiary hiatus ('Palaeogene' box in Figure 8.1) resulting

from a strong current that circulated within the Indian Ocean (Leclaire, 1974). Late Neogene sediment drifts indicate that current velocities slowed down at the MozR in depths similar to modern NADW and AABW (Chapter 6). The occurrence of widespread erosion in AAIW depth suggests that shallow circulation remained vigorous.

The distinct change in the mid-Miocene circulation scheme was caused by a combination of several tectonic (e.g., narrowing of Indonesian Gateway) and climatic (e.g., West Antarctic Glaciation) modifications that occurred both to the east and to the west of the gateway ('Neogene' box in Figure 8.1). A great number of late Neogene PSM structures and neotectonic faults along the lower flanks of the southern MozR provide evidence for its tectono-magmatic reactivation (Chapter 4). This is interpreted as evidence for the highly debated seaward propagation of the Western branch of the EARS.

A Pliocene unconformity is considered to represent the transition towards the modern THC in the A–SO gateway. The onset of renewed drift deposition correlates with the final closure of the CAS and the inception of Northern Hemisphere Glaciation ('Quaternary' box in Figure 8.1). Subhorizontal strong amplitude reflections of the Quaternary seismic unit are interpreted as the consequence of the increase in glaciation cycle frequency during Pleistocene times.

The distribution of the contourite drifts at the southern MozR support a shift of the inflow of AABW into the A–SO gateway to the Agulhas Passage. Predominant pelagic sedimentation at the western flank of the MozR and contemporary current controlled sedimentation in the southern study area in comparable depths indicate the existence of two individual NADW branches.

The weak NADW flow at the western flank is the result of large parts of this NADW branch leaving the A–SO gateway to the north of the MozR. The southern NADW branch enters the Mozambique Basin in a more direct way. Therefore, I suggest that a deep THC (AABW and NADW) through the A–SO gateway without major alteration of flow paths by the MozR was initiated as a result of the Pliocene to Pleistocene tectonic and climatic modifications.

Furthermore, the initiation of contourite drift deposition in AAIW depth indicates a decrease of the previously strong current. This decrease corresponds to the closure of the Indonesian Gateway and a reduction of the strong westward flowing MIOJet, hence implying a positive correlation of AAIW flow speed with MIOJet activity in the Quaternary.

9. Outlook

In the previous chapters the study provided a comprehensive analysis and discussion of the research questions presented in the introduction (chapter 1.4). However, during preparation of the study many additional questions arose. These questions are addressed in this chapter.

First of all, I will focus on how to improve the seismostratigraphic model for the Mozambique Ridge that was developed in this dissertation. Obviously, with the lack of a correlation of the seismic data with geologic data from a drill site, the seismostratigraphic model would greatly benefit from an intersection with DSDP Leg 25 Site 249 (orange star in Figure 9.1).

However, due to the occurrence of a deep depression between the northern MozR and the southern segments of the MozR a direct correlation of the MCS reflection data covering the southern MozR with DSDP Site 249 could pose a problem.

Therefore, I propose the possible locations of two drill sites at the southern MozR (red and green stars in Figure 9.1). Both drill sites penetrate the entire Cretaceous and Cenozoic sedimentary sequence of the seismostratigraphic model and intersect the MCS reflection profiles used in this study (Table 9.1). Drill Site A (red star in Figure 9.1) is located in a water depth of ~2500 m and penetrates ~1135 m of sediments before reaching the basement (black bar with red triangle in Figure 7.1). Its great water depth and its thick total penetration depth may represent a critical issue for a successful completion of the drilling operation.

The second drill site is located at shallower depth (~1600 m water depth) at the eastern flank of the cMozR (green star in Figure 9.1). With a probable penetration depth of ~505 m Drill Site B represents the primary target for a successful correlation with the available MCS reflection data (Figure 9.2). Age dating of the drill cores and the correlation of the results with the MCS reflection data would greatly improve the quality of the already gathered geophysical data and enable an evaluation of the seis-

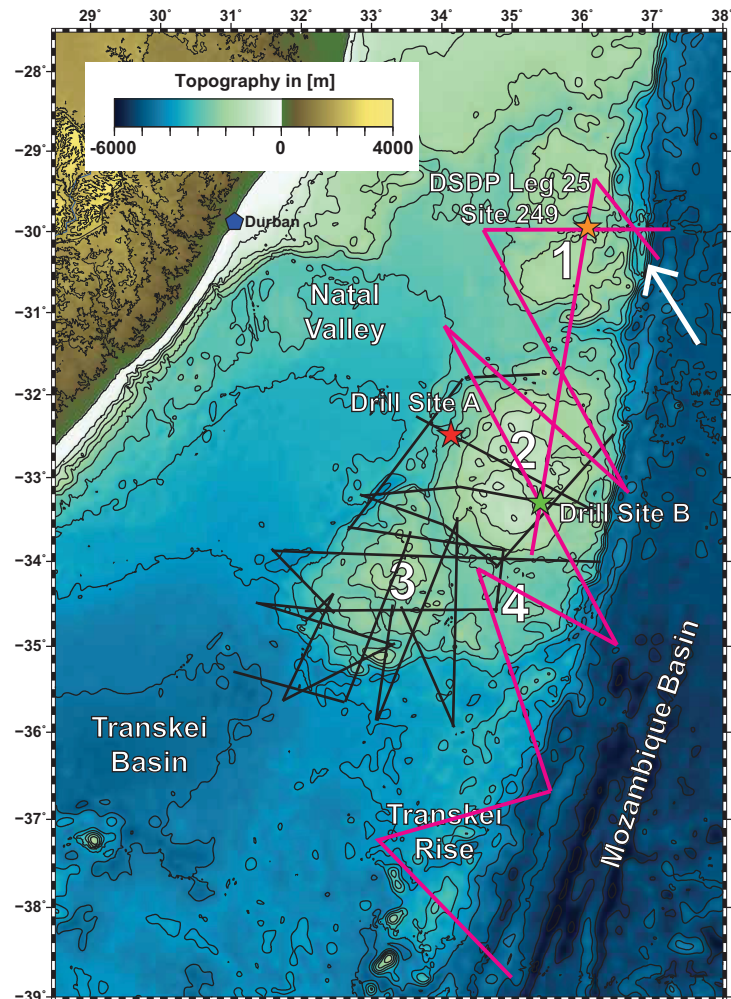


Figure 9.1. Bathymetric map (Weatherall *et al.*, 2015) of the study area showing the key structural units mentioned in this chapter. The magenta lines illustrate the locations of the new proposed MCS reflection profiles, while the red (Drill Site A) and the green stars (Drill Site B) indicate the locations of the proposed drill sites. The white arrow points to the continental fragment east of the nMozR. The black lines represent the MCS profiles used in this study. The orange star corresponds to the location of DSDP Site 249. Durban, South Africa, is marked by a blue pentagram. 1 = northern MozR, 2 = central MozR, 3 = southwestern MozR, 4 = southeastern MozR.

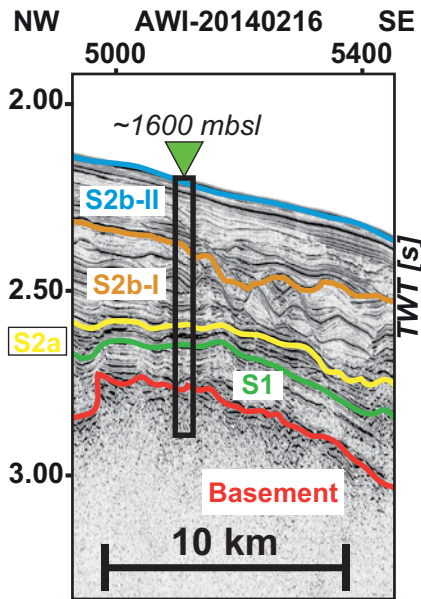


Figure 9.2. Interpreted section of MCS profile AWI-20140216 along proposed Drill Site B. Its location is shown in Figure 9.1. The parameters of Drill Site B are listed in Table 9.1. Seismic stratigraphy as described in chapter 7.

Table 9.1. Parameters of proposed drill sites A and B.

Drill Site	A	B
Water depth [m]	~2500	~1600
Unit S2b-II thickness [m]	~225	~135
Top of unit S2b-I [mbsf]	~225	~135
Unit S2b-I thickness [m]	~100	~180
Top of unit S2a [mbsf]	~325	~315
Unit S2a thickness [m]	~210	~55
Top of unit S1 [mbsf]	~535	~370
Unit S1 thickness [m]	~600	~135
Basement reached [mbsf]	~1135	~505

mostratigraphic model. Furthermore, in case of reaching the basement, samples would provide a basis for the first direct age dating of the basaltic basement of the MozR.

The second objective I am addressing is a necessary extension of the geophysical dataset. Therefore, I propose the acquisition of ten additional MCS reflection profiles (magenta lines in Fig.). The profiles cover the Transkei Rise in the south of the MozR, the seMozR and eastern parts of the cMozR (including transition into the Mozambique Basin), and parts of the nMozR. The proposed profiles intersect DSDP Site 249 and Drill Site B and can thus be used for further improvement of the seismostratigraphic model. The locations of the profiles were selected in order to resolve the following open questions:

- (1) Are there indications for a formation of the Transkei Rise due to (decreased) magmatic activity subsequent to emplacement of the southern MozR?

Gohl *et al.* (2011) proposed the formation of a Southeast African LIP between 140 and 95 Ma. The postulated LIP consisted of the MozR, the Agulhas Plateau, the Transkei Rise, the Maud Rise and the North–East Georgia Rise before its separation. The Southeast African LIP would have comprised a total area of $\sim 1.2 \times 10^6 \text{ km}^2$, which is comparable in size to the greater Kerguelen–Heard Plateau LIP. According to Gohl *et al.* (2011) the Transkei Rise (south of the MozR in Figure 9.1) was emplaced by active LIP magmatism of less intensity that occurred during the interval of MozR and Agulhas Plateau formation. MCS reflection data covering the Transkei Rise and the transition zone from the southern MozR towards it could provide further support for the hypothesis of a Southeast African LIP by confirming the affiliation of both structural units.

- (2) Why is the seMozR substantially less elevated than the other segments of the southern MozR? Does it represent the shift to the phase of strongly reduced LIP magmatism due to shutoff of dike propagation (Karlstrom and Richards, 2011)?

According to several authors (Bryan *et al.*, 2002; Coffin *et al.*, 2002; Jerram and Widowson, 2005) the transition from the main eruption phase to the phase of strongly decreased magmatic output happens abruptly and may introduce a phase of more protracted volcanism where eruptions become more widely distributed.

Additional MCS profiles covering the seMozR (4 in Figure 9.1) are needed for a full evalua-

tion of the areal extent of this part of the ridge. So far, seismic data only covers the edges of the segment, which pose difficulties to assessing its true extent and magmatic volume. This could show if the magmatic output have waned down abruptly or gradually, and could support the hypothesis that the Transkei Rise was a product of less intensive LIP magmatism (Gohl *et al.*, 2011).

- (3) Is there evidence for neotectonic activity at the eastern flank of the MozR?

The MCS reflection profiles across the Andrew Bain Fracture Zone into the Mozambique Valley cover the area of the proposed western boundary of the Lwandle microplate (Stamps *et al.*, 2008; Saria *et al.*, 2014; Stamps *et al.*, 2014). East-west trending (normal) faulting may indicate a correlation with the proposed northeast to southwest direction of the boundary and contribute to the determination of the exact location of it. Together with a reassessment of the neotectonic activity on the basis of the already available MCS reflection data, this could also specify the location of the fault line of the Western branch of the EARS along the western flanks of the MozR.

- (4) Are there differences of the basement structure and sedimentary distribution between the nMozR and the southern MozR? How far does the MozR extent towards the north?

To answer these questions, additional MCS reflection profiles that link the available seismic data covering the southern MozR with the nMozR are required. The suggested MCS reflections profiles intersect the available MCS data in several locations, and enable a correlation with the results of DSDP Site 249 and the proposed Drill Site B (magenta lines in Figure 9.1). Two of the suggested profiles cross a ~110 km long north-south trending structure (white arrow in Figure 9.1) that is separated from the nMozR by a linear depression. The structure was dredged during SO183 and SO232, and it was hypothesized that it represents a continental crustal bloc that was sheared off into the ocean basin during the initial opening of the southeastern Indian Ocean by transform faulting (Jokat, 2006; Uenzelmann-Neben, 2014). Further investigation of the structure via seismic reflection profiling may therefore contribute to the discussion if it can indeed be associated with the initial rifting of Gondwana.

The previously mentioned topics can be addressed with the help of additional geophysical data. In the following, I will give a brief outlook on questions that could be answered by geochemical and petrological investigations.

As illustrated in (Figure 2.2) a total number of 59 dredges with a great variety of rock samples were acquired during RV Sonne expedition SO232 and are further analysed by GEOMAR (Uenzelmann-Neben, 2014). These analyses will provide a better age constraint for the basaltic basement and the PSM structures. In addition, the investigation of the dredge samples in regard to geochemical signatures of palaeocean proxies, such as radiogenic Neodymium and Lead isotopes, could help to identify the water masses that have caused formation of the depositional features.

10. Bibliography

- Arhan, M., Mercier, H., Park, Y.-H., 2003. On the deep water circulation of the eastern South Atlantic Ocean. *Deep Sea Research Part I: Oceanographic Research Papers* 50, 889-916, 10.1016/S0967-0637(03)00072-4.
- Armstrong McKay, D.I., Tyrrell, T., Wilson, P.A., Foster, G.L., 2014. Estimating the impact of the cryptic degassing of Large Igneous Provinces: A mid-Miocene case-study. *Earth and Planetary Science Letters* 403, 254-262, 10.1016/j.epsl.2014.06.040.
- Baksi, A.K., 1989. Reevaluation of the timing and duration of extrusion of the Innaha, Picture Gorge, and Grande Ronde Basalts, Columbia River Basalt Group. *Geological Society of America Special Papers* 239, 105-112, 10.1130/SPE239-p105.
- Barrera, E., Savin, S.M., 1999. Evolution of late Campanian-Maastrichtian marine climates and oceans. *Geological Society of America Special Papers* 332, 245-282, 10.1130/0-8137-2332-9.245.
- Bartoli, G., Sarnthein, M., Weinelt, M., Erlenkeuser, H., Garbe-Schönberg, D., Lea, D.W., 2005. Final closure of Panama and the onset of northern hemisphere glaciation. *Earth and Planetary Science Letters* 237, 33-44, 10.1016/j.epsl.2005.06.020.
- Barton, P.J., 1986. The relationship between seismic velocity and density in the continental crust — a useful constraint? *Geophysical Journal of the Royal Astronomical Society* 87, 195-208, 10.1111/j.1365-246X.1986.tb04553.x.
- Ben-Avraham, Z., Hartnady, C.J.H., Kitchin, K.A., 1997. Structure and tectonics of the Agulhas-Falkland fracture zone. *Tectonophysics* 282, 83-98, 10.1016/S0040-1951(97)00213-8.
- Ben-Avraham, Z., Hartnady, C.J.H., le Roex, A.P., 1995. Neotectonic activity on continental fragments in the Southwest Indian Ocean: Agulhas Plateau and Mozambique Ridge. *Journal of Geophysical Research* 100, 6199-6211, 10.1029/94jb02881.
- Ben-Avraham, Z., Niemi, T.M., Hartnady, C.J.H., 1994. Mid-Tertiary changes in deep ocean circulation patterns in the Natal Valley and Transkei basin, Southwest Indian Ocean. *Earth and Planetary Science Letters* 121, 639-646, 10.1016/0012-821X(94)90097-3.
- Bernard, A., Munsch, M., Rotstein, Y., Sauter, D., 2005. Refined spreading history at the Southwest Indian Ridge for the last 96 Ma, with the aid of satellite gravity data. *Geophysical Journal International* 162, 765-778, 10.1111/j.1365-246X.2005.02672.x.
- Bice, K.L., Birgel, D., Meyers, P.A., Dahl, K.A., Hinrichs, K.-U., Norris, R.D., 2006. A multiple proxy and model study of Cretaceous upper ocean temperatures and atmospheric CO₂ concentrations. *Paleoceanography* 21, PA2002, 10.1029/2005PA001203.
- Billups, K., 2002. Late Miocene through early Pliocene deep water circulation and climate change viewed from the sub-Antarctic South Atlantic. *Palaeogeography, Palaeoclimatology, Palaeoecology* 185, 287-307, 10.1016/S0031-0182(02)00340-1.

- Bond, D.P.G., Wignall, P.B., 2014. Large igneous provinces and mass extinctions: An update. *Geological Society of America Special Papers* 505, 29-55, 10.1130/2014.2505(02).
- Brady, E.C., DeConto, R.M., Thompson, S.L., 1998. Deep water formation and poleward ocean heat transport in the warm climate extreme of the Cretaceous (80 Ma). *Geophysical Research Letters* 25, 4205-4208, 10.1029/1998GL900072.
- Brown, E., Colling, A., Park, D., Phillips, J.D., Rothery, D., Wright, J.B., 1999. *Waves, Tides And Shallow-Water Processes*, 2nd ed. ed. Butterworth-Heinemann, Oxford, 0750642815.
- Bryan, S.E., Ernst, R.E., 2008. Revised definition of Large Igneous Provinces (LIPs). *Earth-Science Reviews* 86, 175-202, 10.1016/j.earscirev.2007.08.008.
- Bryan, S.E., Ferrari, L., 2013. Large igneous provinces and silicic large igneous provinces: Progress in our understanding over the last 25 years. *Geological Society of America Bulletin*, 10.1130/B30820.1.
- Bryan, S.E., Peate, I.U., Peate, D.W., Self, S., Jerram, D.A., Mawby, M.R., Marsh, J.S., Miller, J.A., 2010. The largest volcanic eruptions on Earth. *Earth-Science Reviews* 102, 207-229, 10.1016/j.earscirev.2010.07.001.
- Bryan, S.E., Riley, T.R., Jerram, D.A., Stephens, C.J., Leat, P.T., 2002. Silicic volcanism: An undervalued component of large igneous provinces and volcanic rifted margins, in: Menzies, M.A., Klemperer, S.L., Ebinger, C.J., Baker, J. (Eds.), *Volcanic Rifted Margins*. Geological Society of America Special Paper, Boulder, Colorado, pp. 99-120, 10.1130/0-8137-2362-0.97.
- Calais, E., Ebinger, C., Hartnady, C., Nocquet, J.M., 2006. Kinematics of the East African Rift from GPS and earthquake slip vector data. *Geological Society, London, Special Publications* 259, 9-22, 10.1144/GSL.SP.2006.259.01.03.
- Camp, V.E., Ross, M.E., Hanson, W.E., 2003. Genesis of flood basalts and Basin and Range volcanic rocks from Steens Mountain to the Malheur River Gorge, Oregon. *Geological Society of America Bulletin* 115, 105-128, 10.1130/0016-7606(2003)115<0105:GOFBAB>2.0.CO;2.
- Campbell, I.H., 2007. Testing the plume theory. *Chemical Geology* 241, 153-176, 10.1016/j.chemgeo.2007.01.024.
- Cane, M.A., Molnar, P., 2001. Closing of the Indonesian seaway as a precursor to east African aridification around 3-4 million years ago. *Nature* 411, 157-162, 10.1038/35075500.
- Castelino, J.A., Eagles, G., Jokat, W., 2016. Anomalous bathymetry and palaeobathymetric models of the Mozambique Basin and Riiser Larsen Sea. *Earth and Planetary Science Letters* 455, 25-37, 10.1016/j.epsl.2016.09.018.
- Castelino, J.A., Reichert, C., Klingelhoefer, F., Aslanian, D., Jokat, W., 2015. Mesozoic and Early Cenozoic sediment influx and morphology of the Mozambique Basin. *Marine and Petroleum Geology* 66, Part 4, 890-905, 10.1016/j.marpetgeo.2015.07.028.

- Chapman, D.C., Haidvogel, D.B., 1992. Formation of Taylor caps over a tall isolated sea-mount in a stratified ocean. *Geophysical & Astrophysical Fluid Dynamics* 64, 31-65, 10.1080/03091929208228084.
- Chetty, P., Green, R.W.E., 1977. Seismic Refraction Observations In The Transkei Basin And Adjacent Areas. *Marine Geophysical Researches* 3, 197-208, 10.1007/BF00310110.
- Chorowicz, J., 2005. The East African rift system. *Journal of African Earth Sciences* 43, 379-410, 10.1016/j.jafrearsci.2005.07.019.
- Claerbout, J.F., 1985a. *Fundamentals of geophysical data processing*. Blackwell Science Inc, Oxford, 9780865423053.
- Claerbout, J.F., 1985b. *Imaging the earth's interior*. Blackwell Science Inc, Oxford, 9780865423046.
- Coates, A.G., Collins, L.S., Aubry, M.-P., Berggren, W.A., 2004. The Geology of the Darien, Panama, and the late Miocene-Pliocene collision of the Panama arc with northwestern South America. *Geological Society of America Bulletin* 116, 1327-1344, 10.1130/B25275.1.
- Coffin, M.F., Eldholm, O., 1991. Large Igneous Provinces: JOI/USSAC Workshop Report, Technical Report. University of Texas, Austin Institute for Geophysics, p. 79 pp.
- Coffin, M.F., Eldholm, O., 1994. Large igneous provinces: crustal structure, dimensions, and external consequences. *Reviews of Geophysics* 32, 1-36, 10.1029/93RG02508.
- Coffin, M.F., Pringle, M.S., Duncan, R.A., Gladchenko, T.P., Storey, M., Müller, R.D., Gahagan, L.A., 2002. Kerguelen Hotspot Magma Output since 130 Ma. *Journal of Petrology* 43, 1121-1137, 10.1093/petrology/43.7.1121.
- Coffin, M.F., Rabinowitz, P.D., 1988. Evolution of the conjugate East African - Madagascan margins and the western Somali Basin. *Geological Society of America Special Papers* 226, 1-79, 10.1130/SPE226-p1.
- Corti, G., van Wijk, J., Cloetingh, S., Morley, C.K., 2007. Tectonic inheritance and continental rift architecture: Numerical and analogue models of the East African Rift system. *Tectonics* 26, Tc6006, 10.1029/2006TC002086.
- Courtillot, V., Davaille, A., Besse, J., Stock, J., 2003. Three distinct types of hotspots in the Earth's mantle. *Earth and Planetary Science Letters* 205, 295-308, 10.1016/S0012-821X(02)01048-8.
- Courtillot, V.E., Renne, P.R., 2003. On the ages of flood basalt events. *Comptes Rendus Geoscience* 335, 113-140, 10.1016/S1631-0713(03)00006-3.
- Cramer, B.S., Miller, K.G., Barrett, P.J., Wright, J.D., 2011. Late Cretaceous–Neogene trends in deep ocean temperature and continental ice volume: Reconciling records of benthic foraminiferal geochemistry ($\delta^{18}\text{O}$ and Mg/Ca) with sea level history. *Journal of Geophysical Research: Oceans* 116, C12023, 10.1029/2011JC007255.

- Crisp, J.A., 1984. Rates of magma emplacement and volcanic output. *Journal of Volcanology and Geothermal Research* 20, 177-211, 10.1016/0377-0273(84)90039-8.
- Cross, T.A., Lessenger, M.A., 1988. Seismic Stratigraphy. *Annual Review of Earth and Planetary Sciences* 16, 319-354, 10.1146/annurev.ea.16.050188.001535.
- de Ruijter, W.P.M., Biastoch, A., Drijfhout, S.S., Lutjeharms, J.R.E., Matano, R.P., Pichevin, T., van Leeuwen, P.J., Weijer, W., 1999. Indian-Atlantic interocean exchange: Dynamics, estimation and impact. *Journal of Geophysical Research-Oceans* 104, 20885-20910, 10.1029/1998jc900099.
- Diekmann, B., Fälker, M., Kuhn, G., 2003. Environmental history of the south-eastern South Atlantic since the Middle Miocene: evidence from the sedimentological records of ODP Sites 1088 and 1092. *Sedimentology* 50, 511-529, 10.1046/j.1365-3091.2003.00562.x.
- Dingle, R., Birch, G., Bremner, J., De Decker, R., Du Plessis, A., Engelbrecht, J., Fincham, M., Fitton, T., Flemming, B., Gentle, R., 1987. Deep-sea sedimentary environments around southern Africa (south-east Atlantic and south-west Indian oceans), *Annals of the South African museum*.
- Dingle, R.V., Camden-Smith, F., 1979. Acoustic stratigraphy and current-generated bedforms in deep ocean basins off southeastern Africa. *Marine Geology* 33, 239-260, 10.1016/0025-3227(79)90083-5.
- Dingle, R.V., Goodlad, S.W., Martin, A.K., 1978. Bathymetry and stratigraphy of the northern Natal Valley (SW Indian Ocean): A preliminary account. *Marine Geology* 28, 89-106, 10.1016/0025-3227(78)90099-3.
- Dingle, R.V., Lavelle, M., 2000. Antarctic Peninsula Late Cretaceous-Early Cenozoic palaeoenvironments and Gondwana palaeogeographies. *Journal of African Earth Sciences* 31, 91-105, 10.1016/S0899-5362(00)00075-0.
- Dingle, R.V., Robson, S., 1985. Slumps, canyons and related features on the continental margin off East London, SE Africa (SW Indian Ocean). *Marine Geology* 67, 37-54, 10.1016/0025-3227(85)90147-1.
- Dingle, R.V., Siesser, W.G., Newton, A., 1983. *Mesozoic and Tertiary geology of southern Africa*, 1 ed. A.A.Balkema, Rotterdam, 9061910994.
- Donnadieu, Y., Puceat, E., Moiroud, M., Guillocheau, F., Deconinck, J.-F., 2016. A better-ventilated ocean triggered by Late Cretaceous changes in continental configuration. *Nature Communications* 7, 10.1038/ncomms10316.
- Doucouré, C.M., Bergh, H.W., 1992. Continental origin of the Mozambique Plateau: a gravity data analysis. *Journal of African Earth Sciences (and the Middle East)* 15, 311-319, 10.1016/0899-5362(92)90017-7.
- Durgadoo, J.V., Lutjeharms, J.R.E., Biastoch, A., Ansorge, I.J., 2008. The Conrad Rise as an obstruction to the Antarctic Circumpolar Current. *Geophysical Research Letters* 35, L20606,

- 10.1029/2008GL035382.
- Ebinger, C.J., Deino, A.L., Drake, R.E., Tesha, A.L., 1989. Chronology of volcanism and rift basin propagation: Rungwe Volcanic Province, East Africa. *Journal of Geophysical Research: Solid Earth* 94, 15785-15803, 10.1029/JB094iB11p15785.
- Eldholm, O., Coffin, M.F., 2000. Large Igneous Provinces and Plate Tectonics, The History and Dynamics of Global Plate Motions. American Geophysical Union, pp. 309-326, 10.1029/GM121p0309.
- Elkins-Tanton, L.T., 2005. Continental magmatism caused by lithospheric delamination. *Geological Society of America Special Papers* 388, 449-461, 10.1130/0-8137-2388-4.449.
- Erlank, A.J., Reid, D.L., 1974. Geochemistry, Mineralogy, and Petrology of Basalt, Leg 25, Deep Sea Drilling Project, in: Simpson, E.S.W., Schlich, R., Gieskes, J., Girdley, W.A., Leclaire, L., Marshall, B.V., Moore, C., Müller, C., Sigal, J., Vallier, T.L., White, S.M., Zobel, B. (Eds.), *Initial Reports of the Deep Sea Drilling Project*, Washington.
- Faugères, J.-C., Mulder, T., 2011. Contour Currents and Contourite Drifts, in: Heiko, H., Thierry, M. (Eds.), *Developments in Sedimentology*. Elsevier, pp. 149-214, 10.1016/B978-0-444-53000-4.00003-2.
- Faugères, J.-C., Stow, D.A.V., Imbert, P., Viana, A., 1999. Seismic features diagnostics of contourite drifts. *Marine Geology* 162, 1-38, 10.1016/S0025-3227(99)00068-7.
- Fischer, M.D., Uenzelmann-Neben, G., 2017a. Late Cretaceous onset of current controlled sedimentation in the African–Southern Ocean gateway. *Marine Geology* (in review).
- Fischer, M.D., Uenzelmann-Neben, G., 2017b. Neogene modifications of circulation in the African–Southern Ocean gateway. *Deep-Sea Research Part I* (in review).
- Fischer, M.D., Uenzelmann-Neben, G., Jacques, G., Werner, R., 2017. The Mozambique Ridge: a document of massive multistage magmatism. *Geophysical Journal International* 208, 449-467, 10.1093/gji/ggw403.
- Flores, G., 1973. The Cretaceous and Tertiary sedimentary basins of Mozambique and Zululand, in: Blant, G. (Ed.), *Sedimentary basins of the African coast. Part 2, South and east coast*. Association of African Geological Surveys, Paris, pp. 81-111.
- Frakes, L.A., Kemp, E.M., 1972. Influence of Continental Positions on Early Tertiary Climates. *Nature* 240, 97-100, 10.1038/240097a0.
- Frank, M., Whiteley, N., Kasten, S., Hein, J.R., O’Nions, K., 2002. North Atlantic Deep Water export to the Southern Ocean over the past 14 Myr: Evidence from Nd and Pb isotopes in ferromanganese crusts. *Paleoceanography* 17, 12-11-12-19, 10.1029/2000PA000606.
- Franke, D., Jokat, W., Ladage, S., Stollhofen, H., Klimke, J., Lutz, R., Mahanjane, E.S., Ehrhardt, A., Schreckenberger, B., 2015. The offshore East African Rift System: Structural framework at the toe of a juvenile rift. *Tectonics* 34, 2086-2104, 10.1002/2015TC003922.

- Frey, F.A., Coffin, M.F., Wallace, P.J., Weis, D., 2003. Leg 183 Synthesis: Kerguelen Plateau-Broken Ridge—A Large Igneous Province, in: Frey, F.A., Coffin, M.F., Wallace, P.J., Quilty, P.G. (Eds.), *Proceedings of the Ocean Drilling Program, Scientific Results*.
- Frey, F.A., Coffin, M.F., Wallace, P.J., Weis, D., Zhao, X., Wise Jr, S.W., Wähnert, V., Teagle, D.A.H., Saccocia, P.J., Reusch, D.N., Pringle, M.S., Nicolaysen, K.E., Neal, C.R., Müller, R.D., Moore, C.L., Mahoney, J.J., Keszthelyi, L., Inokuchi, H., Duncan, R.A., Delius, H., Damuth, J.E., Damasceno, D., Coxall, H.K., Borre, M.K., Boehm, F., Barling, J., Arndt, N.T., Antretter, M., 2000. Origin and evolution of a submarine large igneous province: the Kerguelen Plateau and Broken Ridge, southern Indian Ocean. *Earth and Planetary Science Letters* 176, 73-89, 10.1016/S0012-821X(99)00315-5.
- Friedrich, O., Norris, R.D., Erbacher, J., 2012. Evolution of middle to Late Cretaceous oceans—A 55 m.y. record of Earth's temperature and carbon cycle. *Geology* 40, 107-110, 10.1130/G32701.1.
- Ghidella, M.E., Yáñez, G., LaBrecque, J.L., 2002. Revised tectonic implications for the magnetic anomalies of the western Weddell Sea. *Tectonophysics* 347, 65-86, 10.1016/S0040-1951(01)00238-4.
- Girdley, W.A., 1974. Appendix III; carbon and carbonate analyses, Leg 25. *Initial Reports of the Deep Sea Drilling Project covering Leg 25 of the cruises of the drilling vessel Glomar Challenger, Port Louis, Mauritius to Durban, South Africa, June-August 1972* 25, 841, 0080-8334.
- Girdley, W.A., Leclaire, L., Moore, C., Vallier, T.L., White, S.M., 1974. Lithologic summary, Leg 25, Deep Sea Drilling Project, in: Simpson, E.S.W., Schlich, R., Gieskes, J., Girdley, W.A., Leclaire, L., Marshall, B.V., Moore, C., Müller, C., Sigal, J., Vallier, T.L., White, S.M., Zobel, B. (Eds.), *Initial Reports of the Deep Sea Drilling Project covering Leg 25 of the cruises of the drilling vessel Glomar Challenger, Port Louis, Mauritius to Durban, South Africa, June-August 1972*. Univ. Cape Town, Rondebosch, South Africa, Washington, pp. 725-741.
- Gladczenko, T.P., Hinz, K., Eldholm, O., Meyer, H., Neben, S., Skogseid, J., 1997. South Atlantic volcanic margins. *Journal of the Geological Society* 154, 465-470, 10.1144/gsjgs.154.3.0465.
- Gohl, K., Uenzelmann-Neben, G., 2001. The crustal role of the Agulhas Plateau, southwest Indian Ocean: evidence from seismic profiling. *Geophysical Journal International* 144, 632-646, 10.1046/j.1365-246x.2001.01368.x.
- Gohl, K., Uenzelmann-Neben, G., Grobys, N., 2011. Growth and Dispersal of a Southeast African Large Igneous Province. *South African Journal of Geology* 114, 379-386, 10.2113/gssa-jg.114.3-4.379.
- Goodlad, S.W., Martin, A.K., Hartnady, C.J.H., 1982. Mesozoic magnetic anomalies in the southern Natal Valley. *Nature* 295, 686-688, 10.1038/295686a0.
- Gourlan, A.T., Meynadier, L., Allègre, C.J., 2008. Tectonically driven changes in the Indian Ocean circulation over the last 25 Ma: Neodymium isotope evidence. *Earth and Planetary Science*

- Letters 267, 353-364, 10.1016/j.epsl.2007.11.054.
- Granot, R., Dymant, J., 2015. The Cretaceous opening of the South Atlantic Ocean. *Earth and Planetary Science Letters* 414, 156-163, 10.1016/j.epsl.2015.01.015.
- Gruetzner, J., Uenzelmann-Neben, G., 2016. Contourite drifts as indicators of Cenozoic bottom water intensity in the eastern Agulhas Ridge area, South Atlantic. *Marine Geology* 378, 350-360, 10.1016/j.margeo.2015.12.003.
- Hajnal, Z., Lucas, S., White, D., Lewry, J., Bezdan, S., Stauffer, M.R., Thomas, M.D., 1996. Seismic reflection images of high-angle faults and linked detachments in the Trans-Hudson Orogen. *Tectonics* 15, 427-439, 10.1029/95TC02710.
- Hales, A.L., Nation, J.B., 1973. A seismic refraction study in the southern Indian Ocean. *Bulletin of the Seismological Society of America* 63, 1951-1966.
- Hartnady, C.J.H., Ben-Avraham, Z., Rogers, J., 1992. Deep-ocean basins and submarine rises off the continental-margin of South-eastern Africa: New geological research. *South African Journal of Science* 88, 534-539.
- Hay, W.W., 2011. Can humans force a return to a 'Cretaceous' climate? *Sedimentary Geology* 235, 5-26, 10.1016/j.sedgeo.2010.04.015.
- Hernández-Molina, F.J., Larter, R.D., Rebesco, M., Maldonado, A., 2006. Miocene reversal of bottom water flow along the Pacific Margin of the Antarctic Peninsula: Stratigraphic evidence from a contourite sedimentary tail. *Marine Geology* 228, 93-116, 10.1016/j.margeo.2005.12.010.
- Hernández-Molina, F.J., Maldonado, A., Stow, D.A.V., 2008. Abyssal Plain Contourites, in: Rebesco, M., Camerlenghi, A. (Eds.), *Contourites*. Elsevier, pp. 345-378, 10.1016/S0070-4571(08)10018-8.
- Hernández-Molina, F.J., Paterlini, M., Somoza, L., Violante, R., Arecco, M.A., de Isasi, M., Rebesco, M., Uenzelmann-Neben, G., Neben, S., Marshall, P., 2010. Giant mounded drifts in the Argentine Continental Margin: Origins, and global implications for the history of thermohaline circulation. *Marine and Petroleum Geology* 27, 1508-1530, 10.1016/j.marpetgeo.2010.04.003.
- Hinz, K., Neben, S., Schreckenberger, B., Roeser, H.A., Block, M., Souza, K.G.d., Meyer, H., 1999. The Argentine continental margin north of 48°S: sedimentary successions, volcanic activity during breakup. *Marine and Petroleum Geology* 16, 1-25, 10.1016/S0264-8172(98)00060-9.
- Hooper, P.R., 1988. The Columbia River Basalt, in: Macdougall, J.D. (Ed.), *Continental Flood Basalts*. Springer Netherlands, Dordrecht, pp. 1-33, 10.1007/978-94-015-7805-9_1.
- Huber, B.T., Hodell, D.A., Hamilton, C.P., 1995. Middle–Late Cretaceous climate of the southern high latitudes: Stable isotopic evidence for minimal equator-to-pole thermal gradients. *Geological Society of America Bulletin* 107, 1164-1191,

- 10.1130/0016-7606(1995)107<1164:MLCCOT>2.3.CO;2.
- Huber, B.T., Norris, R.D., MacLeod, K.G., 2002. Deep-sea paleotemperature record of extreme warmth during the Cretaceous. *Geology* 30, 123-126, 10.1130/0091-7613(2002)030<0123:DSPROE>2.0.CO;2.
- Inoue, H., Coffin, M.F., Nakamura, Y., Mochizuki, K., Kroenke, L.W., 2008. Intrabasement reflections of the Ontong Java Plateau: Implications for plateau construction. *Geochemistry, Geophysics, Geosystems* 9, Q04014, 10.1029/2007GC001780.
- Jackson, C.A.L., 2012. Seismic reflection imaging and controls on the preservation of ancient sill-fed magmatic vents. *Journal of the Geological Society* 169, 503-506, 10.1144/0016-76492011-147.
- Jacques, G., Werner, R., Hauff, F., Hoernle, K., Uenzelmann-Neben, G., 2015. Preliminary Geochemical Results from the Mozambique Ridge, SW Indian Ocean, AGU Annual Convention 2015, San Francisco.
- Jerram, D.A., Widdowson, M., 2005. The anatomy of Continental Flood Basalt Provinces: geological constraints on the processes and products of flood volcanism. *Lithos* 79, 385-405, 10.1016/j.lithos.2004.09.009.
- Jokat, W., 2006. Southeastern Atlantic and southwestern Indian Ocean: reconstruction of the sedimentary and tectonic development since the Cretaceous; AISTEK-II: Mozambique Ridge and Mozambique Basin, *Berichte zur Polar- und Meeresforschung*. Alfred Wegener Institute, p. 73.
- Jokat, W., Boebel, T., König, M., Meyer, U., 2003. Timing and geometry of early Gondwana breakup. *Journal of Geophysical Research: Solid Earth* 108, 10.1029/2002JB001802.
- Jokat, W., Ritzmann, O., Reichert, C., Hinz, K., 2004. Deep Crustal Structure of the Continental Margin off the Explora Escarpment and in the Lazarev Sea, East Antarctica. *Marine Geophysical Researches* 25, 283-304, 10.1007/s11001-005-1337-9.
- Kampunzu, A.B., Bonhomme, M.G., Kanika, M., 1998. Geochronology of volcanic rocks and evolution of the Cenozoic Western Branch of the East African Rift System. *Journal of African Earth Sciences* 26, 441-461, 10.1016/S0899-5362(98)00025-6.
- Karlstrom, L., Richards, M., 2011. On the evolution of large ultramafic magma chambers and timescales for flood basalt eruptions. *Journal of Geophysical Research: Solid Earth* 116, B08216, 10.1029/2010JB008159.
- Katz, M.E., Cramer, B.S., Toggweiler, J.R., Esmay, G., Liu, C., Miller, K.G., Rosenthal, Y., Wade, B.S., Wright, J.D., 2011. Impact of Antarctic Circumpolar Current Development on Late Paleogene Ocean Structure. *Science* 332, 1076-1079, 10.1126/science.1202122.
- Kent, P.E., 1974. Leg 25 results in relation to East African coastal stratigraphy. Initial Reports of the Deep Sea Drilling Project covering Leg 25 of the cruises of the drilling vessel *Glomar Challenger*, Port Louis, Mauritius to Durban, South Africa, June-August 1972 25, 679-684,

0080-8334.

- Kerr, A.C., 1998. Oceanic plateau formation: a cause of mass extinction and black shale deposition around the Cenomanian–Turonian boundary? *Journal of the Geological Society* 155, 619-626, 10.1144/gsjgs.155.4.0619.
- Kerr, A.C., 2005. Oceanic LIPs: The Kiss of Death. *Elements* 1, 289-292, 10.2113/gselements.1.5.289.
- Kerr, A.C., 2014. Oceanic Plateaus, in: Holland, H., Turekian, K. (Eds.), *Treatise on Geochemistry (Second Edition)*, 2nd ed. Elsevier, Oxford, pp. 631-667, 10.1016/B978-0-08-095975-7.00320-X.
- King, S.D., Anderson, D.L., 1998. Edge-driven convection. *Earth and Planetary Science Letters* 160, 289-296, 10.1016/S0012-821X(98)00089-2.
- Klimke, J., Franke, D., Gaedicke, C., Schreckenberger, B., Schnabel, M., Stollhofen, H., Rose, J., Chaheire, M., 2015. How to identify oceanic crust—Evidence for a complex break-up in the Mozambique Channel, off East Africa. *Tectonophysics*, 10.1016/j.tecto.2015.10.012.
- König, M., Jokat, W., 2006. The Mesozoic breakup of the Weddell Sea. *Journal of Geophysical Research: Solid Earth* 111, B12102, 10.1029/2005JB004035.
- König, M., Jokat, W., 2010. Advanced insights into magmatism and volcanism of the Mozambique Ridge and Mozambique Basin in the view of new potential field data. *Geophysical Journal International* 180, 158-180, 10.1111/j.1365-246X.2009.04433.x.
- Kuhlbrodt, T., Griesel, A., Montoya, M., Levermann, A., Hofmann, M., Rahmstorf, S., 2007. On the driving processes of the Atlantic meridional overturning circulation. *Reviews of Geophysics* 45, RG2001, 10.1029/2004RG000166.
- Kuhnt, W., Holbourn, A., Hall, R., Zuvela, M., Käse, R., 2004. Neogene History of the Indonesian Throughflow, Continent-Ocean Interactions Within East Asian Marginal Seas. *American Geophysical Union*, pp. 299-320, 10.1029/149GM16.
- Lancelot, Y., Embley, R.W., 1977. Piercement structures in deep oceans. *AAPG Bulletin* 61, 1991, 1558-9153.
- Lawver, L.A., Gahagan, L.M., Coffin, M.F., 1992. The Development of Paleoseaways Around Antarctica, *The Antarctic Paleoenvironment: A Perspective on Global Change: Part One*. American Geophysical Union, pp. 7-30, 10.1029/AR056p0007.
- Leckie, R.M., Bralower, T.J., Cashman, R., 2002. Oceanic anoxic events and plankton evolution: Biotic response to tectonic forcing during the mid-Cretaceous. *Paleoceanography* 17, 13-11-13-29, 10.1029/2001PA000623.
- Leclaire, L., 1974. Late Cretaceous and Cenozoic pelagic deposits; paleoenvironment and paleoceanography of the central western Indian Ocean, in: Simpson, E.S.W., Schlich, R., Gieskes, J., Girdley, W.A., Leclaire, L., Marshall, B.V., Moore, C., Müller, C., Sigal, J.,

- Vallier, T.L., White, S.M., Zobel, B. (Eds.), Initial Reports of the Deep Sea Drilling Project covering Leg 25 of the cruises of the drilling vessel Glomar Challenger, Port Louis, Mauritius to Durban, South Africa, June-August 1972. Univ. Cape Town, Rondebosch, South Africa, Washington, pp. 481-513.
- Linnert, C., Robinson, S.A., Lees, J.A., Bown, P.R., Pérez-Rodríguez, I., Petrizzo, M.R., Falzoni, F., Littler, K., Arz, J.A., Russell, E.E., 2014. Evidence for global cooling in the Late Cretaceous. *Nature Communications* 5, 4194, 10.1038/ncomms5194.
- Ludwig, W.J., Nafe, J.E., Simpson, E.S.W., Sacks, S., 1968. Seismic-refraction measurements on the Southeast African Continental Margin. *Journal of Geophysical Research* 73, 3707-3719, 10.1029/JB073i012p03707.
- Lutjeharms, J.R.E., 1996. The Exchange of Water Between the South Indian and South Atlantic Oceans, in: Wefer, G., Berger, W.H., Siedler, G., Webb, D.J. (Eds.), *The South Atlantic: Present and Past Circulation*. Springer Berlin Heidelberg, Berlin, Heidelberg, pp. 125-162, 10.1007/978-3-642-80353-6_8.
- Lutjeharms, J.R.E., 2006. *The Agulhas Current*, 1 ed. Springer, Berlin, 10.1007/3-540-37212-1.
- Lyakhovskiy, V., Ben-Avraham, Z., Reznikov, M., 1994. Stress distribution over the Mozambique Ridge. *Tectonophysics* 240, 21-27, 10.1016/0040-1951(94)90261-5.
- Macgregor, D., 2015. History of the development of the East African Rift System: A series of interpreted maps through time. *Journal of African Earth Sciences* 101, 232-252, 10.1016/j.jafrearsci.2014.09.016.
- MacLeod, K.G., Isaza Londono, C., Martin, E.E., Jimenez Berrocoso, A., Basak, C., 2011. Changes in North Atlantic circulation at the end of the Cretaceous greenhouse interval. *Nature Geoscience* 4, 779-782, 10.1038/ngeo1284.
- Maia, M., Diament, M., Recq, M., 1990. Isostatic response of the lithosphere beneath the Mozambique Ridge (SW Indian Ocean) and geodynamic implications. *Geophysical Journal International* 100, 337-348, 10.1111/j.1365-246X.1990.tb00689.x.
- Mantyla, A.W., Reid, J.L., 1995. On the origins of deep and bottom waters of the Indian Ocean. *Journal of Geophysical Research: Oceans* 100, 2417-2439, 10.1029/94JC02564.
- Martin, A.K., Goodlad, S.W., Salmon, D.A., 1982. Sedimentary basin in-fill in the northernmost Natal Valley, hiatus development and Agulhas Current palaeo-oceanography. *Journal of the Geological Society* 139, 183-201, 10.1144/gsjgs.139.2.0183.
- Martin, E.E., MacLeod, K.G., Jiménez Berrocoso, A., Bourbon, E., 2012. Water mass circulation on Demerara Rise during the Late Cretaceous based on Nd isotopes. *Earth and Planetary Science Letters* 327-328, 111-120, 10.1016/j.epsl.2012.01.037.
- McCave, I.N., Hall, I.R., 2006. Size sorting in marine muds: Processes, pitfalls, and prospects for paleoflow-speed proxies. *Geochemistry, Geophysics, Geosystems* 7, Q10N05, 10.1029/2006GC001284.

- Meyers, P.A., Dickens, G.R., 1992. Accumulations of Organic Matter in Sediments of the Indian Ocean: a Synthesis of Results from Scientific Deep Sea Drilling, Synthesis of Results from Scientific Drilling in the Indian Ocean. American Geophysical Union, pp. 295-309, 10.1029/GM070p0295.
- Miura, S., Suyehiro, K., Shinohara, M., Takahashi, N., Araki, E., Taira, A., 2004. Seismological structure and implications of collision between the Ontong Java Plateau and Solomon Island Arc from ocean bottom seismometer-airgun data. *Tectonophysics* 389, 191-220, 10.1016/j.tecto.2003.09.029.
- Moiroud, M., Pucéat, E., Donnadiou, Y., Bayon, G., Guiraud, M., Voigt, S., Deconinck, J.-F., Monna, F., 2016. Evolution of neodymium isotopic signature of seawater during the Late Cretaceous: Implications for intermediate and deep circulation. *Gondwana Research* 36, 503-522, 10.1016/j.gr.2015.08.005.
- Mougenot, D., Gennesseaux, M., Hernandez, J., Lepvrier, C., Malod, J.A., Raillard, S., Vanney, J.R., Villeneuve, M., 1991. The Mozambique Ridge (Indian-Ocean) - a Continental Fragment Shaped during the Transform Motion of American and Antarctic Plates Along East-Africa. *Comptes Rendus De L Academie Des Sciences Serie Ii* 312, 655-662, 1251-8069.
- Mougenot, D., Recq, M., Virlogeux, P., Lepvrier, C., 1986. Seaward extension of the East African Rift. *Nature* 321, 599-603, 10.1038/321599a0.
- Müller-Michaelis, A., Uenzelmann-Neben, G., Stein, R., 2013. A revised Early Miocene age for the instigation of the Eirik Drift, offshore southern Greenland: Evidence from high-resolution seismic reflection data. *Marine Geology* 340, 1-15, 10.1016/j.margeo.2013.04.012.
- Murphy, D.P., Thomas, D.J., 2012. Cretaceous deep-water formation in the Indian sector of the Southern Ocean. *Paleoceanography* 27, Pa1211, 10.1029/2011PA002198.
- Murphy, D.P., Thomas, D.J., 2013. The evolution of Late Cretaceous deep-ocean circulation in the Atlantic basins: Neodymium isotope evidence from South Atlantic drill sites for tectonic controls. *Geochemistry, Geophysics, Geosystems* 14, 5323-5340, 10.1002/2013GC004889.
- Neal, C.R., Coffin, M.F., Arndt, N.T., Duncan, R.A., Eldholm, O., Erba, E., Farnetani, C., Fitton, J.F., Ingle, S.P., Ohkouchi, N., Rampino, M.R., Reichow, M.K., Self, S., Tatsumi, Y., 2008. Investigating Large Igneous Province Formation and Associated Paleoenvironmental Events: A White Paper for Scientific Drilling. *Sci. Dril.* 6, 4-18, 10.5194/sd-6-4-2008.
- Nielsen, T., Knutz, P.C., Kuijpers, A., 2008. Seismic Expression of Contourite Depositional Systems, in: Rebesco, M., Camerlenghi, A. (Eds.), *Developments in Sedimentology. Contourites*. Elsevier, pp. 301-321, 10.1016/S0070-4571(08)10016-4.
- Niemi, T.M., Ben-Avraham, Z., Hartnady, C.J.H., Reznikov, M., 2000. Post-Eocene seismic stratigraphy of the deep ocean basin adjacent to the southeast African continental margin: a record of geostrophic bottom current systems. *Marine Geology* 162, 237-258, 10.1016/S0025-3227(99)00062-6.
- Nyblade, A.A., Brazier, R.A., 2002. Precambrian lithospheric controls on the development of the

- East African rift system. *Geology* 30, 755-758, 10.1130/0091-7613(2002)030<0755:PL-COTD>2.0.CO;2.
- O'Dea, A., Lessios, H.A., Coates, A.G., Eytan, R.I., Restrepo-Moreno, S.A., Cione, A.L., Collins, L.S., de Queiroz, A., Farris, D.W., Norris, R.D., Stallard, R.F., Woodburne, M.O., Aguilera, O., Aubry, M.-P., Berggren, W.A., Budd, A.F., Cozzuol, M.A., Coppard, S.E., Duque-Caro, H., Finnegan, S., Gasparini, G.M., Grossman, E.L., Johnson, K.G., Keigwin, L.D., Knowlton, N., Leigh, E.G., Leonard-Pingel, J.S., Marko, P.B., Pyenson, N.D., Rachello-Dolmen, P.G., Soibelzon, E., Soibelzon, L., Todd, J.A., Vermeij, G.J., Jackson, J.B.C., 2016. Formation of the Isthmus of Panama. *Science Advances* 2, 10.1126/sciadv.1600883.
- Ogg, J.G., 2012. Chapter 5 - Geomagnetic Polarity Time Scale, *The Geologic Time Scale 2012*, 1st ed. Elsevier, Boston, pp. 85-113, 10.1016/B978-0-444-59425-9.00005-6.
- Otto-Bliesner, B.L., Brady, E.C., Shields, C., 2002. Late Cretaceous ocean: Coupled simulations with the National Center for Atmospheric Research Climate System Model. *Journal of Geophysical Research: Atmospheres* 107, ACL 11-11-ACL 11-14, 10.1029/2001JD000821.
- Parsieglia, N., Gohl, K., Uenzelmann-Neben, G., 2008. The Agulhas Plateau: structure and evolution of a Large Igneous Province. *Geophysical Journal International* 174, 336-350, 10.1111/j.1365-246X.2008.03808.x.
- Pekar, S.F., DeConto, R.M., 2006. High-resolution ice-volume estimates for the early Miocene: Evidence for a dynamic ice sheet in Antarctica. *Palaeogeography, Palaeoclimatology, Palaeoecology* 231, 101-109, 10.1016/j.palaeo.2005.07.027.
- Petit, C., Ebinger, C., 2000. Flexure and mechanical behavior of cratonic lithosphere: Gravity models of the East African and Baikal rifts. *Journal of Geophysical Research: Solid Earth* 105, 19151-19162, 10.1029/2000JB900101.
- Pietsch, R., Uenzelmann-Neben, G., 2015. The Manihiki Plateau—A multistage volcanic emplacement history. *Geochemistry, Geophysics, Geosystems* 16, 2480-2498, 10.1002/2015GC005852.
- Pietsch, R., Uenzelmann-Neben, G., 2016. The Manihiki Plateau—a key to missing hotspot tracks? *Geophysical Journal International* 206, 731-741, 10.1093/gji/ggw166.
- Poore, H.R., Samworth, R., White, N.J., Jones, S.M., McCave, I.N., 2006. Neogene overflow of Northern Component Water at the Greenland-Scotland Ridge. *Geochemistry, Geophysics, Geosystems* 7, Q06010, 10.1029/2005GC001085.
- Poulsen, C.J., Barron, E.J., Arthur, M.A., Peterson, W.H., 2001. Response of the Mid-Cretaceous global oceanic circulation to tectonic and CO₂ forcings. *Paleoceanography* 16, 576-592, 10.1029/2000PA000579.
- Poulsen, C.J., Gendaszek, A.S., Jacob, R.L., 2003. Did the rifting of the Atlantic Ocean cause the Cretaceous thermal maximum? *Geology* 31, 115-118, 10.1130/0091-7613(2003)031<0115:DTROTA>2.0.CO;2.

- Rahmstorf, S., 2002. Ocean circulation and climate during the past 120,000 years. *Nature* 419, 207-214, 0028-0836.
- Raillard, S., 1990. Les Marges de l'Afrique de l'est et les Zones de Fracture associées: Chaîne Davie et Ride du Mozambique. Pierre and Marie Curie University, Paris, p. 272.
- Ramsay, A.T.S., Sykes, T.J.S., Kidd, R.B., 1994. Waxing (and Waning) lyrical on hiatuses: Eocene - Quaternary Indian Ocean hiatuses as proxy indicators of water mass production. *Paleoceanography* 9, 857-877, 10.1029/94PA01397.
- Ramsay, D.C., Colwell, J.B., Coffin, M.F., Davies, H.L., Hill, P.J., Pigram, C.J., Stagg, H.M.J., 1986. New findings from the Kerguelen Plateau. *Geology* 14, 589-593, 10.1130/0091-7613(1986)14<589:NFFTKP>2.0.CO;2.
- Read, J.F., Pollard, R.T., 1999. Deep inflow into the Mozambique Basin. *Journal of Geophysical Research* 104, 3075, 10.1029/1998jc900078.
- Rebesco, M., Camerlenghi, A., Van Loon, A.J., 2008. Contourite Research: A Field in Full Development, in: Rebesco, M., Camerlenghi, A. (Eds.), *Developments in Sedimentology. Contourites*. Elsevier, pp. 1-10, 10.1016/S0070-4571(08)10001-2.
- Rebesco, M., Hernández-Molina, F.J., Van Rooij, D., Wåhlin, A., 2014. Contourites and associated sediments controlled by deep-water circulation processes: State-of-the-art and future considerations. *Marine Geology* 352, 111-154, 10.1016/j.margeo.2014.03.011.
- Rebesco, M., Stow, D., 2001. Seismic expression of contourites and related deposits: a preface. *Marine Geophysical Researches* 22, 303-308, 10.1023/A:1016316913639.
- Recq, M., Goslin, J., 1981. Etude de l'équilibre isostatique dans le sud-ouest de l'océan Indien à l'aide des résultats de réfraction sismique. *Marine Geology* 41, M1-M10, 10.1016/0025-3227(81)90101-8.
- Reznikov, M., Ben-Avraham, Z., Hartnady, C., Niemi, T.M., 2005. Structure of the Transkei Basin and Natal Valley, Southwest Indian Ocean, from seismic reflection and potential field data. *Tectonophysics* 397, 127-141, 10.1016/j.tecto.2004.11.002.
- Roberts, D.G., Hogg, N.G., Bishop, D.G., Flewellen, C.G., 1974. Sediment distribution around moated seamounts in the Rockall Trough. *Deep Sea Research and Oceanographic Abstracts* 21, 175-184, 10.1016/0011-7471(74)90057-6.
- Robinson, S.A., Murphy, D.P., Vance, D., Thomas, D.J., 2010. Formation of "Southern Component Water" in the Late Cretaceous: Evidence from Nd-isotopes. *Geology* 38, 871-874, 10.1130/G31165.1.
- Robinson, S.A., Vance, D., 2012. Widespread and synchronous change in deep-ocean circulation in the North and South Atlantic during the Late Cretaceous. *Paleoceanography* 27, Pa1102, 10.1029/2011PA002240.
- Roden, G.I., 1991. Mesoscale flow and thermohaline structure around Fieberling seamount. *Jour-*

- nal of Geophysical Research: Oceans 96, 16653-16672, 10.1029/91JC01747.
- Rohde, J.K., van den Bogaard, P., Hoernle, K., Hauff, F., Werner, R., 2013. Evidence for an age progression along the Tristan-Gough volcanic track from new $^{40}\text{Ar}/^{39}\text{Ar}$ ages on phenocryst phases. *Tectonophysics* 604, 60-71, 10.1016/j.tecto.2012.08.026.
- Sager, W.W., Bull, J.M., Krishna, K.S., 2013a. Active faulting on the Ninetyeast Ridge and its relation to deformation of the Indo-Australian plate. *Journal of Geophysical Research: Solid Earth* 118, 4648-4668, 10.1002/jgrb.50319.
- Sager, W.W., Zhang, J., Korenaga, J., Sano, T., Koppers, A.A.P., Widdowson, M., Mahoney, J.J., 2013b. An immense shield volcano within the Shatsky Rise oceanic plateau, northwest Pacific Ocean. *Nature Geoscience* 6, 976-981, 10.1038/ngeo1934.
- Sandwell, D.T., Smith, W.H.F., 2009. Global marine gravity from retracked Geosat and ERS-1 altimetry: Ridge segmentation versus spreading rate. *Journal of Geophysical Research: Solid Earth* 114, B01411, 10.1029/2008JB006008.
- Saria, E., Calais, E., Stamps, D.S., Delvaux, D., Hartnady, C.J.H., 2014. Present-day kinematics of the East African Rift. *Journal of Geophysical Research: Solid Earth* 119, B010901, 10.1002/2013JB010901.
- Saunders, A.D., 2005. Large Igneous Provinces: Origin and Environmental Consequences. *Elements* 1, 259-263, 10.2113/gselements.1.5.259.
- Schlüter, P., Uenzelmann-Neben, G., 2007. Seismostratigraphic analysis of the Transkei Basin: A history of deep sea current controlled sedimentation. *Marine Geology* 240, 99-111, 10.1016/j.margeo.2007.02.015.
- Schlüter, P., Uenzelmann-Neben, G., 2008a. Conspicuous seismic reflections in Upper Cretaceous sediments as evidence for black shales off South Africa. *Marine and Petroleum Geology* 25, 989-999, 10.1016/j.marpetgeo.2007.10.003.
- Schlüter, P., Uenzelmann-Neben, G., 2008b. Indications for bottom current activity since Eocene times: The climate and ocean gateway archive of the Transkei Basin, South Africa. *Global and Planetary Change* 60, 416-428, 10.1016/j.gloplacha.2007.07.002.
- Schneider, B., Schmittner, A., 2006. Simulating the impact of the Panamanian seaway closure on ocean circulation, marine productivity and nutrient cycling. *Earth and Planetary Science Letters* 246, 367-380, 10.1016/j.epsl.2006.04.028.
- Sclater, J.G., Grindlay, N.R., Madsen, J.A., Rommevaux-Jestin, C., 2005. Tectonic interpretation of the Andrew Bain transform fault: Southwest Indian Ocean. *Geochemistry, Geophysics, Geosystems* 6, Q09K10, 10.1029/2005GC000951.
- Self, S., Jay, A.E., Widdowson, M., Keszthelyi, L.P., 2008. Correlation of the Deccan and Rajahmundry Trap lavas: Are these the longest and largest lava flows on Earth? *Journal of Volcanology and Geothermal Research* 172, 3-19, 10.1016/j.jvolgeores.2006.11.012.

- Self, S., Widdowson, M., Thordarson, T., Jay, A.E., 2006. Volatile fluxes during flood basalt eruptions and potential effects on the global environment: A Deccan perspective. *Earth and Planetary Science Letters* 248, 518-532, 10.1016/j.epsl.2006.05.041.
- Shanmugam, G., 2008. Deep-water Bottom Currents and their Deposits, in: Rebesco, M., Cammerlenghi, A. (Eds.), *Developments in Sedimentology. Contourites*. Elsevier, pp. 59-81, 10.1016/S0070-4571(08)10005-X.
- Sheriff, R.E., 1977. Limitations on resolution of seismic reflections and geologic detail derivable from them, in: Payton, C.E. (Ed.), *Seismic Stratigraphy—Applications to Hydrocarbon Exploration*. AAPG Memoirs, pp. 3-14.
- Shevenell, A.E., Kennett, J.P., Lea, D.W., 2008. Middle Miocene ice sheet dynamics, deep-sea temperatures, and carbon cycling: A Southern Ocean perspective. *Geochemistry, Geophysics, Geosystems* 9, Q02006, 10.1029/2007GC001736.
- Sigal, J., 1974. Comments on Leg 25 sites in relation to the Cretaceous and Paleogene stratigraphy in the eastern and southeastern Africa coast and Madagascar regional setting. Initial Reports of the Deep Sea Drilling Project covering Leg 25 of the cruises of the drilling vessel *Glomar Challenger*, Port Louis, Mauritius to Durban, South Africa, June-August 1972 25, 687-723, 0080-8334.
- Sijp, W.P., von der Heydt, A.S., Dijkstra, H.A., Flögel, S., Douglas, P.M.J., Bijl, P.K., 2014. The role of ocean gateways on cooling climate on long time scales. *Global and Planetary Change* 119, 1-22, 10.1016/j.gloplacha.2014.04.004.
- Simpson, E.S.W., Schlich, R., Gieskes, J., Girdley, W.A., Leclaire, L., Marshall, B.V., Moore, C., Müller, C., Sigal, J., Vallier, T.L., White, S.M., Zobel, B., 1974. Site 249, in: Simpson, E.S.W., Schlich, R., Gieskes, J., Girdley, W.A., Leclaire, L., Marshall, B.V., Moore, C., Müller, C., Sigal, J., Vallier, T.L., White, S.M., Zobel, B. (Eds.), *Initial Reports of the Deep Sea Drilling Project covering Leg 25 of the cruises of the drilling vessel Glomar Challenger*, Port Louis, Mauritius to Durban, South Africa, June-August 1972. Univ. Cape Town, Rondebosch, South Africa, Washington, pp. 287-346.
- Sleep, N.H., 1992. Hotspot Volcanism And Mantle Plumes. *Annual Review of Earth and Planetary Sciences* 20, 19-43, 10.1146/annurev.earth.20.050192.000315.
- Sobolev, S.V., Sobolev, A.V., Kuzmin, D.V., Krivolutskaya, N.A., Petrunin, A.G., Arndt, N.T., Radko, V.A., Vasiliev, Y.R., 2011. Linking mantle plumes, large igneous provinces and environmental catastrophes. *Nature* 477, 312-316, 10.1038/nature10385.
- Stamps, D.S., Calais, E., Saria, E., Hartnady, C., Nocquet, J.-M., Ebinger, C.J., Fernandes, R.M., 2008. A kinematic model for the East African Rift. *Geophysical Research Letters* 35, L05304, 10.1029/2007GL032781.
- Stamps, D.S., Flesch, L.M., Calais, E., Ghosh, A., 2014. Current kinematics and dynamics of Africa and the East African Rift System. *Journal of Geophysical Research: Solid Earth* 119, 5161-5186, 10.1002/2013JB010717.

- Storey, B.C., 1995. The role of mantle plumes in continental breakup: case histories from Gondwanaland. *Nature* 377, 301-308, 10.1038/377301a0.
- Stothers, R.B., 1998. Far Reach of the Tenth Century Eldgjá Eruption, Iceland. *Climatic Change* 39, 715-726, 10.1023/A:1005323724072.
- Stow, D.A.V., Faugères, J.-C., Howe, J.A., Pudsey, C.J., Viana, A.R., 2002. Bottom currents, contourites and deep-sea sediment drifts: current state-of-the-art, in: Stow, D.A.V., Pudsey, C.J., Howe, J.A., Faugères, J.C., Viana, A.R. (Eds.), *Deep-Water Contourite Systems: Modern Drifts and Ancient Series, Seismic and Sedimentary Characteristics*. Geological Society, London, *Memoirs*, pp. 7-20, 10.1144/GSL.MEM.2002.022.01.02.
- Stow, D.A.V., Faugères, J.C., 2008. Contourite Facies and the Facies Model, in: Rebesco, M., Camerlenghi, A. (Eds.), *Developments in Sedimentology. Contourites*. Elsevier, pp. 223-256, 10.1016/S0070-4571(08)10013-9.
- Stow, D.A.V., Hernández-Molina, F.J., Llave, E., Sayago-Gil, M., Díaz del Río, V., Branson, A., 2009. Bedform-velocity matrix: The estimation of bottom current velocity from bedform observations. *Geology* 37, 327-330, 10.1130/G25259A.1.
- Stow, D.A.V., Hunter, S., Wilkinson, D., Hernández-Molina, F.J., 2008. The Nature of Contourite Deposition, in: Rebesco, M., Camerlenghi, A. (Eds.), *Developments in Sedimentology. Contourites*. Elsevier, pp. 143-156, 10.1016/S0070-4571(08)10009-7.
- Thompson, G., Bryan, W.B., Frey, F.A., Dickey, J.S., Davies, H., 1982. Petrology, geochemistry and original tectonic setting of basalts from the Mozambique Basin and Ridge (DSDP Sites 248, 249 and 250), and from the Southwest Indian Ridge (DSDP Site 251). *Marine Geology* 48, 175-195, 10.1016/0025-3227(82)90096-2.
- Tikku, A.A., Marks, K.M., Kovacs, L.C., 2002. An Early Cretaceous extinct spreading center in the northern Natal valley. *Tectonophysics* 347, 87-108, 10.1016/S0040-1951(01)00239-6.
- Tomczak, M., Godfrey, J.S., 1994. *Hydrology of the Indian Ocean, Regional Oceanography: An Introduction*. Pergamon, Amsterdam, pp. 221-236, 10.1016/B978-0-08-041021-0.50016-3.
- Toole, J.M., Warren, B.A., 1993. A hydrographic section across the subtropical South Indian Ocean. *Deep Sea Research Part I: Oceanographic Research Papers* 40, 1973-2019, 10.1016/0967-0637(93)90042-2.
- Tucholke, B.E., Carpenter, G.B., 1977. Sediment distribution and Cenozoic sedimentation patterns on the Agulhas Plateau. *Geological Society of America Bulletin* 88, 1337-1346, 10.1130/0016-7606(1977)88<1337:SDACSP>2.0.CO;2.
- Tucholke, B.E., Embley, R.W., 1984. Cenozoic Regional Erosion of the Abyssal Sea Floor Off South Africa, in: Schlee, J.S. (Ed.), *Interregional Unconformities and Hydrocarbon Accumulation*. American Association Petroleum Geologists Memoir, pp. 145-164, 10.1306/M36440C11.
- Tucholke, B.E., Houtz, R.E., Barrett, D.M., 1981. Continental crust beneath the Agulhas Plateau,

- southwest Indian Ocean. *Journal of Geophysical Research: Solid Earth* 86, 3791-3806, 10.1029/JB086iB05p03791.
- Uenzelmann-Neben, G., 2001. Seismic characteristics of sediment drifts: An example from the Agulhas Plateau, southwest Indian Ocean. *Marine Geophysical Researches* 22, 323-343, 10.1023/A:1016391314547.
- Uenzelmann-Neben, G., 2002. Contourites on the Agulhas Plateau, SW Indian Ocean: indications for the evolution of currents since Palaeogene times. Geological Society, London, *Memoirs* 22, 271-288, 10.1144/GSL.MEM.2002.022.01.20.
- Uenzelmann-Neben, G., 2013. Volcanology: Magma giant. *Nature Geoscience* 6, 902-903, 10.1038/ngeo1958.
- Uenzelmann-Neben, G., 2014. The Expedition of the Research Vessel "Sonne" to the Mozambique Ridge in 2014 (So 232), in: Uenzelmann-Neben, G. (Ed.), *Reports on polar and marine research*. Alfred Wegener Institute for Polar and Marine Research, Bremerhaven, Germany, p. 207.
- Uenzelmann-Neben, G., Clift, P.D., 2015. A Sediment Budget for the Transkei Basin, Southwest Indian Ocean. *Marine Geophysical Research* 36, 281-291, 10.1007/s11001-015-9250-3.
- Uenzelmann-Neben, G., Gohl, K., 2014. Early glaciation already during the Early Miocene in the Amundsen Sea, Southern Pacific: Indications from the distribution of sedimentary sequences. *Global and Planetary Change* 120, 92-104, 10.1016/j.gloplacha.2014.06.004.
- Uenzelmann-Neben, G., Gohl, K., Ehrhardt, A., Seargent, M., 1999. Agulhas Plateau, SW Indian Ocean: New Evidence for Excessive Volcanism. *Geophysical Research Letters* 26, 1941-1944, 10.1029/1999GL900391.
- Uenzelmann-Neben, G., Huhn, K., 2009. Sedimentary deposits on the southern South African continental margin: Slumping versus non-deposition or erosion by oceanic currents? *Marine Geology* 266, 65-79, 10.1016/j.margeo.2009.07.011.
- Uenzelmann-Neben, G., Schlüter, P., Weigelt, E., 2007. Cenozoic oceanic circulation within the South African gateway: indications from seismic stratigraphy. *South African Journal of Geology* 110, 275-294, 10.2113/Gssaig.110.2-3.275.
- Uenzelmann-Neben, G., Watkeys, M.K., Kretzinger, W., Frank, M., Heuer, L., 2011. Palaeoceanographic Interpretation of a Seismic Profile from the Southern Mozambique Ridge, Southwestern Indian Ocean. *South African Journal of Geology* 114, 449-458, 10.2113/gssa-jg.114.3-4.449.
- Uenzelmann-Neben, G., Weber, T., Grützner, J., Thomas, M., 2016. Transition from the Cretaceous ocean to Cenozoic circulation in the western South Atlantic — A twofold reconstruction. *Tectonophysics*, 10.1016/j.tecto.2016.05.036.
- Vail, P.R., Mitchum, R.M., Todd, R.G., Widmier, J.M., Thompson, S., Sangree, J.B., Bubb, J.N., Hatlelid, W.G., 1977. Seismic Stratigraphy and Global Changes of Sea Level, in: Payton, C.E.

- (Ed.), *Seismic Stratigraphy – Applications to Hydrocarbon Exploration*. American Association of Petroleum Geologists, pp. 49-386, 9780891813026.
- Vallier, T.L., 1974. Volcanogenic sediments and their relation to landmass volcanism and sea floor-continent movements, western Indian Ocean, Leg 25, Deep Sea Drilling Project. Initial Reports of the Deep Sea Drilling Project covering Leg 25 of the cruises of the drilling vessel *Glomar Challenger*, Port Louis, Mauritius to Durban, South Africa, June-August 1972 25, 515-542, 0080-8334.
- Vallier, T.L., Kidd, R.B., 1977. Volcanogenic sediments in the Indian Ocean. 87-118, 10.1029/SP009p0087.
- van Aken, H.M., 2007. *The Oceanic Thermohaline Circulation: An Introduction*. Springer, New York, 10.1007/978-0-387-48039-8.
- van Aken, H.M., Ridderinkhof, H., de Ruijter, W.P.M., 2004. North Atlantic deep water in the south-western Indian Ocean. *Deep Sea Research Part I: Oceanographic Research Papers* 51, 755-776, 10.1016/j.dsr.2004.01.008.
- Verron, J., Le Provost, C., 2006. A numerical study of quasi-geostrophic flow over isolated topography. *Journal of Fluid Mechanics* 154, 231-252, 10.1017/S0022112085001501.
- Via, R.K., Thomas, D.J., 2006. Evolution of Atlantic thermohaline circulation: Early Oligocene onset of deep-water production in the North Atlantic. *Geology* 34, 441-444, 10.1130/G22545.1.
- Voigt, S., Jung, C., Friedrich, O., Frank, M., Teschner, C., Hoffmann, J., 2013. Tectonically restricted deep-ocean circulation at the end of the Cretaceous greenhouse. *Earth and Planetary Science Letters* 369–370, 169-177, 10.1016/j.epsl.2013.03.019.
- Wagner, T., Pletsch, T., 1999. Tectono-sedimentary controls on Cretaceous black shale deposition along the opening Equatorial Atlantic Gateway (ODP Leg 159). *Geological Society, London, Special Publications* 153, 241-265, 10.1144/GSL.SP.1999.153.01.15.
- Weatherall, P., Marks, K.M., Jakobsson, M., Schmitt, T., Tani, S., Arndt, J.E., Rovere, M., Chayes, D., Ferrini, V., Wigley, R., 2015. A new digital bathymetric model of the world's oceans. *Earth and Space Science* 2, 331-345, 10.1002/2015EA000107.
- White, R.S., McKenzie, D., 1995. Mantle plumes and flood basalts. *Journal of Geophysical Research: Solid Earth* 100, 17543-17585, 10.1029/95JB01585.
- White, S.M., Crisp, J.A., Spera, F.J., 2006. Long-term volumetric eruption rates and magma budgets. *Geochemistry, Geophysics, Geosystems* 7, Q03010, 10.1029/2005GC001002.
- Wignall, P.B., 2001. Large igneous provinces and mass extinctions. *Earth-Science Reviews* 53, 1-33, 10.1016/S0012-8252(00)00037-4.
- Wignall, P.B., 2005. The Link between Large Igneous Province Eruptions and Mass Extinctions. *Elements* 1, 293-297, 10.2113/gselements.1.5.293.

- Wildeboer Schut, E., Uenzelmann-Neben, G., Gersonde, R., 2002. Seismic evidence for bottom current activity at the Agulhas Ridge. *Global and Planetary Change* 34, 185-198, 10.1016/S0921-8181(02)00114-5.
- Wiles, E., Green, A., Watkeys, M., Jokat, W., Krocker, R., 2014. Anomalous seafloor mounds in the northern Natal Valley, southwest Indian Ocean: Implications for the East African Rift System. *Tectonophysics* 630, 300-312, 10.1016/j.tecto.2014.05.030.
- Wunsch, C., 2002. What is the Thermohaline Circulation? *Science* 298, 1179-1180, 10.1126/science.1079329.
- Wyrki, K., 1973. Physical Oceanography of the Indian Ocean, in: Zeitzschel, B., Gerlach, S.A. (Eds.), *The Biology of the Indian Ocean*. Springer Berlin Heidelberg, Berlin, Heidelberg, pp. 18-36, 10.1007/978-3-642-65468-8_3.
- Yilmaz, Ö., 2001. *Seismic Data Analysis: Processing, Inversion, and Interpretation of Seismic Data*. Society of Exploration Geophysicists, 10.1190/1.9781560801580.
- You, Y., 1999. Diapycnal mixing, transformation and transport of the deep water of the Indian Ocean. *Deep Sea Research Part I: Oceanographic Research Papers* 46, 109-148, 10.1016/S0967-0637(98)00058-2.
- You, Y., Lutjeharms, J.R.E., Boebel, O., de Ruijter, W.P.M., 2003. Quantification of the interocean exchange of intermediate water masses around southern Africa. *Deep Sea Research Part II: Topical Studies in Oceanography* 50, 197-228, 10.1016/S0967-0645(02)00384-3.
- Zachos, J., Pagani, M., Sloan, L., Thomas, E., Billups, K., 2001. Trends, Rhythms, and Aberrations in Global Climate 65 Ma to Present. *Science* 292, 686-693, 10.1126/science.1059412.

11. Danksagung

Hier möchte Ich denen herzlich danken, die mich während der Anfertigung meiner Dissertation begleitet und unterstützt haben.

Mein großer Dank gebührt Gabriele Uenzelmann-Neben, die dieses Projekt beantragt und mir somit die Möglichkeit eröffnet hat diese Doktorarbeit am AWI zu schreiben. Ich danke Dir, dass du mir geholfen hast Klarheit in meine oft ellenlangen Sätze zu bringen und selbst dann noch den Sinn oder Unsinn meiner Aussagen entziffern konntest, als ich mich schon längst selbst nur noch kopfschüttelnd hinterfragen konnte. Danke für deine stets hilfreichen Tipps und die rasend schnellen Korrekturen meiner Manuskripte und dafür, mir immer zum richtigen Zeitpunkt in den Hintern getreten zu haben. Zudem möchte Ich Dir dafür danken, dass Du es mir ermöglicht hast an zwei Expeditionen teilzunehmen, durch die ich meinen Horizont um tolle Erfahrungen erweitern konnte.

Wilfried Jokat und Katrin Huhn möchte ich dafür danken, dass sie meine Arbeit begutachten und bewerten.

Wilfried Jokat möchte ich zusätzlich dafür danken, dass er mir ermöglicht hat der Reflexionsseismik treu zu bleiben, obwohl ich diese beinahe mit der Refraktionsseismik hintergangen hätte. Des Weiteren möchte Ich Ihm dafür danken, immer ein offenes Ohr und eine flinke Hand für Unterschriften jedweder Art parat gehabt zu haben. Und natürlich dafür, dass Ich mich ein zweites Mal im Indischen Ozean auf Expedition begeben konnte, frei nach dem Motto "Warum nicht?".

Ich möchte meinen Kollegen für die vielen hilfreichen Tipps, Diskussionen und die erlebnisreiche Zeit danken. Ohne Euch wäre der Arbeitsalltag eine ganze Spur trister gewesen.

Meiner Familie möchte Ich für die unentwegte Unterstützung und den Rückhalt danken, den ich nicht erst seit Beginn meiner Arbeit am AWI erfahren habe. Ihr habt immer an mich geglaubt, auch wenn ich bereits nah an der Verzweiflung war. Ganz besonders gilt mein Dank meinem Onkel Marc, welcher mir hilfreich bei der Korrektur meiner englischen Wortkonstrukte zur Seite stand.

Zu guter Letzt möchte Ich meiner Freundin Iman danken, die immer für mich da war wenn mir die Decke auf den Kopf fiel. Danke, dass du die mehr als drei Jahre des hin- und herpendelns auch ohne den Anreiz eines Bremerhavener Strandbads ertragen hast. Ohne deinen Beistand wäre es mir nicht möglich gewesen diese Arbeit erfolgreich zu Ende zu führen.

Appendix

The Appendix provides an overview of the parameters of the MCS reflection profiles (Table A.1) and shows the 22 time-migrated MCS reflection profiles used in this study. The locations of the profiles are shown in Figure A.1. The processing steps that were applied to all profiles are described in chapter 2.2.1.

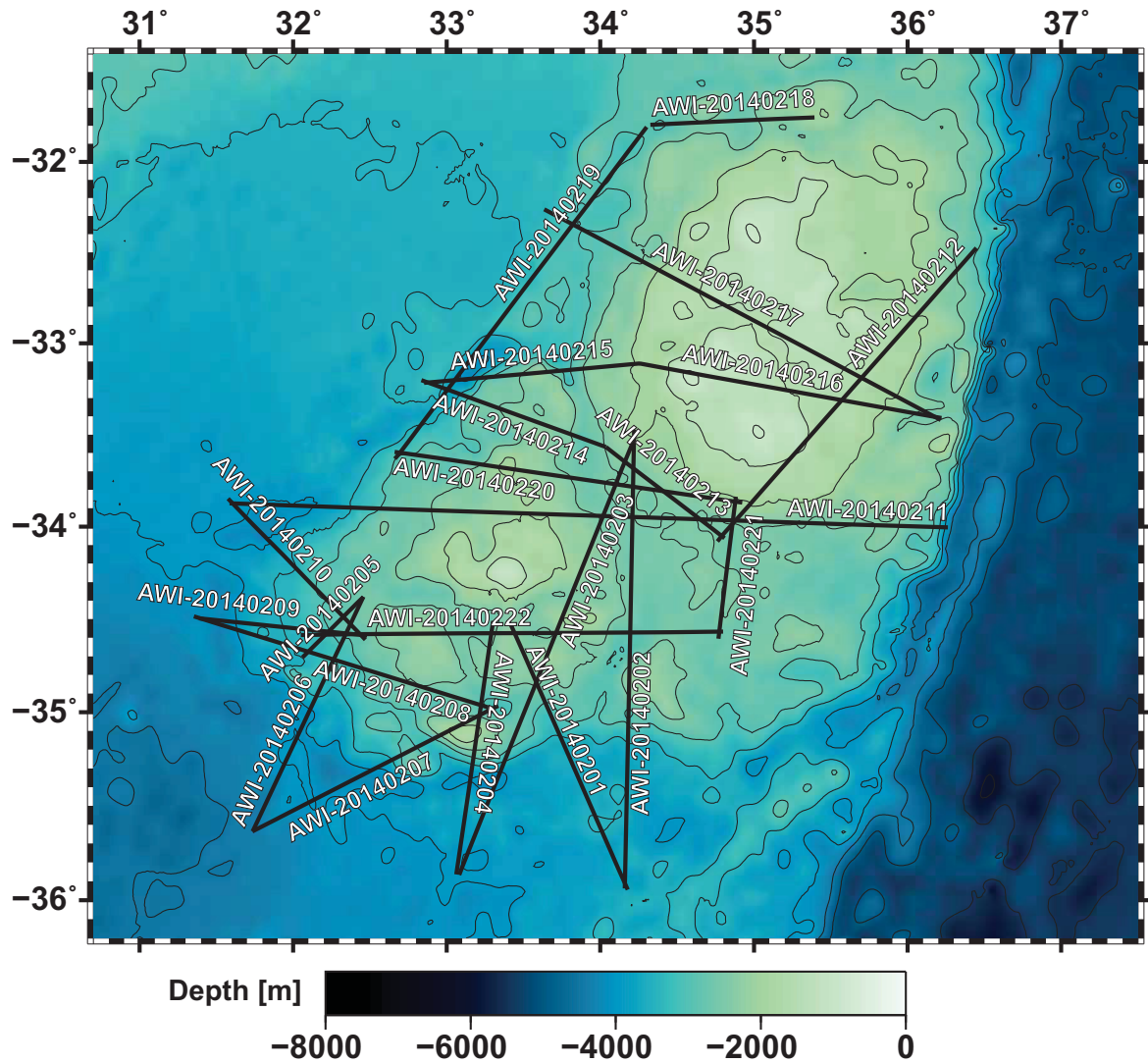


Figure A.1. Bathymetric map (Weatherall *et al.*, 2015) of the study area showing the locations of the 22 new MCS reflection profiles gathered during expedition SO232.

Table A.1. Parameters of the MCS reflection profiles

Profile	Start		End		Length [km]	No of CDPs
	Lat	Lon	Lat	Lon		
AWI-20140201	-34.53233	33.41895	-35.94361	34.17836	168.532	6980
AWI-20140202	-35.9376	34.1585	-33.4726	34.2199	270.392	11069
AWI-20140203	-35.5214	34.2208	-35.866	33.0807	283.356	11358
AWI-20140204	-35.8636	33.0623	-34.5102	33.3018	164.828	6191
AWI-20140205	-34.706	32.061	-34.38	32.456	50.004	2167
AWI-20140206	-34.379	32.457	-35.636	31.737	168.532	6285
AWI-20140207	-35.636	31.735	-34.965	33.335	172.236	6658
AWI-20140208	-34.982	33.298	-34.485	31.345	179.644	7580
AWI-20140209	-34.49499	31.38786	-34.58864	32.4864	100.008	4151
AWI-20140210	-34.61063	32.47065	-33.84847	31.57718	116.676	4839
AWI-20140211	-33.87365	31.58651	-34.004	36.26258	448.184	17513
AWI-20140212	-32.476	36.447	-34.08	34.761	227.796	9597
AWI-20140213	-34.062	34.809	-33.568	34.036	83.34	3732
AWI-20140214	-33.568	34.036	-33.203	32.835	116.676	4883
AWI-20140215	-33.217	32.8527	-33.1115	34.2566	138.9	5387
AWI-20140216	-33.1115	34.2566	-33.4097	36.2201	200.016	7573
AWI-20140217	-33.42	36.2157	-32.2626	33.6245	261.132	11094
AWI-20140218	-31.7529	35.3944	-31.7931	34.3253	92.6	4124
AWI-20140219	-31.8061	34.3012	-33.6317	32.6623	235.204	10247
AWI-20140220	-33.5936	32.6608	-33.8696	34.9234	212.98	8549
AWI-20140221	-33.8377	34.8814	-34.6051	34.7681	109.268	3536
AWI-20140222	-34.5665	34.7988	-34.5848	32.0501	237.056	10205

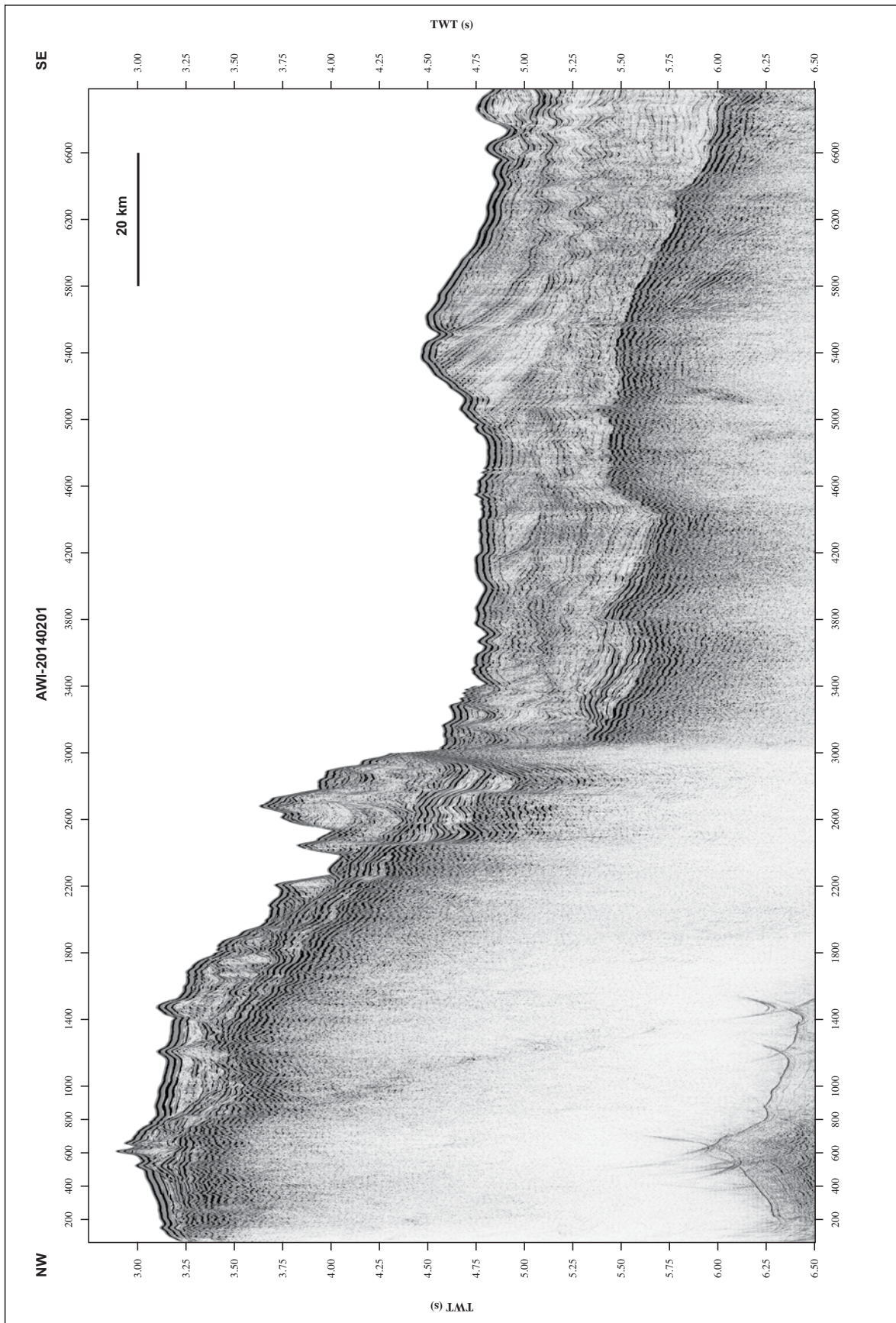


Figure A.2. Profile AWI-20140201.

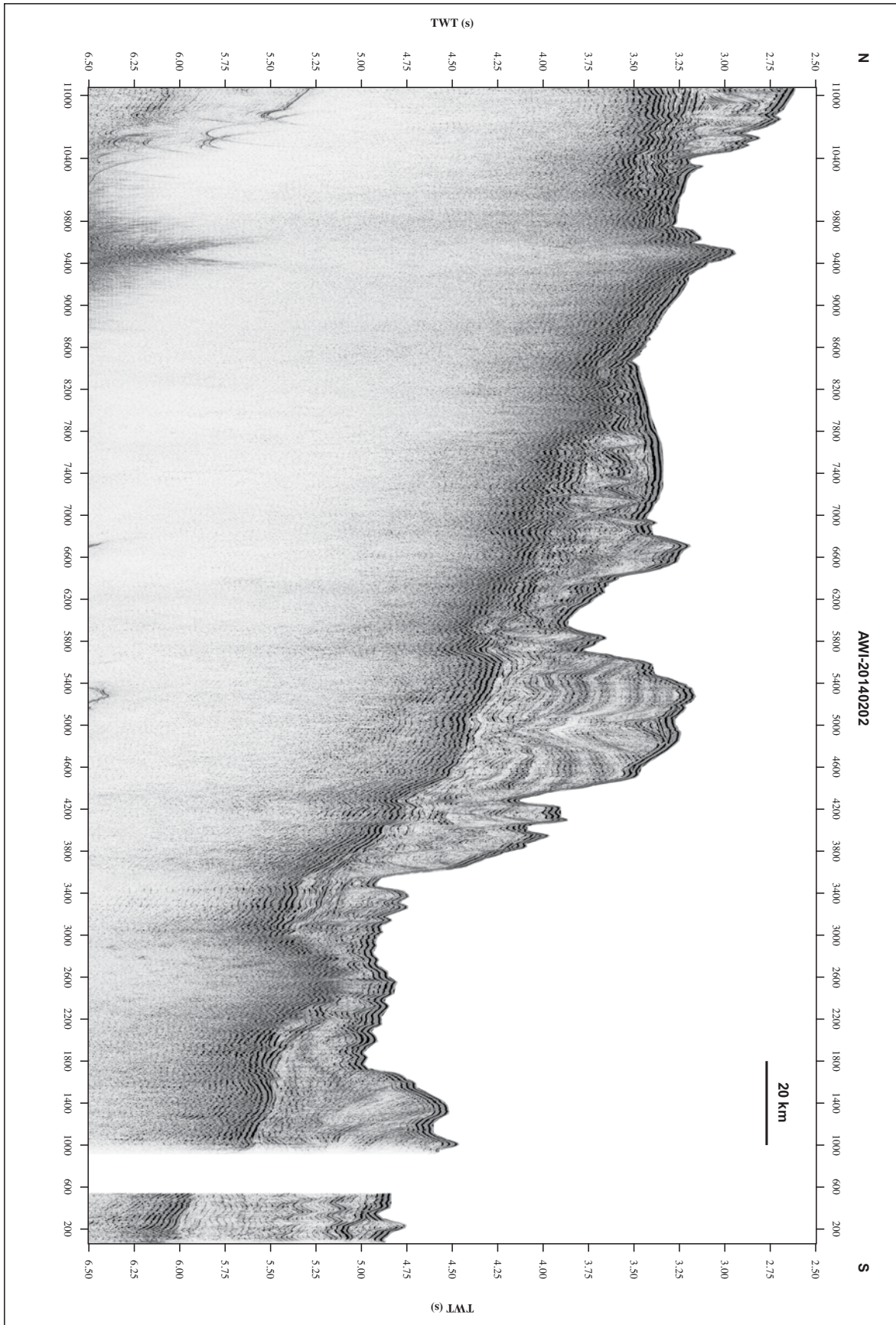


Figure A.3. Profile AWI-20140202

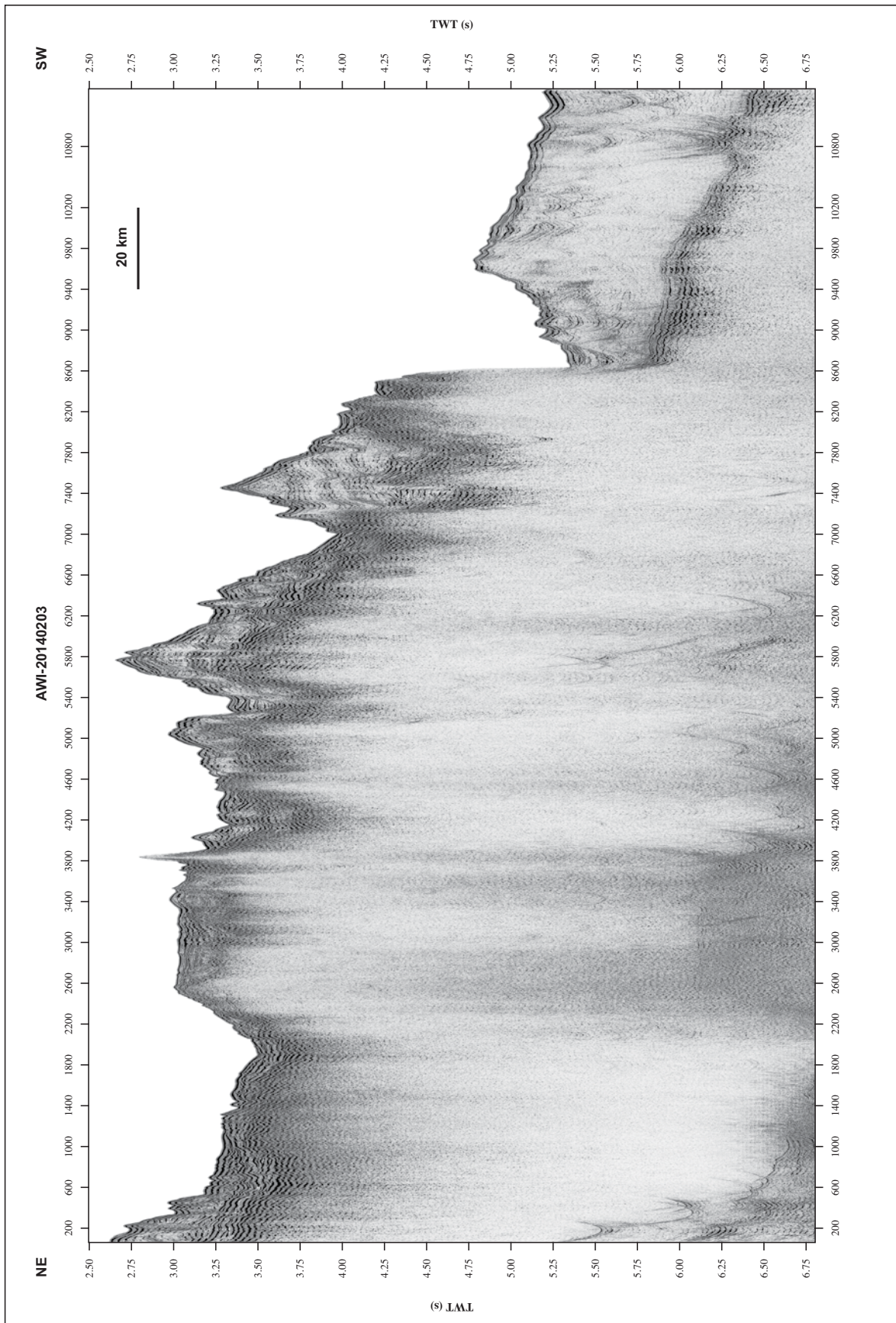


Figure A.4. Profile AWI-20140203.

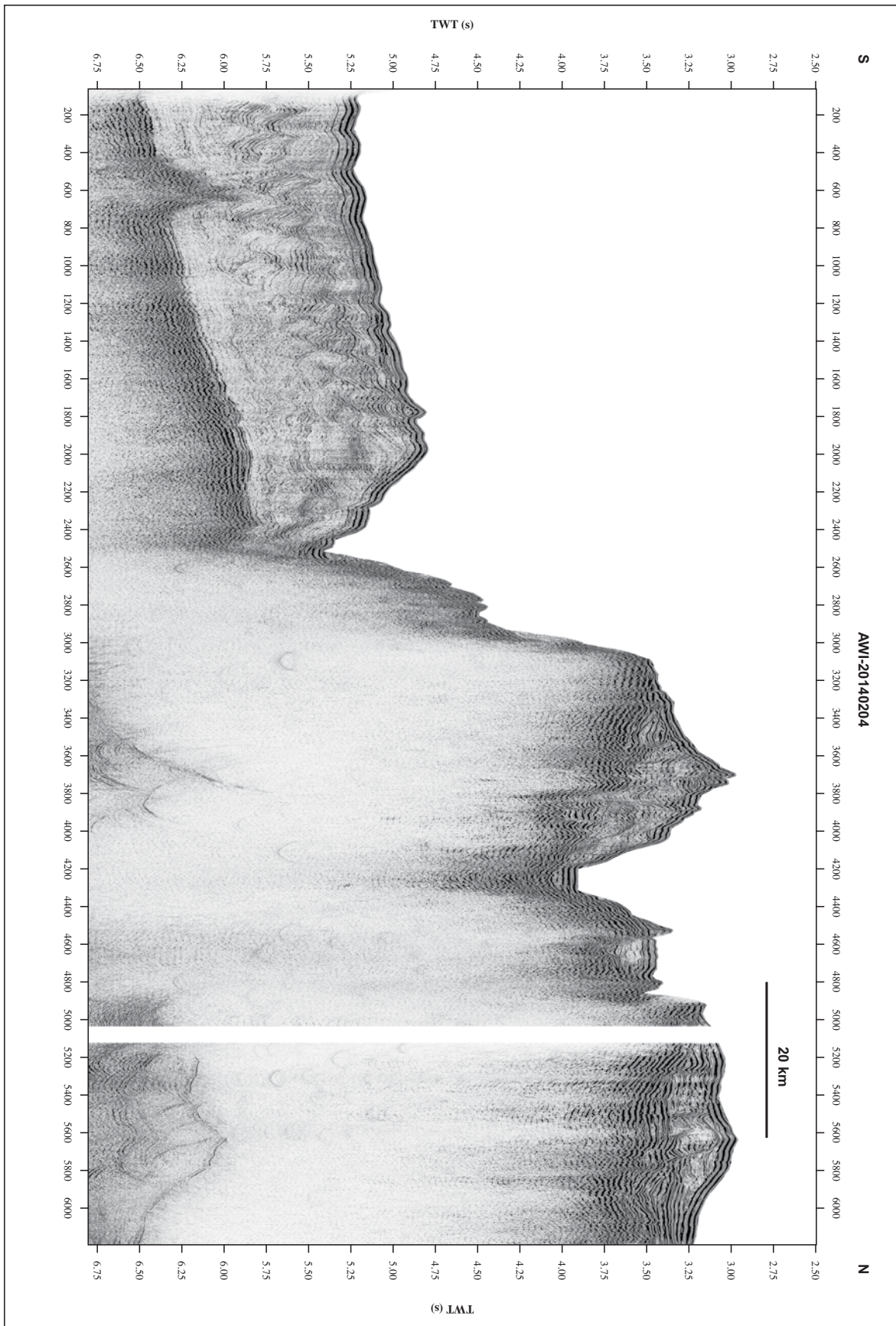


Figure A.5. Profile AWI-20140204.

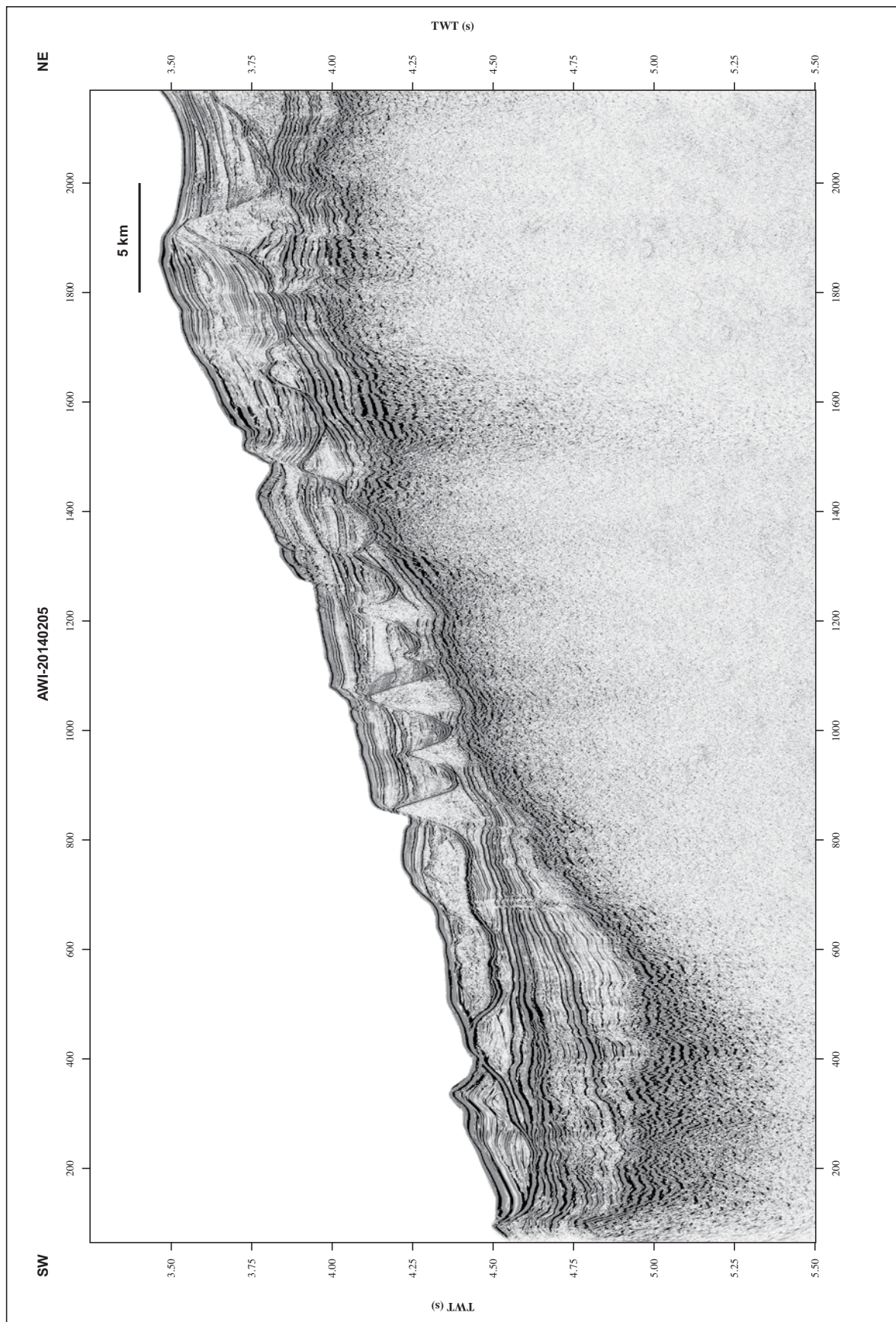


Figure A.6. Profile AWI-20140205.

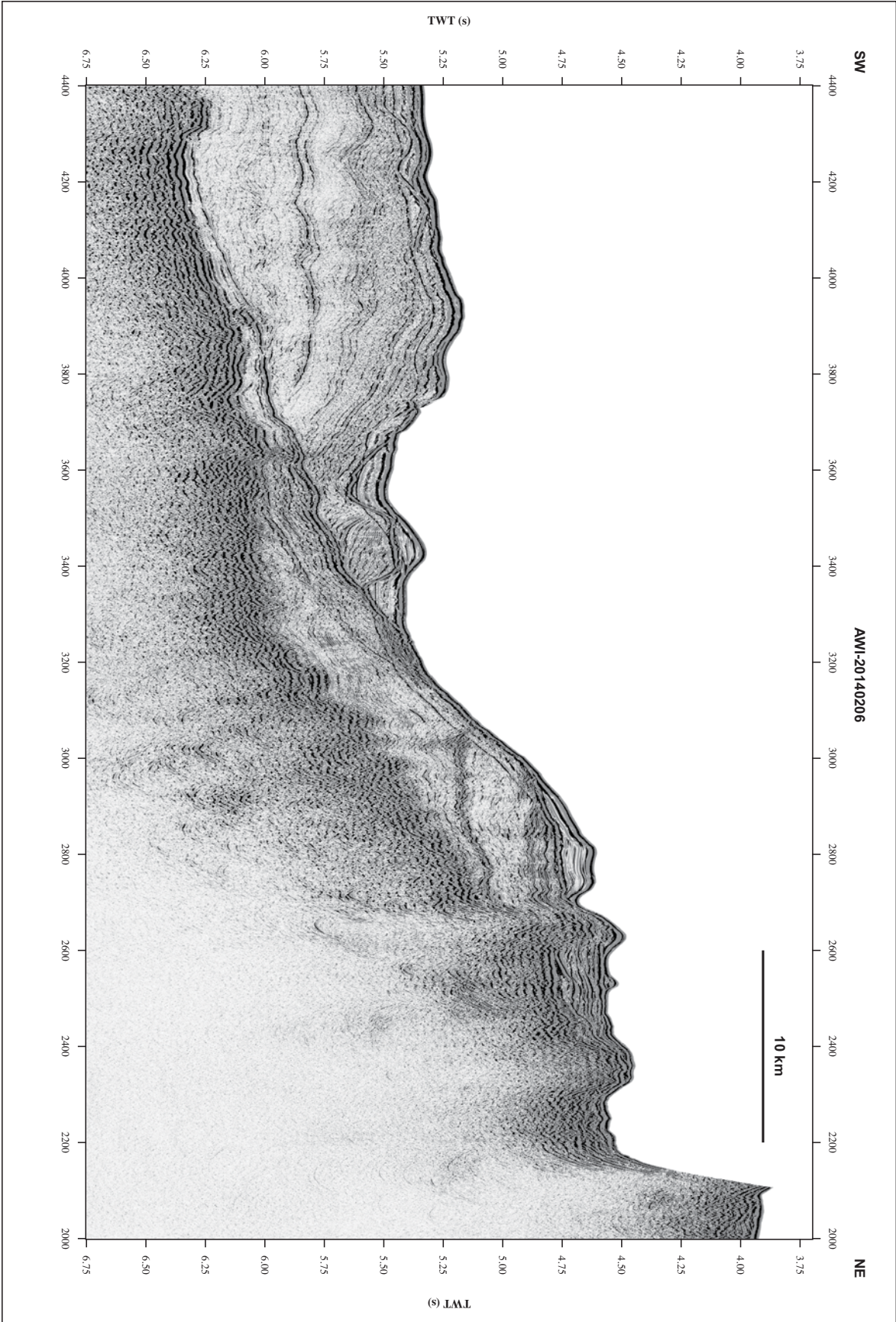


Figure A.7. Profile AWI-20140206.

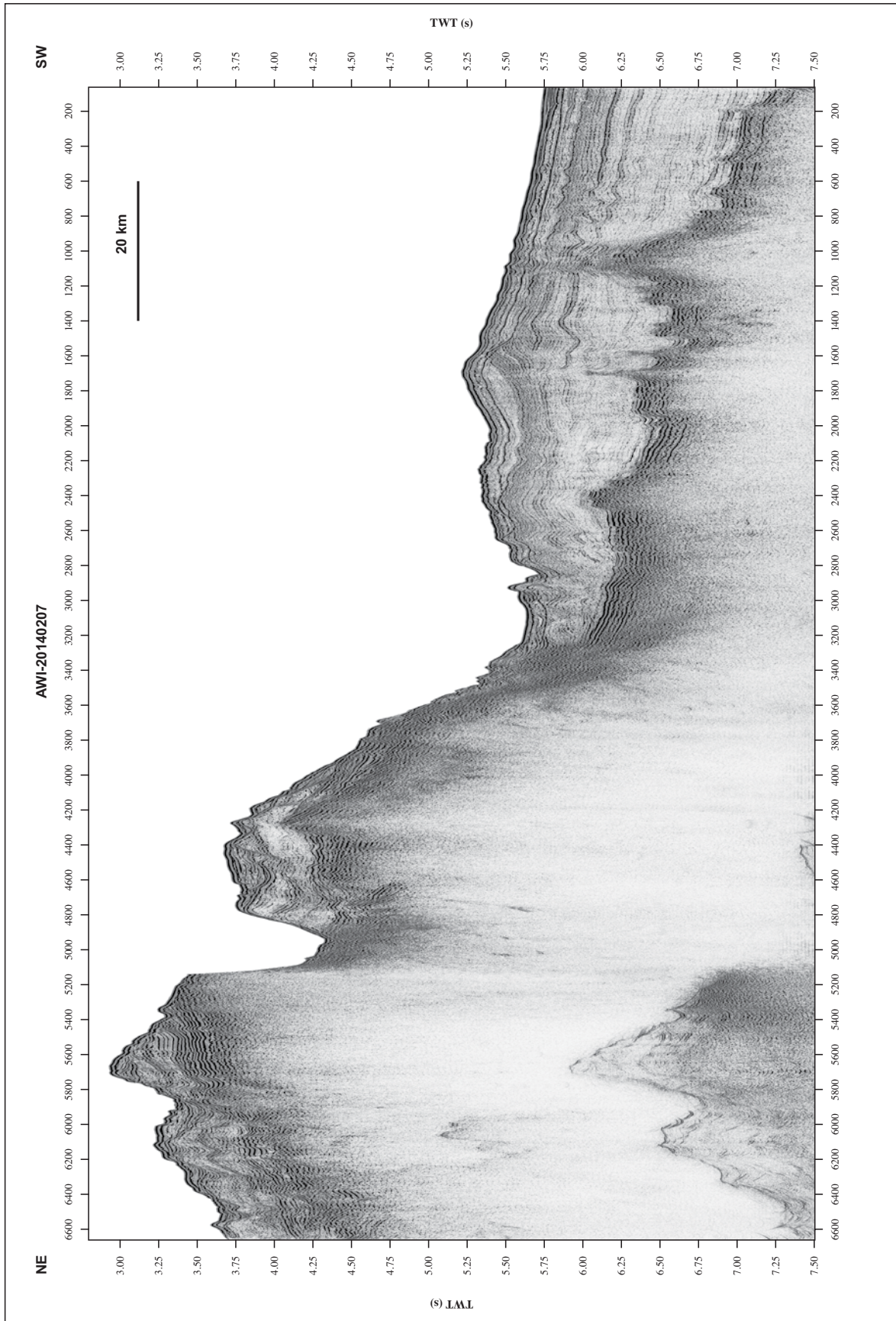


Figure A.8. Profile AWI-20140207.

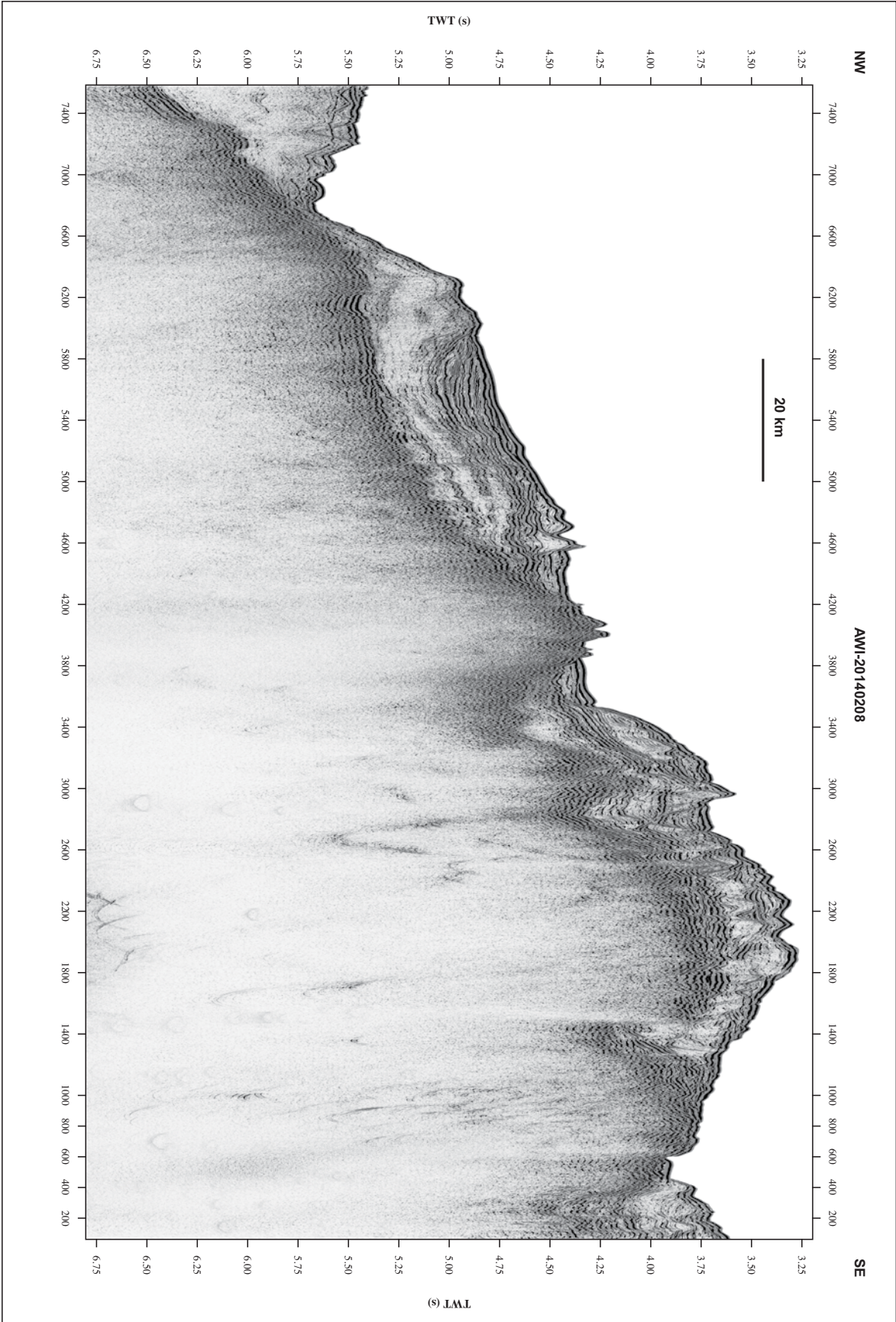


Figure A.9. Profile AWI-20140208.

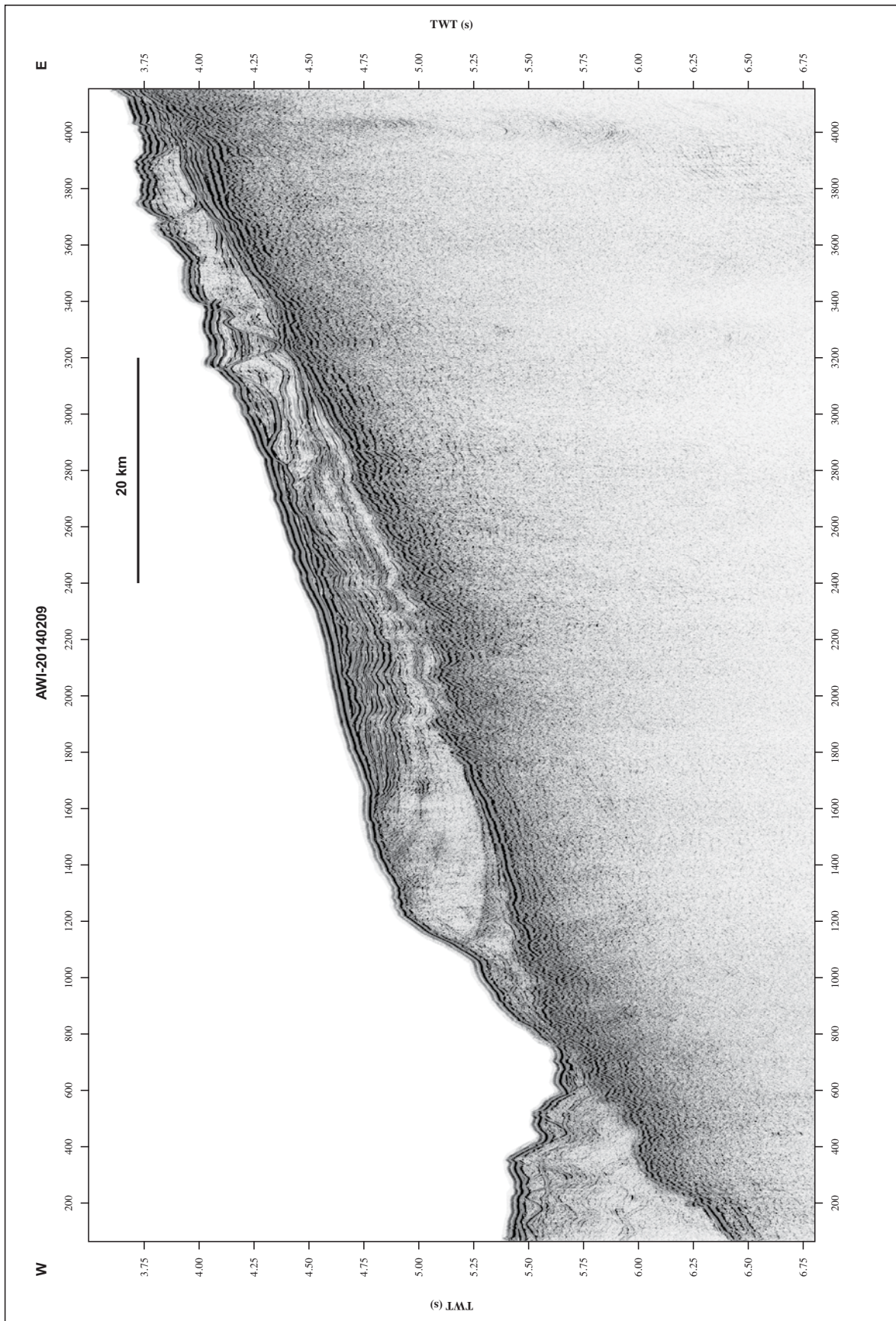


Figure A.10. Profile AWI-20140209.

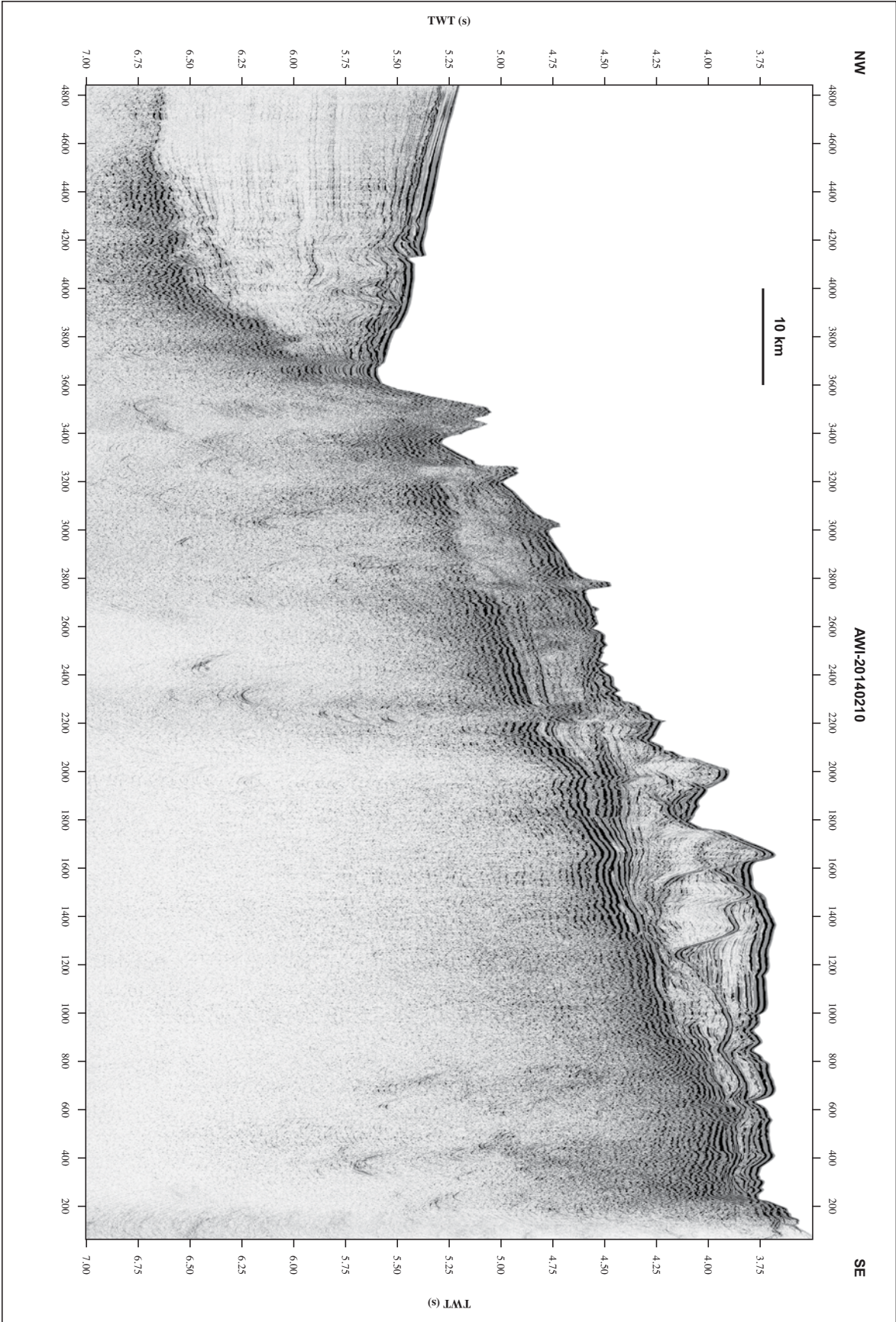


Figure A.11. Profile AWI-20140210.

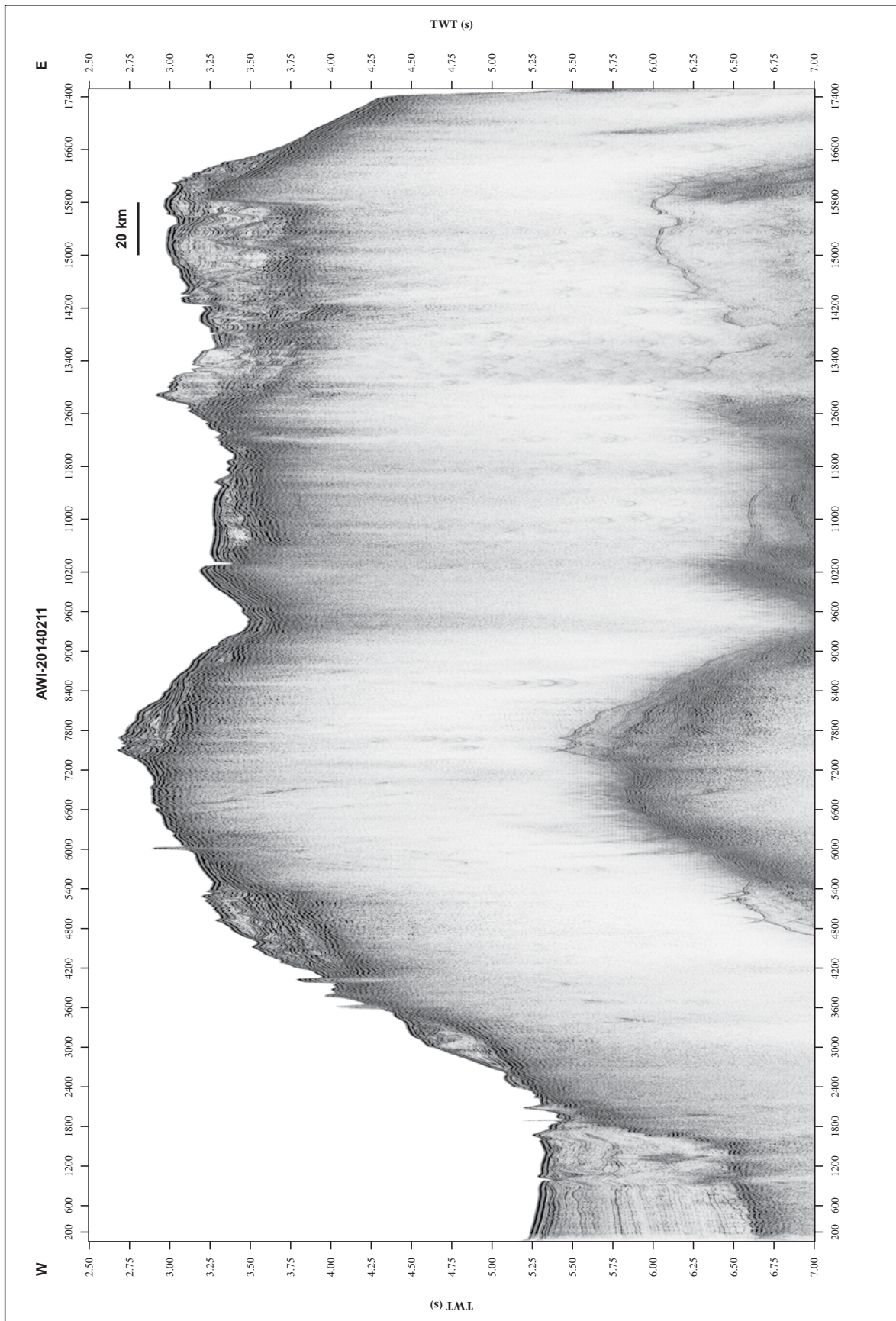


Figure A.12. Profile AWI-20140211.

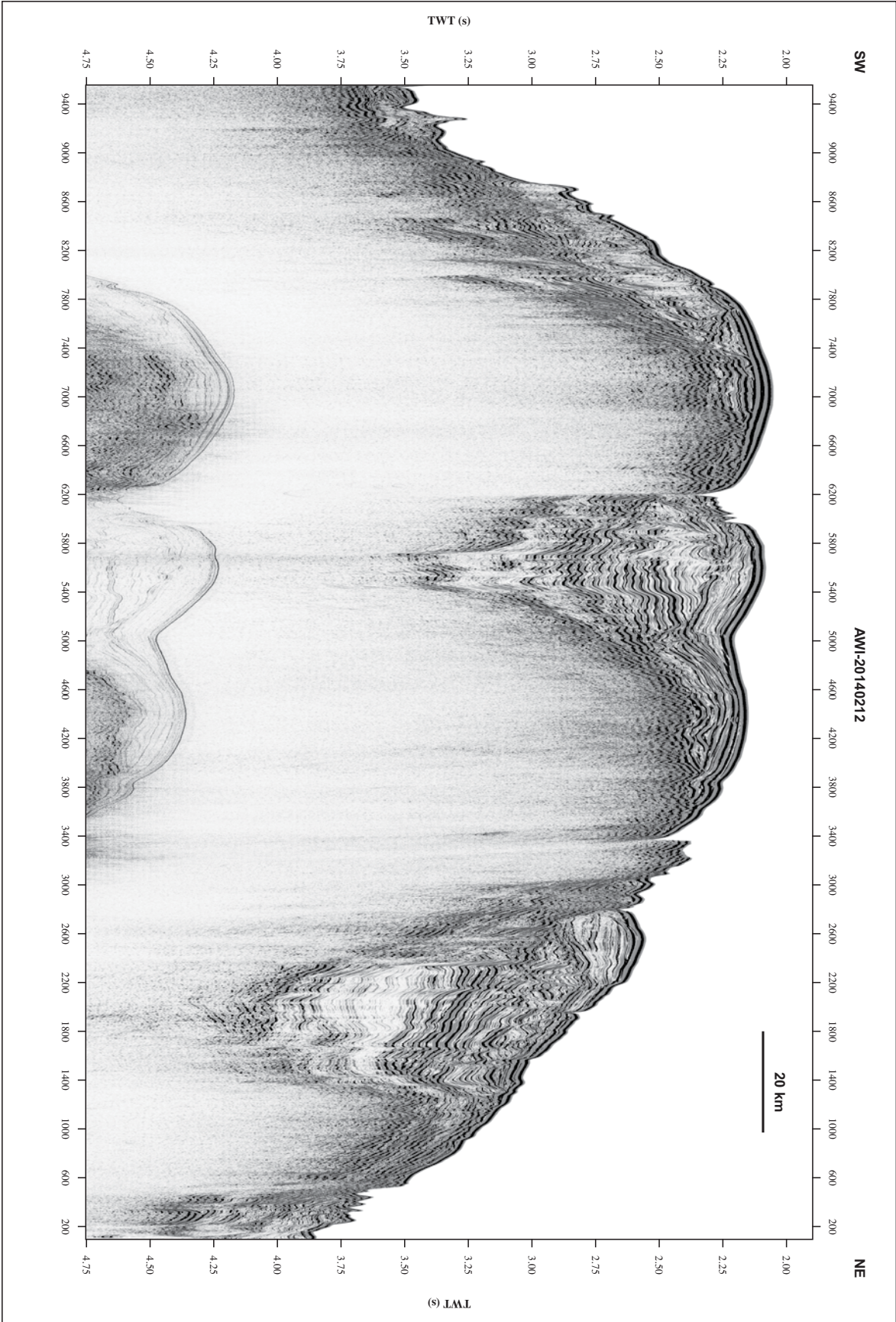


Figure A.13. Profile AWI-20140212.

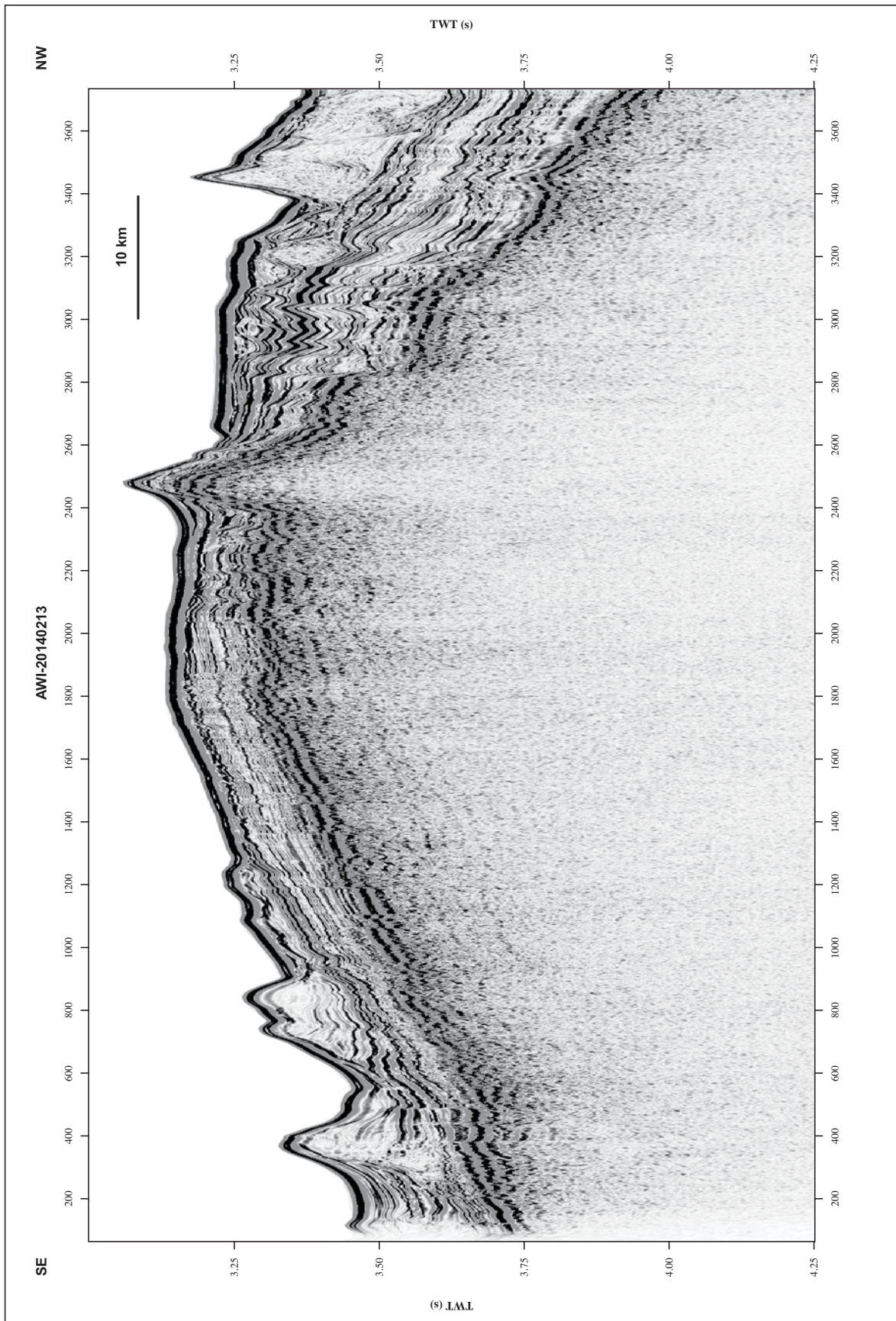


Figure A.14. Profile AWI-20140213.

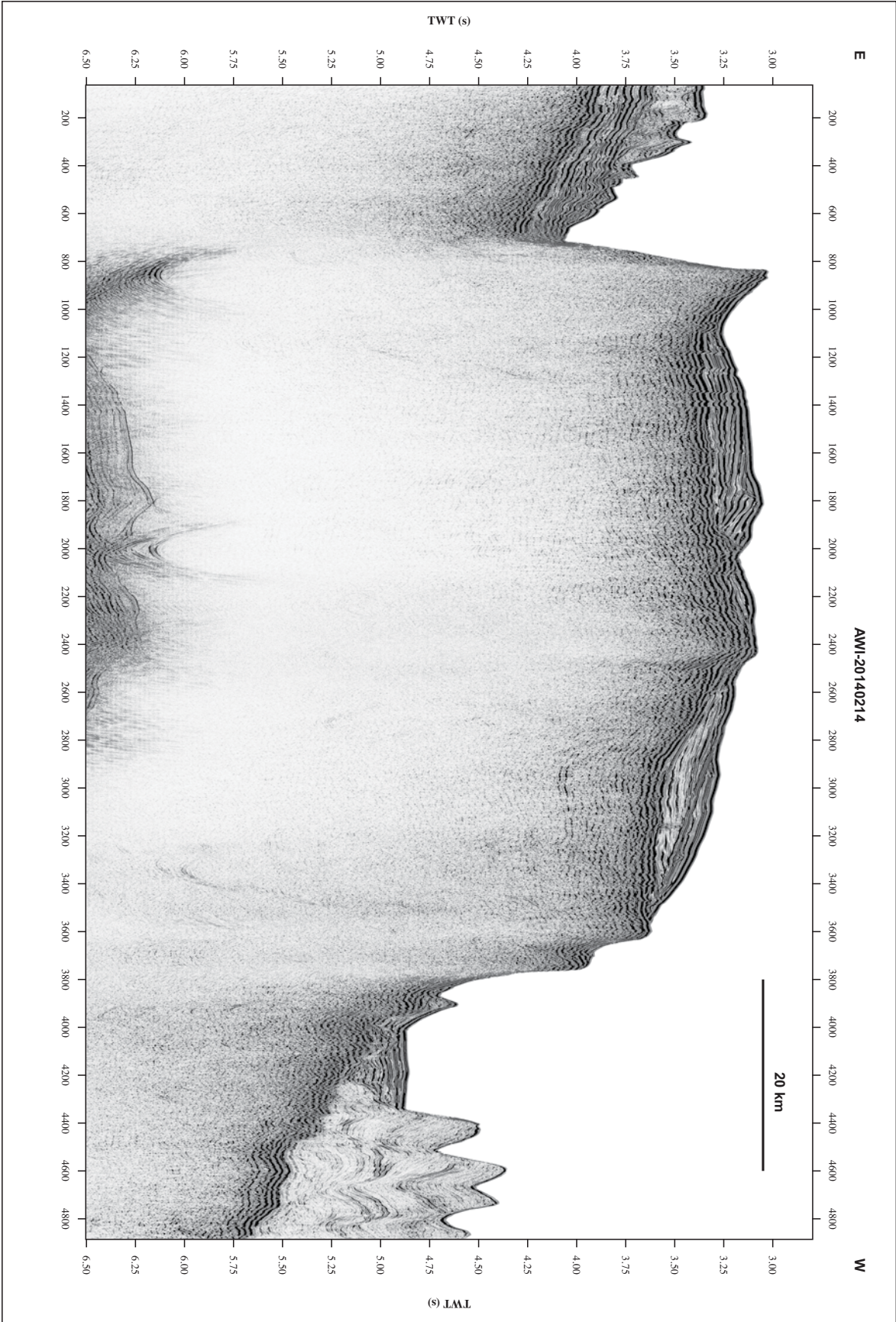


Figure A.15. Profile AWI-20140214.



Figure A.16. Profile AWI-20140215.

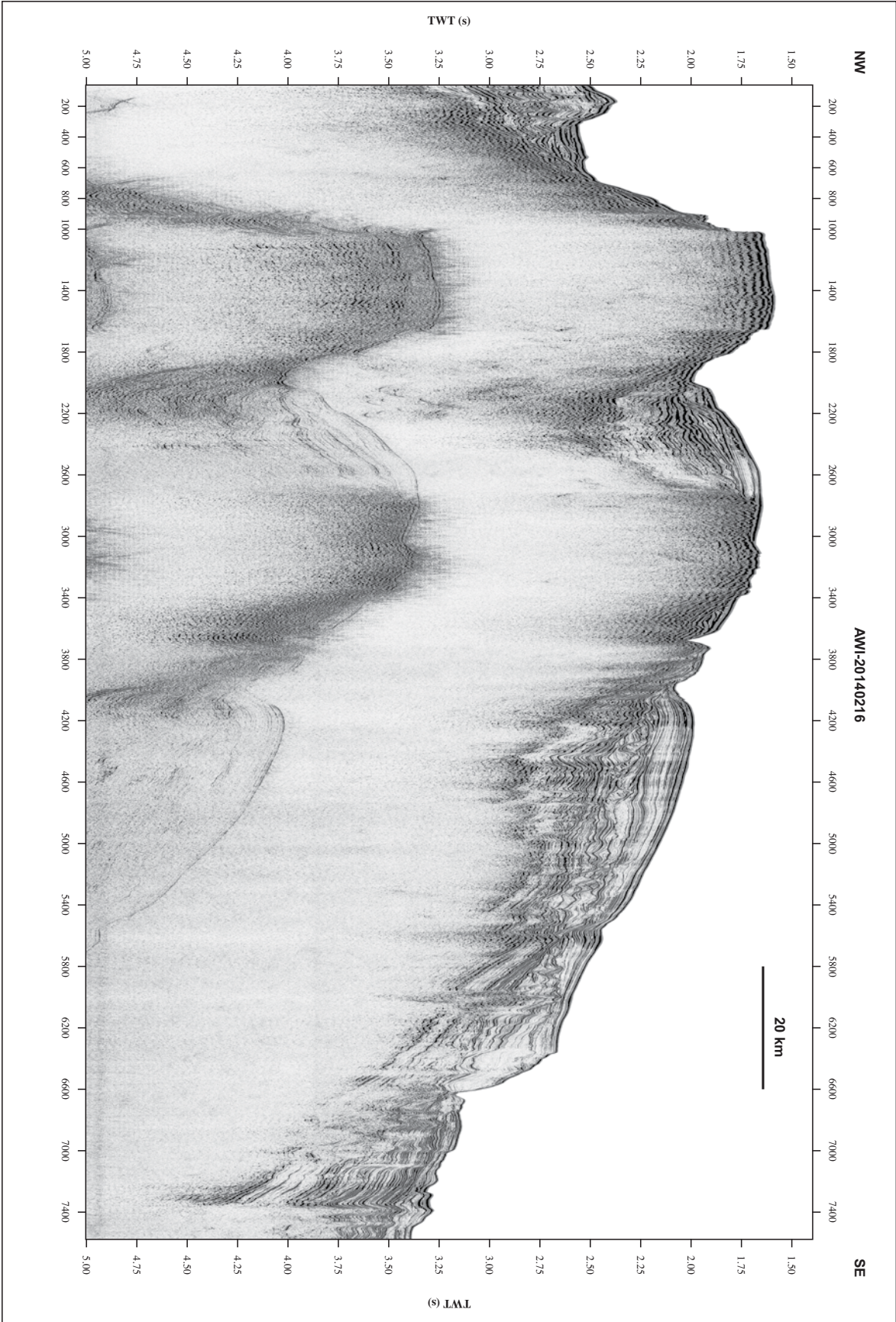


Figure A.17. Profile AWI-20140216.

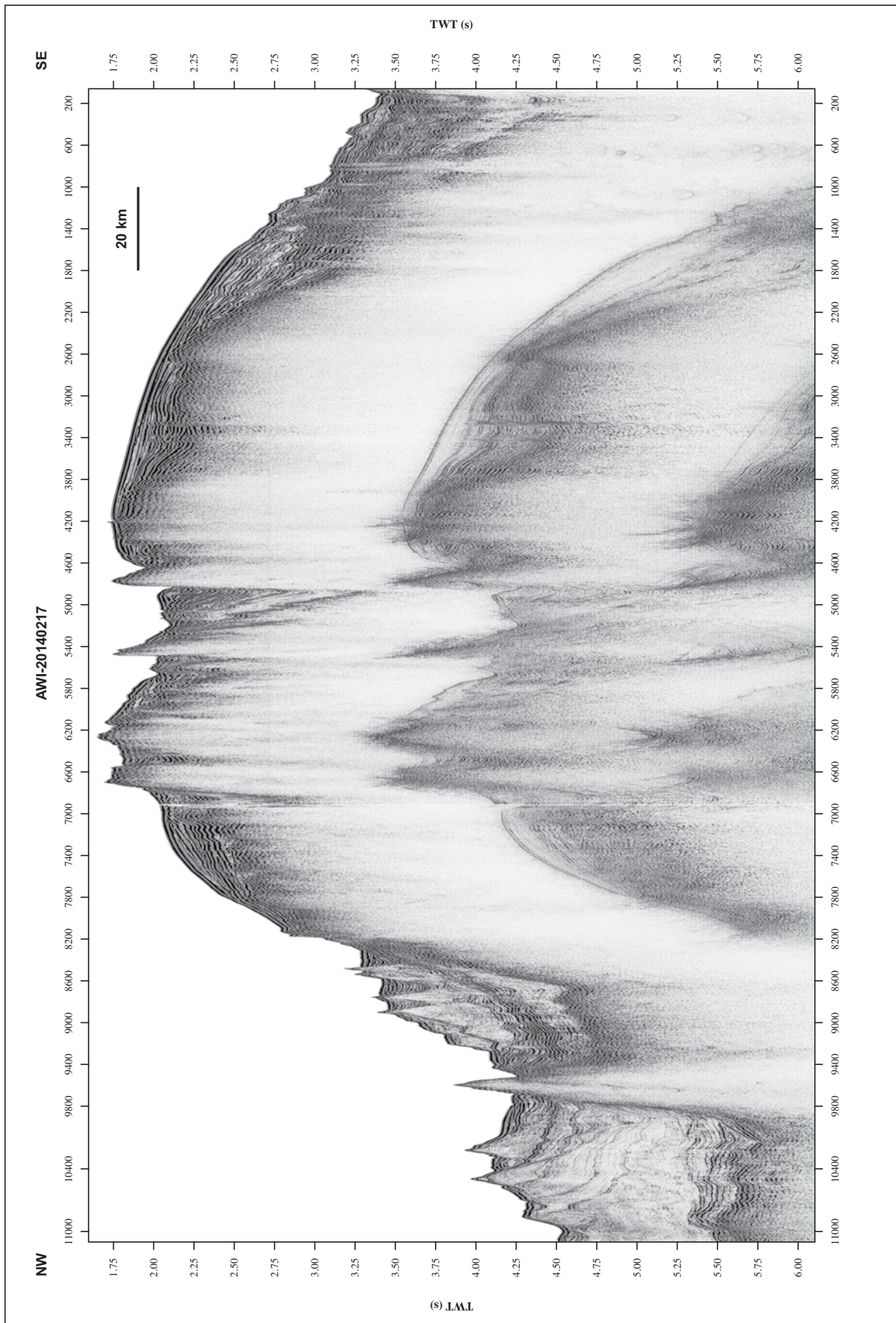


Figure A.18. Profile AWI-20140217.

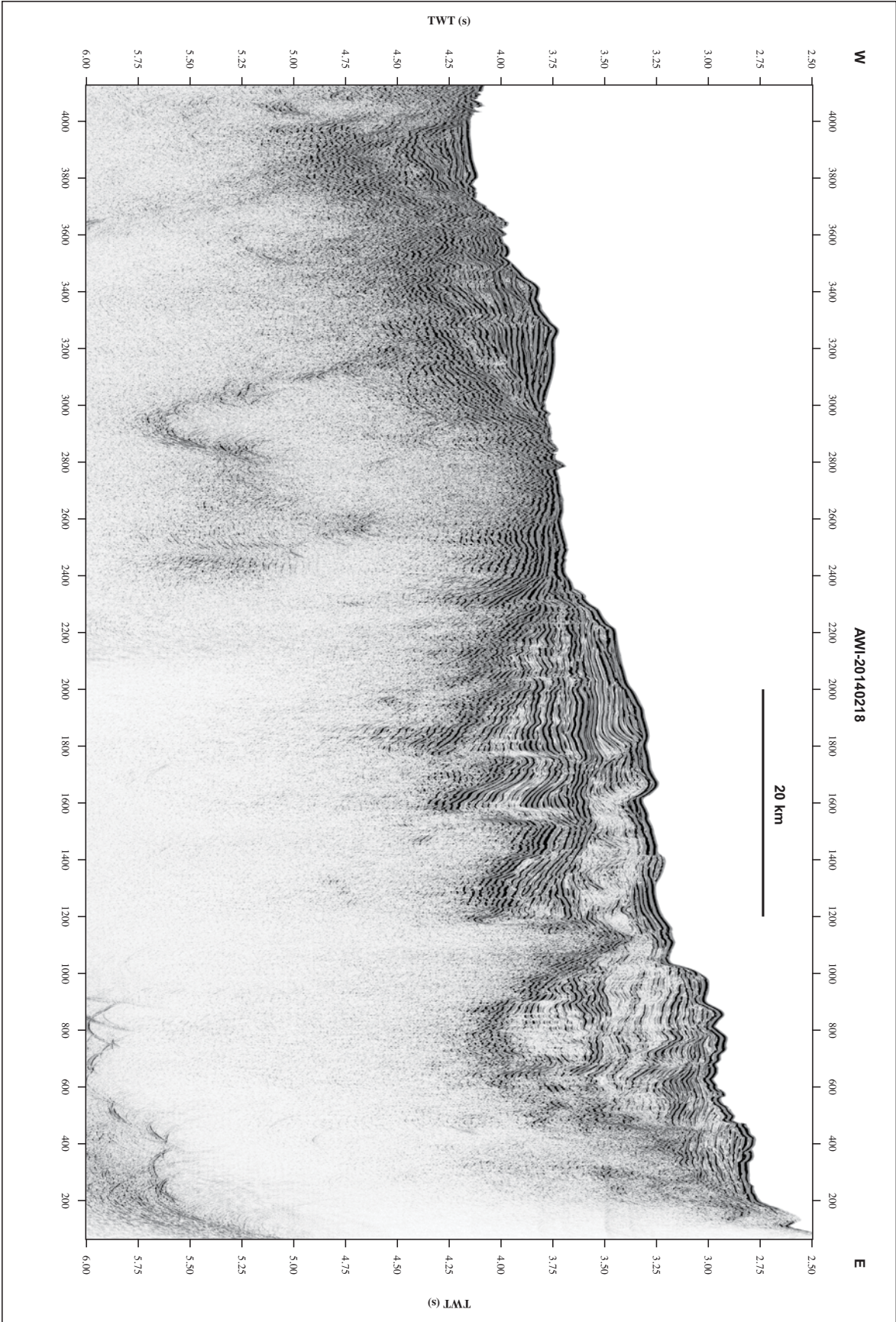


Figure A.19. Profile AWI-20140218.

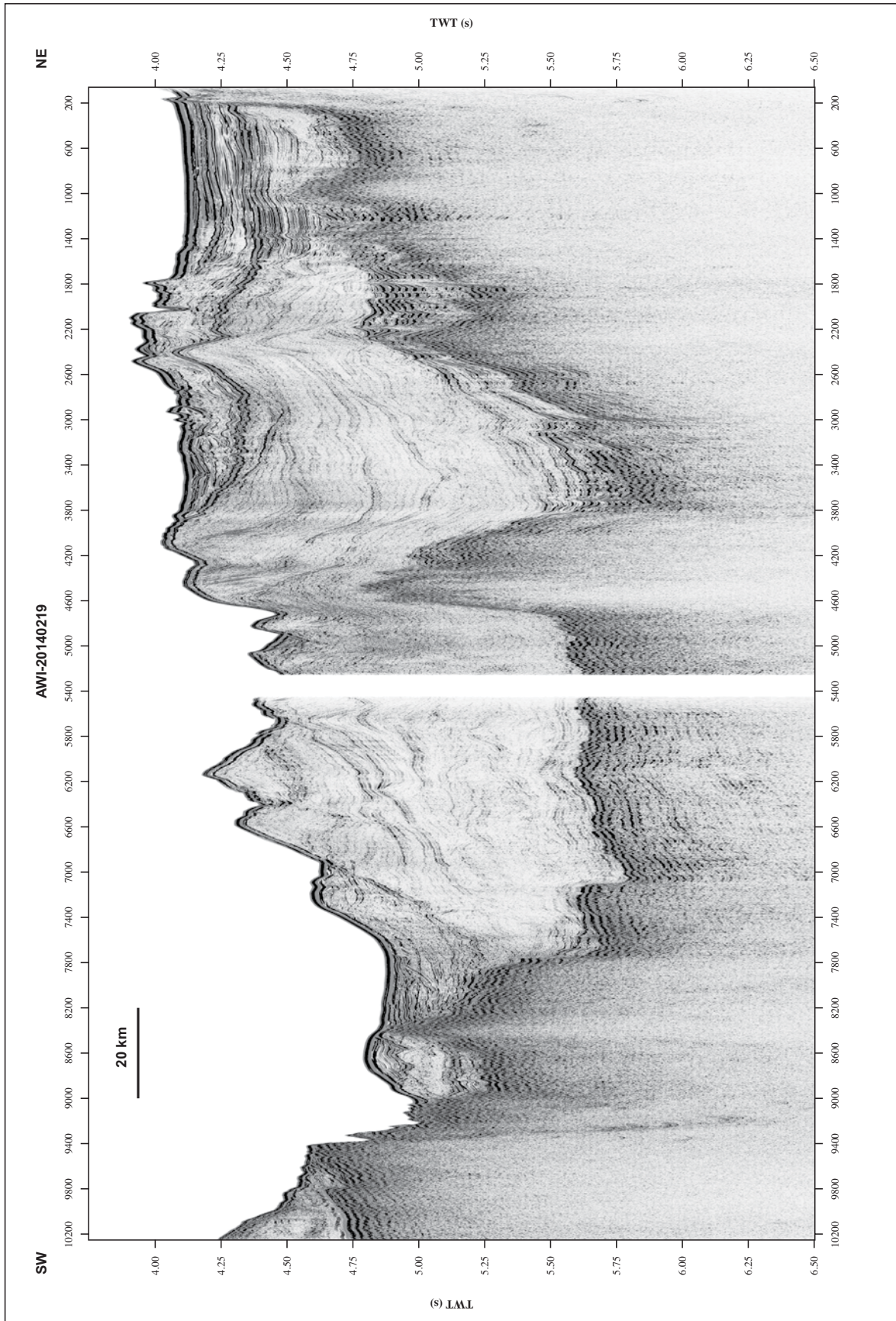


Figure A.20. Profile AWI-20140219.

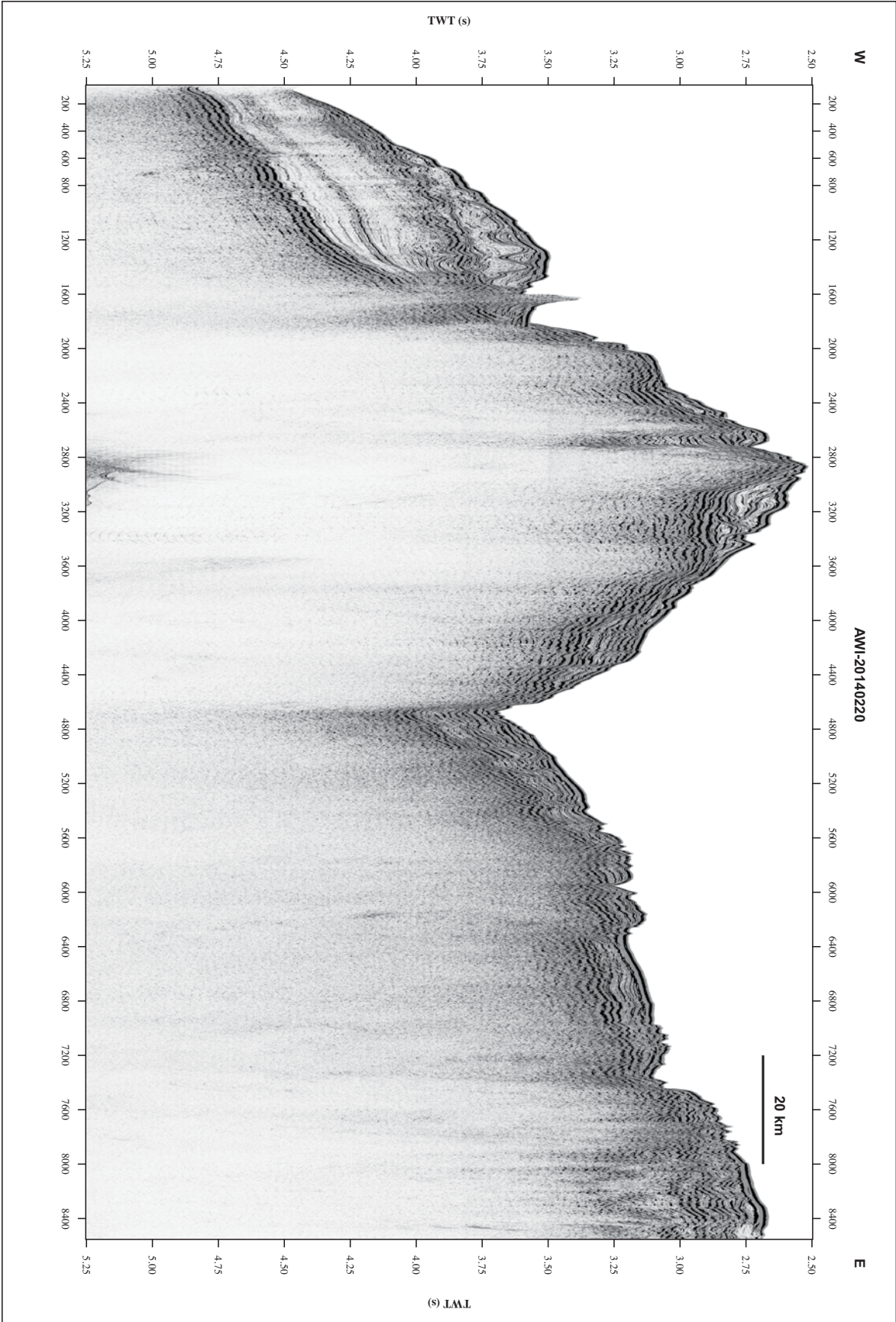


Figure A.21. Profile AWI-20140220.

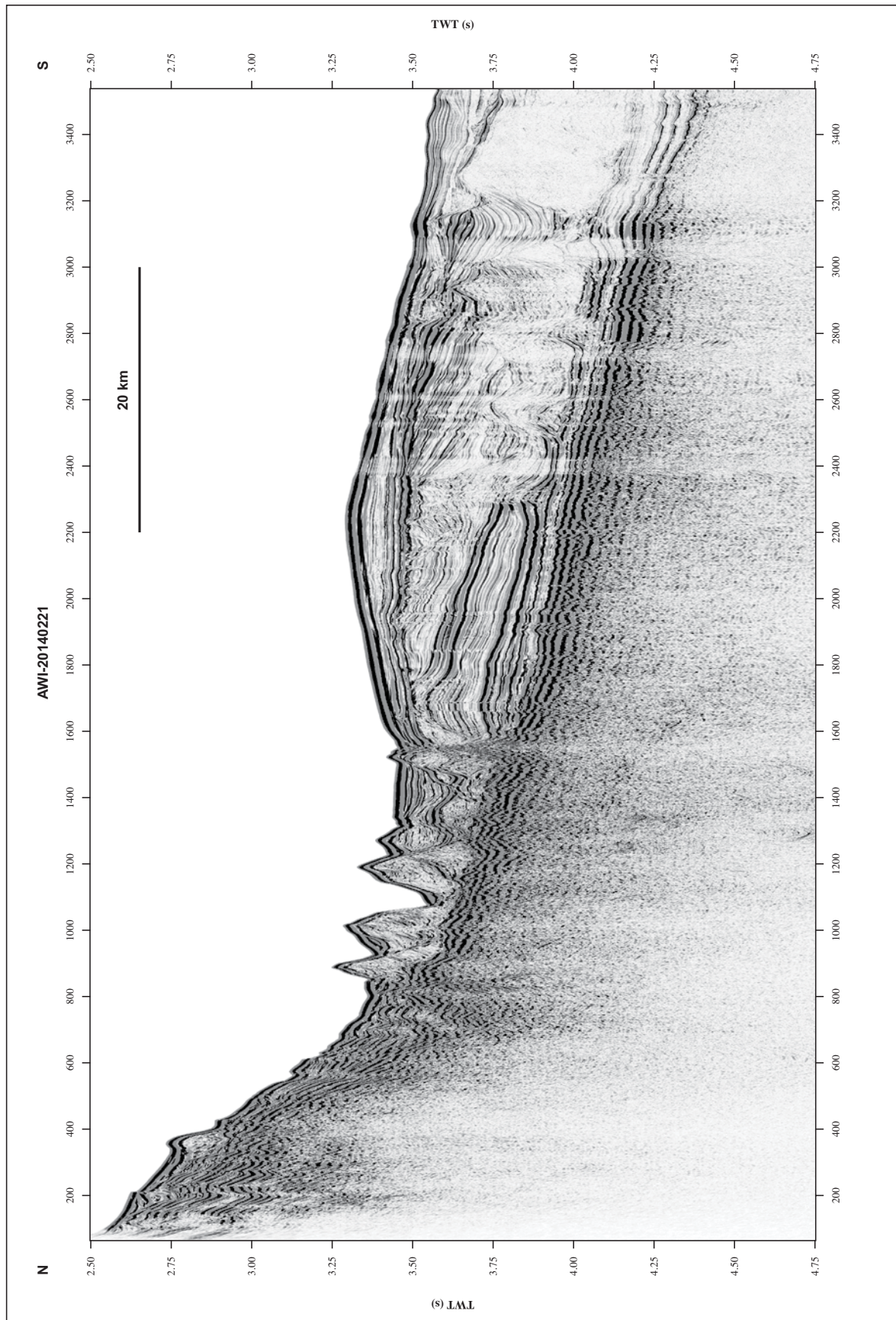


Figure A.22. Profile AWI-20140221.

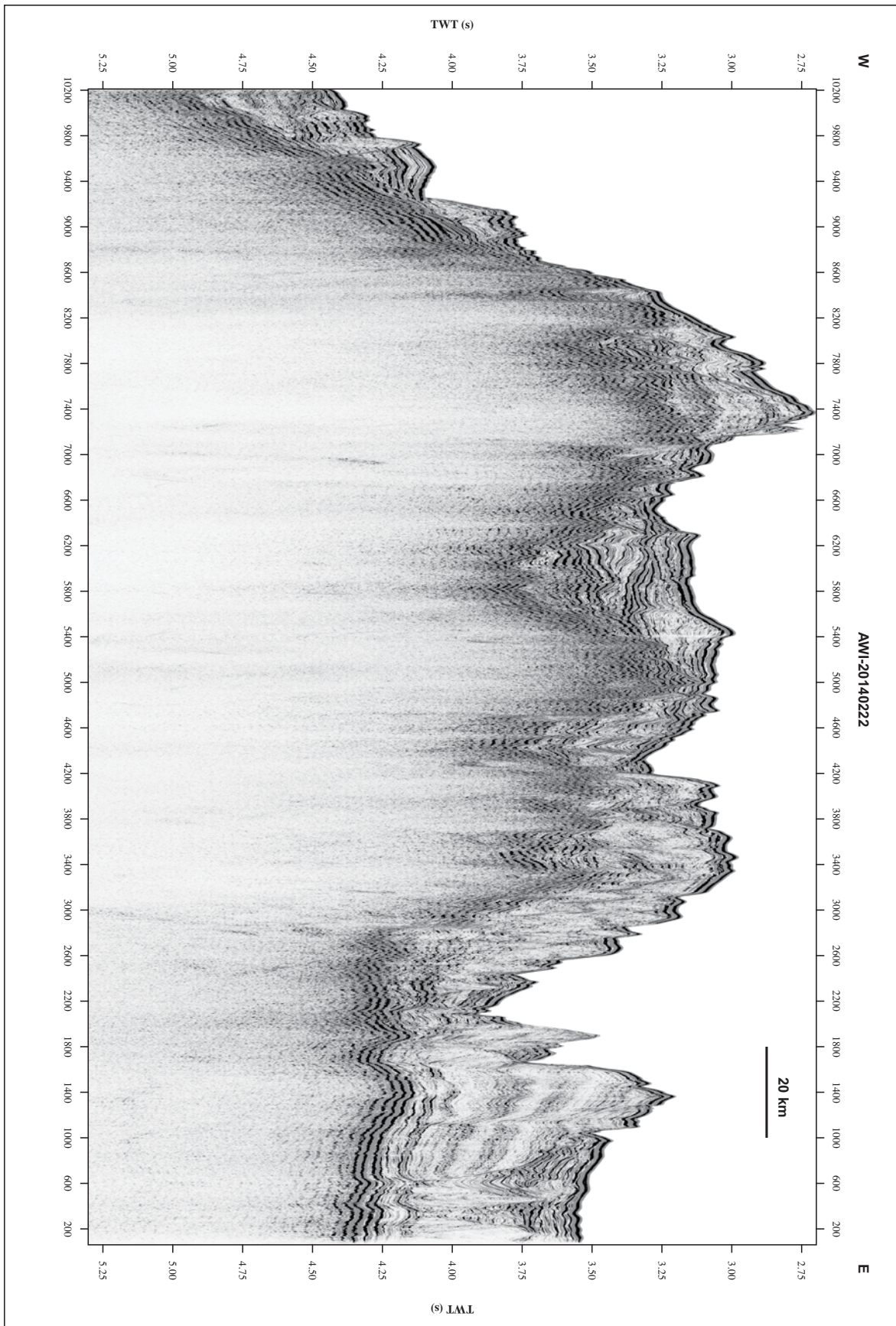


Figure A.23. Profile AWI-20140222.

